
Louisiana Transportation Research Center

Final Report 384

Strengthening of Bridge Beams using Fiber Reinforced Polymers (FRP)

by

Vijay Gopu, Ph.D., P.E.
LTRC

Paul H. Ziehl, Ph.D., P.E.
University of South Carolina



4101 Gourrier Avenue | Baton Rouge, Louisiana 70808
(225) 767-9131 | (225) 767-9108 fax | www.ltrc.lsu.edu

TECHNICAL REPORT STANDARD PAGE

1. Report No. FHWA/LA.16/384		2. Government Accession No.	3. Recipient's Catalog No.
4. Title and Subtitle Strengthening of Bridge Beams using Fiber Reinforced Polymers (FRP)		5. Report Date November 2016	
		6. Performing Organization Code LTRC Project Number: 03-4ST State Project Number: 736-99-1135	
7. Author(s) Vijay Gopu, Ph.D., P.E. and Paul H. Ziehl, Ph.D., P.E.		8. Performing Organization Report No.	
9. Performing Organization Name and Address Department of Civil and Environmental Engineering Louisiana State University Baton Rouge, LA 70803		10. Work Unit No.	
		11. Contract or Grant No.	
12. Sponsoring Agency Name and Address Louisiana Department of Transportation and Development P.O. Box 94245 Baton Rouge, LA 70804-9245		13. Type of Report and Period Covered Final Report July 2003 – December 2007	
		14. Sponsoring Agency Code	
15. Supplementary Notes Conducted in Cooperation with the U.S. Department of Transportation, Federal Highway Administration			
16. Abstract A literature review was conducted with regard to FRP strengthening of reinforced concrete bridge beams. The literature review focused primarily on field applications and analytical and design considerations. Selected laboratory investigations related to field implementation projects are also included in the literature review. Based on the literature review and the experience of the investigators, three different strengthening systems were selected for implementation on an existing bridge in Baton Rouge, Louisiana. The design of the three strengthening systems involving carbon fiber reinforced polymers (CFRP) wet layup, CFRP pre-cured plates, and near surface mounted CFRP rods and their installation on spans two and three of the White Bayou Bridge in Zachary, Louisiana, are described in detail. The moment capacity of the CFRP strengthened beams increased from 15% to 32% depending on the system used. The shear capacity of the member was not an issue. The live load testing and installation of the long term monitoring system were carried out by Bridge Diagnostics Inc. (BDI) and are discussed in this report (See Appendix A). The bridge was instrumented with several strain and displacement sensors and the first set of live load tests were conducted before the bridge was strengthened using three different load paths. The second set of tests was performed with identical procedures to the first load test so that direct comparisons of the response could be made. The load tests permitted the assessment of the lateral load distribution that occurred in the structure and the confirmation that continuity was minimal. The member capacities that were calculated using the Standard Specifications for Highway Bridges, and the load rating factors for the standard AASHTO H-20, HS-20, Type 3, Type 3-3, and Type 3S3 vehicles that were computed according to the LFD rating method are presented in this report. The ultimate moment capacity of the strengthened beams and the associated load rating factors for each of the strengthening systems were calculated and compared with the un-strengthened member values. Recommendations for the installing of the CFRP reinforcement, factors to be considered in field monitoring and load testing, and a summary related to the cost of the FRP strengthening systems and the relative performance of each system are included.			
17. Key Words Strengthening, Fiber Reinforced Polymer, FRP, Load Rating,		18. Distribution Statement Unrestricted. This document is available through the National Technical Information Service, Springfield, VA 21161.	
19. Security Classif. (of this report)	20. Security Classif. (of this page)	21. No. of Pages 220	22. Price

Strengthening of Bridge Beams using Fiber Reinforced Polymers (FRP)

by

Vijay Gopu, Ph.D., P.E.
Tulane University
School of Science and Engineering
New Orleans, LA

and

Paul H. Ziehl, Ph.D., P.E.
U. South Carolina
Dept. of Civil and Environmental Engineering
Columbia, SC

LTRC Project No. 03-4ST
State Project No. 736-99-1135

conducted for

Louisiana Department of Transportation and Development
Louisiana Transportation Research Center

The contents of this report reflect the views of the author/principal investigator who is responsible for the facts and the accuracy of the data presented herein. The contents do not necessarily reflect the views or policies of the Louisiana Department of Transportation and Development or the Louisiana Transportation Research Center. This report does not constitute a standard, specification, or regulation.

November 2016

ABSTRACT

A literature review was conducted with regard to FRP strengthening of reinforced concrete bridge beams. The literature review focused primarily on field applications and analytical and design considerations. Selected laboratory investigations related to field implementation projects are also included in the literature review. Based on the literature review and the experience of the investigators, three different strengthening systems were selected for implementation on an existing bridge in Baton Rouge, Louisiana.

The design of the three strengthening systems involving carbon fiber reinforced polymers (CFRP) wet layup, CFRP pre-cured plates, and near surface mounted CFRP rods and their installation on spans two and three of the White Bayou Bridge in Zachary, Louisiana, are described in detail. The moment capacity of the CFRP strengthened beams increased from 15% to 32% depending on the system used. The shear capacity of the member was not an issue.

The live load testing and installation of the long term monitoring system were carried out by Bridge Diagnostics Inc. (BDI) and are discussed in this report (See Appendix A). The bridge was instrumented with several strain and displacement sensors and the first set of live load tests were conducted before the bridge was strengthened using three different load paths. The second set of tests was performed with identical procedures to the first load test so that direct comparisons of the response could be made. The load tests permitted the assessment of the lateral load distribution that occurred in the structure and the confirmation that continuity was minimal.

The member capacities that were calculated using the Standard Specifications for Highway Bridges, and the load rating factors for the standard AASHTO H-20, HS-20, Type 3, Type 3-3, and Type 3S3 vehicles that were computed according to the LFD rating method are presented in this report. The ultimate moment capacity of the strengthened beams and the associated load rating factors for each of the strengthening systems were calculated and compared with the un-strengthened member values.

Recommendations for the installing of the CFRP reinforcement, factors to be considered in field monitoring and load testing, and a summary related to the cost of the FRP strengthening systems and the relative performance of each system are included.

ACKNOWLEDGMENTS

Work on this project was performed primarily by Tulane University Department of Civil and Environmental Engineering, with substantial input from Drs. Myers and Nanni of the University of Missouri-Rolla Department of Civil, Architectural, and Environmental Engineering under the sponsorship of the Louisiana Transportation Research Center, and in cooperation with the Louisiana Department of Transportation and Development. Gill Gautreau, Bridge Maintenance Engineer of the Louisiana Department of Transportation and Development, selected two candidate bridges for strengthening and provided maintenance reports. Paul Fossier, Bridge Engineer Administrator of the Louisiana Department of Transportation and Development, provided structural plans of the bridge and escorted the investigators to the bridge sites. Dr. Walid Alaywan, Sr. Structures Research Engineer of the Louisiana Transportation Research Center, provided load rating calculations and administrative management for the project.

Also acknowledged is the work of Yizhuo Chen, Francisco Barrios, Adam Ridge, and Zhiwei Liu, graduate students at Tulane University when this work was completed, and Dr. Anthony Lamanna, also of Tulane University when this work was completed.

The strengthening was performed by Structural Preservation Systems, and the input of Tarek Alkhrdaji and Jay Thomas is appreciated. Bridge Diagnostics Incorporated conducted the live load test and installed the long-term monitoring system.

IMPLEMENTATION STATEMENT

Weight restrictions on existing bridges are harmful to commerce in Louisiana. Furthermore, the state of the aging infrastructure may lead to a reduction in the safety of older bridges over time. Load postings of bridges are difficult to enforce and the passage of overweight vehicles on load-posted bridges is likely to continue. This can substantially reduce the fatigue life of the bridges. If strengthening with FRP materials is found to be a reliable and cost-effective approach, the long-term safety of weight restricted bridges could be substantially increased. The useful life of strengthened bridges will be significantly extended and therefore substantial cost savings can be realized over time.

Results of this research have been implemented in the form of FRP strengthening of an existing bridge. Three different strengthening schemes were recommended for implementation. Two of the three recommended systems (CFRP wet layup and near surface mounted strips) were implemented on a bridge in Zachary, Louisiana. The third was not implemented on this bridge (mechanically fastened CFRP post-tensioned strips) due to the scarcity of post-tensioned CFRP systems in practice and the observed failure by tearing of the strips in service. These factors coupled with budgetary considerations led to the implementation of a CFRP pre-cured strip system in lieu of the post-tensioned strip system.

The implementation provides an excellent opportunity to compare the advantages and disadvantages of the different strengthening systems. The load testing and subsequent long-term monitoring of the different strengthening systems likewise offers an excellent opportunity to determine the performance and durability of the selected systems in real world conditions. Through this project, DOTD has gained considerable experience with the FRP strengthening approach, and this will likely lead to more widespread implementation. If the FRP strengthening approach is feasible, this can lead to a reduction in the number of weight restricted bridges in Louisiana and to longer service lives for the strengthened bridges.

TABLE OF CONTENTS

ABSTRACT.....	iii
ACKNOWLEDGMENTS	v
IMPLEMENTATION STATEMENT	vii
TABLE OF CONTENTS.....	ix
LIST OF TABLES.....	xi
LIST OF FIGURES	xiii
INTRODUCTION	1
Literature Review	1
Field Applications	1
Laboratory Investigations.....	7
OBJECTIVES.....	25
SCOPE	27
METHODOLOGY	29
Description of Bridge and Selection of Strengthening Systems	29
CFRP Wet Layup (Fabric)	32
CFRP Near Surface Mounted Strips or Rods.....	33
CFRP Post-Tensioned Strips or Rods	34
Description of CFRP Strengthening Systems and Calculation Procedures	36
Description of CFRP Strengthening Systems	36
Calculation Procedures.....	39
Live Load Testing Procedures	47
DISCUSSION OF RESULTS.....	61
Preliminary Data Review Observations	61
Reproducibility and Linearity	61
Distribution.....	61
Continuity of Spans	61
Response Symmetry	62
Influence of Cracks	62
Neutral Axis Measurements	62
Unusual Responses(s).....	62
High Speed Tests.....	63
Strengthening.....	63
Modeling, Analysis and Data Correlation	68
Model Calibration Results	70
Element Stiffness.....	70

Deck Stiffness.....	70
Pier Support Conditions	71
Load Rating Procedures and Results.....	71
Description of Long-Term Monitoring.....	76
Long-Term Monitoring System.....	76
CONCLUSION.....	81
Field Applications.....	81
Laboratory Investigations	81
Analysis and Design Considerations.....	82
RECOMMENDATIONS.....	83
ACRONYMS, ABBREVIATIONS, AND SYMBOLS	87
REFERENCES	89
APPENDIX A BRIDGE DIAGNOSTICS, INC. REPORT	95
APPENDIX B SHEAR RATING CALCULATIONS	200

LIST OF TABLES

Table 1	Properties of installed strengthening systems.....	45
Table 2	Calculated increase in moment capacity.....	46
Table 3	Calculated shear capacity.....	47
Table 4	Structure description and testing notes.....	47
Table 5	Testing vehicle information.....	49
Table 6	Analysis and model details.....	69
Table 7	Model accuracy and parameter values.....	71
Table 8	Load and resistance factors.....	72
Table 9	Girder section and steel details.....	73
Table 10	Tee beam moment capacities.....	74
Table 11	Load rating factors for H-20.....	74
Table 12	Load rating factors for HS-20.....	74
Table 13	Load rating factors for Type 3.....	75
Table 14	Load rating factors for Type 3-3.....	75
Table 15	Load rating factors for Type 3S3.....	75
Table 16	Moment capacities and load rating factors of strengthened beams.....	76

LIST OF FIGURES

Figure 1	View of sub-structure and super-structure of White Bayou Bridge	30
Figure 2	View of pile cap, beam, and deck of White Bayou Bridge	30
Figure 3	CFRP wet layup (schematic)	33
Figure 4	Near surface mounted CFRP strips (schematic)	34
Figure 5	CFRP post tensioned strips (schematic)	35
Figure 6	CFRP strengthening schemes - plan view	36
Figure 7	CFRP strengthening schemes - cross-section views	37
Figure 8	Overall view of White Bayou Bridge	37
Figure 9	Wet lay-up	38
Figure 10	CFRP NSM strips	38
Figure 11	Instrumentation plan (layout view)	50
Figure 12	Instrumentation plan (span 2 gauge locations – test setup 1)	51
Figure 13	Instrumentation plan (span 3 gauge locations – test setup 1)	52
Figure 14	Instrumentation plan (span 4 gauge locations –test setup 1)	53
Figure 15	Instrumentation plan (cross-section view, span 2 – test setup 1)	54
Figure 16	Instrumentation plan (cross-section view, span 3 – Test Setup 1)	55
Figure 17	Instrumentation plan (cross-section view, span 3 – test setup 1)	56
Figure 18	Instrumentation plan (span 2 – test setup 2)	57
Figure 19	Instrumentation plan (span 3 gauge locations – test setup 2)	58
Figure 20	Instrumentation plan (span 4 gauge locations – test setup 2)	59
Figure 21	Photograph showing strain and displacement instrumentation	60
Figure 22	Test truck footprint – single rear axle dump truck (Test 1)	60
Figure 23	Reproducibility and linearity of test results	64
Figure 24	Lateral load distribution (LVDT results)	64
Figure 25	Pier support details	65
Figure 26	Damaged beam bearing at Pier 4	65
Figure 27	Slight continuity between spans	66
Figure 28	Influence of cracks on strain	66
Figure 29	High-speed test results (measured impact)	67
Figure 30	Pre and post strengthening strain comparison – 3 locations on interior beam	67
Figure 31	Pre and post strengthening displacement comparison – interior beam	68
Figure 32	Pre and post strengthening displacement comparison – exterior beam	68
Figure 33	Finite element model of superstructure	69
Figure 34	Tee beam steel details	73
Figure 35	Long-term instrumentation plan – Span 2	78

Figure 36 Long-term instrumentation plan – Span 3	79
Figure 37 Long-term instrumentation plan – Span 4	80

INTRODUCTION

Literature Review

This chapter summarizes field applications, laboratory investigations, and analysis and design considerations.

Field Applications

Alkhrdaji, Nanni, Chen, and Barker published a report titled *Destructive and Nondestructive Testing of Bridge J857, Phelps County, Missouri; Volume I: Strengthening and Testing to Failure of Bridge Decks [1]*. This report summarizes an investigation regarding the feasibility and effectiveness of strengthening full-scale reinforced concrete bridge decks with carbon fiber reinforced polymers (CFRP). Through theoretical calculations and experimental research, two different CFRP strengthening schemes were selected to strengthen flat slab bridge systems. An actual bridge structure was then strengthened and destructively tested to further understand its behavior after strengthening. The research program included three main parts:

- Strengthening and static load testing to failure of three bridge decks.
- Dynamic testing of the bridge.
- Strengthening and destructive experiments on bridge piers.

The research summarized is concerned only with the first part. Bridge J857, located in Phelps County, Missouri, was the candidate bridge for strengthening and evaluation. The bridge was a three span simply supported skewed deck (15 degrees) made of reinforced concrete slabs. The research included:

- Investigation and recording of the existing bridge geometry and condition.
- The capacity of the bridge was calculated based on Missouri Department of Transportation (MoDOT) procedures and recommended material properties.
- Two different strengthening design schemes were developed for two of the three spans. One span was strengthened with near surface mounted (NSM) CFRP rods. For this system 7/16-inch (11-mm) diameter CFRP rods were placed into 3/4-inch (19-mm) deep by 9/16-inch (14-mm) wide grooves that were saw-cut in the field. The second span was strengthened with externally bonded CFRP fabric sheets. The third span served as a control span and was not strengthened.
- Static tests were then conducted in the field. The experiments included: strain and deflection measurements, concrete strength obtained from cores, and pull-off tests of the CFRP strips to measure bond quality.

- The experimental results from static testing to failure of the bridge decks were then analyzed.

The following conclusions were drawn:

- Using CFRP to strengthen concrete bridge decks did not obviously improve stiffness prior to yielding of the steel reinforcement.
- Application of CFRP strengthening for concrete bridges has the favorable characteristics of speed and ease of installation. However, installation can be deceptively simple and care must be taken, particularly in regard to surface preparation.
- Different failure characteristics were observed after strengthening with external bonded CFRP strips and near surface mounted CFRP rods.
- The stiffness of the strengthened spans was not significantly increased.
- Failure of the NSM span was by rupture of the CFRP rods. Failure of the span strengthened with CFRP fabric sheets was by a combination of rupture and debonding of the sheets.
- The strengthened spans exhibited ductility prior to failure. This was due to yielding of the steel prior to failure of the FRP systems.
- The application of the NSM rods required no surface preparation and therefore required much less time than the installation of the CFRP sheets.
- An increase in ultimate load capacity of approximately 23 and 33 percent was realized for the CFRP fabric sheet and CFRP near surface mounted systems, respectively.
- The non-strengthened span had significantly more capacity than was predicted through calculations. This was attributed to higher actual material properties, strain hardening, and some degree of end fixity.
- Long term durability of the systems included in the study should be investigated.

Hag-Elsafi, Kunin, Alampalli, and Conway published a FHWA report titled “Strengthening of Route 378 Bridge over Wynantskill Creek in New York using FRP Laminates” [2]. The objectives of this study were to evaluate effectiveness of an FRP strengthening system and investigate its influence on the bridge structural behavior, using results from load tests conducted before and after installation of the system. The bridge carries State Route 378 over the Wynantskill Creek in the city of South Troy, Rensselaer County, New York. This simple span, reinforced concrete, tee-beam structure was built with an integral deck in 1932. The bridge is 40 ft. (12.19 m) long, 120 ft (36.6 m) wide, and is supported by a total of 26 beams spaced at 4.5 ft (1.37 m) center to center.

The laminate system was the Replark system®, consisting of Replark 30® unidirectional carbon fibers and three types of Ephoterm, primer, putty, and resin, all manufactured by Mitsubishi Chemical Corporation of Japan. The system had a reported ultimate strength of 493,000 psi (3,400 Mpa) corresponding to a guaranteed ultimate strain of 0.015.

A primer was applied, followed by putty at the locations where the FRP laminates were to be installed. The primer was expected to penetrate the concrete surface, increase its strength and improve laminate bonding to the surface. An epoxy resin was applied to the surface, followed by placement of the laminates. Roller pressure was applied to impregnate the laminate in accordance with specifications and heaters were used to control curing temperatures.

Nine beams were instrumented to obtain transverse live-load distribution. For flexural evaluation, reinforcing steel and laminate strains were acquired at midspan. Three other locations on the center beam were also instrumented: near the support to investigate the effect of the strengthening system on shear, and at quarter and midspan to assess laminate bond to concrete and laminate stresses.

Two types of conventional strain gauges were used for measuring strains. Ten foil strain gauges were mounted on steel reinforcing and 13 were mounted on the concrete surfaces before the installation of the laminates. An additional 18 foil gauges were bonded to the surface of the laminates after installation. Four trucks with an average weight of approximately 44 kips (196 kN) were used in the load test.

Linear behavior of the bridge structure was investigated, for the before and after installation tests, using calculated moments and measured midspan strains. Relatively small scatter of the recorded data was observed about the best fit-lines. The results did not show a significant change in the stiffness after installation of the laminates.

Comparing the distribution factors from the before and after installation tests, it can be concluded that live load distribution improved by approximately 12 percent after the laminates were installed. A comparison between before and after installation stresses obtained from test data clearly shows that installation of the FRP laminates moderately reduced the stress in the reinforcing bars.

The bond between the concrete and FRP was better for the laminates located above the neutral axis. The weaker bond may be attributed to the level of precision in strain measurements and/or a lack of full bond development between the laminates and concrete at the time the test was conducted.

Shear stresses and forces were calculated using data from strain rosettes and applied truck loads. After comparing the before and after installation results, a slight increase in concrete shear stress was noted after the laminates were installed. However, the presence of the U-jacketed laminates is expected to provide confinement of web concrete and shear resisting interlock mechanism, hence improving its ultimate shear capacity. The comparison of the shear results obtained in the test with a classical analysis indicates good agreement between the experimental and analytical results and linear behavior was noted under both approaches.

Test results were analyzed and compared with those obtained using a classical analysis. The main conclusions were:

- Under service live load, after the laminates were installed, main rebar stresses were moderately reduced, concrete stresses (flexural and shear) moderately increased, and transverse live-load distribution to the beams slightly improved. Although the laminates participated in load carrying, compatibility of strains was not satisfied at some locations, and is attributed to the level of precision in strain measurements and/or a lack of full bond development at the time of the testing.
- Unintended fixity of the beam-ends was discovered, which substantially reduced anticipated live load moments.
- As expected, after the laminates were installed, the neutral axis migrated downwards.

It was noted that the benefits of the FRP laminate system may not be fully realized within the loading range used in the testing program. The maximum load applied during the testing program was not sufficient to induce nonlinear behavior. However, using bonded FRP laminates provided an opportunity for New York State Department of Transportation (NYSDOT) to demonstrate their use and investigate their feasibility as a cost-effective bridge rehabilitation technique. The project caused minimal traffic interruptions. Total cost of the rehabilitation was estimated at \$300,000, as compared to an estimated \$1.2 million for replacement of the structure.

Hag-Elsafi, Lund, and Alampalli published a FHWA report titled “Strengthening of Church Street Bridge Pier Capbeam Using Bonded FRP Composite Plates: Strengthening and Load Testing” [3]. A preliminary analysis of the East Church Street Bridge indicated possible cap beam deficiencies in both moment and shear capacities under current service loads. A decision was made to use bonded FRP materials to strengthen the cracked beams, demonstrate the materials use, and investigate their feasibility as a cost-effective technique for bridge rehabilitation. Two types of materials were considered: bonded-FRP laminates and pre-cured FRP plates. Design objectives were set, based on the preliminary analysis, to

increase the shear and moment capacities of the beam by about 10 and 20 percent, respectively. The bridge was constructed in 1954 and carries State Route 352 in the city of Elmira, New York. It is a four-span multi-stringer steel structure, with a total length approximately 220 ft (67 m). It has two 12 ft. (3.66 m) wide lanes.

Flexural and shear plates, made of carbon/glass hybrid and glass materials, were used for strengthening of one cap beam. The flexural plates were 0.5 in. (13-mm) thick, 10 in. (254-mm) wide and 17 ft. (5.18 m) long. The shear plates were 0.28 in. (7-mm) thick, 3.6 ft. (1.1 m) wide and 5.6 ft. (1.7 m) long. The modulus of elasticity of the hybrid flexure plate material [0, 0] was 10,000 ksi (69,000 Mpa) and its ultimate strain was 0.0005. The shear modulus for the [+45, -45] glass shear plates material was 1,000 ksi (6,900 Mpa) and its maximum shear strain was 0.0003.

The cap beam was pressure-washed with water to remove any loose materials that could lead to plate debonding. A proprietary epoxy mix, consisting of a resin and a hardener, was then applied to the plate or the concrete surface and anchor bolts were installed at predrilled locations to mechanically maintain tight contact between the plates and concrete surface. A load test was conducted 14 days after installation of the plates.

For the load test prior to installation, flexural strains were measured in the steel reinforcement bars and concrete in both positive and negative moment regions. Concrete strains, in a rosette setting, were also measured near the center pier at the beam mid-depth. For the load test following installation, flexural strains in the FRP plates in both positive and negative moment regions were measured. Four trucks with an average weight of approximately 44 kips (196 kN) were used for the load test.

The test results can be summarized as follows:

- The results demonstrated linear behavior during the testing and proved consistency of the test data. Comparing the before and after installation results for the negative moment region, it was concluded that the FRP plate system reduced service load stresses in the steel reinforcing bars by approximately 10 percent. For the positive moment region, it was concluded that the FRP plate system reduced service load stresses in the steel reinforcement bar by approximately six percent.
- The neutral axis moved slightly downward after the FRP plate system was installed.
- Concerning the bond between the FRP plates and concrete: Estimated strains were consistently higher (about 100 percent) than those measured. This discrepancy may be attributed to sensitivity of computed FRP strains to the noise in the measured steel and concrete strains and/or improper bonding of the FRP plate to the cap beam

concrete.

- Concerning the shear investigation, when comparing the before and after installation concrete shear strain results, it was concluded that installation of the FRP plates reduced shear strains by approximately 10 percent.

The test results indicated that the system moderately reduced live load stresses in the steel reinforcement bars in the negative and positive moment regions by approximately 10 and six percent, respectively. The location of the neutral axis in the positive moment region shifted downwards, as expected, after strengthening. Analysis of shear strain data showed that concrete shear strain at the critical section near the center pier was reduced by approximately 10 percent.

This project provided an opportunity for the NYSDOT to demonstrate the feasibility of using FRP materials as a cost-effective bridge retrofit technique. Compared to conventional repair methods, the retrofit system used proved to be a cost-effective solution (\$18,000 versus \$150,000). The system was reported to be relatively easy to install and to cause minimal interruption to traffic, always important features, particularly for applications in highly populated areas.

Hag-Elsafi, Kunin, and Alampalli published a FHWA report titled “In-Service Evaluation of a Concrete Bridge FRP Strengthening System,” [4]. Due to concerns regarding section loss of reinforcing steel to corrosion and overall safety, a bridge was selected for strengthening with FRP laminates in 1999. The bridge was built in 1932 and carries Route 378 over the Wynantskill Creek in the city of South Troy, NY. It is a 40 ft. (12.19 m) long, 120 ft. (36.58 m) wide reinforced concrete structure, consisting of 26 simply supported T-beams, spaced at 4.5 ft (1.37 m) on centers, with an integral concrete deck. The main reinforcement consists of 8, 1¼ x 1¼ in.² (32 x 32 mm²) square steel bars.

The purpose of the strengthening was to improve flexural and shear capacities, and to contain observed freeze-thaw cracking in the bridge beams. The bridge was instrumented and load tested before and after installation of the FRP laminates, to evaluate effectiveness of the strengthening system.

The Replark® laminate system was used in the bridge retrofit design. The system consisted of Replark 30® unidirectional carbon fibers and three types of Ephoterm materials (primer, putty, and resin) all manufactured by Mitsubishi Chemical Corporation of Japan.

The ultimate strength of the laminate system was reported as 493 ksi (3,400 MPa), corresponding to a guaranteed ultimate tensile strain of 0.015.

Nine beams were instrumented to provide information on transverse load distribution on the bridge. General purpose 350-ohm self-temperature-compensating constantan foil strain gauges with large measuring grids were bonded using an epoxy resin. The bridge was load tested in 1999 and again in 2001. The average weight of each of the load trucks was approximately 44 kips (196 kN).

The following summarizes the load test results:

- Strain compatibility can be used to assess the bond between the FRP laminates and concrete by observing laminate and concrete strains at similar locations on the structure. After comparing the results for the 2001 and 1999 tests, it was concluded that the quality of the bond, at the instrumented locations, had not deteriorated during the two years in service. Thermographic imaging using an infrared (IR) camera did not show significant debonding in the system laminates.
- After comparing the respective factors for the two test years, it was concluded that the manner in which load on the bridge was distributed had not changed, implying that the retrofit system had not deteriorated between the two test years.

The 2001 load test indicated that recorded strains were generally lower than those measured during the 1999 test. The results also indicated that the quality of the bond between the FRP laminates and concrete and effectiveness of the retrofit system had not changed after two years in service. Thermographic imaging provided images supporting this conclusion on bond quality.

Laboratory Investigations

Brena published a dissertation titled “Strengthening Reinforced Concrete Bridges Using Carbon Fiber Reinforced Polymer Composites” at the University of Texas at Austin, Department of Civil Engineering [5]. The dissertation summarized is related to the following TXDOT reports:

- Brena, Bramblett, Benouaich, Wood, and Kreger (2001) - *Use of Carbon Fiber Reinforced Polymer Composites to Increase the Flexural Capacity of Reinforced Concrete Beams* - Report FHWA-TX-0-1776-1
- Brena, Wood, and Kreger (2001) - *Increasing the Flexural Capacity of Typical Reinforced Concrete Bridges in Texas Using Carbon Fiber Reinforced Polymers* - Report FHWA-TX-0-1776-2

The objectives of this research were to evaluate the behavior of pan-joist and flat-slab bridges after strengthening with CFRP and to develop a reliable design guideline for the implementation of these materials in existing bridges.

The research was performed in three different phases. In Phase One, 22 rectangular beams were tested to investigate the effect of CFRP composites on the flexural strength of reinforced concrete elements, to determine the bond length required to develop the rupture stress of the composites before the CFRP debonded from the concrete surface and to develop strengthening schemes to produce repeatable response of the specimens. In Phase Two, eight rectangular beams were subjected to cyclic fatigue using different load amplitude to take into account the effect of fatigue on the response of the beams. In Phase Three, four full-scale laboratory specimens representative of reinforced concrete bridges were constructed and tested.

Phase One. The main variables evaluated in this phase were the effects of a) CFRP composites on the flexural strength of reinforced concrete elements, b) external anchorage using composites straps, and c) long term wetting and drying cycles. All beams were simply supported and subjected to four point bending.

Four strengthening configurations were applied in this phase. Two configurations had the CFRP composites attached to the bottom of the beam, with and without transverse straps along the bonded length. The other two configurations had the CFRP bonded to the sides of the beam, also with and without transverse straps. The tests indicated that debonding was delayed by the addition of transverse straps along the span of the specimens.

Two beams were tested statically to failure after being exposed to cycles of wet and dry conditions. A sustained load equal to 20 percent of the yield load was also applied to one of the beams. The results of these tests indicated that the bond between the CFRP and the concrete was not affected by exposure to moisture or sustained load.

As a result of this phase, a conservative value of the CFRP strain was obtained to design of the strengthening schemes in Phase Three. The maximum strain that could be reliably developed in the CFRP composites was assumed to be 0.007.

Phase Two. Eight rectangular beams were subjected to fatigue loading using different load amplitudes. The experimental setup was identical to the one used in Phase One but the load was controlled using a close-loop system. The load was applied cyclically from approximately zero to the load that generated the desired stress in the steel reinforcement.

The load amplitude was selected initially to represent service-load conditions in an existing bridge. Therefore, four beams were subjected to repeated loads that generated stresses equal to 30 or 50 percent of the yield stress on the longitudinal steel reinforcement. The beams were subjected to either 10,000 or 1,000,000 cycles of load and then tested statically to failure. Results from these tests indicated that the bond between the composites and the surface of the concrete did not deteriorate with service-level fatigue loading. Subsequently, the remaining beams were subjected to higher stress ranges to cause fatigue failure either between the composite and surface of the concrete or in the reinforcing steel. Results from these tests indicated that fatigue failures were only generated after cycling to very high stress ranges.

Phase Three. Four full-scale laboratory specimens, two pan-joint and two flat slab geometries, representative of reinforced concrete bridges were constructed and tested in this Phase. As a part of this phase, an analytical model was developed to calculate the moment-curvature and load-deflection response of reinforced concrete members strengthened using CFRP composites. This analytical model is described later.

Two identical full-scale pan-joint bridge specimens were constructed and tested to compare the behavior of the system after strengthening with CFRP pre-cured plates or CFRP fabric. Each test specimen consisted of two interior joists. Concrete diaphragms were cast at each end of the specimen to replicate field conditions. The specified yield stress for all reinforcing steel used was 60 ksi (414 MPa), and the design 28-day compressive strength was 3,500 psi (24.1 MPa).

Two laboratory specimens were tested to compare the behavior of slabs strengthened with CFRP pre-cured plates or CFRP fabric. The specimens represent a six-ft wide section of the slab in a prototype bridge. Only the slab was modeled in the laboratory to study the behavior of the strengthened specimens without the contribution from the structural curbs. Reinforcement consisted of two mats of uniformly spaced reinforcement.

Three types of instruments were used in the tests: linear potentiometers, strain gauges, and load cells. Linear potentiometers were used to monitor global specimen response. Strains were monitored on the steel reinforcement, concrete surface and CFRP composites.

The following conclusions were drawn:

- The CFRP composites had little influence on the response of the specimens up to the yield load. A marginal increase in stiffness was observed after strengthening under low load levels; the yield load of the reinforced concrete elements, however, was not

increased significantly.

- The stiffness of the specimens after yielding was much higher than the stiffness expected of a bare reinforced concrete element. The measured strength exceeded the nominal capacity calculated during design of the test specimens.
- Examination of the load-deflection response during the tests demonstrated CFRP composites are effective in increasing the flexural strength of existing reinforced concrete elements.
- The maximum strength of the specimens was always controlled by CFRP debonding from the concrete surface.
- Placement of the longitudinal CFRP pre-cured plates on the sides of the cross section, rather than on the bottom, reduced the tendency of the CFRP pre-cured plates to pry off the surface of the concrete at locations where the laminates crossed existing cracks.
- All specimens exhibited significant inelastic behavior before the CFRP composites debonded from the surface of the concrete.
- Fatigue loading, sustained service-level loads, and exposure to wetting and drying cycles did not affect the behavior of the strengthened elements.

Kachlakev and McCurry published a FHWA report titled *Testing of Full-Size Reinforced Concrete Beams Strengthened with FRP Composites: Experimental Results and Design Methods Verification*, [6]. This report describes the full-scale testing performed to simulate FRP-strengthening performed on portions of the Horsetail Creek Bridge in Oregon. The existing reinforced concrete bridge beams were constructed without shear reinforcement; load rating calculations revealed that the structure had rating factors of 0.50 and 0.06 for flexural and shear stresses, respectively.

Four reinforced concrete beam specimens spanning 18 feet (5.5 m) were prepared with dimensions and steel reinforcement configurations similar to the existing bridge beams. Three of the four beam specimens were strengthened with FRP.

- One test beam was fitted with carbon fiber flexural FRP reinforcement.
- Another beam was strengthened in shear with a glass fiber U-wrap FRP application.
- The third test beam received both; flexural and shear FRP strengthening.
- The fourth beam served as the control specimen and was not strengthened with FRP.

The four test beams were subjected to third point bending tests to failure in accordance with ASTM C78.

The results of the program indicated that the test beams fitted with FRP for only flexural or shear reinforcement experienced an increase in load of 45 percent over the unstrengthened control specimen, though failing in different modes. The test beam strengthened in both flexure and shear with FRP was found to exceed the strength of the control specimen by at least 50 percent in shear and 99 percent in flexure. Limitations associated with the testing equipment prevented this test beam from being loaded to failure. The post-cracking stiffness of the FRP strengthened test beams exceeded the control specimen by 30 percent. The use of the FRP strengthening for shear, flexure, or both shear and flexure resulted in greater beam deflections at failure than those associated with the unstrengthened control specimen.

Kachlakev, Yim, Miller, and Seamanontaprianya published a FHWA report titled "Behavior of FRP Composite-Strengthened Beams Under Static and Cyclic Loading," which discusses the testing that was performed on 38 small-scale concrete beam specimens measuring 6 x 6 x 20.9 in. (150 x 150 x 530-mm) [7]. Eight combinations of FRP reinforcing utilizing high and low modulus epoxy resins and one or two layers of glass or carbon fiber materials were applied to 24 concrete beam specimens. These beams, along with three plain concrete control specimens, were subjected to third point bending tests to failure in accordance with ASTM C78. The remaining 11 specimens were tested in fatigue in a third point bending configuration at 0.5 Hz with the loads applied as varying percentages of the ultimate static load. The minimum load for the fatigue testing was 151 pounds (0.67 kN) for all specimens. Five of the fatigue tested beams were strengthened with a low-modulus resin and one layer of glass fiber, five were strengthened with a high-modulus resin and two layers of carbon fiber, and one beam was a plain concrete control specimen.

The results from the testing performed indicate that in a wet lay-up application, increasing the modulus of the resin may increase the flexural capacity of FRP strengthened beams. However, the research revealed that this effect diminished for failure modes other than flexural bending. Due to the fact that fatigue performance is dependent upon the ultimate capacity of the member, the modulus of the resin may improve the fatigue performance of FRP strengthened beams. Further testing with full-sized beams was recommended to investigate the relationship between resin modulus and member performance.

Shahrooz, Boy, and Baseheart published a paper in the ACI Structural Journal titled "Flexural Strengthening of Four 76-Year-Old T-Beams with Various Fiber-Reinforced Polymer Systems: Testing and Analysis," [8]. This paper describes the strengthening of four 76-year-old T-beams that were removed from two bridges. Four different strengthening systems were investigated. Theoretical analysis and experimental study of the T-beams was

conducted, with the goal of developing simple but effective design methods for cases where current ACI design guidelines were unavailable.

Four concrete T-beams were removed from bridges that were constructed in 1924. The T-beams were 32.8 ft. (10 m) long. All of the beams were subjected to essentially the same traffic load and environmental conditions. Mechanical tests were conducted on reinforcing bars obtained from similar beams to obtain mechanical properties. The concrete compressive strength was measured by rebound hammer.

The four T-beams were retrofitted with four different strengthening methods as described below:

- T-beam 1: This beam was retrofitted with four 0.37 in. (9.5-mm) external CFRP post-tensioning rods, two on each side of the web. The anchorage systems were 13.4 ft. (4.1 m) and 15.1 ft. (4.6 m) from the centerline of the beam. Each rod was post-tensioned to 13 kips (57.8 KN), which corresponded to 45 percent of the nominal ultimate capacity of the rods.
- T-beam 2: Two 3 in. (76.2-mm) wide \times 0.053 in. (1.34-mm) thick unidirectional CFRP plates were bond to the bottom face of the web. Due to miscalculations, one plate was bonded from face to face of the supports. The other plate was terminated 8.5 in. (216-mm) away from the face of one support and extended 8.5 in. (216-mm) beyond the face of the other support.
- T-beam 3: Two 12 in. (305-mm) wide layers of unidirectional carbon fabric were bonded to the soffit of the web. The fabric was bonded from face to face of the supports. The web and bottom face of the flange were also wrapped with two U-shaped layers of carbon fabrics along the entire clear span as shear reinforcement.
- T-beam 4: Two 4 in. (102-mm) wide \times 0.19 in. (4.8-mm) thick plates were bonded to the soffit of the web and anchored at each end with 3 in. (76.2-mm) long A325 anchors. Anchor bolts were also used along the entire plate to prevent failure by debonding.
- The test methodology and instrumentation were as follows:
 - Prior to retrofitting, each beam was loaded to 50 percent of the yield strain in the bottom longitudinal reinforcing bars at midspan.
 - Each beam was unloaded and retrofitted with the different FRP systems mentioned above.
 - Each retrofitted beam was then loaded to produce large displacements and

extensive damage.

- Load-deflection relationships were obtained at the quarter points and midspan.
- Strain was monitored in the lowest longitudinal bars at midspan.
 - The strain profile through the depth was also obtained at midspan.
 - The concrete surface strain on the web soffit was obtained at the quarter points
 - Strains in the FRP material at midspan and quarter points were obtained for beams 2, 3, and 4.
 - The load-deflection behavior, stiffness characteristics, failure mode, and strain distribution between the bonded FRP plates or fabrics and the substrate was investigated and used to draw conclusions regarding the behavior of each retrofitted T-beam.
 - T-beam 1: After release of the jacking force, the measured force in the rod was 11.6 kips (51.7 kN), which was a 10.5% loss when compared with the theoretical post-tensioning force of 13 kips (57.8 kN). The experimental data showed that external post-tensioning increased the initial stiffness of the beam by approximately 9 percent and the ultimate capacity by 14 percent. Theoretical analyses were conducted which indicated that if the post-tensioning force were increased to 75 percent of ultimate capacity and a lower position used for the post-tensioning bars, the beam capacity could then be increased by 22 percent.
 - T-beam 2: The stiffness and ultimate capacity of the retrofitted beam were increased by 9 percent and 10 percent, respectively, due to the addition of the CFRP plates.
 - T-beam 3: The stiffness of beam after retrofit with 2 layers of longitudinal and transverse carbon fabrics was much higher than that achieved in beam 2. T-beam 3 also exhibited better ductility.
 - T-beam 4: The flexural stiffness inferred from experiment was twice the computed value. The mechanical anchorage at the ends of the FRP plates prevented complete debonding between the plates and concrete. The CFRP plates were found to be effective despite some parts debonding.

The retrofit system used in beams 1 and 4 was the most effective in increasing the capacity of the beams. After retrofitting, the ultimate capacity in beams 1, 2, 3, and 4 were enhanced by 14.2, 9.9, 9.2, and 17.5 percent, respectively. This was due to the use of mechanical anchorage in these beams. Compared with other retrofit systems, T-beam 3 was found to

prevent major spalling and damage of concrete more efficiently than the other systems. The following conclusions were drawn:

- Current ACI design guidelines are suitable for predicting ultimate capacity of retrofitted old concrete beams.
- If adequate methods can be used to prevent anchorage failure, the retrofit in T-beams 1 and 4 would be the most desirable.
- The retrofit system used for T-beam 3 exhibited better ductility than the other systems.
- Simple analytical models can provide effective methods for current ACI design guidelines which do not have specific recommendations for particular retrofitting systems.

Analysis and Design Considerations

In her dissertation titled “Strengthening Reinforced Concrete Bridges Using Carbon Fiber Reinforced Polymer Composites,” Brena developed an analytical model and compared the results obtained from this model with the test results obtained from the experimental investigation described earlier in this literature review [5]. The following assumptions were used in the initial analytical model:

- Strains increase proportionally with distance from the neutral axis.
- No slip occurs between the steel reinforcement and concrete surrounding it.
- Perfect bond exists between the CFRP material and concrete surface.
- Failure is reached when the extreme fiber in compression reaches the maximum usable concrete strain.

The third assumption was refined in later models because the CFRP material was observed to slip relative to the concrete surface during the experimental phase of the project. Similar to most analytical models for calculating flexural response of reinforced concrete elements, the cross section was divided into horizontal slices and the total response of the section was obtained by adding the contribution of each slice.

- *Concrete:* The uniaxial stress-strain behavior of concrete in compression was modeled using the curve proposed by Hognestad [9, 10]. Concrete in tension was assumed to behave linearly up to the stress corresponding to its tensile capacity, and after this point, the tensile strength was assumed to be equal to zero.
- *Reinforcing Steel:* The stress-strain relationship for steel reinforcement with a well-defined yield point was idealized using three linear segments. The initial elastic modulus was 29,000 ksi. After yielding the slope of the curve was equal to zero until

the strain corresponding to initiation of strain hardening was reached. Reinforcement steel that did not exhibit a well-defined yield point was approximated using the model proposed by Menegotto and Pinto [11].

- *Fiber reinforced polymer composites:* The uniaxial behavior of the CFRP was assumed to be linear to failure. The properties published by the manufacturers were used to define the material models for the different CFRP composites.
- *Load-deflection response:* Deflections were calculated using the moment-area method because this method is applicable to members that have a non-linear curvature relationship.

Evaluation of previous experimental work indicated that the maximum measured strains developed in the CFRP composites varied significantly. This strain was dependent on the ability of the CFRP to deform without debonding from the surface of the concrete. The limiting CFRP strain value selected for the design of the large-scale specimens was 0.007.

Recommended design procedures were developed based on the analytical model and the results of the laboratory tests of strengthened full-scale bridge components as follows:

Nominal Flexural Capacity of Strengthened Sections. In order to calculate the flexural capacity of the elements, it was necessary to anticipate the failure mode that governs the flexural behavior of the section. The failure mode for strengthened reinforced concrete elements depends on the characteristics of the bare reinforced concrete section and the amount of CFRP composite used to strengthen the element. For the elements in this research project, failure was always governed by debonding of the CFRP from the concrete surface. Debonding occurred after the yielding of the reinforcing bars and before concrete crushing in the extreme compression fiber.

Strain Distribution. Because bridge elements are typically subjected to dead-load moments before CFRP composites are applied to the surface of the concrete, the existing dead-load strain distribution must be determined before the capacity of the strengthened sections can be calculated. Cracked section properties should be used in calculations because of the likelihood the section has been cracked due to the application of service live loads during its lifetime.

Preliminary Estimate of the Area of CFRP Composite. The area of CFRP composite can be calculated for preliminary design based on an assumed distribution of compressive stresses in the concrete. The use of the equivalent rectangular stress block commonly applied for the design of reinforced concrete flexural members was not generally applicable because the failure mode was typically debonding of the CFRP from the surface of the concrete. The initial estimate of the required area of CFRP was calculated by solving the equations of equilibrium of horizontal forces and moments simultaneously.

Maximum Recommended Area of CFRP Composite. A criterion was established to calculate the maximum area of CFRP similar to the limit set on the maximum area of reinforcing steel in the design of reinforced concrete members. The maximum recommended area was calculated from horizontal force equilibrium, assuming that the commonly used rectangular stress block could be used to represent the distribution of compressive stresses.

Anchoring Straps. The longitudinal CFRP composites were restrained from debonding by CFRP straps positioned at spacing equal to $h/2$ along the length of the beam. The straps were provided where debonding was expected to start and this was always near the section of maximum moment. Strap spacing was based on the assumption that diagonal cracks would be oriented 45° from horizontal and that these cracks would trigger local debonding of the CFRP composite.

Length of the CFRP Composites. It was recommended that the CFRP composites be extended at least a distance equal to the height of the member (h) from the theoretical cut-off point. For short span bridges, it was recommended that the CFRP composite be applied throughout the entire span.

Kachlakev, Miller, Yim, Chanasat, and Potisuk published a FHWA report titled “Finite Element Modeling of Reinforced Concrete Structures Strengthened with FRP Laminates,” [12]. The objective of the study discussed in this report was to establish a methodology for utilizing structural modeling software for the analysis of reinforced concrete elements strengthened with FRP materials. Four concrete test beams of similar dimensions and configuration to beams strengthened with FRP on the Horsetail Creek Bridge were fabricated and tested. One beam was provided with glass fiber shear strengthening, one with carbon fiber flexural strengthening, one with both shear and flexural strengthening, and the remaining beam served as an unstrengthened control specimen. Third point bending tests to failure were performed in accordance with ASTM C78. Finite element models of the test beams were prepared and loaded in similar fashion to the test specimens and the results were compared.

Utilizing a non-linear smeared cracking approach, the ANSYS finite element program (1998) was used to simulate the behavior of the four test beams. The behavior of the finite element models showed reasonable agreement with the test beams in regard to load-deflection plots, load-strain plots, load carrying capacity of the shear and flexure strengthened test beam, and crack pattern prediction. The finite element models indicated higher stiffness than the test beams in both the linear and non-linear range and the predicted ultimate loads were found to be five to 24 percent lower than the results obtained from the testing.

Some of the recommendations concerning the use of finite element analysis for FRP strengthened reinforced concrete beams included:

- Models should be simplified in order to avoid discontinuities and reduce model size and difficulty.
- Non-linear analysis should be used after cracking develops in the concrete.
- To realistically simulate cracking, the size of the concrete elements in the finite element model should be no more than two to three times the maximum aggregate size.
- In non-linear analysis, tolerances in convergence criteria should be defined carefully. It may be necessary to relax force and moment criteria to avoid divergence.
- Shear transfer coefficients must be assumed in non-linear analysis. For closed cracks, the assumed value should be 1.0; for open cracks, values of 0.05 to 0.50 should be utilized. In this experiment, values less than 0.20 were tried but caused divergence problems.
- Beam symmetry should be used to reduce model size.
- Steel plates should be added to models at supports to provide better simulation of actual conditions and to avoid stress concentrations.
- In non-linear analyses, applied loads should be increased in small increments to isolate changes in the behavior of the reinforced concrete element and to improve convergence of solutions.

Swenson and Barnes published an interim report titled “Design Procedure for FRP Strengthening of War Memorial Bridge,” [13]. This report was prepared for the Alabama Department of Transportation and dealt with the War Memorial Bridge located in Macon County, Alabama, on Alabama Highway 81. The bridge is constructed of reinforced concrete and was completed in 1945. The continuous portion of the bridge is three spans long and symmetric about the center of the middle span. The end spans are 48 ft. (14.6 m) long and the middle span is 65 ft. (19.8 m) long. Spans are measured relative to the girder

ends. Each span consists of four reinforced concrete girders cast monolithically with a reinforced concrete slab. The depth of the girders varies from minimum of 30.5 in. (775-mm) to a maximum of 71 in. (1.8 m) over the interior supports. The cross section of the bridge is symmetrical about its centerline. Girders are at 88 in. (2.24 m) spacing, measured center-to-center on the girder webs.

The effects of factored loading were calculated on interior and exterior girders in the continuous region of the structure and strength demand curves were developed. The design shear and moment capacities of both interior and exterior girders were determined and compared to the strength demand curves. Maximum factored loads on the girders were obtained at distinct locations in the three-span continuous region of the structure.

The positive moment capacity of both interior and exterior girders was not sufficient in portions of all three spans. Negative moment and shear capacities of the girders were found to be sufficient for all spans. Regions where the moment-demand exceeded the design moment capacity required strengthening. Critical locations were chosen within the deficient regions and were used in the internal FRP design process. The cross section at each location was used to determine the amount of FRP needed for adequate flexural strengthening.

Preliminary calculations showed that the addition of external FRP composites to the girder soffits would increase the cracked-section moment of inertia by four to five percent. A result of the increased cracked-section moment of inertia of the strengthened portion of the structure would be. Given that the increase in stiffness of the strengthened portion of the structure would be limited to approximately five percent, the investigators estimated that the resulting increase in positive moment would be less than two percent. This slight increase was considered when selecting the quantity and extent of the FRP reinforcement.

The flexural design of the FRP strengthened girders was completed using multiple variations of two distinct design procedures. The first design was done according to the recommendations in chapter nine of the ACI committee 440 draft report, *Guide for the Design and Construction of Externally Bonded FRP Systems for Strengthening Concrete Structures* [14]. The second design was performed with a computer spreadsheet that used a nonlinear stress-strain relationship for the compressive stress in the concrete.

ACI Committee 440 Flexural Design. This method was based on ultimate strength design. Force equilibrium, strain compatibility, and the constitutive material relationship of concrete, steel, and FRP were used to derive the equations needed to calculate the nominal amount of external FRP needed for flexural strengthening. The following assumptions must be true in order for the design to be valid:

- All calculations are based on actual member dimensions, locations of reinforcing steel, and material properties of the existing member.
- Strains in the reinforcing steel and concrete are directly proportional to their distance from the neutral axis.
- The maximum compression strain in the concrete is 0.003.
- Any tensile stresses in the concrete are neglected in design.
- The FRP composite behaves in a linear elastic manner until failure.
- Steel is linear elastic prior to yield and perfectly plastic thereafter.
- Perfect bond exists between the steel reinforcement and the concrete and between the concrete and the external FRP composite.
- The compressive stresses in the concrete at failure may be effectively represented by a rectangular stress distribution.

A discontinuity in the strain profile exists at the bottom concrete fiber. The difference is a result of dead loads present on the member when the FRP is applied. Once the FRP has been applied, strain compatibility between the FRP and the rest of the reinforced concrete is assumed.

ACI Committee 440 Design, Variation I. Calculation of the nominal amount of FRP needed for strengthening of the reinforced concrete girder was done with the aid of a simple computer spreadsheet. Given material properties and cross section geometry are used to calculate strains, stresses, and forces. Some changes were made to the equations given in the ACI so that compression steel reinforcement could be included.

ACI Committee 440 Design, Variation II. As in the first variation of the design procedure, all calculations were done by a computer spreadsheet. Only the characterization of the compressive stress in the concrete was changed in this variation. The compressive stresses were modeled as linear elastic. The resulting triangular stress distribution should produce more conservative estimates of the moment capacity of FRP strengthened RC members.

Computer Spreadsheet Design. The second method used to design the FRP strengthened bridge girders used a non-linear stress-strain relationship for the concrete in the member cross section. The computer spreadsheet design was used to accomplish two main goals:

- Determine the most efficient amount of external FRP composite required for adequate strengthening of the bridge girders.
- Check the validity of the design method proposed in the ACI committee 440-Draft report.

Some serviceability concerns related to the strengthening of RC members with external FRP composites were also examined with the use of the computer spread sheet design.

Primary Design of FRP Strengthened RC Member. For this method, a nonlinear stress-strain function for the behavior of the concrete developed by Collins and Mitchell was used [15]. The use of the nonlinear stress-strain function resulted in more accurate calculations of moment capacity and better representation of the moment-curvature behavior of the design cross sections. Force equilibrium, strain compatibility, and constitutive material relationships had to be satisfied for the design to be valid. The following assumptions were made about the cross section and its behavior:

- All calculations based on actual member dimensions, locations of reinforcing steel, and material properties of the existing member.
- Strains in the reinforcing steel and concrete directly proportional to their distance from the neutral axis.
- The maximum compression strain in the concrete is 0.003.
- The FRP composite behaves in linear elastic manner until failure.
- Steel is linear elastic until it yields and perfectly plastic thereafter.
- Perfect bond exists between the steel reinforcement and the concrete and between the concrete and the external FRP composite.
- The nonlinear behavior of concrete, as modeled by a function from Collins and Mitchell, is used in the calculation of the moment capacity [15].

The spreadsheet divides the member cross-section into distinct elements, each element defined by its material properties and position in the cross section.

Secondary Design of FRP Strengthened RC Member. The secondary computer spreadsheet design method uses alternative criteria for limiting the strain in the FRP composite. Other ideas used for design as proposed in ACI, such as the environmental

reduction and bond-dependent coefficient, were incorporated in the calculation of the moment capacity of the section.

Additional Design Requirements. Once the cross-sectional area of FRP had been selected, it became necessary to determine how far the FRP composite would be extended from the critical design sections. ACI 318-99 states that internal reinforcing bars that are terminated in a positive moment region must extend a distance equal to the effective depth of the member and past where they are needed for flexural strength. Using this design guideline, the external FRP composite plates were extended a distance equal to the depth of the beam beyond the points at which they were needed for flexural resistance.

In order to be sure that the design length of the FRP composites was acceptable for anchorage of the plates, a check on the stresses in the FRP composite plate was performed. The procedure by Tedesco and El-Mihilmy was used to determine the shear peeling stresses in the FRP composite under service level loading [16].

The two composites considered were the Tyfo UC composite manufactured by Fyfe Co. and the Fibercote composite. The choice of these composite materials was based on their material properties, the results of initial flexural designs, and economic issues.

ACI Committee 440 Design Method. The strengthening systems used for each type of composite depended on the geometry and material properties of the FRP composite and the geometry of the bridge girder. For the Tyfo UC composite, a constant thickness of 0.055 inches (1.4-mm) was used while the width of the composite sheet was varied. Design of the Fibercote composite was done by varying both the width and the thickness. The nominal moment capacity calculated by Variation I of the ACI committee 440 was 1.8 to 2.3 percent larger than that calculated by Variation II.

An examination of the results from variation II of the design revealed that the Fibercote composite was unable to provide adequate flexural strengthening for all design cross sections. Results from design variations showed that the Fibercote composite was capable of strengthening the exterior girder only if a 14 in. (356-mm) wide, 0.05 in. (1.27-mm) thick plate was used. This plate has nearly the same thickness as the Tyfo UC composite plate, but is almost 50 percent wider.

The Fibercote FRP composite material was used in the computer spreadsheet design to determine if a more refined model of the behavior of the strengthened cross section would produce different results. After the results were assessed, the Fibercote material was eliminated as a strengthening option.

Computer Spreadsheet Design. The 10 in. (254-mm) wide Tyfo UC composite plate provided an adequate amount of flexural strengthening at all three critical sections. All

designs provided developed adequate ductility prior to failure of the cross section. The results of the computer spreadsheet design revealed that an eight in. (203-mm) wide plate would provide adequate flexural strength and ductility at the critical sections used for design; this held true when moment redistribution in the strengthened girders was considered.

Serviceability Design. Analysis of the bridge girders prior to strengthening revealed that the stress in the primary tensile reinforcement was nearly 86 percent of the yield stress under service level loading. Current recommendations stated that the stress in steel reinforcement should be less than 80 percent of the steel yield stress under service level loads. In order to examine the stresses in the primary reinforcing steel, the amount of Tyfo UC composite material used to strengthen the exterior girder was varied.

Comparison of Design Procedures. Results from the ACI Committee 440 design procedure were slightly non-conservative when compared to the results from the computer spreadsheet design. The ACI Committee procedure overestimated the calculated moment capacity of the strengthened girders by one to two percent on average.

The moment capacities of the cross sections calculated by the ACI committee 440-design procedure (variation II) were conservative when compared to computer spreadsheet design results. Moment capacities calculated by variation II of the ACI committee were up to one percent smaller than those calculated by the computer spreadsheet. Using a linear distribution of compressive stresses in the concrete at failure will result in a conservative estimation of the amount of external FRP required for flexural strengthening. Comparison to a design that incorporates the nonlinear behavior of concrete may be done to ensure the design is not overly conservative.

From the results obtained from the flexural design of the FRP strengthened bridge girders, some conclusions were drawn on the accuracy of the design methods used. The flexural design procedure recommended by ACI Committee 440 produced non-conservative designs. Calculated moment capacities were up to two percent larger than those calculated by the computer spreadsheet program.

An alternative design procedure that modeled the compressive stresses in the concrete at failure with a linear distribution was developed. This design procedure produced conservative results for all design cross sections considered. Use of the alternative model of the compressive concrete stresses requires some minor changes to be made to the equations given in chapter nine of the ACI Committee 440 draft report [14]. The use of this procedure may also result in a design that is overly conservative.

In order for the most efficient design of the strengthened member to be made, the stress in the concrete at failure should be modeled as accurately as possible. The computer spreadsheet design accounted for the non-linear stress-strain behavior of concrete under compressive loading. This design gave the most precise results for the FRP strengthened RC members. The moment capacities calculated with this design were about one percent larger than those calculated using a linear distribution of concrete stress. The use of a flexural design procedure that accounts for the non-linear behavior of concrete was recommended for the design of FRP-strengthened reinforced concrete members.

Strengthening of reinforced concrete with epoxy bonded steel plates has been conducted for some time [17]. Due to corrosion of the steel, research was begun into the use of bonded FRP materials as early as 1978 in Germany [18]. Research in Switzerland led to the early applications of FRP strengthening for bridges in 1987 [19, 20]. Research in the United States began in the 1980's and is ongoing. Many states have investigated the use of FRP strengthening of bridges on a limited basis, including the following: Alabama, Texas, Oregon, California, and New York. Missouri has conducted significant field research and is currently undertaking the strengthening of many deficient bridges. Several strengthening projects have included field monitoring.

While a good deal of experimental work has been conducted in the field of FRP strengthening, questions remain about the durability in actual field applications and the cost-effectiveness of different approaches.

A thorough review of literature related to FRP strengthening was carried out to better understand the behavior of FRP strengthened structures. A discussion on the analytical modeling and design consideration is included in the report. A summary of laboratory investigations is presented to highlight the effectiveness of different strengthening schemes in a controlled environment. The subject bridge is located in Zachary, Louisiana, and carries Highway 19 over White Bayou. The primary objective of this research project was to evaluate the feasibility of using CFRP strengthening to increase the live load capacity of existing bridges in Louisiana. Currently, there are many load-rated bridges, and often these bridges are reinforced concrete tee beam bridges that are deficient in flexure. This project is intended as a demonstration of how CFRP materials can be applied in an actual field environment; for that reason, an experienced contractor (Structural Preservation Systems) was employed to install the strengthening systems. While the installed cost of the strengthening system is discussed, however, much of the installation cost is associated with mobilization. Therefore, the costs associated with a minor strengthening effort such as the one undertaken here will not be entirely representative of more significant strengthening

applications. However, the installation is useful from the standpoint of understanding what calculations can be used for the prediction of ultimate capacity, the limitations of those calculation procedures, and complicating factors that are likely to be encountered in field installations.

To better understand the behavior of the bridge both before and after strengthening, Bridge Diagnostics, Inc. (BDI) was contracted to test and evaluate portions of the structure. This procedure was also important to understand the limitations of live load testing as it relates to CFRP strengthened bridges. In addition to the significant live load testing efforts, a long-term monitoring system was installed and the details of that system are described. The closure of the engineering programs at Tulane University and the loss of faculty engaged in this project did not permit the long-term monitoring or data collection after all the tasks planned during the project funding period were concluded.

OBJECTIVES

The objectives of this study are as follows:

- Summarize selected literature that is related to the field implementation of FRP strengthening systems for reinforced concrete bridges.
- Based on the summarized literature and the experience of the investigators, select and describe three different strengthening systems that are appropriate for field implementation on a selected bridge.
- Describe the strengthening systems and related calculation procedures.
- Summarize the results of the live load tests.
- Describe the long-term monitoring system.

SCOPE

The scope of this report is limited to the following:

- Literature review of FRP strengthening field applications, analysis and design methods, and laboratory investigations,
- The selection and description of three different strengthening systems for a selected reinforced concrete bridge,
- Description of calculation procedures for flexural strengthening,
- Results of the live load tests prior to and immediately after strengthening.

METHODOLOGY

A literature review was conducted, focused primarily on field applications of FRP strengthening projects that have been conducted on actual bridges and the analysis and design considerations for those projects. Laboratory investigations were also included, particularly when the laboratory investigations were directly related to field applications. States included are: Alabama, Missouri, Oregon, Texas, and New York. The review gives an overall picture of the systems that are commercially available and the considerations involved in their application.

A candidate bridge for strengthening was selected by the DOTD in cooperation with the LTRC in January of 2004. Photographs of the bridge site were transmitted to a supplier of FRP strengthening systems, along with preliminary strengthening designs. As a result of the literature review, the experience of the investigators, the site visit, and input from the FRP supplier regarding preliminary cost information, three strengthening systems were selected and recommended for field implementation.

Design calculations were subsequently performed with the intent of increasing the flexural capacity of the strengthened bridge spans. A contractor, Structural Group, was contacted to perform the strengthening of two spans and this work was completed in spring of 2007. Bridge Diagnostics, Inc. (BDI) was contacted to perform the load testing and installation of the long term monitoring system. A live load test was conducted on the portion of the bridge to be strengthened both prior to and immediately after strengthening. Based on the results of the installation procedure and live load testing, conclusions regarding the performance of the strengthening systems are drawn.

Description of Bridge and Selection of Strengthening Systems

The bridge selected for strengthening is Bridge Number 2500110141 on Louisiana State Route 19 in Baton Rouge, Louisiana. It is a reinforced concrete T-beam simple span system, constructed in 1951. The design live load was H15 and the current bridge weight limit is 20-35 tons. The current overall structure rating is from the April 2008 DOTD bridge inspection #5. The geographic feature crossed is White Bayou. A site visit to the bridge was conducted in February of 2004. Photographs of the bridge were taken during the visit (Figures 1 and 2) and dimensions as shown on the contract documents were spot checked with a measuring tape. The dimensions shown on the drawings proved to be generally representative of the actual bridge structure. The site visit revealed that four spans are accessible from below.



Figure 1
View of sub-structure and super-structure of White Bayou Bridge



Figure 2
View of pile cap, beam, and deck of White Bayou Bridge

Based on a limited visual inspection, the concrete appeared to be in relatively good condition at locations away from the supports. At the support locations for the White Bayou Bridge, the supports were generally in good condition. However, a few support locations showed signs of significant spalling. At the neighboring Copper Mill Bayou Bridge, some of the

support locations also showed signs of significant spalling. At the areas of spalling, the aggregate was visible and in many instances the aggregate was significantly larger than 3/4 in. (19.1-mm). The spalling also allowed for investigation into the clear cover over the stirrups and this cover was determined to be approximately two inches (50.8-mm) in the location measured. Based on conversations with the LTRC, it is understood that the bridge is deficient in flexure but adequate in shear.

The concrete T-beams were apparently formed with wooden planking, and this resulted in an uneven surface on the bottom and sides of the T-beams. The uneven surface is a consideration for the surface preparation required for the FRP strengthening systems.

The bridge type and condition, as well as accessibility to the underside of the bridge, have a significant impact on the selection of the strengthening systems. For example, if the concrete was determined to be in poor condition or the surface was excessively uneven, the selection of an adhesively bonded wet-layup system may be less desirable than a mechanically affixed system. Similarly, if the concrete cover was less than one in. (25.4-mm) then the use of a near-surface mounted system may be less desirable. In regard to accessibility, if only access to the ends could be provided, then a system with mechanical end attachment would be preferred. For the White Bayou Bridge, a large number of strengthening systems appear to be feasible, including adhesively bonded wet-layup, near surface mounted bars or strips, adhesively bonded pre-cured strips, and post-tensioned pre-cured strips or rods.

Several different fiber and resin combinations are commercially available. Glass fibers have the advantage of low-cost. However, they also have low stiffness and their durability is questionable. Aramid fibers are of higher modulus than glass fibers, but durability is, again, questionable. Carbon fibers are of high strength and stiffness, and are generally considered to have the best durability of the fiber systems. The cost of carbon fibers is high when compared to glass, but the cost of bridge strengthening is typically governed by labor and mobilization. Both glass and aramid fibers are of low conductivity while carbon fibers are highly conductive. Because of this, care should be taken to insulate carbon fibers from direct contact with steel. If carbon fibers are in direct contact with steel for an extended period of time, corrosion may result.

Recently, steel fiber systems (such as the 'hardwire' system) have become available with either polymeric or cement-based matrices. Steel fibers offer high strength and stiffness, but durability can be questioned with a metallic fiber system. Steel fiber systems are relatively new to the market. At this time, it appears that they may be best suited for applications where material cost and/or impact are primary considerations.

In regard to resins, most of the commercially available systems are applied with proprietary resin systems. Epoxies, polyesters, and vinylesters are commercially available. For carbon fibers, epoxies are the most widely used resins. For glass fibers, vinylesters and epoxies are generally considered to provide the best durability.

Due to the desire for widespread implementation, attention should be given to systems that have proven to be satisfactory in the past. Recently developed or developing systems that have clear and demonstrable advantages over the more widely implemented FRP strengthening systems should also be considered and implemented on a trial basis to gain an understanding of the benefits and potential drawbacks of these newer systems.

Due to the shortness of the spans [approximately 25 ft. (7.62 m)] and the relatively small number of beams per span (four beams), an opportunity exists to investigate the feasibility of three different strengthening systems. Carbon fiber offers the advantages of long-term durability, lightness of weight, and availability. The cost of carbon fiber is somewhat higher than glass or steel. However, the cost of bridge strengthening is not generally controlled by material cost, but instead by ease of installation. Therefore, each of the systems selected is based on carbon fibers only.

CFRP Wet Layup (Fabric)

CFRP wet layup (generally with unidirectional fibers) is one of the most widely used strengthening systems. It offers the benefits of ease-of-installation, low out-of-plane stiffness, and large contact area. It is an adhesive system, so surface preparation is critical. However, due to the large amount of surface area, surface preparation is less critical than for pre-cured strips.

Laboratory testing has been conducted with this system at Tulane University and the results indicate that this system is more easily applied than CFRP pre-cured strips [21, 22]. Surface preparation was minimal, whereas the pre-cured strip method required the use of a needle-scaler. Furthermore, the ultimate strength of the wet layup system was higher than that of the pre-cured strip system. A schematic representation of the CFRP wet layup system is shown in Figure 3.

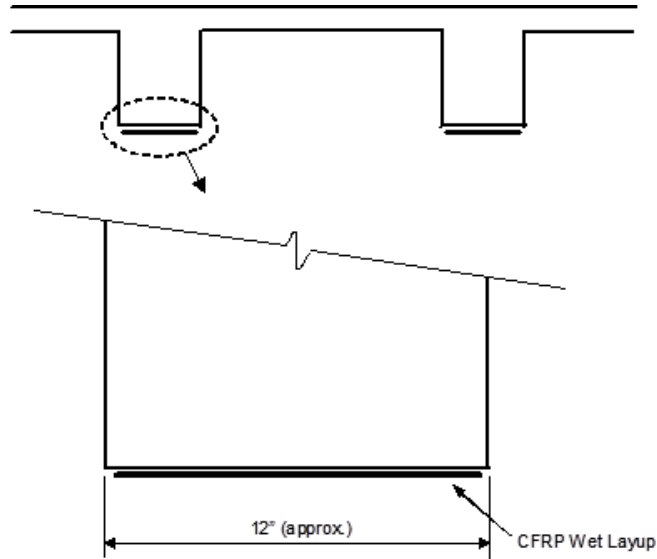


Figure 3
CFRP wet layup (schematic)

CFRP near Surface Mounted Strips or Rods

The use of near surface mounted strips or rods offers the advantage of partially or completely encapsulating the CFRP material. Therefore, the bond between the strips or rods and the concrete is enhanced. With this method, the ultimate strength of the rods or bars can often be achieved. This is in contrast to the wet layup method, where failure of the strengthening system is often controlled by debonding or delamination prior to failure of the strengthening system itself. In the single field application reviewed, the installation was reported to be less time consuming than the wet layup method, primarily due to the lack of surface preparation required with the near surface mounted method. A schematic representation of the CFRP near surface mounted method is shown in Figure 4.

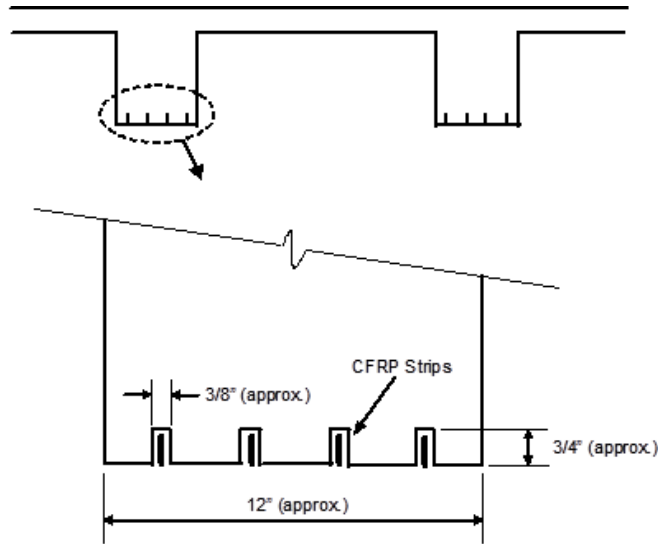


Figure 4
Near surface mounted CFRP strips (schematic)

CFRP Post-Tensioned Strips or Rods

CFRP has an inherently high tensile strength. As mentioned previously, this tensile strength is rarely achieved for the wet layup system. One method that takes advantage of the full tensile strength of the CFRP material is post-tensioning. In the applications reported, the CFRP material has been typically post-tensioned from 40 to 50 percent of ultimate capacity. Because of the mechanical attachments at the ends with these systems, failure of the system is typically controlled by tensile failure of the CFRP strips or rods. Aside from high ultimate strength, this system offers the advantages of improved serviceability through the reduction of tensile stress in the existing steel reinforcing, reduction of in-service deflections that have taken place over time (creep), and reduction of existing crack widths. Each of these factors should have a positive impact on increasing the serviceability and life expectancy of a strengthened structure.

Of the three systems, this is the least understood and has been implemented only on a limited basis in the United States. However, it may also be the most beneficial because it addresses serviceability as well as ultimate strength, while the other systems primarily address ultimate strength. A schematic of the CFRP post-tensioned strip method is shown in Figure 5.

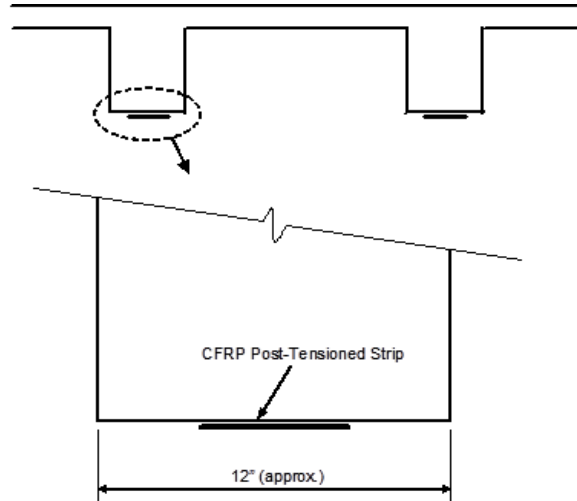


Figure 5
CFRP post tensioned strips (schematic)

Preliminary designs of the CFRP wet layup and CFRP near surface mounted systems were completed in February of 2004 and then transmitted to a representative of Degussa (previously Master Builders) for purposes of preliminary cost estimating. Approximately twenty digital photographs of the bridge site were also transmitted, along with portions of the design drawings. A preliminary cost estimate of the CFRP post-tensioned system was also requested. The results indicated that the installed cost of the CFRP wet layup and CFRP near surface mounted system would be in the vicinity of \$25 per square foot (0.0929 m²) of the strengthened area. For a 25-foot span with four beams, each of one foot width, the installed cost could then be estimated as \$25 * one foot (0.305 m) width * 25 feet (7.62 m) long * 4 beams = \$2,500 per span. This rough estimate was originally discussed over the telephone, and later confirmed by e-mail. The cost estimate for the post-tensioned system was originally estimated at approximately \$35 per square foot (0.0929 m²) over the telephone [as opposed to the \$25 per square foot (0.0929 m²)] for the other systems, but at the time of this writing a confirmed estimate could not be obtained due to limited experience with the system. Later conversations with another representative of Degussa indicated that an estimate of \$15 per square foot of installed area was more appropriate for the wet layup and near surface mounted systems. The figures referenced are only rough cost estimates and actual costs may be significantly different due to several factors including accessibility, the extent of surface preparation required, and the actual amount and type of CFRP material.

Description of CFRP Strengthening Systems and Calculation Procedures

This chapter describes the strengthening systems selected for installation and the calculation procedures used to assess the predicted structural behavior of the installed systems. With CFRP strengthening, beam increases in flexural strength from 10 to 160 percent have been reported. However, for realistic applications, increases in the range of five to 40 percent are more readily achieved. For the strengthened beams described here, the projected increase in flexural strength was in the range of 15 to 32 percent. The shear capacity of the beams was determined as adequate prior to the commencement of the project and shear strengthening was not addressed in this study. For completeness, a brief section is included at the end of this chapter to discuss the shear capacity of the structure.

Description of CFRP Strengthening Systems

This report briefly described the selected bridge and three recommended CFRP strengthening schemes: CFRP wet layup; CFRP near surface-mounted strips; and CFRP post-tensioned strips. Due to scarceness of the post-tensioned CFRP systems in practice, combined with budgetary considerations, it was later decided to substitute a passive CFRP pultruded strip system (not post-tensioned) in place of the post-tensioned strip system.

In lieu of installing each of three strengthening systems on a span for a total of three strengthened spans, it was decided to install the CFRP near surface mounted strip system on Span 2 (all four tee beams) and to install the CFRP pultruded strips and CFRP wet layup system side by side on Span 3. The CFRP pultruded strips were installed on Beams 1 and 2 of Span 3 and the CFRP wet layup was utilized for Beams 3 and 4 of Span 3. A plan view of the strengthening schemes along with schematic cross-sections is shown in Figure 6 and section views of the strengthening schemes are shown in Figure 7. An overall view of the project and photographs of the CFRP wet layup and near surface mounted strengthening systems are shown in Figures 8, 9, and 10.

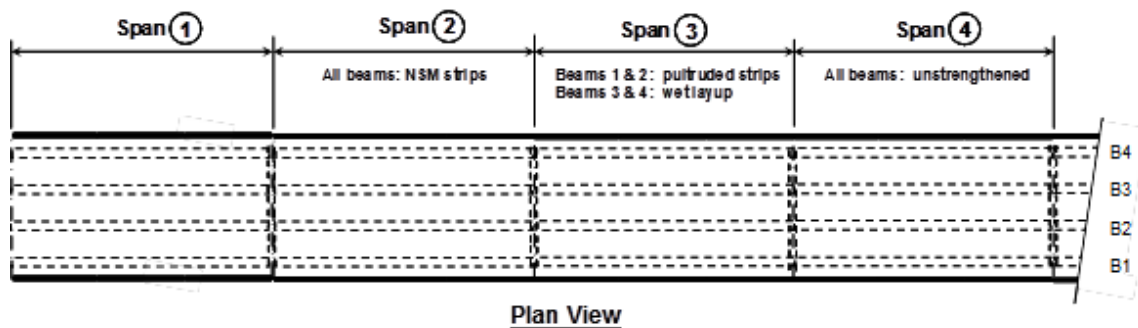


Figure 6
CFRP strengthening schemes - plan view

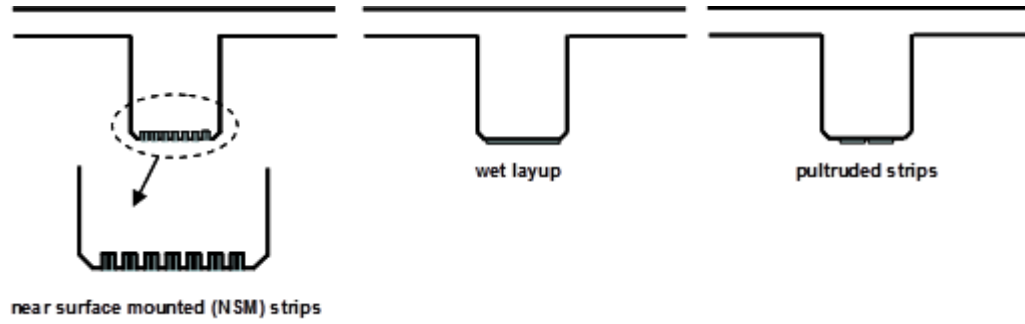


Figure 7
CFRP strengthening schemes - cross-section views



Figure 8
Overall view of White Bayou Bridge



Figure 9
Wet lay-up



Figure 10
CFRP NSM strips

Calculation Procedures

The strengthening calculations were carried out in general conformance with ACI 440.2R-02 [ACI 440.2, 2002]. This method incorporates a limit states design philosophy with consideration to ultimate capacity and serviceability. For ultimate capacity, the pertinent failure modes are assessed. Commonly for externally bonded systems, such as the pultruded strips and the wet layup applied to Span 3, the failure mode is controlled by debonding of the CFRP material from the concrete surface. Shear/tension delamination of the concrete cover is another common failure mode with externally bonded systems. It is important to note that neither of these failure modes will develop the full tensile capacity of the CFRP material and, therefore, the ultimate tensile stress of the CFRP material is of relatively little consequence in predicting the ultimate flexural capacity of the section. The longitudinal and out-of-plane stiffness of the material are more important because these factors contribute to the tendency for the CFRP material to debond and/or delaminate.

For the near surface mounted systems, such as the one installed on Span 2, debonding rarely occurs because the strips are encased on three sides. Delamination can still occur depending on the properties of the concrete and the geometry of the strengthening scheme, and existing reinforcing bars. In contrast to the externally bonded systems, the near surface mounted system is often capable of developing the full tensile strength of the CFRP strips, therefore, with this method, the tensile capacity of the strips is a more significant consideration. For all strengthening systems, the other common failure modes of reinforced concrete flexural members, such as concrete crushing and shear dominated failure, should not be overlooked. Strengthening limits are imposed in the ACI 440 document with the general philosophy that the structure should be able to resist a reasonable level of load without collapse, even if the CFRP system is damaged. This philosophy is described in the following equation:

$$(\phi R_n)_{\text{existing}} \geq (1.2S_{DL} + 0.85S_{LL})_{\text{new}} \quad (1)$$

where,

ϕ = strength reduction factor

R_n = nominal strength of member

S_{DL} = dead load effects

S_{LL} = live load effects

While a detailed investigation of fire resistance is beyond the scope of this report, fire resistance can be a consideration for some installations, including bridges. The polymeric systems that are typically used for CFRP strengthening have a relatively low glass transition

temperature, in the range of 140 to 180 degrees F. In a significant fire event, the stiffness of the resin can be expected to be reduced or completely lost relatively quickly. ACI 216R [ACI 216R, 2001] addresses the loss in concrete and steel strengths due to a fire event. When this approach is followed, it is both conservative and seemingly appropriate to neglect the effect of the CFRP reinforcement. ACI 440.2 recommends that the following equation be satisfied:

$$(R_{n\theta})_{\text{existing}} \geq S_{DL} + S_{LL} \quad (2)$$

where, $R_{n\theta}$ = nominal resistance of member at elevated temperature (see ACI 216R). If the CFRP system is intended to allow greater load-carrying capacity, such as an increase in live load, the load effects should be computed using the greater loads.

Long term effects such as impact tolerance, creep rupture and fatigue, resistance to alkalinity/acidity, and thermal expansion are addressed in 'Environmental Considerations' in ACI 440.2. At the time the document was written, relatively few field applications had been implemented. To compound matters, most field applications were not, and currently are not, monitored with the goal of determining long-term effects. Environmental reduction factors, C_E , are nonetheless described in ACI 440.2R-02 for different types FRP systems and exposure conditions.

The following assumptions are made for calculation of the flexural resistance of CFRP strengthened reinforced concrete beam sections:

- Design calculations are based on actual dimensions and material properties
- Plane sections remain plane after loading
- No relative slip occurs between the CFRP and the concrete
- Shear deformation within the adhesive (epoxy) layer is neglected
- Ultimate compressive strain in concrete is 0.003
- Tensile strength of the concrete is neglected
- The CFRP reinforcement behaves linear-elastically to failure

Calculation of Nominal Strength. Strength design is accomplished with the same general principles as those normally used for reinforced concrete flexural members. Namely, the design flexural strength must meet or exceed the required moment strength as expressed in the following equation:

$$\phi M_n \geq M_u \quad (3)$$

where,

M_n = Nominal moment strength

M_u = Factored moment at section

The nominal flexural strength of a CFRP strengthened flexural section can be calculated based on strain compatibility, internal force equilibrium, and determination of the controlling failure mode. Failure modes include:

- Crushing of concrete in compression prior to yielding of tensile steel
- Yielding of tensile steel followed by rupture of CFRP laminate
- Yielding of tensile steel followed by concrete crushing
- Shear/tension delamination of the concrete cover
- Debonding of the CFRP from the concrete

Concrete crushing is assumed to occur if the strain in the concrete reaches 0.003. Rupture of the laminate is assumed to occur if the rupture strain of the laminate is reached. This occurs rarely for externally bonded installations. Usually either cover delamination or debonding controls the failure mode. It is noted that significant ductility can still exist after either of these two failure modes is reached, albeit at the unstrengthened load capacity. In an attempt to set a limiting usable strain on the laminate, and to thereby indirectly predict the onset of delamination or debonding, a 'bond-dependent coefficient', κ_m , is defined as follows:

$$\kappa_m = \frac{1}{60\varepsilon_{fu}} \left(1 - \frac{nE_f t_f}{2,000,000} \right) \leq 0.90 \quad \text{for } nE_f t_f \leq 1,000,000 \quad (4a)$$

$$\kappa_m = \frac{1}{60\varepsilon_{fu}} \left(\frac{500,000}{nE_f t_f} \right) \leq 0.90 \quad \text{for } nE_f t_f > 1,000,000 \quad (4b)$$

where,

ε_{fu} = design rupture strain of CFRP reinforcement
 n = number of plies of CFRP reinforcement
 E_f = tensile modulus of elasticity of CFRP reinforcement
 t_f = nominal thickness of one ply of CFRP reinforcement

The factor κ_m is a factor no greater than 0.90 that may be multiplied by the CFRP rupture strain to arrive at a strain limitation. This factor recognizes the fact that laminates, having greater stiffness, are more prone to delamination and debonding. For laminates with unit stiffness greater than 1,000,000 lb./in., the factor limits the force in the laminate, effectively placing an upper bound on the total force that can be developed in the laminate regardless of the number of plies. The width of the laminate is not included in the equations because an increase in width results in a proportional increase in bond area. This equation is based largely on experience and, as such, is not expected to be highly accurate. Nevertheless, it is important to realize that delamination and debonding are very important and common failure modes for externally bonded CFRP systems and some attempt must be made to address this behavior.

The maximum or effective strain level in the CFRP reinforcement at ultimate can be found by:

$$\varepsilon_{fe} = \varepsilon_{cu} \left(\frac{h-c}{c} \right) - \varepsilon_{bi} \leq \kappa_m \varepsilon_{fu} \quad (5)$$

where,

ε_{fe} = effective strain level in CFRP reinforcement; strain level attained at section failure
 ε_{cu} = maximum usable compressive strain of concrete
 h = overall thickness of a member
 c = distance from extreme compression fiber to the neutral axis
 ε_{bi} = strain level in the concrete substrate at the time of the CFRP installation

The effective stress level in the CFRP reinforcement can be found from the effective strain level and the assumption of elastic behavior:

$$f_{fe} = E_f \varepsilon_{fe} \quad (6)$$

where, f_{fe} is the effective stress in the CFRP reinforcement attained at section failure.

Ductility. Because CFRP strengthening systems effectively increase the tensile reinforcement ratio, combined with the fact that they behave elastically to failure, it is to be expected that the ductility of the strengthened system will be reduced. Although this should be recognized and accounted for, this is not a cause for alarm due to two reasons: a) flexural systems with lessened ductility are allowed and addressed by the ACI code with appropriate strength reduction factors; and b) if the failure mode is delamination, debonding, or CFRP rupture, as is commonly the case, a significant amount of ductility is still present in the system, approaching the ductility that existed prior to installation of the reinforcement. However the capacity after failure is essentially reduced to that prior to strengthening.

The philosophy used for selecting the strength reduction factor in ACI 440.2 is similar to that found in ACI 318-05. The equations set the reduction factor at 0.90 for ductile sections and at 0.70 for brittle sections. A linear transition is used between the two extremes:

$$\phi = 0.90 \quad \text{for } \varepsilon_s \geq 0.005 \quad (7a)$$

$$\phi = 0.70 + \frac{0.20(\varepsilon_s - \varepsilon_{sy})}{0.005 - \varepsilon_{sy}} \quad \text{for } \varepsilon_{sy} < \varepsilon_s < 0.005 \quad (7b)$$

$$\phi = 0.70 \quad \text{for } \varepsilon_s \leq \varepsilon_{sy} \quad (7c)$$

where,

ε_s = strain level in the nonprestressed steel reinforcement

ε_{sy} = strain corresponding to the yield strength of nonprestressed steel reinforcement

Serviceability. In addition to the ultimate strength requirements, the strengthened section should also satisfy applicable serviceability criteria, as described in ACI 318-05. For purposes of serviceability analysis, it is often convenient to use a transformed section approach. ACI 440.2 recommends that the service level stress in the tensile reinforcing steel be limited to 80 percent of the yield strength as follows:

$$f_{s,s} \leq 0.80f_y \quad (8)$$

where,

$f_{s,s}$ = stress level in nonprestressed steel reinforcement at service loads

f_y = specified yield strength of nonprestressed steel reinforcement

Creep-Rupture and Fatigue Stress Limits. Creep rupture and fatigue failure occur at differing values of applied stress for different resin/fiber combinations. For CFRP strengthening systems the ACI 440.2 document references 91 percent of the ultimate stress as the creep rupture limit. The level of sustained load stress in the CFRP material should be calculated and compared to this value. The maximum stress induced by fatigue should also be investigated and the following equation is given:

$$\text{Sustained plus cyclic stress limit} \geq f_{f,s} \quad (9)$$

where, $f_{f,s}$ is the stress level in the CFRP caused by a moment within the elastic range of the member. A value for the sustained plus cyclic stress limit for CFRP is given as $0.55f_{fu}$, where f_{fu} is the design ultimate tensile strength of the CFRP.

Calculations Performed for the Strengthening Systems Used. As discussed previously, three different flexural strengthening systems were installed on two bridge spans. The strengthening systems are described as near surface mounted, wet layup, and pultruded strips. The details of the systems are summarized in the Table 1.

Table 1
Properties of installed strengthening systems

	NEAR SURFACE MOUNTED STRIPS†	WET LAYUP	PULTRUDED† STRIPS
Trade identifier	Carbodur S512	V-Wrap C100	Carbodur S512
Env. reduction factor, C_E	1.0	1.0	1.0
Fiber type	carbon	carbon	carbon
Ultimate stress of CFRP, f_{fu}	380,000 psi	550,000 psi*	380,000 psi
Ultimate strain of CFRP, ϵ_{fu}	0.017	0.015	0.017
Modulus of CFRP, E_f	22,000,000 psi	33,000,000 psi*	22,000,000 psi
Thickness of CFRP, t_f	0.05 in	0.0065 in*	0.05 in
Width of CFRP, w_f	5.25 in***	10 in	6 in**
Number of plies, n	1***	4	1
Concrete compr. stress, f_c	5,000 psi	5,000 psi	5,000 psi
Tensile steel cross-sect. area, A_s	6.625 in ²	6.625 in ²	6.625 in ²
Tensile steel yield stress, f_y	40,000 psi	40,000 psi	40,000 psi
Distance to tensile steel, d	19.80 in	19.80 in	19.80 in
Moment due to dead load, M_{DL}	647.9 k-in	647.9 k-in	647.9 k-in
Moment due to service load, M_S	1,231 k-in	1,231 k-in	1,231 k-in
Member height, h	22.5 in	22.5 in	22.5 in
2nd MOI of section (cracked), I_{CR}	10,940 in ⁴	10,940 in ⁴	10,940 in ⁴
Calculated bond coefficient, κ_m	1.0	0.63	0.53
Calculated strength red. factor, ϕ	0.9	0.90	0.90

* = values reported are associated with the fibers only in the case of the wet layup system. The calculations for the κ_m factor are also based on the product of the $nE_f t_f$ values shown in the table and based on the fibers only. This is not strictly correct but has been shown to produce reasonable results in the past [Ridge, 2004 and Ridge and Ziehl, 2006]. Furthermore, the calculated κ_m value of 0.63 appears to be reasonable.

** = for pultruded strips, (2) 3 in. wide strips were used, equaling (1) 6 in. wide strip

*** = for near surface mounted strips, (7) 0.75 in. vertical strips were installed on each beam, equaling (1) 5.25 in. wide strip

† = for pultruded strips and near surface mounted strips, material properties were taken from ACI 440.2R-02, Table 14.2.

Note that for calculations of the CFRP wet layup system, the ultimate stress values that are used are not for the CFRP material but rather for the carbon fibers themselves. To provide consistent results, the thickness of the CFRP is not used, but is instead replaced by the thickness of one layer of carbon fibers. This value ($t = 0.0065$ inches) was found in literature from the manufacturer. For the near surface mounted system, the bond dependent coefficient was set equal to unity due to the ability of this system to sometimes develop the full tensile capacity of the CFRP strips. For all systems, the environmental reduction factor was set equal to unity because it is believed that the factors shown in ACI 440.2R-02 may be overly conservative. In all cases, the calculated strength reduction factor was equal to 0.90, indicating ductile behavior at ultimate, as would be expected for a tee beam system due to the very wide concrete compressive zone available in the slab.

The values shown in the table above were used in general conformance with ACI 440.2R-02 to arrive at values for calculated flexural capacity, with each of the three different systems as shown in Table 2. The calculated percentage increases are also shown in Table 2.

Table 2
Calculated increase in moment capacity

	Near Surface Mounted	Wet Layup	Pultruded Stips
Trade identifier	Carbodur S512	V-Wrap C100	Carbodur S512
Unstrengthened moment capacity, ϕMn	4,407 k-in	4,407 k-in	4,407 k-in
Strengthened moment capacity, ϕMn_{CFRP}	5,844 k-in	5,525 k-in	5095 k-in
Increase in moment capacity	32%	25%	15%

Shear Capacity. The concrete shear capacity of the T-Beam section of the bridge can be conservatively calculated assuming that only the rectangular web portion (including the flange depth) is effective in resisting shear. For a more accurate estimation of the T-beam shear capacity the contribution of the flange can be considered.

Table 3 gives the shear capacity of the beam determined by considering only the concrete shear capacity of the web and the stirrups. As can be seen from the values in the table, the shear strength of the member is not a concern and as such was not addressed in this study.

Table 3
Calculated shear capacity

(The design/ultimate shear for HS-20 loading, $V_u = 82.1$ kips)

	Concrete Shear Capacity, ϕV_c (kips)	Stirrups Shear Capacity ϕV_s (kips)	Total Shear Capacity ϕV_n (kips)	RF_{INV}	RF_{OPR}
Case I: Concrete Shear Capacity of Web + Shear Capacity of Stirrups	28.6	49.4	77.9	1.19	1.98

The shear rating calculations shown in the above table are included in the Appendix for clarification and justification of the results presented.

Live Load Testing Procedures

The live load testing and installation of the long term monitoring system were carried out by Bridge Diagnostics Inc. (BDI) with input from the LTRC. Much of the text and many of the figures that are included in this and the following chapter are excerpted directly or paraphrased from the BDI report that was generated under a separate contract [BDI, 2007]. Field notes are shown in Table 4.

Table 4
Structure description and testing notes

ITEM	DESCRIPTION
STRUCTURE NAME	White Bayou
BDI PROJECT NUMBER	040702
TESTING DATE	April 17, 2007 / May 1, 2007
LOCATION/ROUTE	Zachary Slaughter Hwy over White Bayou
STRUCTURE TYPE	Reinforced Concrete
TOTAL NUMBER OF SPANS	8
SPAN LENGTH(S)	24'
SKEW	0°
STRUCTURE/ROADWAY WIDTH	23'-9"
DECK TYPE	Asphalt

ITEM	DESCRIPTION
OTHER STRUCTURE INFO	
SPANS TESTED	2,3,4
TEST REFERENCE LOCATION (X=0,Y=0)	Inside Curb, North West Corner
TEST VEHICLE DIRECTION	South Bound
TEST BEGINNING POINT	North end of structure
LATERAL LOAD POSITION(S)	1.6' from west curb, 1.6' from east curb, center line
NUMBER/TYPE OF SENSORS	40 Strain Gauges / 2 LVDT's / 2 String Pots
STS SAMPLE RATE	40 Hz
NUMBER OF TEST VEHICLES	1
STRUCTURE ACCESS TYPE	Preinstalled scaffolding
STRUCTURE ACCESS PROVIDED BY	Tulane University
TRAFFIC CONTROL PROVIDED BY	LA DOTD
TOTAL FIELD TESTING TIME	2 days
FIELD NOTES	See Appendix B
VISUAL CONDITION	Fair

Prior to the first live load test, the bridge was instrumented with several strain and displacement sensors, as described in Table 4 and illustrated by Figures 11 through 17. Several controlled load tests were performed, during which strains and displacements were recorded while the test vehicle crossed the bridge at crawl speed (5 mph). The truck was driven across the bridge along prescribed paths and the longitudinal position of the truck was monitored remotely and recorded with the response data. Tests were performed on three different truck paths, each path being repeated at least twice to ensure reproducibility of the test procedures and the structural performance. Details regarding the load test vehicles are given in Table 5.

Table 5
Testing vehicle information

VEHICLE TYPE - SINGLE REAR AXLE DUMP TRUCK	
GROSS VEHICLE WEIGHT (GVW) (same truck used during both tests)	25,900 lbs (Test 1) 25,550 lbs (Test 2)
WHEEL ROLLOUT 5 REVS	51.4' (10.28'/rev)
NO. OF SEMI-STATIC PASSES	6 passes – 3 paths
NO. OF HIGH SPEED PASSES/SPEED	2 passes – 2 paths

After the first set of load tests was performed, Spans 2 and 3 were strengthened with the CFRP strengthening methods. Span 2 beams were strengthened with the near surface mounted CFRP strips, while Beams 1 and 2 of Span 3 were strengthened with CFRP pultruded strips affixed to the bottom surface, and Beams 3 and 4 of Span 3 were strengthened with the CFRP wet layup system. Span 4 was not strengthened and was used as a control span for testing.

Tests were initially performed on April 17, 2007, prior to strengthening. Tests were repeated again on May 1, 2007, after all three CFRP strengthening systems were installed on Spans 2 and 3. The second set of tests was performed with identical procedures to the first so that direct comparisons of the response could be made. Figures 18 through 20 show the instrumentation plan for the second set of tests. The BDI report included in the Appendix provides figures corresponding to Figures 11-20 that are of higher clarity. Figure 21 shows a photograph of the strain and displacement instrumentation and Figure 22 shows a test truck footprint for Test 1.

Access to the structure was provided by Tulane University, LTRC, and DOTD. Scaffolding was installed under the bridge that extended the whole width of the superstructure for Spans 1 through 4. The work platform made for convenient access for instrumentation of the bridge. Traffic control and the load vehicle were provided by the DOTD. The test vehicle wheel weights were obtained by the Louisiana Highway Patrol.

The BDI Structural Testing System (STS) was used for measuring strains at 40 locations and displacements at six locations on the superstructure while it was subjected to a moving truck load. The response data was then used to calibrate a finite element model of the structure, which was in turn used to compute load ratings for standard design and rating vehicles using

the AASHTO Load Factor Design (LFD) approach. The finite element software that was used for the modeling was a BDI code proprietary software and not public domain.

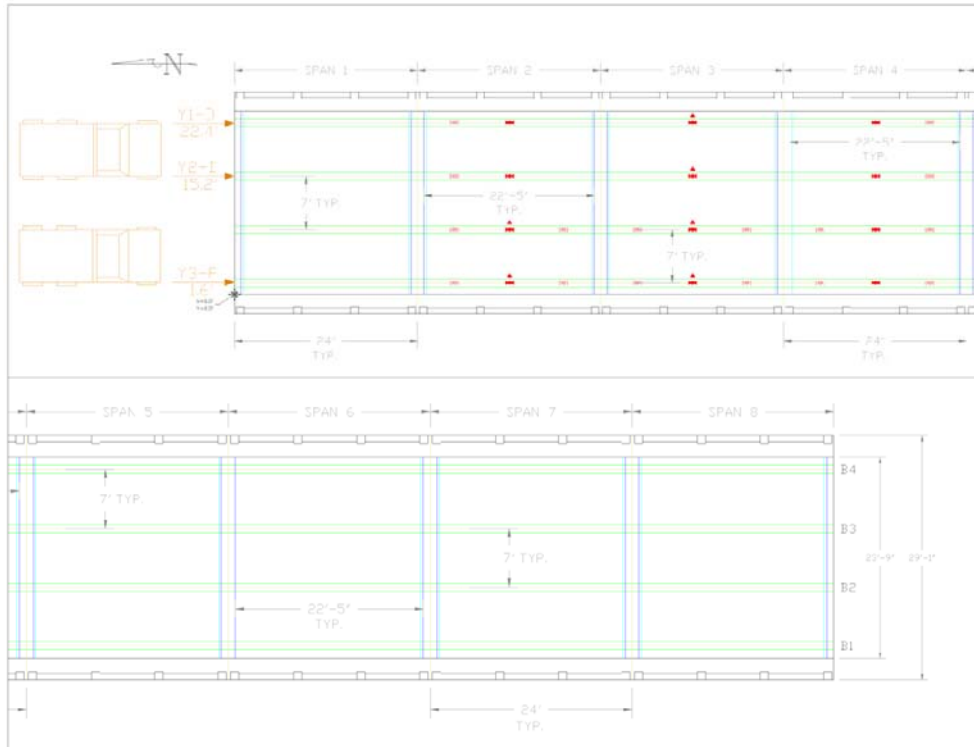


Figure 11
Instrumentation plan (layout view)

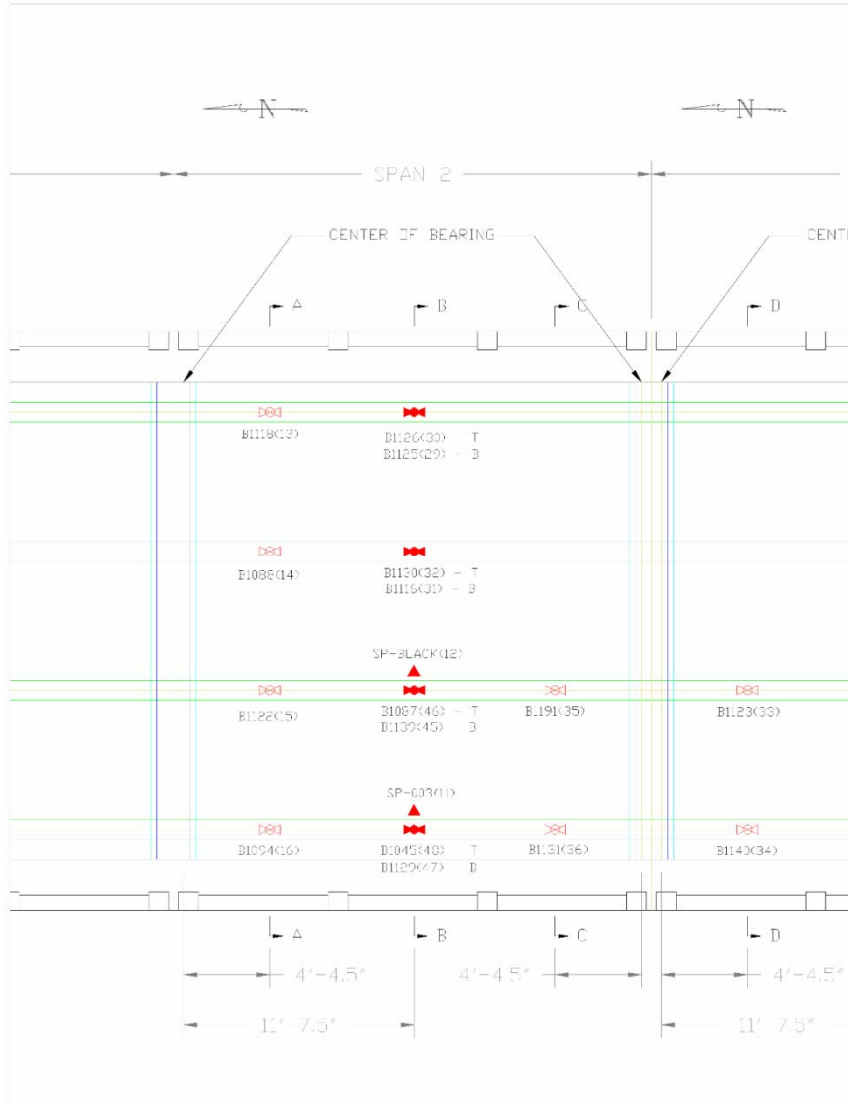


Figure 12
Instrumentation plan (span 2 gauge locations – test setup 1)

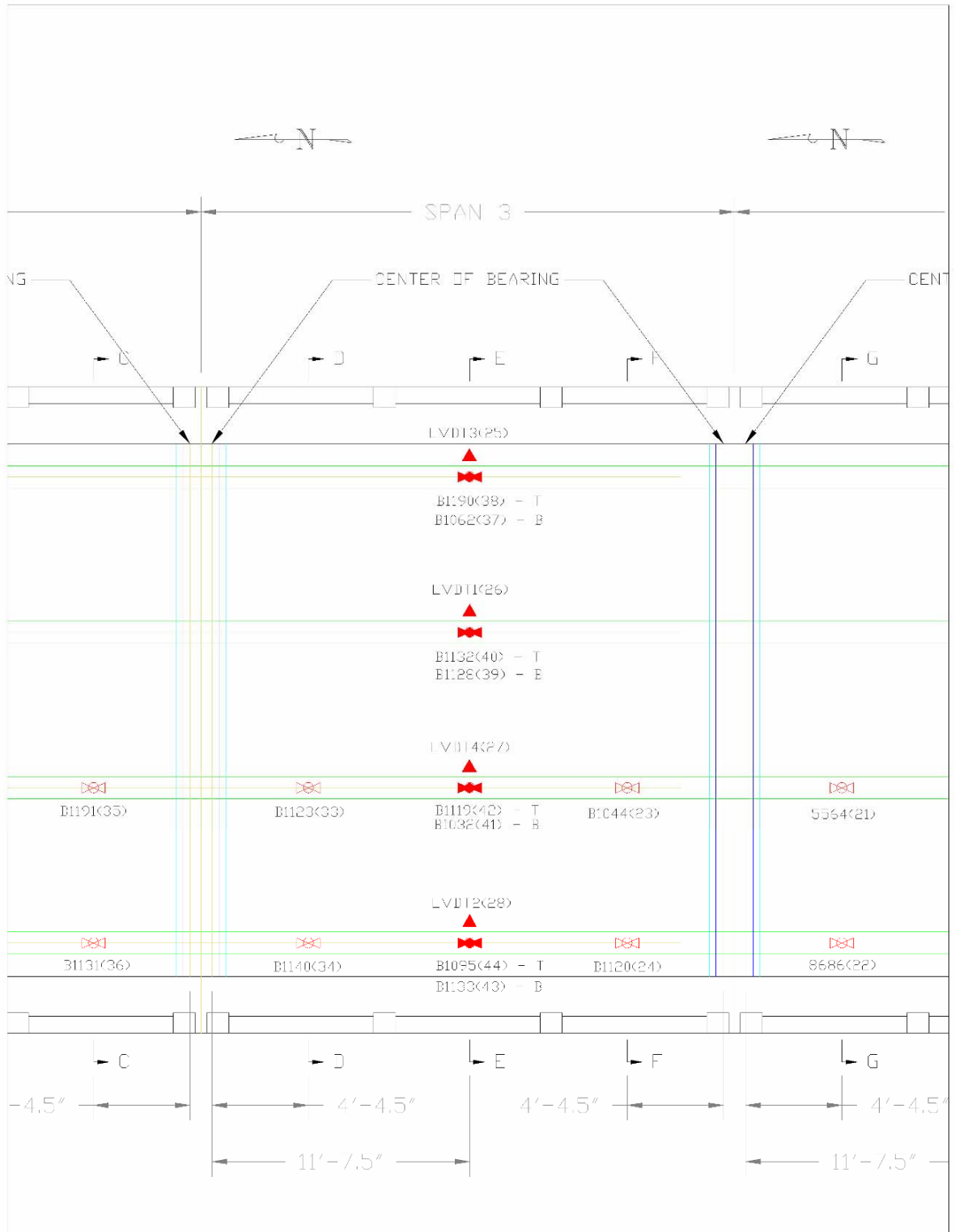


Figure 13
Instrumentation plan (span 3 gauge locations – test setup 1)

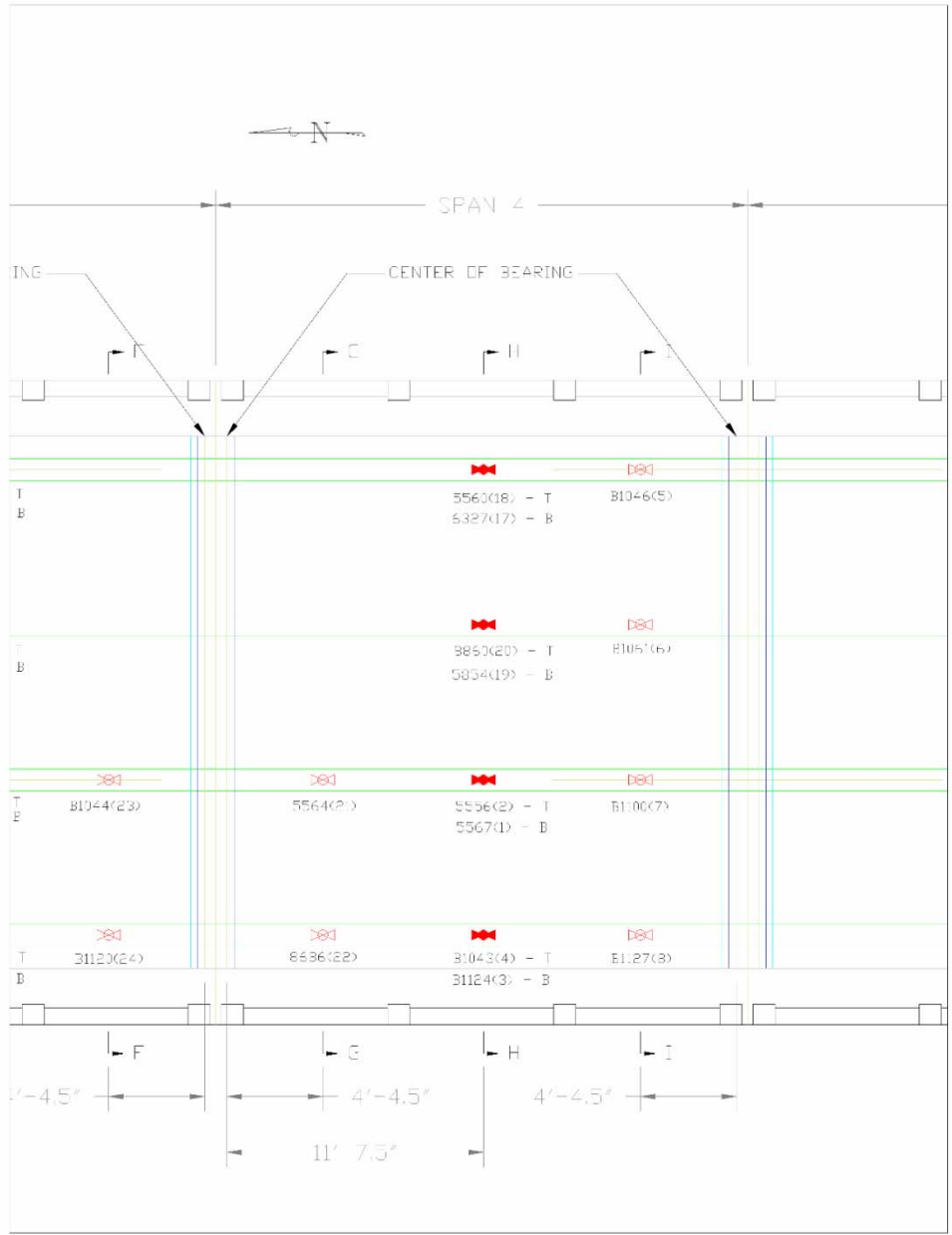


Figure 14
Instrumentation plan (span 4 gauge locations –test setup 1)

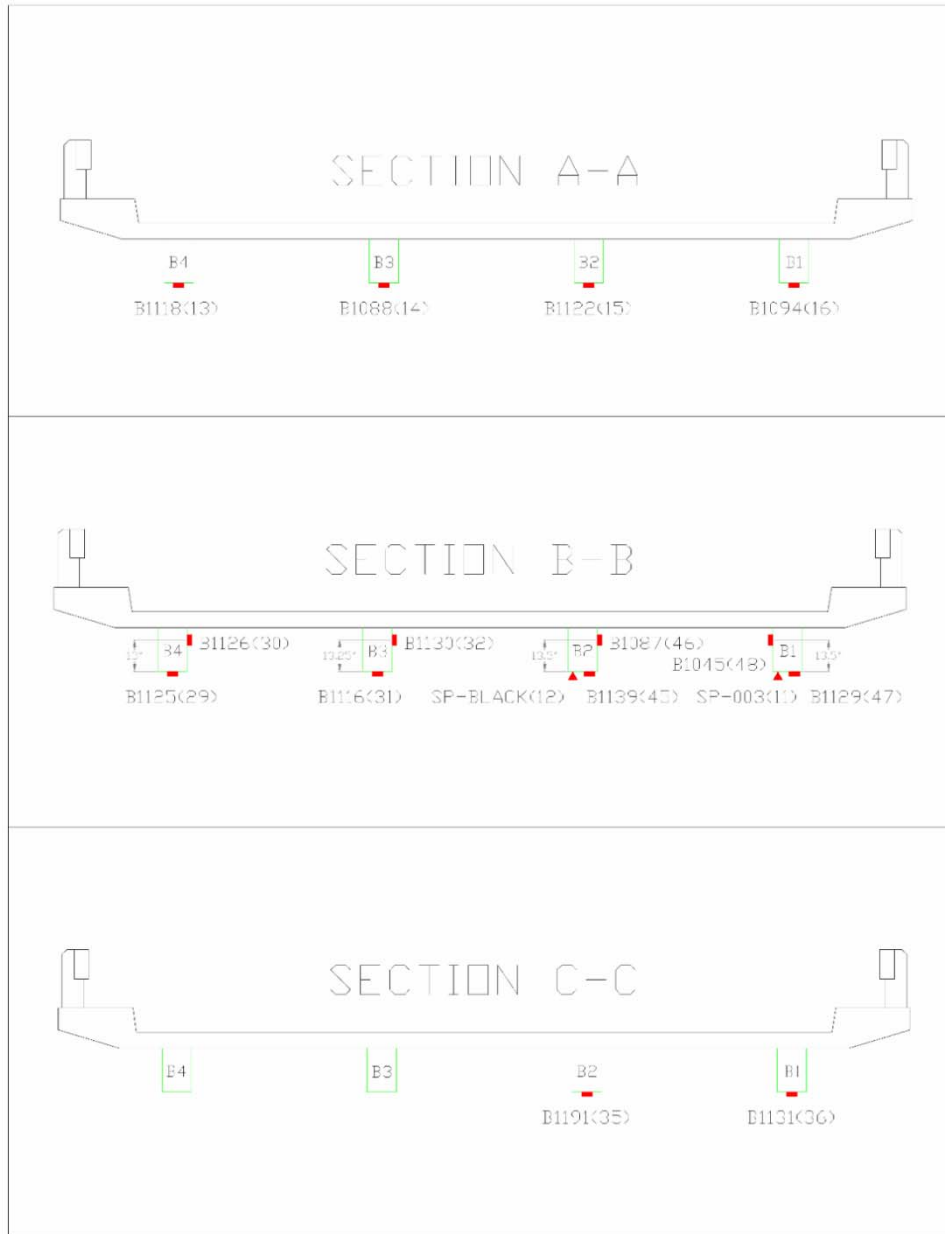


Figure 15
Instrumentation plan (cross-section view, span 2 – test setup 1)

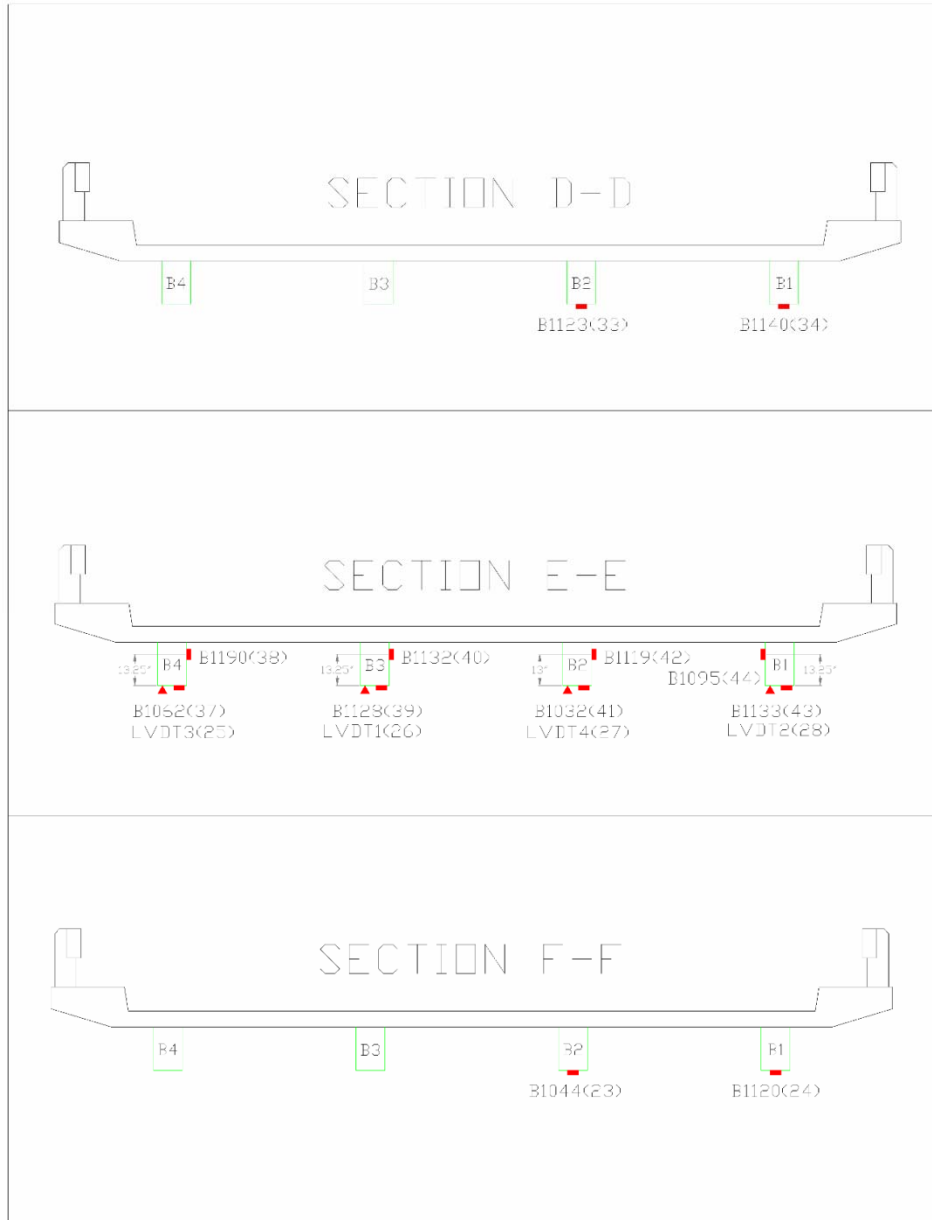


Figure 16
Instrumentation plan (cross-section view, span 3 – Test Setup 1)

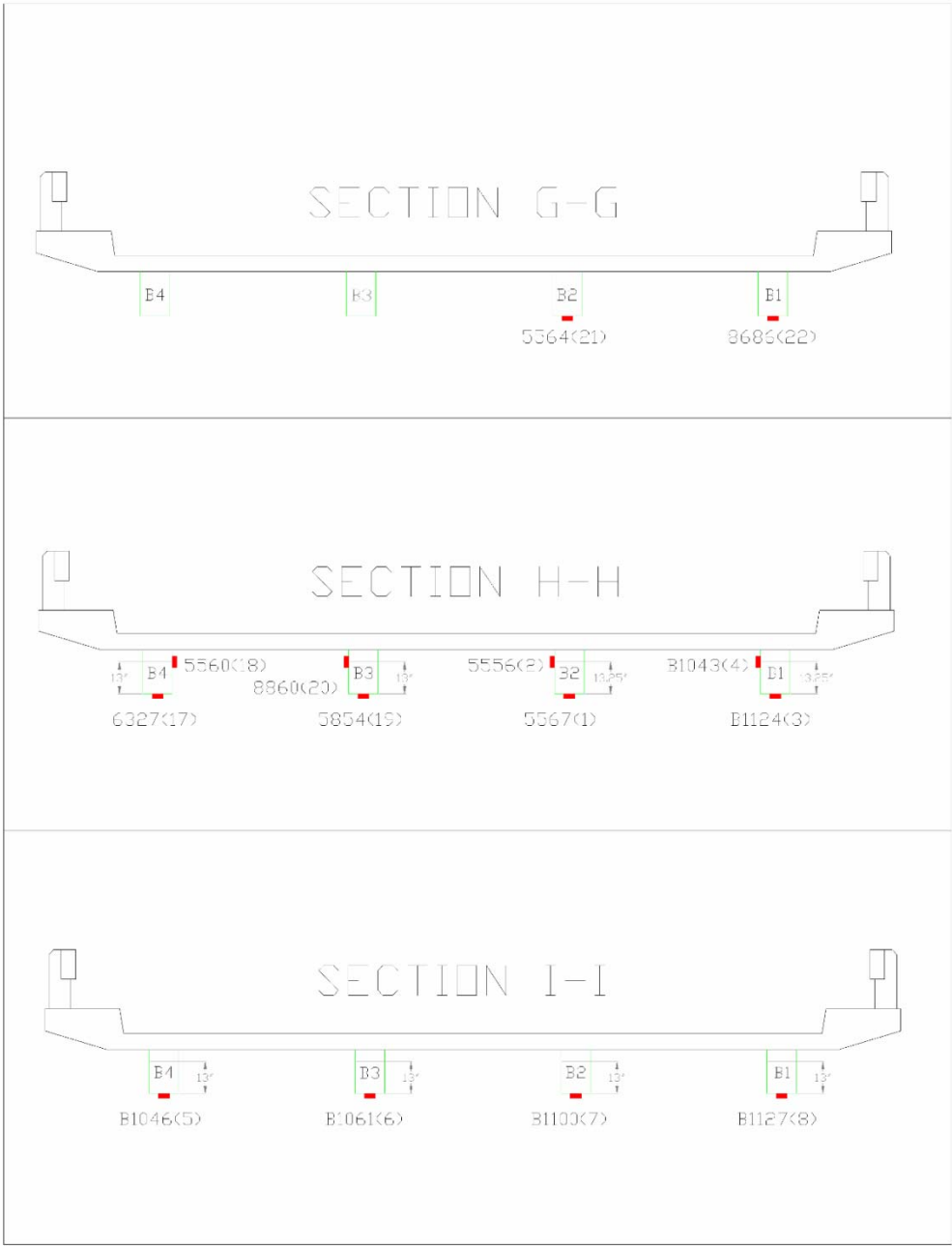


Figure 17
Instrumentation plan (cross-section view, span 3 – test setup 1)

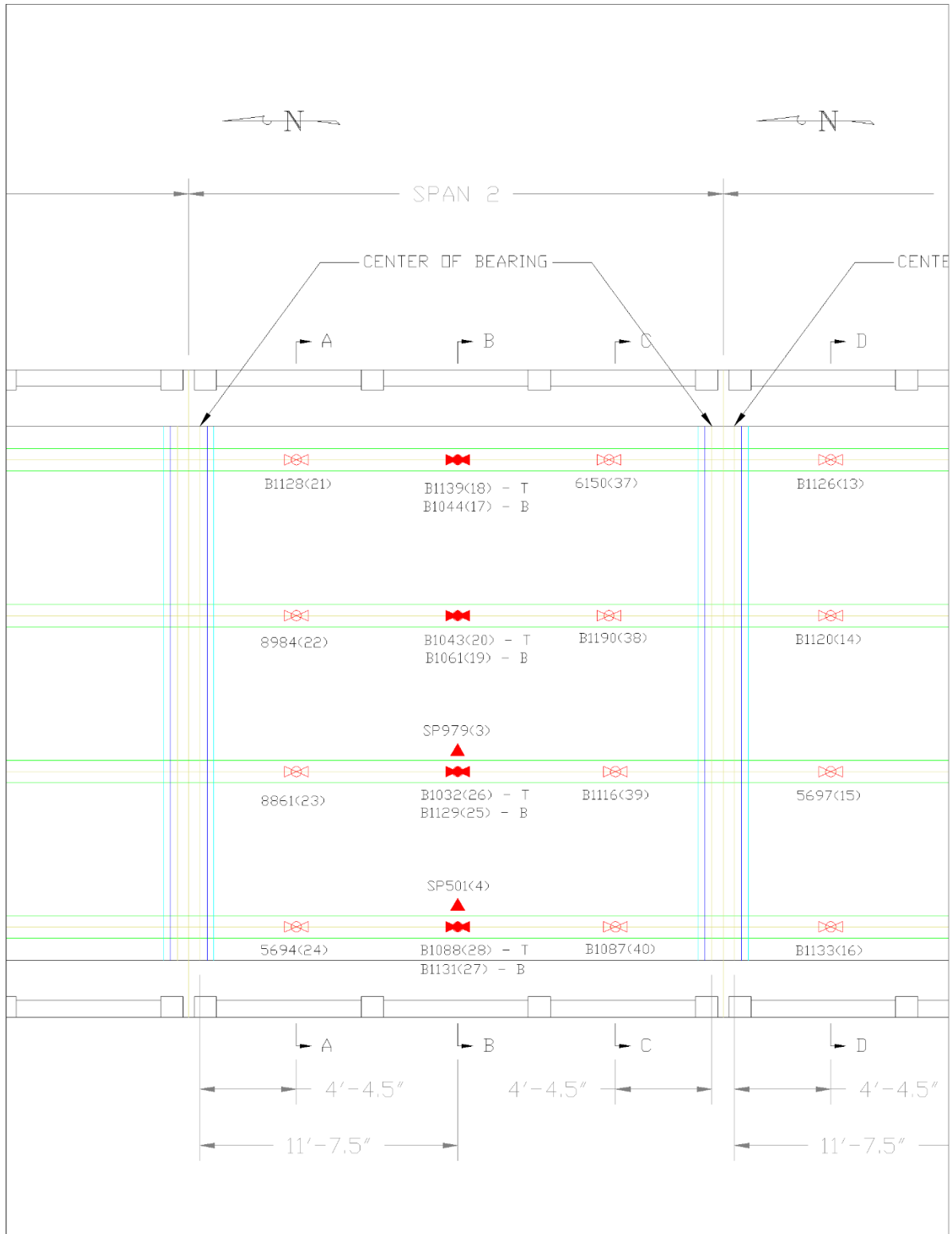


Figure 18
Instrumentation plan (span 2 – test setup 2)

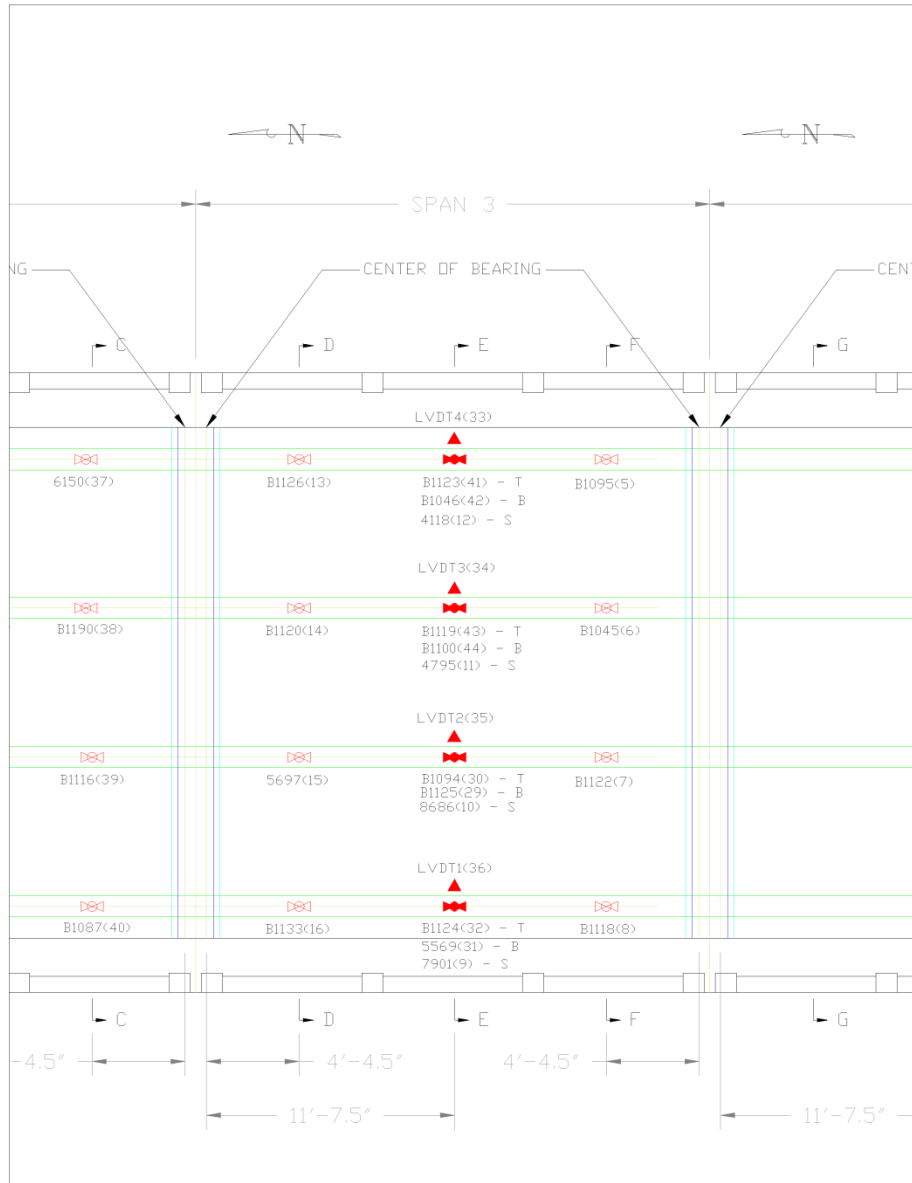


Figure 19
Instrumentation plan (span 3 gauge locations – test setup 2)

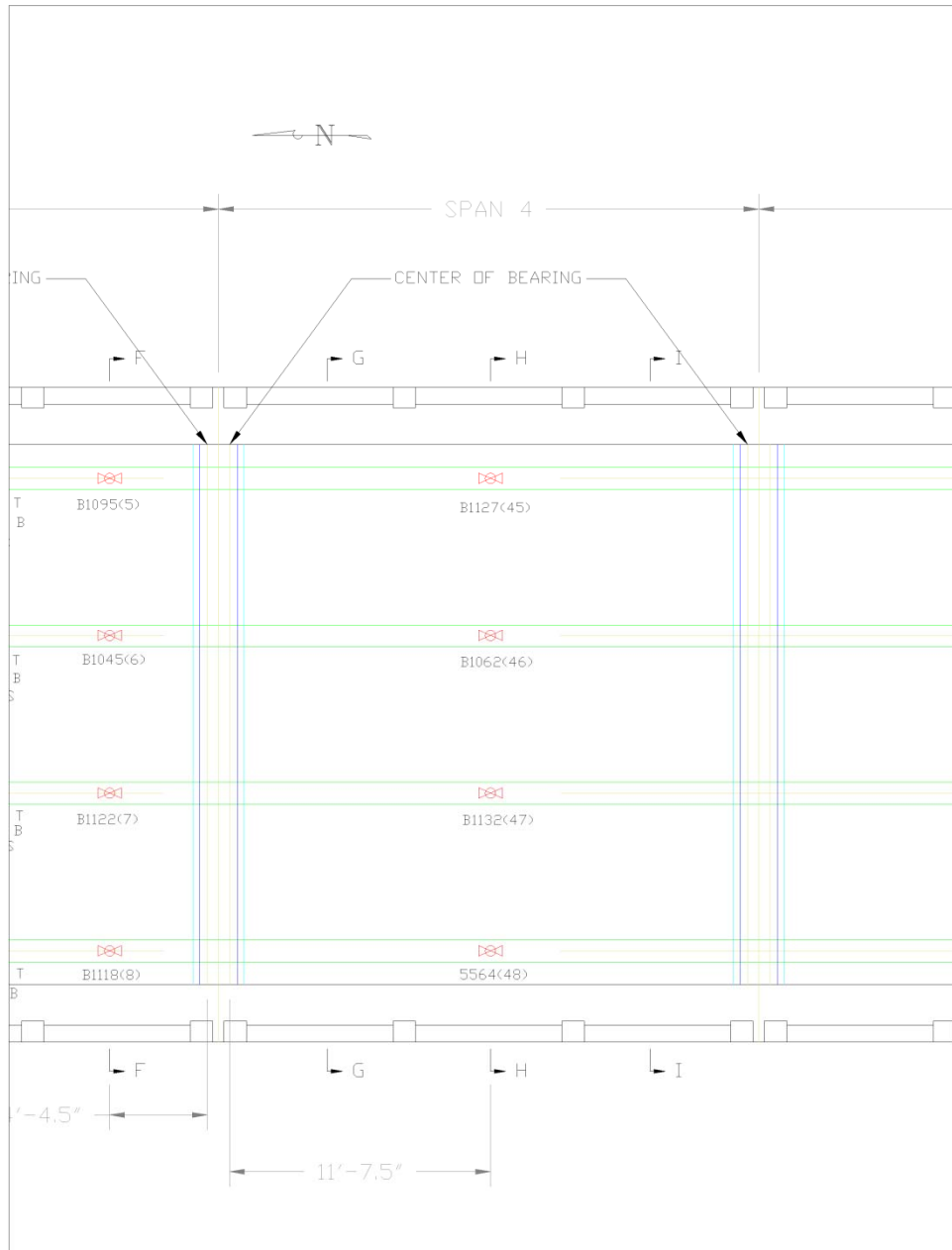


Figure 20
Instrumentation plan (span 4 gauge locations – test setup 2)



Figure 21
Photograph showing strain and displacement instrumentation

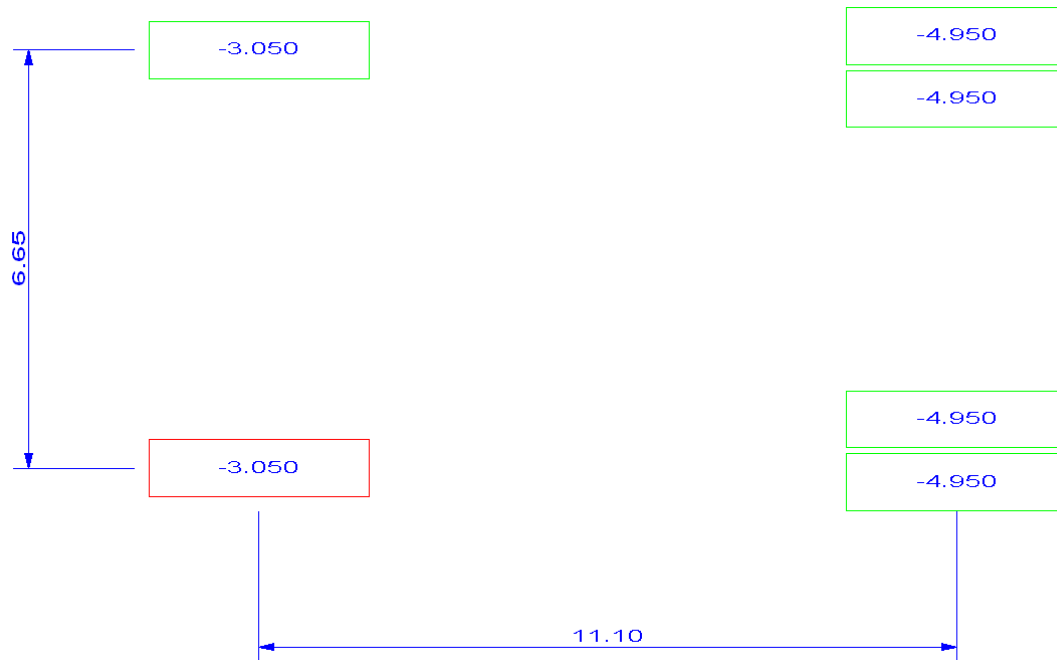


Figure 22
Test truck footprint – single rear axle dump truck (Test 1)

(Note: Numbers in boxes are wheel loads in lbs.)

DISCUSSION OF RESULTS

First, all of the field data was examined graphically to determine its quality and to provide a qualitative assessment of the structure's live-load response. Some of the indicators of data quality included reproducibility between identical truck crossings, elastic behavior (strains returning to zero after truck crossing), and any unusual-shaped responses that might indicate nonlinear behavior or possible gauge malfunctions.

In addition to providing a data "quality check," the information obtained during the preliminary investigation was used to determine appropriate modeling procedures and helped establish the direction that the analysis should take. The majority of discussion on the bridge response behavior was obtained from the initial set of tests. A comparison of data is made between the two sets of tests to evaluate any change in performance.

Preliminary Data Review Observations

Reproducibility and Linearity

Responses from identical truck paths were reproducible, as shown in Figure 23. In addition, all strains appeared to be linear with respect to load magnitude (truck position) and all strains returned to zero, indicating that the structure was acting in a linear elastic manner. Also seen in this graph are the responses from Beam B1 at the mid-span of spans 1, 2, and 3 for the western truck path. The test was conducted by using two passes with the supplied dump truck. All of the strain histories had a similar degree of reproducibility.

Distribution

The lateral load distribution of this structure was measured at several cross-sections using both strain transducers and displacement (LVDT) sensors. The results obtained from the LVDT sensors were the best representation of the lateral load distribution of the structure since the flexural cracks that were present did not affect displacement measurements as much as the strain measurements. Figure 24 displays the results from the VDTs at maximum midspan deflection.

Continuity of Spans

As expected, continuity was very minimal at all tested bearing locations. End spans were not tested and therefore end-restraint due to abutments could not be analyzed. The instrumented beams were simply-supported at the piers and provided only minimal continuity. The small amount of continuity between spans was likely the result of slight translational movement at the top of the pier. Figure 25 shows the slight continuity observed between spans. See Figure 26 for a photo of the pier support conditions. Based on these responses and bearing

type, only translational restraint springs were used for the pier supports. A small eccentric element would also be used to connect the two spans to simulate the continuity that was observed. The condition of the bearings varied significantly. Figure 27 shows a beam bearing with substantial damage and very little remaining bearing surface. Because of this variability in condition, any end-restraint resulting from the model calibration process should be removed prior to load rating calculations.

Response Symmetry

Overall, the shapes of the response histories responses indicated that the structure was deforming in a symmetric manner. Displacement measurements provided the best indication of the global behavior and it was apparent from the LVDT measurements in Figure 24 that the structures' deformations were symmetric. There was a larger variation in strain magnitudes from beam to beam, but this is to be expected from reinforced concrete.

Influence of Cracks

During the sensor installation, visible flexural cracks and shear cracks were noticed. The density and size of the cracks appeared normal for a reinforced concrete bridge. While the use of transducer extensions helps minimize the effects of cracks on the measurements by averaging them over a longer gauge length, the effects cannot be eliminated entirely. For example, if the gauge/extension unit spans additional cracks, the output will be higher than expected. The opposite is true if there is a large crack immediately adjacent to a gauge location. Figure 28 shows the response history for two locations that should have very similar magnitudes. The variation in strain magnitude indicates the measurements are likely influenced by cracks. It is important to have an idea of how much crack influence there is prior to comparing analysis results with load test data. In this case, the influence of cracks was not significant enough to warrant modeling the local effects of the cracks.

Neutral Axis Measurements

Neutral axis locations were determined by examining the strain histories at multiple depths on the T-beam webs. Due to the presence of the cracks, the neutral axis locations varied slightly throughout the structure. Despite this, they were sufficiently close to the theoretical values for both the interior and exterior beams. Note that the neutral axis locations for the exterior beams were slightly higher than the interior beams, indicating the curbs and railings contributed to the exterior beam stiffness.

Unusual Responses(s)

The results recorded from all top flange gauges located near supports were very low in magnitude (less than 10 micro-strain) and relatively varied since they were extremely close

to the neutral axes locations; these gauges were examined to substantiate basic beam cross-section properties, but should not be used in the model calibration process.

High Speed Tests

Two high-speed tests were conducted to evaluate the live-load impact on the superstructure. None of the high-speed responses showed any significant change between high speed and low speed passes along the same vehicle path. This suggests that the actual impact factor was lower than the LFD value of 30 percent. Figure 29 shows a direct comparison of data captured during a slow and high-speed truck crossing. Note that dynamic testing was done to verify that the code specified impact factor was conservative. A much more thorough test procedure would be required to justify modifying the impact factor. There are numerous factors that influence the dynamic responses, so numerous tests would need to be run with different vehicles and at differing speeds.

Strengthening

A direct comparison of the pre- and post- strengthened test data was made. It was expected that the small volume of FRP would have minimal effect on the structural stiffness during service loads. Since the test vehicle and test procedures were nearly identical, it was expected that the strain and displacement histories would be nearly identical. The results however, indicated that the interior beam's strain and deflection values reduced by approximately 10 percent during the second load test while the exterior beams had very similar magnitudes, as shown in Figure 30 and Figure 31. While the changes were not particularly large, the observation was curious because essentially no change was expected. Furthermore, the change was relatively consistent among all three spans. There were no strengthening methods applied to Span 4, so it is not likely that the response change was related to the addition of the CFRP. Figure 32 contains strain comparisons from three locations on an interior beam. The plot shows that the strains at the L/5 locations increased during the second test by a few micro-strain while the midspan strains decreased by approximately the same magnitude. This response was typical of all interior beams. The basic change in magnitude, with respect to the location on the beam, is not consistent with what would be expected from the strengthening approach or by any changes in end-restraint at the beam bearings. The most likely cause of the change in response behavior is some type of temperature effect. The mean temperature in Zachary, LA, during the second test (76°F) was 13°F degrees warmer than it was on the first test (63°F). The change in temperature may have changed how the asphalt influenced the effective depth and stiffness of the T-beams. Slight changes in neutral axis values between the two tests supports this theory, and it would also explain why the interior beams seem to be influenced more than the exterior beams.

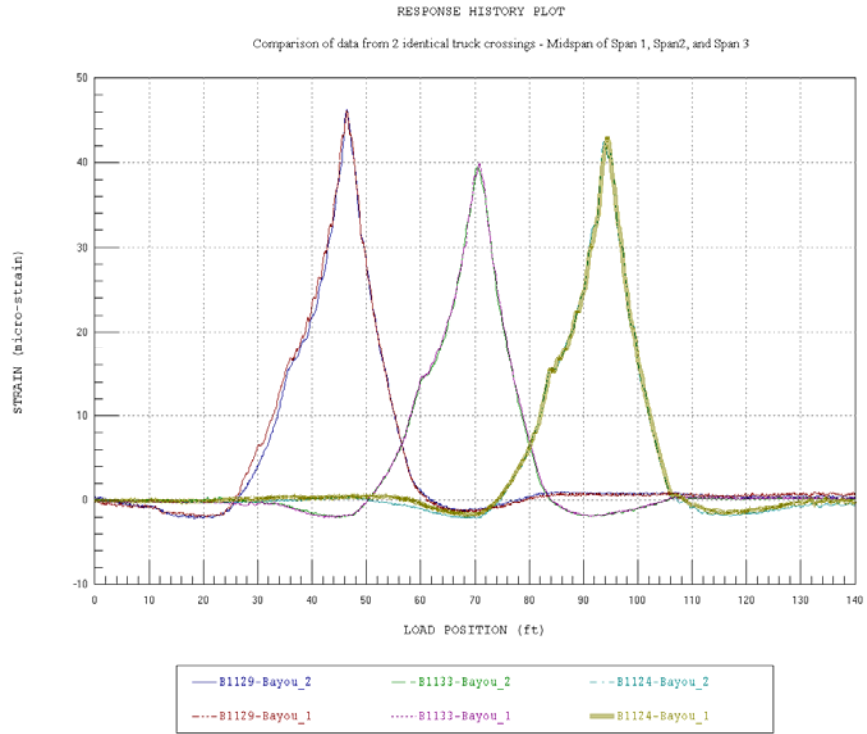


Figure 23
Reproducibility and linearity of test results

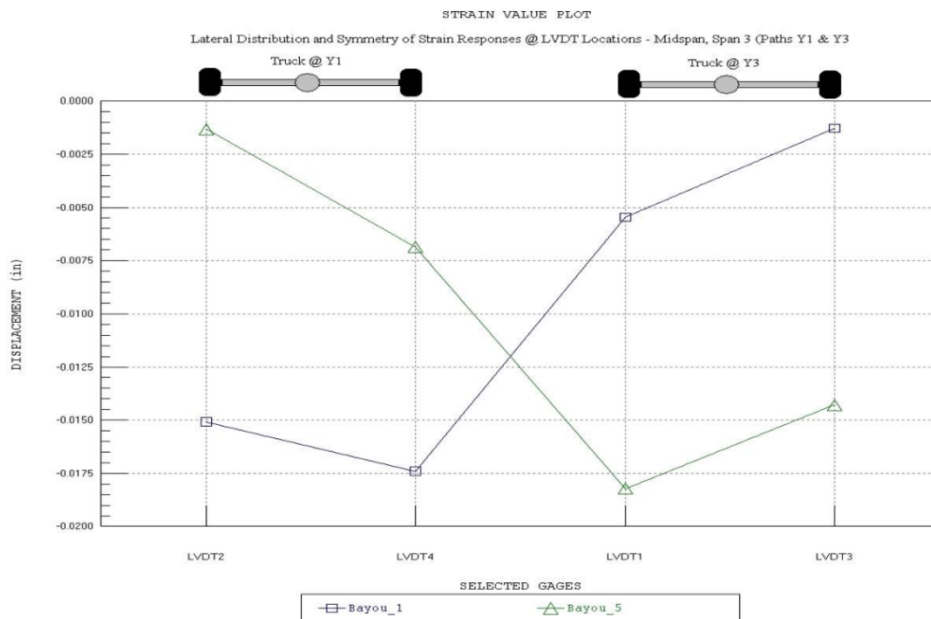


Figure 24
Lateral load distribution (LVDT results)



Figure 25
Pier support details



Figure 26
Damaged beam bearing at Pier 4

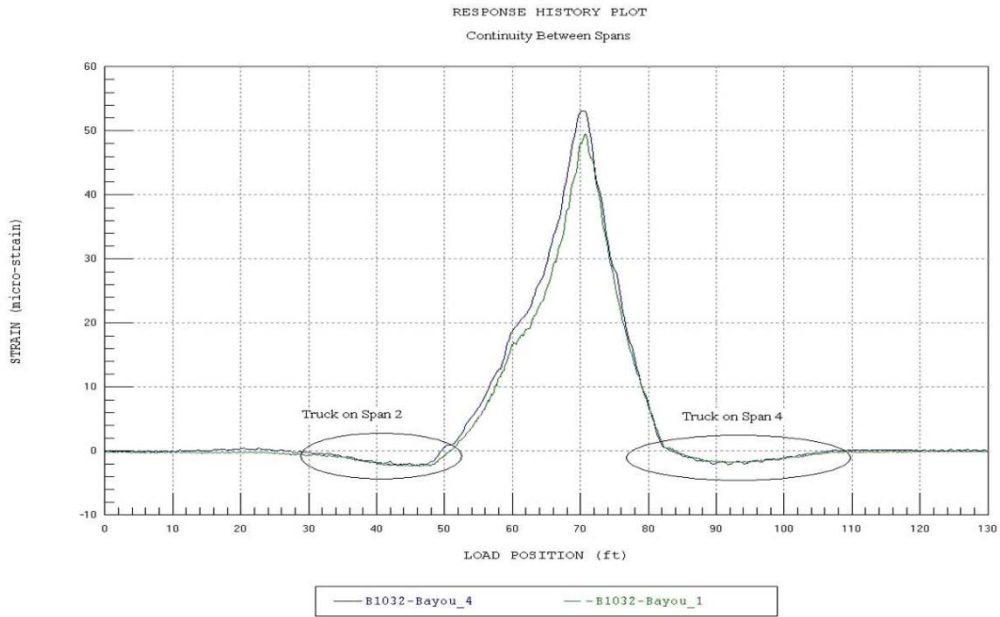


Figure 27
Slight continuity between spans

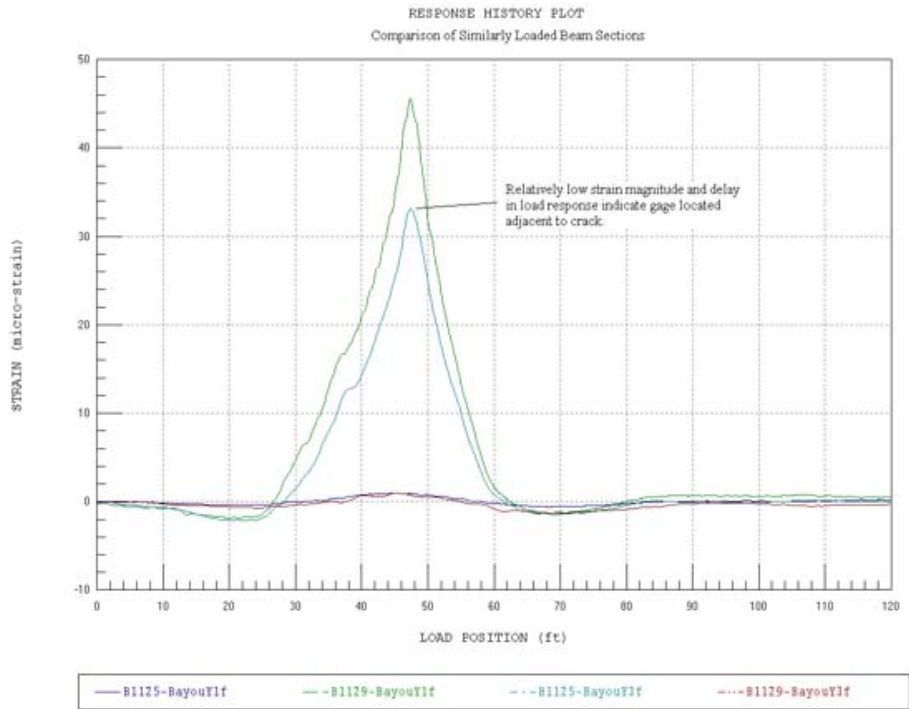


Figure 28
Influence of cracks on strain

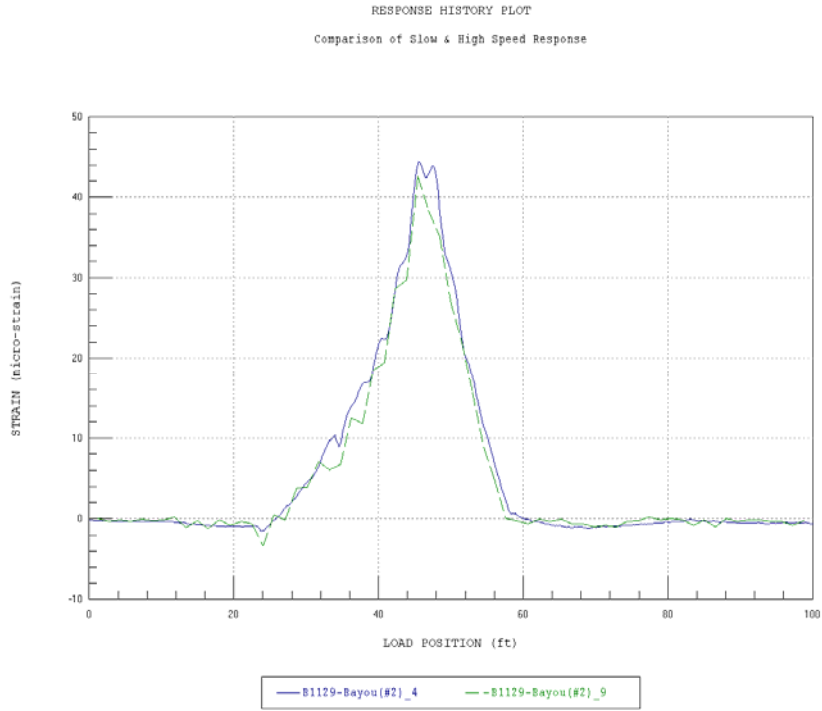


Figure 29
High-speed test results (measured impact)

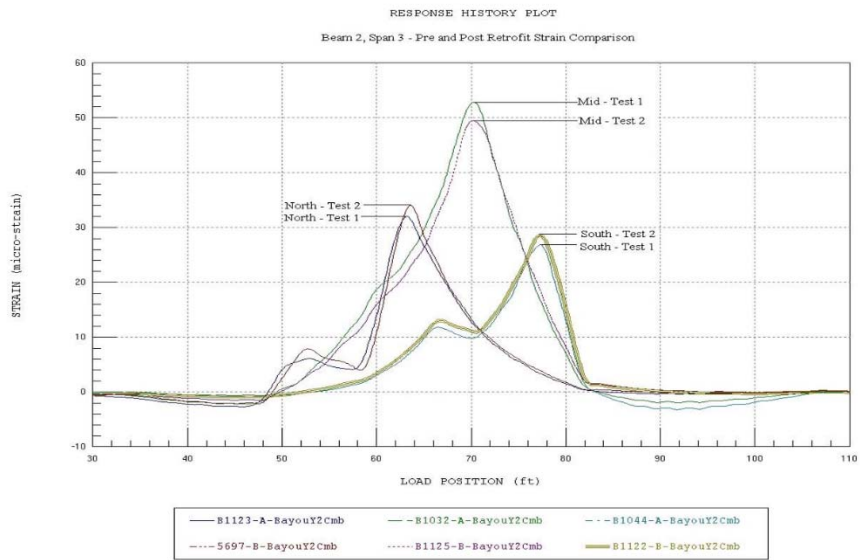


Figure 30
Pre and post strengthening strain comparison – 3 locations on interior beam

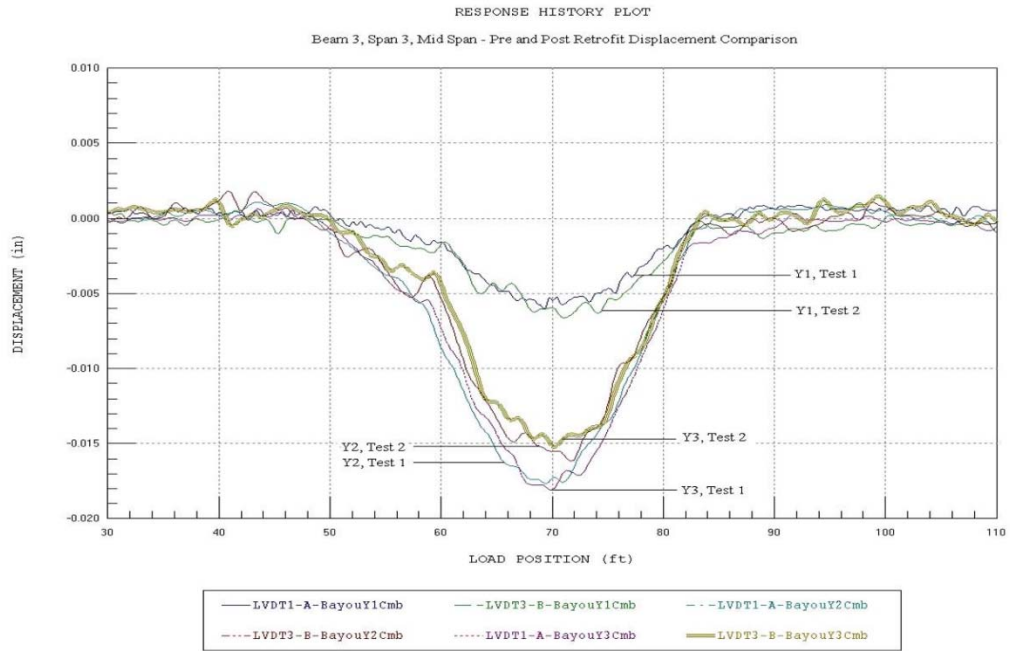


Figure 31
Pre and post strengthening displacement comparison – interior beam

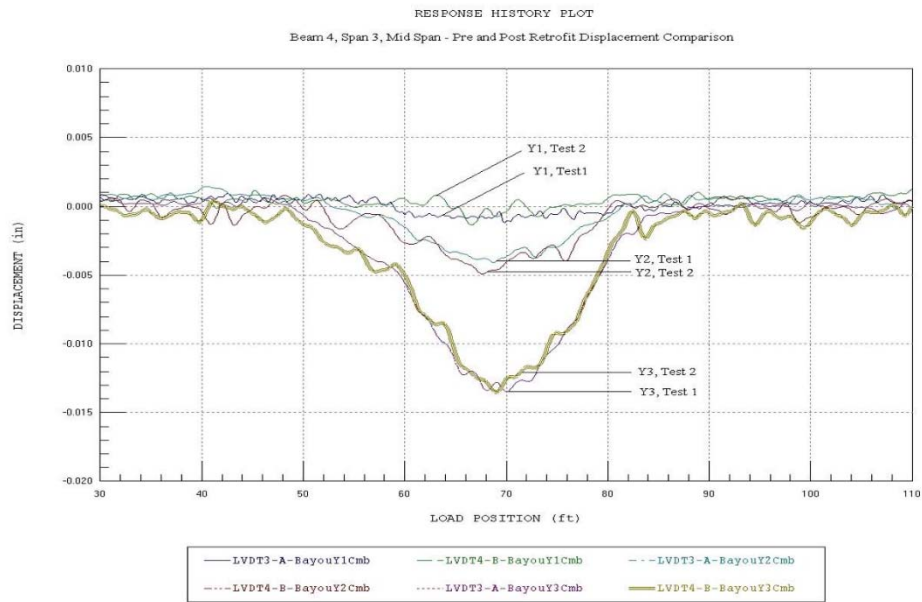


Figure 32
Pre and post strengthening displacement comparison – exterior beam

Modeling, Analysis and Data Correlation

The above information was determined by simply viewing the field data. Observations made during the preliminary investigation were then used to generate a representative finite

element model, as seen below in Figure 33. Details regarding the structure model and analysis procedures are provided in Table 6.

Once the model was developed, the load testing procedures were essentially reproduced in the model. A two-dimensional footprint of the loading vehicle was applied to the model along the same paths that the actual test vehicle used to cross the bridge. A direct comparison of strain values was then made between the analytical predictions and the experimentally-measured results. The initial model was then calibrated by modifying various properties and boundary conditions until the results matched those measured in the field.

In this case, the bridge model was calibrated using the response data from the first set of load tests (pre-strengthening). Responses from the second set of load tests were later compared with the calibrated model to evaluate any changes in response behavior.

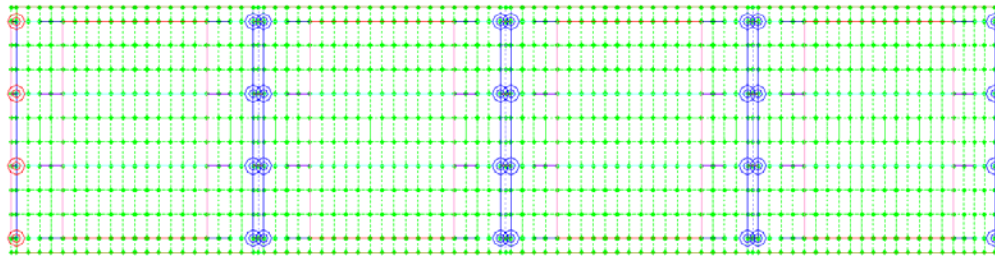


Figure 33
Finite element model of superstructure

Table 6
Analysis and model details

Analysis Type	Linear-elastic finite element - stiffness method.
Model Geometry	Planar-grid composed of shell elements, beam elements, and springs.
Nodal Locations	Nodes placed at all bearing locations. Nodes at all four corners of each plate element.
Model Components	Plates for all slab elements. Eccentric beam elements for each beam line, diaphragm, and curb. Springs elements at each support.
Live-Load	2-D footprint of test truck consisting of 6 vertical point loads for the dump truck. Truck paths simulated by series of load cases with truck moving at 2-foot increments.
Dead-Load	Self-weight of structure.
Number of Load Case Positions Compared	50 x 4 lateral load paths = 200 Load case positions compared
Total Number of Strain Comparisons	40 strain points x 200 load positions = 8000 Strain Comparisons
Model Statistics	1080 Nodes

	696 Elements 12 Cross-section/Material types 50 Load Cases 40 Gauge locations
Adjustable Parameters for Model Calibration	1. Rotational springs at abutment support and Piers (F_x & M_y) 3. Deck slab Young's modulus (E) 4. Exterior beams Young's modulus (E) 5. Interior beams Young's modulus (E) 6. Curb Young's modulus (E) 7. Construction Joints Young's modulus (E)

Model Calibration Results

Several stiffness parameters were modified to obtain the best correlation between the measured and computed strain responses. The parameter values used in the initial model and obtained for the final model are provided in Table 7. Note that the stiffness parameters typically selected for modification were the modulus of the beam or slab sections. The resulting element modulus represented the effective homogenous material stiffness and includes the effect of crack density and the volume of steel in the reinforced concrete. Resulting modulus values should, therefore, not be considered as a true representation of the actual concrete modulus. The relative difference in material stiffness generally provides a measure of relative crack density at the various locations on the structure. Following the optimization procedures, the model produced a .9800 correlation. The initial and final correlation, as well as other statistical error values are also provided in Table 7.

Element Stiffness

The effective mid-span stiffness and end section stiffness of the interior and exterior beams increased significantly from the initial assumed values. The difference between these two stiffness values was expected due to a higher crack density at mid-span. The concrete overlay on the bridge deck increased the effective thickness of the slab and contributed to the higher “effective” modulus values for both the beam and slab components.

Deck Stiffness

Overall effective stiffness of the deck increased. This could be a result of a few inches of asphalt on top of the structure and/or the significantly high strength aggregate used in the original concrete. There was talk of exceptionally hard concrete on this bridge, but the resulting modulus values were very high.

Pier Support Conditions

Since the pier support conditions were such that there was a physical gap between the spans, axial restraint springs alone were used to simulate the friction at the beam bearings. The concrete beams were bearing directly on the pier, causing a small amount of pier movement and slight continuity between spans. At a few locations, the beam bearing location was damaged. The axial forces generated by temperature effects and end rotation likely caused the deterioration at the supports.

Parapet/Curb Stiffness

The effective stiffness for the parapet/curb increased since the interaction between the parapet and exterior beams had a significant effect on the structure's edge stiffness. This type of response significantly improved the effective lateral load distribution of the bridge deck.

Table 7
Model accuracy and parameter values

MODELING PARAMETER (UNITS)	INITIAL MODEL VALUE	FINAL MODEL VALUE
Pier axial spring (kips/in)	0	687.3
Beam stiffness – mid-span (ksi)	3,600	7,086
Beam stiffness - end (ksi)	3,600	9,567
Beam stiffness - bearing (ksi)	3,600	2,875
Deck stiffness (ksi)	3,600	6,474
Curb stiffness (ksi)	3,600	10,700
ERROR PARAMETERS	INITIAL MODEL VALUE	FINAL MODEL VALUE
Absolute Error	41,102	8,546
Percent Error	149.3%	4.0%
Scale Error	13.2%	2.0%
Correlation Coefficient	0.9674	0.9800

Load Rating Procedures and Results

The goal of producing an accurate model was to predict the actual live load behavior of the structure when subjected to design or rating loads. This approach is essentially identical to

standard load rating procedures, except that a field verified model is used instead of a typical beam analysis combined with load distribution factors.

Once the finite element model was calibrated to field conditions, engineering judgment was used to address any optimized parameters that may change over time or that may be unreliable with heavy loads or future damage. In this case, the optimized stiffness values for the beams, deck, and curb were used as rating since there was no evidence to support adjusting the values manually. The pier springs were reduced to zero since some of the beam bearings were damaged and because it is likely that the friction is time-dependent with respect to load duration and load rates. Reducing end-restraint values is a conservative approach which results in an increase in live load mid-span moment and a lower load rating.

Member capacities were calculated using the Standard Specifications for Highway Bridges, 17th Edition - 2002. Load rating factors for the standard AASHTO H-20, HS-20, Type 3, Type 3-3, and Type 3S3 vehicles were computed according to the LFD rating method. Load and resistance factors used in the rating are listed in Table 8.

Table 8
Load and resistance factors

LOAD	TYPE	FACTOR
Dead Load	Structural	1.30
Live Load	Inventory	2.17
	Operating	1.30
Impact Factor	IM	0.30
Multiple Lane Factor, <i>m</i>	No. of Lanes	
	1	1.00
	2	1.00

Section capacities were calculated based on the set of standard Louisiana Department of Transportation Specifications, which was provided for the structure. From the standards provided, it was found that the steel reinforcement allowable stress (f_s) was 20 ksi, which, based on the design code at the time this bridge was built, corresponds to a yield stress (f_y) of 40 ksi. Figure 34 and Table 9 show typical beam reinforcement and rebar arrangements, respectively. The concrete was assumed to have a compressive strength (f'_c) of 5,000 psi. This is a high compressive strength for standard reinforced concrete, but justified and still conservative based on the model optimization results. The computed moment capacities for the interior and exterior girders are provided in Table 10.

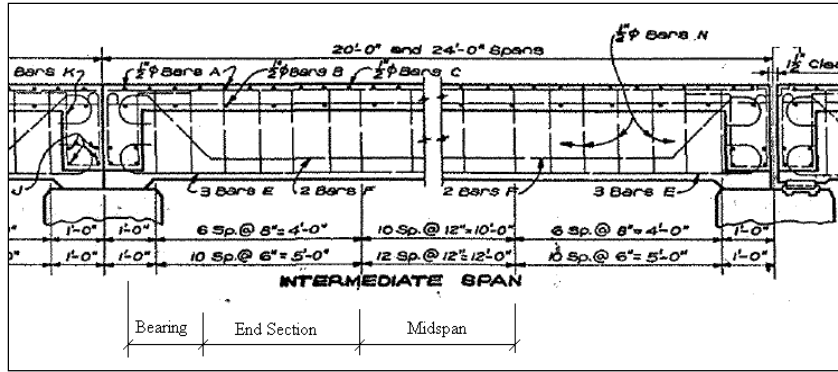


Figure 34
Tee beam steel details

Table 9
Girder section and steel details

Section	Details					
	Shear			Moment		
	-	-	-	M Bars	# Bars	Area Steel
Midspan	-	-	-	1 1/8" sq.	5	6.328
End	-	-	-	1 1/8" sq.	5	6.328
Bearing	-	-	-	1 1/8" sq.	3	3.800

Table 10
Tee beam moment capacities

MEMBER	MOMENT CAPACITY, $\phi_f M_n$ (kip-in)
Interior Girders – Mid-span	4407
Interior Girders – End	4407
Interior Girders – Bearing	4407
Exterior Girders – Mid-span	4407
Exterior Girders – End	4407
Exterior Girders – Bearing	4407

Maximum live and dead load moment responses for each load configuration were obtained from the field verified finite-element model. The live load moment values present in Table 11 through Table 15 are the un-factored live load and dead load responses. Rating factors for the bridge prior to any strengthening procedures were computed for the H-20, HS-20, Type 3, Type 3-3, and Type 3S3 are also provided.

Table 11
Load rating factors for H-20

Group	Name	Mode	RF	Element#	Node	Envelope	DL Response	LL Response
1	Ext_Girders_Midspan	+My	1.71	123	2	6	543.7	764.9
2	Int_Girders_Midspan	+My	1.03	212	2	6	647.9	1231.3
12	Int_Girders_End	+My	1.59	205	2	6	411.2	865.2
13	Ext_Girders_End	+My	2.56	160	2	6	361.6	545.5

Table 12
Load rating factors for HS-20

Group	Name	Mode	RF	Element#	Node	Envelope	DL Response	LL Response
1	Ext_Girders_Midspan	+My	1.69	123	2	6	543.7	775.7
2	Int_Girders_Midspan	+My	1.03	212	2	6	647.9	1231.3
12	Int_Girders_End	+My	1.39	205	2	6	411.2	991.8
13	Ext_Girders_End	+My	2.2	160	2	6	361.6	633.2

Table 13
Load rating factors for Type 3

Group	Name	Mode	RF	Element#	Node	Envelope	DL Response	LL Response
1	Ext_Girders_Midspan	+My	1.9	122	2	6	548.6	688.6
2	Int_Girders_Midspan	+My	1.12	211	2	6	653.9	1127.3
12	Int_Girders_End	+My	1.86	205	2	6	411.2	739.7
13	Ext_Girders_End	+My	3.08	160	2	6	361.6	453.3

Table 14
Load rating factors for Type 3-3

Group	Name	Mode	RF	Element#	Node	Envelope	DL Response	LL Response
1	Ext_Girders_Midspan	+My	2.31	122	2	6	548.6	566.5
2	Int_Girders_Midspan	+My	1.37	211	2	6	653.9	923.9
12	Int_Girders_End	+My	2.16	205	2	6	411.2	637.6
13	Ext_Girders_End	+My	3.5	116	2	6	361.8	398.9

Table 15
Load rating factors for Type 3S3

Group	Name	Mode	RF	Element#	Node	Envelope	DL Response	LL Response
1	Ext_Girders_Midspan	+My	2.06	122	2	6	548.6	636.5
2	Int_Girders_Midspan	+My	1.22	233	2	6	653.9	1037.5
12	Int_Girders_End	+My	1.92	227	2	6	411.2	715.4
13	Ext_Girders_End	+My	3.17	160	2	6	361.6	440.5

To evaluate the benefit of the various FRP strengthening procedures, load ratings were performed on each of the strengthened beam types. Modified moment capacities, based on the geometry of the strengthening schemes used and published material properties, were calculated as described in Chapter 2. The capacities were calculated in general conformance with ACI 440.2R-02 [ACI, 2002]. Table 16 contains the ultimate moment capacities of the original beam and each of the strengthened beam types. To provide an indication of the increased live-load capacity presented by the FRP strengthening, HS-20 load rating factors are also supplied for each beam type. A substantial increase can be seen in all the load rating factors.

Table 16
Moment capacities and load rating factors of strengthened beams

Beam Type	ΦM_n (kip-in)	HS-20 Load Ratings			
		RF _{Inv.}	Tons	RF _{Oper.}	Tons
Original T-beam	4,407	0.93	33	1.54	56
Carbodur S512 – Near surface mounted strips	5,844	1.32	48	2.21	79
Vwrap C100 - Wet layup	5,525	1.24	44	2.06	74
Carbodur S512 – Pultruded strips	5,095	1.12	40	1.86	67

It is important to note that the rating results provided for the strengthened sections are not intended to be representative of the overall bridge load capacity. The flexural strengthening applied was not intended to improve the shear capacity. Shear strengthening was not required since the shear capacity of the existing structure was adequate. The flexural strengthening was only performed on two of the eight spans. The primary purpose of the research project was to evaluate the feasibility and long-term performance of the various strengthening methods. Therefore, the current posted load limits should not be changed. In the event that strengthening of all spans is to take place in the future, shear strengthening should be fully evaluated.

Description of Long-Term Monitoring

In addition to the load test and subsequent analyses procedures, a long-term monitoring system was installed to help evaluate the long-term performance of the CFRP strengthening systems. The monitoring system was designed primarily to evaluate slow-speed responses due to temperature and permanent responses due to settlement and/or damage. The monitoring system can also be used to perform static live-load tests as a means of periodic evaluations. Strain sensors are mounted to both the surface mounted FRP and the concrete on Span 3 with the intent of detecting possible delamination during a pure static load test.

Long-Term Monitoring System

In order to monitor the long-term performance of the strengthening methods, a structural monitoring system was installed on the bridge. The long-term monitoring system includes several strain and crack measurement sensors that are monitored on a continuous basis. There are numerous temperature sensors which obtain the ambient temperature, temperature of each displacement type sensor, and the internal temperature of the concrete beams. A relative humidity sensor is also installed.

The monitoring system is intended to measure and record slow-speed and permanent movements, such as those from temperature, settlement, creep, and/or damage. The system is not intended to measure any live-load responses, except under a complete static situation. Measurement cycles occur at a 60 second interval so that responses due to normal traffic conditions will not be captured.

Figures 35 through 37 contain the long-term instrumentation plans for Spans 2, 3, and 4. The two strengthened spans and the unstrengthened control span are instrumented in a manner similar to the live load tests. In general, the midspan strains are measured along with a crack opening displacement. Strain gauges were installed on both the concrete and on the CFRP at Span 3 where the surface mounted FRP was applied. Sensor locations designated at S# refer to strain gauges, C# refer to crack displacement, and T# indicates an embedded thermistor.

The data logger setup consists of a Campbell Scientific, Inc. CR10X measurement and control device. The system is powered with a 20 watt solar panel and contains a 12 V battery to maintain operation at night. A cell modem is provided so that data can be retrieved and the logger control can be performed remotely. A custom program was written for the logger to measure the specific sensors and perform various data processing tasks. The original program was written to measure each sensor on a 60 second interval and then to compute and store the averages and extreme values from each sensor once an hour. The logger operation can be controlled remotely via modem or by a PC connected directly to the logger. However, as mentioned in an earlier section, the closure of the engineering programs at Tulane University and the loss of faculty engaged in this project did not permit the long-term monitoring or data collection using the cell modem after all the tasks planned during the project funding period were concluded. Despite this, there is no reason to believe that the modem is not operational or unable to allow the collection of data if the cellular service was available.

An option exists to record the raw data on every measurement cycle (60 seconds). This feature is useful to run static load tests on a periodic basis. The continuous measurement cycle can be initiated and run for a few minutes after which a specific load can then be applied to the bridge and left in place for another two minutes. Various load conditions can be applied, but each change in load condition should remain in place for at least two minutes to ensure that all sensors have recorded the new load condition. It will be very important to record the logger time during each load event. Following any procedures during which data is recorded continuously, it will be important to turn off the continuous recording feature. The logger memory will fill up within hours during the continuous recording; whereas, several months of data can be stored when only the hourly recording is performed.

All communication and control of the logger is performed with the CSI LoggerNet software. Complete instructions are available in the LoggerNet software manual. Basic information on how LoggerNet is used to communicate with the White Bayou data logger and specific details on the data-logger program are provided in the report by BDI related to this project.

The data logger is not intended to replace visual inspection. It should be viewed as a tool to help with visual inspection and provide information as to what areas may need to be examined.

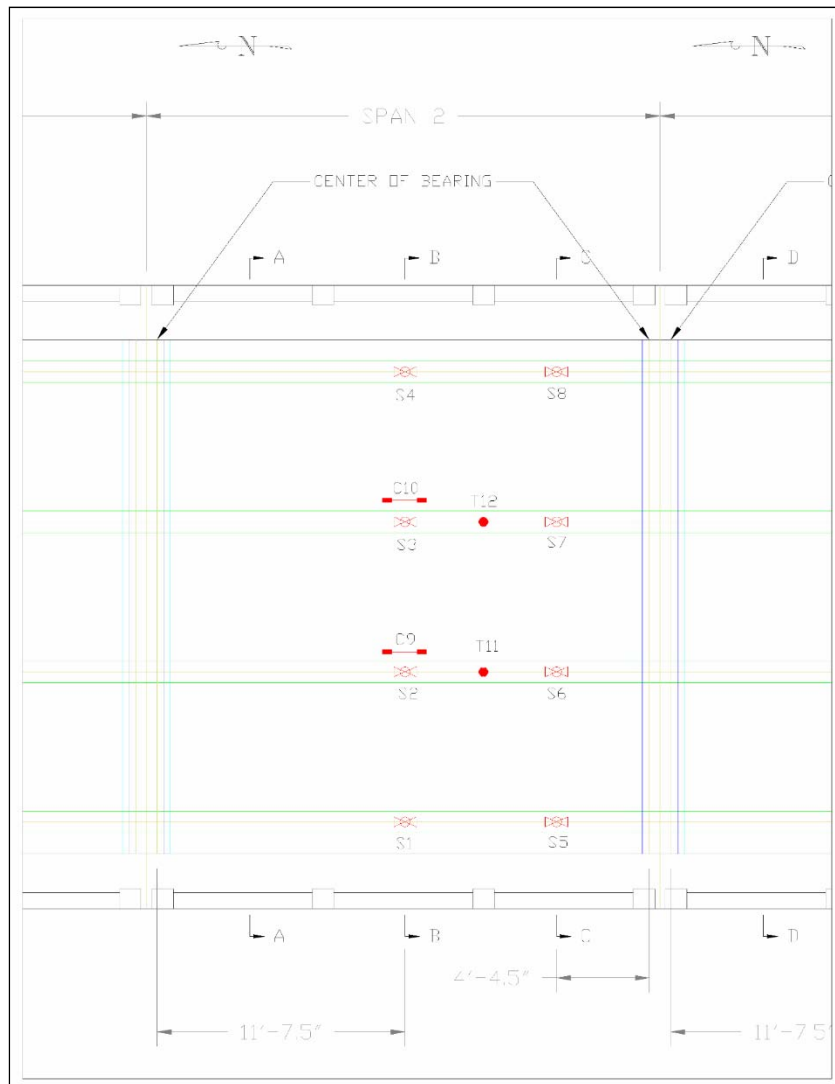


Figure 35
Long-term instrumentation plan – Span 2

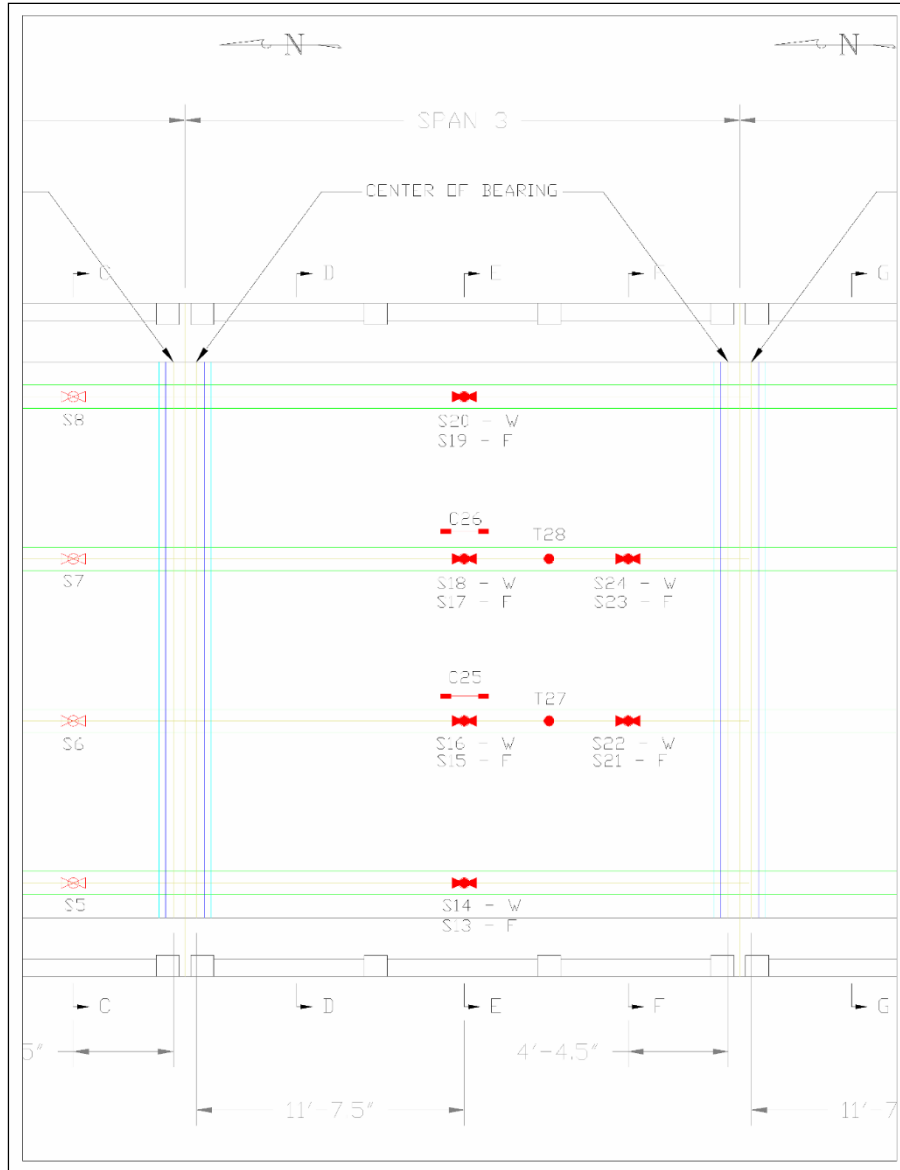


Figure 36
Long-term instrumentation plan – Span 3

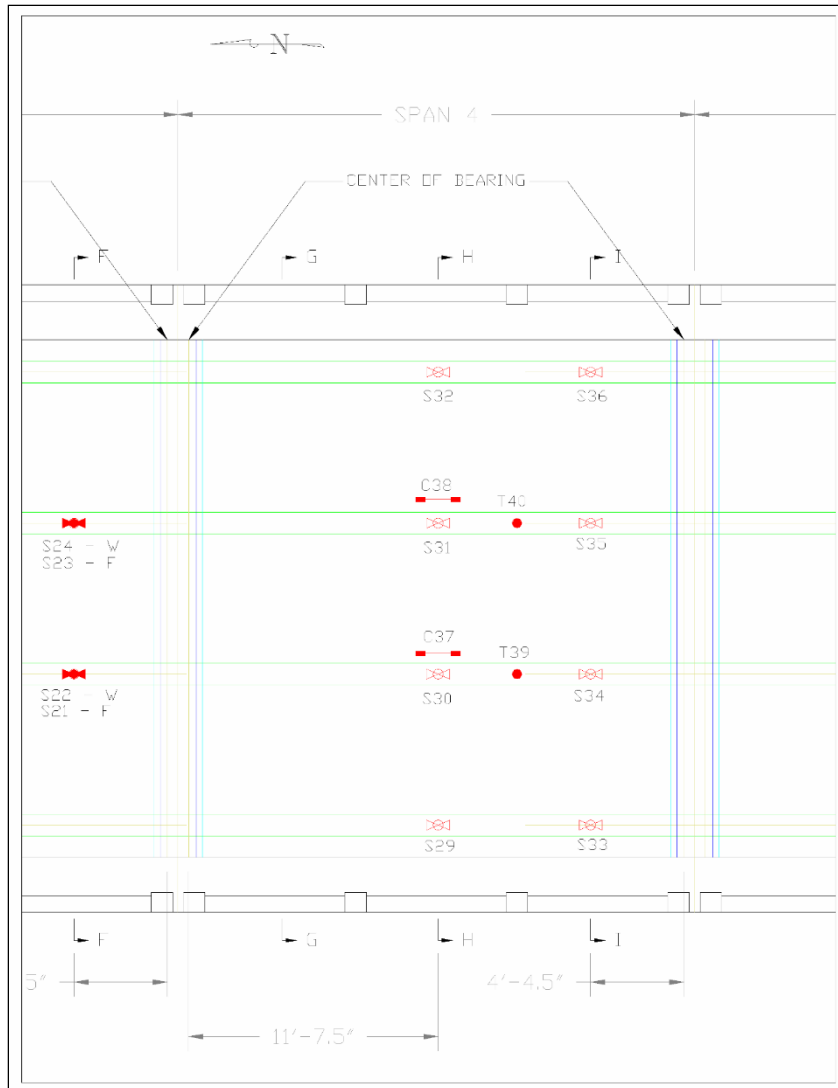


Figure 37
Long-term instrumentation plan – Span 4

CONCLUSION

The literature review and the experience of the investigators led to the selection and installation of three different strengthening systems to be installed on White Bayou Bridge.

Field Applications

From the review of the existing literature, it was found that CFRP wet layup as well as CFRP pre-cured plates have been widely used in the past. In one instance, near surface mounted CFRP rods were used. Each of these systems appears to be easily implemented in the field. In the case where CFRP wet layup and near surface mounted rods were used on the same project, it was mentioned that the near surface mounted method was more readily installed. Both systems produced good results when the strengthened spans (flat-slabs) were tested to failure. The CFRP wet layup system was noticed to fail prematurely due to debonding, in some instances.

In addition to the published literature, during the January 2004 meeting of the Transportation Research Board, a presentation was made regarding a field application of a post-tensioned CFRP system. In this case, a post-tensioned CFRP system was applied to an existing prestressed bridge in Ohio. The application was reported as generally successful. A CFRP post-tensioned system has also recently been successfully applied to a steel stringer bridge in Iowa [23].

When field applications were conducted in combination with load testing, it was generally noted that the strengthening systems increased the overall stiffness of the structures. However, this increase in stiffness was small. This suggests a need for additional methods of assessment, as well as good resolution for strain and displacement measurements.

Laboratory Investigations

Several different methods of strengthening were studied in full or large-scale laboratory investigations. These included CFRP wet layup, CFRP pre-cured strips, and CFRP post-tensioned rods. When CFRP pre-cured strips were adhesively bonded to the surface of the specimens, the strips generally were found to debond at lower levels of ultimate than the CFRP wet layup method. This is due to the increased out-of-plane stiffness and smaller contact area for adhesive bonding of the pre-cured plates. In one study, the pre-cured plates were bonded not to the bottom but rather to the sides of the specimens to delay the debonding mechanism. Transverse wet layup straps were used for both CFRP wet layup and pre-cured strips, also to delay debonding. The use of mechanical anchorages at the ends of the pre-

cured strips was investigated, as well, and found to provide satisfactory results. The use of CFRP post-tensioned rods provided satisfactory results.

Analysis and Design Considerations

The finite element method was found to provide reasonably accurate results, both for the prediction of stiffness and ultimate strength. For the study summarized, the predicted strengths were generally less than those obtained from laboratory investigations.

In regard to analytical models, the ACI 440 method (2000 edition) was investigated and found to provide reasonable results in one study. However, it was noted that the ACI method is based on the use of the Whitney stress block and this may not be appropriate for beams that have been externally strengthened. The debonding coefficient given in the ACI method may also be questioned in certain instances. It is noted that the ACI 440 document has recently been revised.

RECOMMENDATIONS

It is recommended that finalized designs based on the three systems be developed and a particular manufacturer selected. The CFRP post-tensioned systems that are currently available are often proprietary. The differences in the systems are centered primarily on the end connections. It is recommended that a short list of qualified suppliers and installers be developed with input from the project investigators. Once the short-list is developed, the LA DOTD and LTRC should select a single supplier and installer (sole source), again with input from the project investigators. The materials and installation methods will be similar among the different suppliers, but some variation is to be expected. Once a supplier and installer are selected, construction documents should then be developed and a price and timetable for the strengthening installation established. Since all three reinforcing methods provided adequate flexural strengthening, a decision on the particular method to be used needs to be based on cost and the results of reasonable long-term performance monitoring—18 to 24 months—of the systems.

For strengthening applications, proper installation of the systems is critical to both the short and long-term performance. Furthermore, it will be to the benefit of the state to assess the quality of FRP systems that are installed by qualified personnel. Because of this, it is not recommended that inexperienced personnel (such as graduate research assistants or inexperienced contractors) install the strengthening systems.

In regard to field monitoring and load testing, systems that are durable and that have sufficient sensitivity to assess the different strengthening systems should be selected and implemented.

The primary objective of this research project was to evaluate the feasibility of using CFRP strengthening to increase the live load capacity of existing bridges in Louisiana. Currently, there are many load-rated bridges and often these bridges are reinforced concrete tee beam bridges that are deficient in flexure.

A demonstration bridge was selected in cooperation with the LTRC and DOTD. The bridge is located in Zachary, Louisiana, and carries Highway 19 over White Bayou. Portions of the bridge were live load tested both before and after strengthening in the spring of 2007. Two spans of the bridge were strengthened; one span was strengthened entirely with CFRP near surface mounted strips, the other by CFRP wet layup on two of the four beams and with CFRP pultruded strips on the adjacent two beams. One of the spans was instrumented but was not strengthened and used as a control span. In addition to the significant live load

testing efforts, a long term monitoring system was installed and the details of that system are described. Shear strengthening was not an issue for this bridge.

Conclusions made from the live load test data were qualitative in nature and indicated that the structure was behaving typical for a reinforced concrete structure. The structure appeared to be in fair condition with visible flexural and shear cracks. All strain measurements indicated that the structure was behaving linearly with respect to load magnitude (truck position) and all responses were elastic. It was also noted that some of the beam bearing locations had experienced damage. The damaged beam bearings have not yet significantly altered the structural performance but a significant reduction in bearing area has occurred.

As is typical of RC structures, flexural cracks were observed at various locations on the beams. Load test results and subsequent model calibration indicated a higher density of cracks at mid-span (higher flexibility) than near the beam ends. This result was expected since crack formation is related to the moment magnitude. The resulting member stiffness was exceptionally high compared to what was initially assumed. Exact reasons for this are not definitively known, though it is possible the actual deck thickness is greater than what was indicated by the Louisiana design standard.

Load tests were performed before and after the implementation of CFRP strengthening to two of the spans. While a change in ultimate capacity was expected, it was not expected that the responses within the serviceability limits would be noticeably different. Load test procedures and load magnitudes were nearly identical between the two load tests, yet the measurements indicated a reduction of midspan strains and midspan displacement of approximately 10 percent on the interior girders for the second load test (after strengthening). It is important to note that the same level of change was observed on both the strengthened and un-strengthened (control) spans. Therefore it does NOT appear that the increased stiffness of the interior girders was a result of the CFRP strengthening.

The CFRP strengthening had a significant effect on the load rating factors resulting from moment capacity. The CFRP strengthening methods used were not intended to increase shear capacity; however, it is possible that shear capacity was marginally increased in some cases due an increased value of 'effective depth' caused by the CFRP strengthening. The primary focus of this study was to evaluate the feasibility of CFRP flexural strengthening and to help evaluate the long-term performance of the systems. It was not intended to increase the actual load limit on the bridge, as only two of the eight spans were strengthened. Therefore current posted load limits should be unaffected based on the CFRP strengthening.

The costs associated with the CFRP strengthening methods were as follows:

- a) CFRP strengthening materials - \$8,500 (estimated)
- b) Installation of all three systems - \$18,500 (completed by Structural Preservation Systems)
- c) Scaffolding - \$15,000 (provided by DOTD)

Because of the relatively small amount of strengthening that was provided and the research-based nature of the work, the costs that are noted above are not likely to be reflective of what would be encountered in practice for more significant strengthening projects. The cost of strengthening projects is highly dependent on access to the structure and ease with which a work crew can be mobilized. However, some information can still be gained.

In conversations with the contractor responsible for the strengthening, it was clear that the wet layup technique was preferred due to its ease of installation, past positive experience, and perceived reliability. The pultruded strip method was viewed in a similar light. Both methods required surface preparation prior to installation. The near surface mounted strip method, by contrast, had been little used in the past and was viewed as being the most difficult to install. This was true even though this method did not require as much surface preparation. It is generally believed by the authors that the wet layup system has a high degree of reliability and the pultruded strip method perhaps less so. This is partially due to the smaller contact area with the pultruded strip method, but is also due to the method of application itself, which involves impregnating in place in the case of the wet layup method, as opposed to pressing or rolling the cured strip in place in the case of the pultruded strip method. The near surface mounted method is believed to be the most reliable due to the relatively high amount of contact area between the strips and the surrounding concrete.

The near surface mounted system is also less intrusive visually and very little of the CFRP material is exposed to vandalism. It would seem that this method affords a larger degree of fire resistance than the other two methods, but this was not directly assessed and is beyond the scope of the project. One way to verify these statements is through destructive testing of portions of the bridge, recommended to be done after the bridge is taken out of service. This can be done either in place or sections can be cut from the bridge and the resulting tee beams tested in a laboratory setting.

When viewing the cost data, it seems most expedient to compare costs on a per square foot of bridge basis so that projections can be made for other strengthening projects. If this approach is taken, the costs would be approximately \$7 per sq. ft. of bridge for materials and \$16 per sq. ft. of bridge for labor. It is emphasized that these costs will vary for each strengthening

application and are likely to be lower in practice for more significant applications. The costs of strengthening should be considered against the cost of replacement and the costs associated with load posting of the bridge (transportation costs). It is clear from the project that the systems can be readily installed, and it is likewise clear that it is at least theoretically feasible to remove load restrictions from posted bridges, if the reasons for posting are related to structural concerns such as flexural capacity.

If strengthening with CFRP materials is to be conducted on a more widespread basis in the future, the durability of the strengthening systems will be of utmost importance. For this reason a long-term monitoring system has been installed on the bridge and the data should be recorded for as long as possible. Any significant changes in the data should be investigated as soon as feasible through visual inspection of the affected areas of the bridge. While the addition of CFRP strengthening is expected to reduce the live load stress in the reinforcing bars and, therefore, to increase the fatigue life of the tensile reinforcing, gauges were not placed on the steel reinforcing bars to verify the extent of this effect. It is noted that the long-term monitoring system is not a replacement for scheduled visual (or other) inspections.

ACRONYMS, ABBREVIATIONS, AND SYMBOLS

AASHTO	American Association of State Highway and Transportation Officials
ACI	American Concrete Institute
ASTM	American Society of Testing methods
BDI	Bridge Diagnostic Inc.
CDF	cumulative distribution function
CFRP	Carbon Fiber Reinforced Polymer
CSI	Campbell Scientific Inc.
DL	Dead load
DOTD	Louisiana Department of Transportation and Development
f'_c	28-day Compressive Strength of Concrete
FHWA	Federal Highway Administration
FRP	Fiber Reinforced Polymer
fs	Allowable tensile stress
ft.	foot (feet)
ft./sec	feet per second
IM	Impact Factor
GVW	Gross Vehicular Weight
km	kilometer(s)
ksi	1000 pounds per square inch
kN	Kilo Newton
LA	Louisiana
LFD	Load Factor Design
LL	Live Load
LTRC	Louisiana Transportation Research Center
LVDT	Linear Variable Differential transformer
m	multiple lane factor
MoDOT	Missouri Department of Transportation
MPa	Mega Pascal
NSM	Near Surface Mounted
NYSDOT	New York State Department of transportation
PSI	pound per square inch
R.C.	Reinforced Concrete
RF	Rating Factor
RF_{inv}	Inventory Rating factor
RF_{opr}	Operating Rating factor

R_n	Nominal Strength of member
ϕ_f	Strength reduction factor
STS	Structural Testing Systems
TXDOT	Texas Department of Transportation
US	United States

REFERENCES

1. Alkhrdaji, T; Nanni, A; Chen, G; and Barker, M. (1999), *Destructive and Nondestructive Testing of Bridge J857, Phelps County, Missouri - Volume I: Strengthening and Testing to Failure of Bridge Decks*, Report CIES 99-08A, 116 pp.
2. Hag-Elsafi, S.; Kunin, J.; Alampalli, S.; and Conway, T. (2001), *Strengthening of Route 378 Bridge over Wynantskill Creek in New York using FRP Laminates*, Report FHWA-NY-SR-01-135, 33 pp.
3. Hag-Elsafi, S.; Lund, R.; Alampalli, S. (2002), *Strengthening of Church Street Bridge Pier Capbeam Using Bonded FRP Composite Plates: Strengthening and Load Testing*, Report FHWA-NY-SR-02-138, 32 pp.
4. Hag-Elsafi, S.; Kunin, J.; Alampalli, S. (2003), *In-Service Evaluation of a Concrete Bridge FRP Strengthening System*, Report FHWA-NY-SR-03-139, 21 pp.
5. Brena (2000), *Strengthening Reinforced Concrete Bridges Using Carbon Fiber Reinforced Polymer Composites*, Dissertation, The University of Texas at Austin, Department of Civil Engineering, 435 pp.
6. Kachlakev, D. and McCurry, D. (2000), *Testing of Full-Size Reinforced Concrete Beams Strengthened with FRP Composites: Experimental Results and Design Methods Verification - Final Report SPR 387*, Report FHWA-OR-RD-00-19, 36 pp.
7. Kachlakev, D.; Yim, S.; Miller, T.; and Seamanontapriya, D. (2001), *Behavior of FRP Composite-Strengthened Beams Under Static and Cyclic Loading - Summary Report SPR 387.011*, Report FHWA-OR-RD-01-20, 11 pp.
8. Shahrooz, B.; Boy, S.; and Baseheart, T. (2002), "Flexural Strengthening of Four 76-Year-Old T-Beams with Various Fiber-Reinforced Polymer Systems: Testing and Analysis", *ACI Structural Journal*, Vol. 99, No. 5, September-October, pp. 681-691.
9. Hognestad, E. (1950), *An Experimental Study of Combined Bending and Axial Load in Reinforced Concrete Members*, University of Illinois, Engineering Experiment Station, October 1950.
10. Hognestad, E., Hanson, N., and McHenry, D., (1955), "Concrete Stress Distribution in Ultimate Strength Design", *Journal of the American Concrete Institute*, Vol. 27, No. 4, December 1955, pp. 455-479.

11. Menegotto, M., and Pinto, P. (1973), "Method of Analysis for Cyclically Loaded Reinforced Concrete Plane Frames Including Changes in Geometry and Nonelastic Behavior of Elements Under Combined Normal Force and Bending", *IABSE Symposium on the Resistance and Ultimate Deformability of Structures Acted on by Well-Defined Repeated Loads*, Lisbon, 1973.
12. Kachlakev, D.; Miller, T.; Yim, S.; Chanasat, K.; and Potisuk, T. (2001), Finite Element Modeling Of Reinforced Concrete Structures Strengthened With FRP Laminates - Final Report SPR 316, Report Fhwa-Or-Rd-01-17, 111 Pp.
13. Swenson, K. and Barnes, R. (2002), *Design Procedure for FRP Strengthening of War Memorial Bridge - Interim Report 930-466*, prepared for the Alabama Department of Transportation, 62 pp.
14. American Concrete Institute Committee 440 (ACI 440) (2000), Guide for the Design and Construction of Externally Bonded FRP Systems for Strengthening Concrete Structures, unpublished draft version, July 2000.
15. Collins, M., and Mitchell, D., (1991) - *Prestressed Concrete Structures*, Englewood Cliffs, New Jersey; Prentice Hall.
16. Tedesco, J. and El-Mihilmy, M. (2001), "Prediction of Anchorage Failure for Reinforced Concrete Beams Strengthened with Fiber-Reinforced Polymers," *ACI Structural Journal*, Vol. 98, No. 3, May-June 2001, pp. 301-314.
17. Fleming, C. and King, J., (1967), "The Development of Structural Adhesives for Three Original Uses in South Africa," *RILEM International Symposium, Synthetic Resins in Building Construction*, Paris, pp. 75-92.
18. Wolf, R., and Meissler, H., (1989), "Erfahrungen Mit Glasfaserverbundstaben", *HLV-Spannglieder in der Praxis*, Beton, 2, pp. 47-51 (in German).
19. Meier, U. (1987), "Bridge Repair with High Performance Composite Materials", *Material and Technik*, Vol. 4, pp. 125-128 (in German).
20. Rostasy, F., (1987), "Bonding of Steel and GRFP Plates in the Area of Coupling Joints, Talbrucke Kattensbusch", *Research Report No. 3126/1429*, Federal Institute for Materials Testing, Germany (in German).
21. Ridge, A. (2004) "Nondestructive Techniques for Field Evaluation of FRP Strengthened

Reinforced Concrete Bridge Beams”, *Masters’ thesis, Tulane University, Dept. of Civil and Environmental Engineering*, New Orleans, Louisiana.

22. Ridge, A., and Ziehl, P., (2006), “Nondestructive Evaluation of Strengthened RC Beams: Cyclic Load Test and Acoustic Emission Methods”, *ACI Structural Journal*, Volume 103, Issue 6, pp. 832-841.
23. Wipf, T., Phares, B., Klaiber, F., and Lee, Y. (2003) *Evaluation of Post-Tension Strengthened Steel Girder Bridge Using FRP Bars - CTRE Project 01-99*, prepared for the Iowa Department of Transportation, 71 pp.

APPENDICES

APPENDIX A

Bridge Diagnostics, Inc. Report

**FIELD TESTING AND LOAD RATING REPORT:
HIGHWAY 10 OVER WHITE BAYOU (RC T-BEAM BRIDGE)
ZACHARY, LOUISIANA**

DRAFT



SUBMITTED TO:



Tulane University
Department of Civil and Environmental
Engineering
205 Walter E. Blessey Hall
New Orleans, LA 70118-5698
504-865-5779

SUBMITTED BY:



BRIDGE DIAGNOSTICS, INC.
1965 57th Court North, Suite 106
Boulder, CO 80301
303.494.3230
www.bridgetest.com

May 2007

EXECUTIVE SUMMARY

As part of a research project performed by Tulane University, in which various FRP strengthening methods were investigated, Bridge Diagnostics, Inc. (BDI) was contracted to test and evaluate a multi-span RC T-beam bridge. This bridge was located in Zachary, LA and carried Highway 19 over the White Bayou. . Load tests were performed before and after structural modifications were made. The goal of the live-load testing was to obtain and then utilize field measurements to verify and calibrate an analytical model. The two sets of tests were performed in an identical manner with the intent of identifying any changes in the live-load behavior.

The BDI Structural Testing System (STS) was used for measuring strains at 40 locations and displacements at 6 locations on the superstructure while it was subjected to a moving truck load. The response data was then used to “calibrate” a finite element model of the structure, which was in turn used to compute load ratings for standard design and rating vehicles using the AASHTO Load Factor Design (LFD) approach.

Based on the calibrated model, the critical structural component was the shear capacity of the interior beams. Table 1 contains the critical load rating factors and load limits for the standard AASHTO design and rating vehicles. These rating factors were generated from the model prior to any strengthening. Since the strengthening techniques were designed to improve moment capacity it was desirable to compare the original flexural strength load ratings with those obtained from the three different strengthening methods. Table 2 contains flexural moment HS-20 load rating results for the each beam type.

Table 1 Critical load rating factors and weights for pre-structural rehabilitation.

TRUCK	LOCATION	LFD INVENTORY		LFD OPERATING	
		RF	TONS	RF	TONS
H-20	Interior Girder - Midspan	0.87	17	1.45	52
HS-20	Interior Girder - Midspan	0.81	29	1.35	49
Type-3	Interior Girder - Midspan	0.92	23	1.54	38
Type-3S2	Interior Girder - Midspan	1.01	36	1.69	61
Type-3-3	Interior Girder - Midspan	1.15	46	1.92	77

Table 2 HS-20 Flexural Strength Load Rating Results for each Beam Type.

BEAM TYPE	LOCATION	LFD INVENTORY		LFD OPERATING	
		RF	TONS	RF	TONS
Initial Beam	Interior Girder - Midspan	1.04	37	1.74	62
CFRP Fabric	Interior Girder - Midspan	1.36	49	2.27	82
CRFP Pultruded Strips	Interior Girder - Midspan	1.24	45	2.07	75
CRFP Near Surface Mounted	Interior Girder - Midspan	1.46	53	2.44	88

It is important to note that the rating results provided for the strengthened sections are not representative of the overall bridge load capacity. First of all, load limits are controlled by the shear capacity of the interior T-beams at all spans and the strengthening methods did not improve the shear strength. Secondly, the retrofits were only performed on selected beams from two of the 8 spans. The primary purpose of the research project was to evaluate the feasibility and long-term performance of the various strengthening methods. Therefore the current posted load limits for this bridge should remain in place.

In addition to the load test and subsequent analyses procedures. A long-term monitoring system was installed to help evaluate the long term performance of the FRP strengthening methods employed at the White Bayou Bridge. The monitoring system was designed primarily to evaluate slow-speed responses due to temperature and permanent responses due to settlement and/or damage. The monitoring system can be used to perform static live-load tests as a means of periodic evaluations. Strain sensors are mounted to both the surface mounted FRP and the concrete on Span 3. It should be possible to detect any delamination during a pure static load test.

This report is limited to the work performed by BDI and only relates to the load test procedures and results and information relating to the long-term monitoring system. Any information regarding FRP (material and application methods) was provided by others.

TABLE OF CONTENTS

EXECUTIVE SUMMARY	1
TABLE OF CONTENTS	3
LIST OF TABLES.....	4
LIST OF FIGURES.....	5
STRUCTURAL TESTING INFORMATION	7
STRUCTURAL TESTING INFORMATION	7
PRELIMINARY INVESTIGATION OF TEST RESULTS.....	21
MODELING, ANALYSIS, AND DATA CORRELATION.....	28
LOAD RATING PROCEDURES AND RESULTS.....	31
LONG-TERM MONITORING SYSTEM	36
CONCLUSIONS AND RECOMMENDATIONS.....	41
APPENDIX A - MEASURED AND COMPUTED STRAIN COMPARISONS	42
APPENDIX B – FIELD NOTES (SCANNED)	59
APPENDIX C - FIELD TESTING PROCEDURES	75
APPENDIX D - DATA LOGGER SUPPORT SOFTWARE GUIDE	80
CSI-LOGGERNET SOFTWARE.....	80
LTRC_WB.DLD DATA LOGGER PROGRAM OPERATION	82
<i>Scheduling</i>	83
DATA LOGGER DATA FORMAT	84
INSTRUMENTATION NOTES	85
APPENDIX E – SPECIFICATIONS: BDI STRAIN TRANSDUCERS.....	91
APPENDIX F – SPECIFICATIONS: BDI STRUCTURAL TESTING SYSTEM.....	92
APPENDIX G – SPECIFICATIONS: BDI AUTOCLICKER	93
APPENDIX H - MODELING AND ANALYSIS: THE INTEGRATED APPROACH.....	94
APPENDIX I - LOAD RATING PROCEDURES.....	100
APPENDIX J - REFERENCED MATERIAL	104

LIST OF TABLES

Table 1 Critical load rating factors and weights for pre-structural rehabilitation.....	1
Table 2 HS-20 Flexural Strength Load Rating Results for each Beam Type.....	2
Table 3 Structure description & testing notes.....	7
Table 4 Testing vehicle information.....	19
Table 5 Analysis and model details.....	29
Table 6 Model accuracy & parameter values.....	31
Table 7 Load and Resistance Factors.....	32
Table 8 Girder section and steel details.....	33
Table 9 T-Beam Moment and Shear Capacities.....	33
Table 10 Load rating factors for H-20.....	34
Table 11 Load rating factors for HS-20.....	34
Table 12 Load rating factors for Type 3.....	35
Table 13 Load rating factors for Type 3-3.....	35
Table 14 Load rating factors for Type 3S3.....	36
Table 15 Moment Capacities and Load Rating Factors of Strengthened Beams.....	36
Table 16 Array 1 Data Format – Average Sensor Values – Recorded Hourly.....	84
Table 17 Array 2 Data Format – Average Temperatures – Recorded Hourly.....	84
Table 18 Array 3 Data Format – Minimum Sensor Values – Recorded Hourly.....	84
Table 19 Array 4 Data Format – Maximum Sensor Values – Recorded Hourly.....	85
Table 20 Array 5 Data Format – sensor values – recorded @ 60 sec interval (Flag 2 On).....	85
Table 21 Array 6 Data Format – temperatures – recorded @ 60 sec interval (Flag 2 On).....	85
Table 22 Instrumentation connectivity and channel numbers.....	89
Table 23. Gage Wiring Sequence.....	90
Table 24 Error Functions.....	99

LIST OF FIGURES

Figure 1 Instrumentation plan (layout view).	9
Figure 2 Instrumentation plan (span 2 gage locations – Test Setup 1).....	10
Figure 3 Instrumentation plan (span 3 gage locations – Test Setup 1).....	11
Figure 4 Instrumentation plan (span 4 gage locations – Test Setup 1).....	12
Figure 5 Instrumentation plan (cross-section view, span 2 – Test Setup 1).	13
Figure 6 Instrumentation plan (cross-section view, span 3 – Test Setup 1).	14
Figure 7 Instrumentation plan (cross-section view, span 4 – Test Setup 1).	15
Figure 8 Instrumentation plan (span 2 gage locations – Test Setup 2).....	16
Figure 9 Instrumentation plan (span 3 gage locations – Test Setup 2).....	17
Figure 10 Instrumentation plan (span 4 gage locations – Test Setup 2).....	18
Figure 11 Photograph showing strain and displacement instrumentation.	19
Figure 12 Test truck footprint – Single rear axle dump truck (Test 1).....	20
Figure 13 Reproducibility and linearity of test results.....	23
Figure 14 Lateral load distribution (LVDT results).....	24
Figure 15 Pier support details.	24
Figure 16 Damaged Beam Bearing @ Pier 4.....	25
Figure 17 Slight continuity between spans.	25
Figure 18 Influence of cracks on strain measurements.....	26
Figure 19 High-speed test results (measured impact).....	26
Figure 20 Pre and Post Retrofit Strain Comparison – 3 Locations on Interior Beam.	27
Figure 21 Pre and post retrofit displacement comparison – interior beam.	27
Figure 22 Pre and post retrofit displacement comparison – exterior beam.	28
Figure 23 Finite element model of superstructure	29
Figure 24 T-Beam Steel Details.....	32
Figure 25 Long-term Instrumentation Plan – Span 2.....	38
Figure 26 Long-term Instrumentation Plan – Span 3.....	39
Figure 27 Long-term Instrumentation Plan – Span 4.....	40
Figure 28 Beam 1, cross-section A-A – bottom.	42
Figure 29 Beam 2, cross-section A-A – bottom.	43
Figure 30 Beam 3, cross-section A-A – bottom.	43
Figure 31 Beam 4, cross-section A-A – bottom.	44
Figure 32 Beam 1, cross-section B-B – bottom.....	44
Figure 33 Beam 2, cross-section B-B – bottom.....	45
Figure 34 Beam 3, cross-section B-B – bottom.....	45
Figure 35 Beam 4, cross-section B-B – bottom.....	46
Figure 36 Beam 1, cross-section C-C – bottom.....	46
Figure 37 Beam 2, cross-section C-C – bottom.....	47
Figure 38 Beam 1, cross-section D-D – bottom.	47
Figure 39 Beam 2, cross-section D-D – bottom.	48
Figure 40 Beam 1, cross-section E-E – bottom.	48
Figure 41 Beam 2, cross-section E-E – bottom.	49
Figure 42 Beam 3, cross-section E-E – bottom.	49
Figure 43 Beam 4, cross-section E-E – bottom.	50
Figure 44 Beam 1, cross-section E-E – displacement.....	50
Figure 45 Beam 2, cross-section E-E – displacement.....	51

Figure 46 Beam 3, cross-section E-E – displacement.....	51
Figure 47 Beam 4, cross-section E-E – displacement.....	52
Figure 48 Beam 1, cross-section F-F – bottom.....	52
Figure 49 Beam 2, cross-section F-F – bottom.....	53
Figure 50 Beam 1, cross-section G-G – bottom.	53
Figure 51 Beam 2, cross-section G-G – bottom.	54
Figure 52 Beam 1, cross-section H-H – bottom.	54
Figure 53 Beam 2, cross-section H-H – bottom.	55
Figure 54 Beam 3, cross-section H-H – bottom.	55
Figure 55 Beam 4, cross-section H-H – bottom.	56
Figure 56 Beam 1, cross-section I-I – bottom.....	56
Figure 57 Beam 2, cross-section I-I – bottom.....	57
Figure 58 Beam 3, cross-section I-I – bottom.....	57
Figure 59 Beam 4, cross-section I-I – bottom.....	58
Figure 60 Strain Transducers Mounted on Steel Girder	77
Figure 61 Transducers w/Gage Extensions Mounted On R/C Slab.....	77
Figure 62 AutoClicker Mounted on Test Vehicle.....	78
Figure 63 Long-term Instrumentation Plan – Span 2.....	86
Figure 64 Long-term Instrumentation Plan – Span 3.....	87
Figure 65 Long-term Instrumentation Plan – Span 4.....	88
Figure 66 Illustration of Neutral Axis and Curvature Calculations	95
Figure 67 Moment Diagram of Beam with Rotational End Restraint.	96
Figure 68 Relationship Between Spring Stiffness and Fixity Ratio.	97
Figure 69 AASHTO Rating and Posting Load Configurations.	103

STRUCTURAL TESTING INFORMATION

Prior to the load test, the bridge was instrumented with several strain and displacement sensors as described in Table 3 and illustrated by Figure 1 through Figure 7. Several controlled load tests were performed during which strains and displacements were recorded while the test vehicle crossed the bridge at crawl speed (5mph). The truck was driven across the bridge along prescribed paths and the longitudinal position of the truck was monitored remotely and recorded with the response data. Tests were performed on three different truck paths and each path was repeated at least twice to ensure reproducibility of the test procedures and the structural performance.

After the first set of load tests were performed, Spans 2 and 3 were retrofitted with three different FRP strengthening methods. Span 2 beams were strengthened with the near surface carbon fiber strips, while Beams 1 & 2 of Span 3 were strengthened with carbon fiber strips glued to the bottom surface of the girders, and the Beams 3 & 4 of Span 3 were strengthened with the wet layup of a carbon fiber mat. Span 4 did not have any modifications and was used as a control span for the two sets of tests.

Tests were initially performed on April 17 before any retrofits were performed. Tests were repeated again on May 1st after FRP strengthening procedures were applied to Spans 2 and 3. The second set of tests was performed in an identical procedure so that a direct comparison of responses could be made. Figure 8 through Figure 10 show the instrumentation plan for the second set of tests.

Access to the structure was provided by Tulane University. Because of the work to be performed for installing the FRP on Spans 2 and 3, scaffolding was installed under the bridge that extended the whole width of the superstructure for Spans 1 through 4. The work platform made for extremely easy access for instrumenting the bridge. Traffic control and the load vehicle were provided by the Louisiana Department of Transportation. The test vehicle wheel weights were obtained by the Louisiana Highway Patrol.

Table 3 Structure description & testing notes.

ITEM	Description
STRUCTURE NAME	White Bayou
BDI PROJECT NUMBER	040702
TESTING DATE	April 17, 2007 / May 1, 2007
CLIENT'S STRUCTURE ID #	
LOCATION/ROUTE	Zachary Slaughter Hwy over White Bayou
STRUCTURE TYPE	Reinforced Concrete
TOTAL NUMBER OF SPANS	8
SPAN LENGTH(S)	24'
SKEW	0°
STRUCTURE/ROADWAY WIDTH	23'-9"

ITEM	Description
DECK TYPE	Asphalt
OTHER STRUCTURE INFO	
SPANS TESTED	2,3,4
TEST REFERENCE LOCATION (X=0,Y=0)	Inside Curb, North West Corner
TEST VEHICLE DIRECTION	South Bound
TEST BEGINNING POINT	North end of structure
LATERAL LOAD POSITION(S)	1.6' from west curb, 1.6' from east curb, center line
NUMBER/TYPE OF SENSORS	40 Strain Gages / 2 LVDT's / 2 String Pots
STS SAMPLE RATE	40 Hz
NUMBER OF TEST VEHICLES	1
STRUCTURE ACCESS TYPE	Preinstalled scaffolding
STRUCTURE ACCESS PROVIDED BY	Tulane University
TRAFFIC CONTROL PROVIDED BY	Unknown
TOTAL FIELD TESTING TIME	2 days
FIELD NOTES	See Appendix B
VISUAL CONDITION	Fair

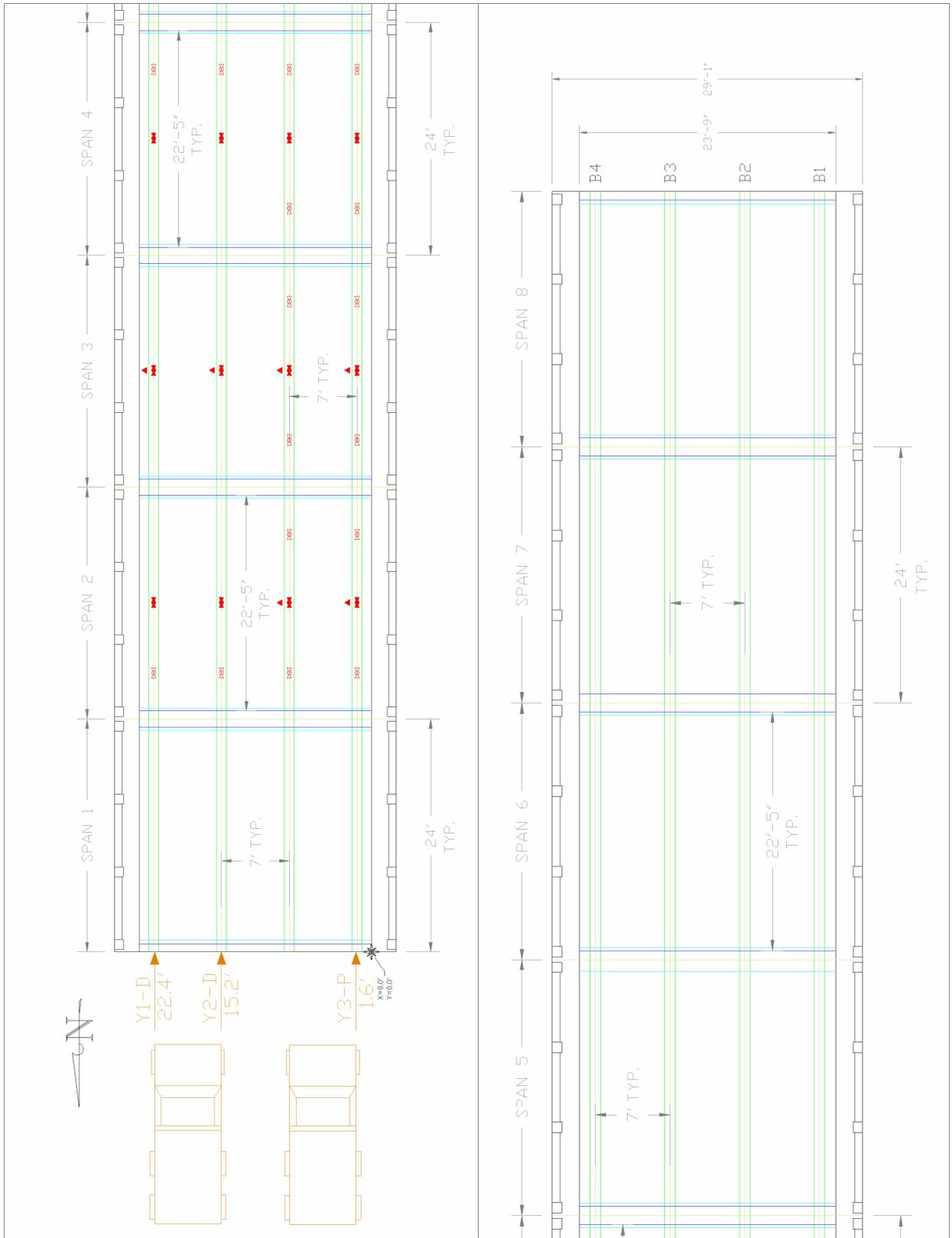


Figure 1 Instrumentation plan (layout view).

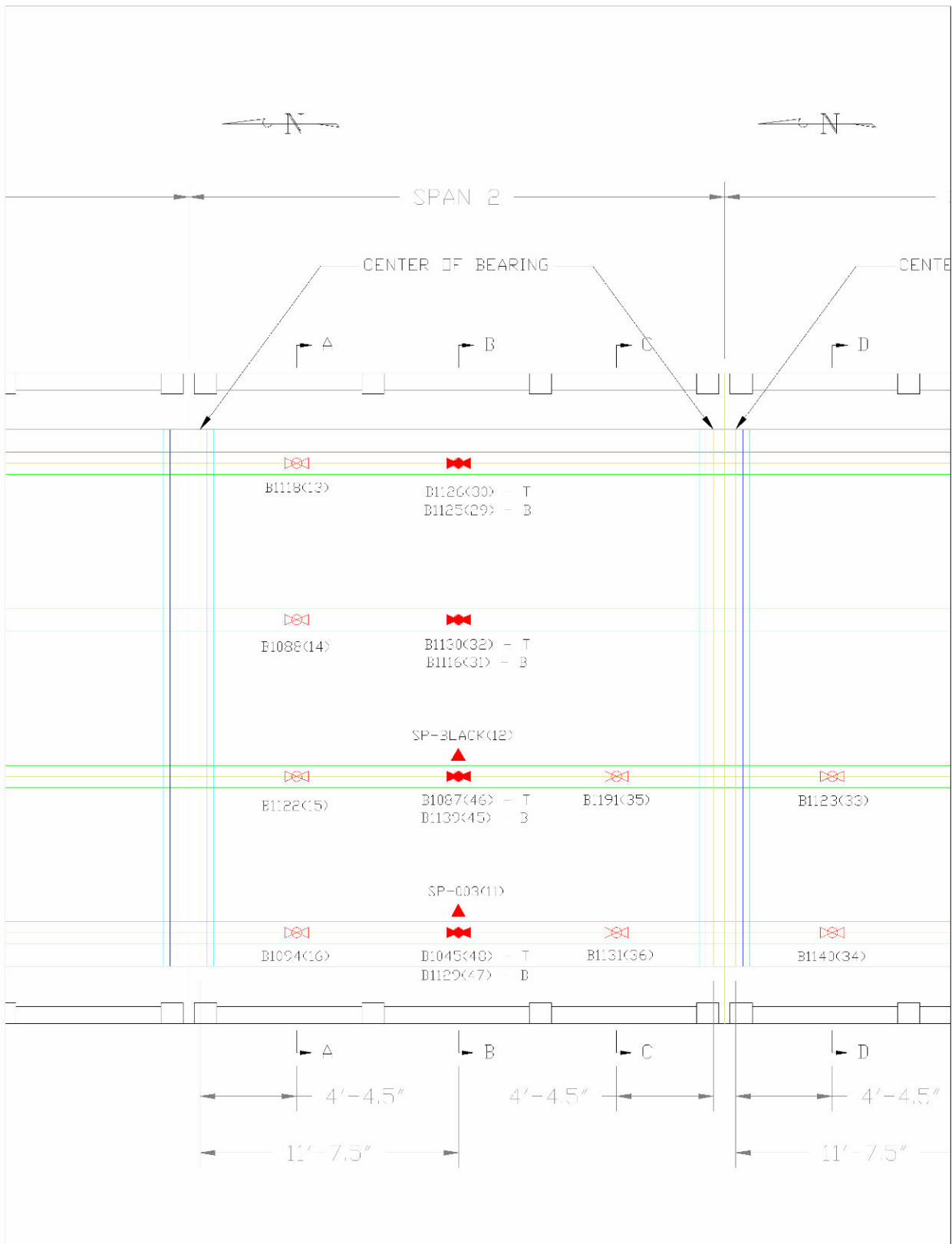


Figure 2 Instrumentation plan (span 2 gage locations – Test Setup 1).

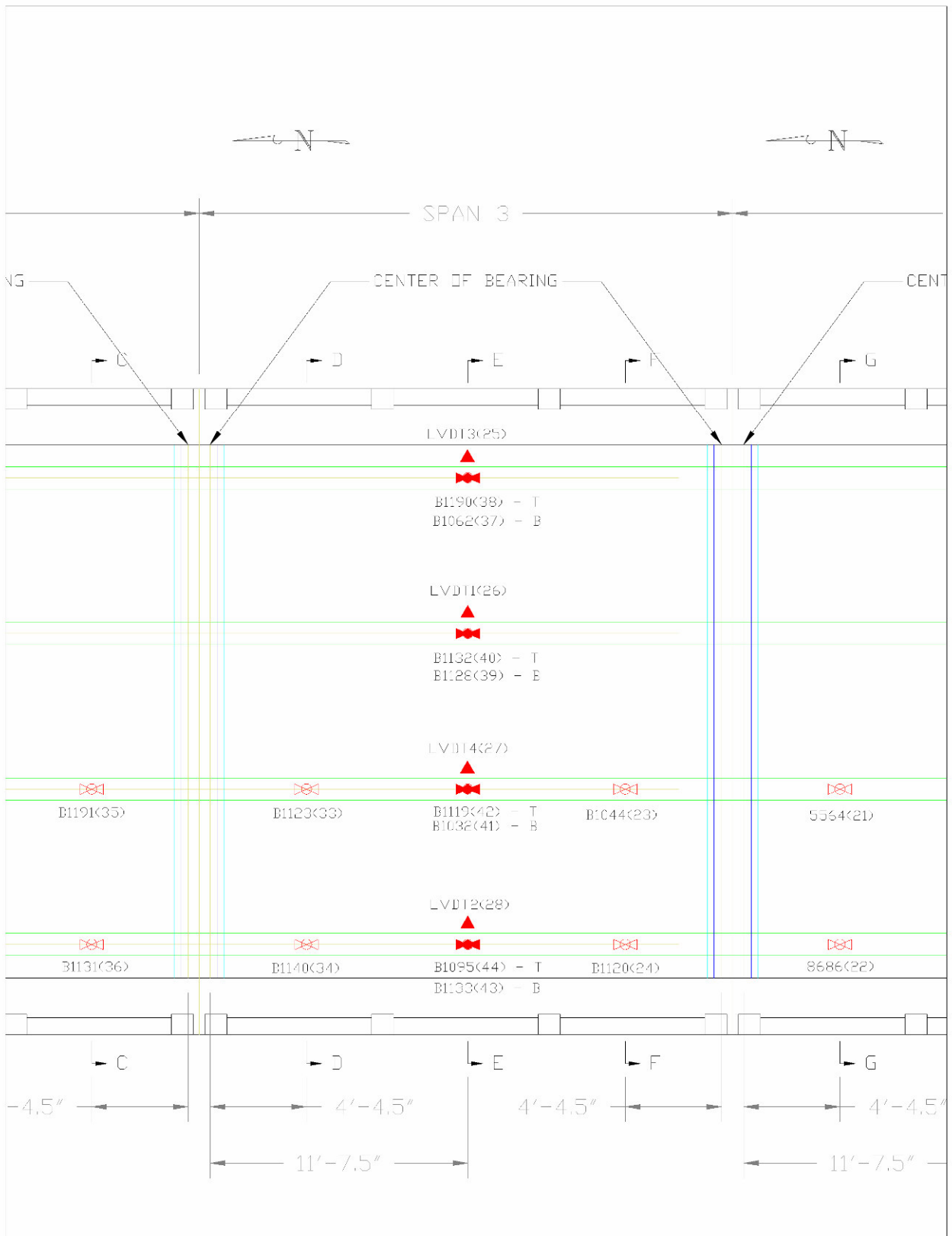


Figure 3 Instrumentation plan (span 3 gage locations – Test Setup 1).

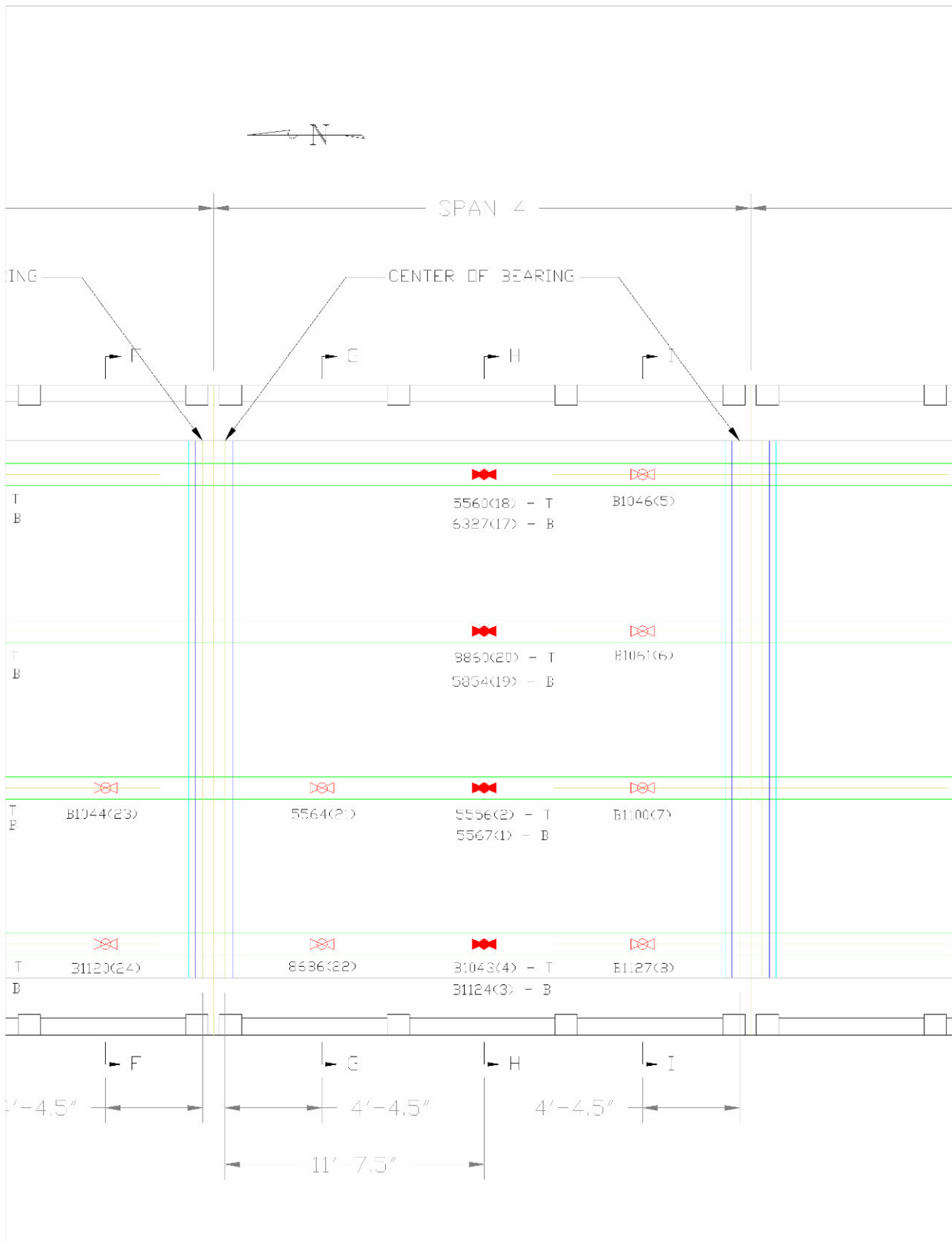


Figure 4 Instrumentation plan (span 4 gage locations – Test Setup 1).

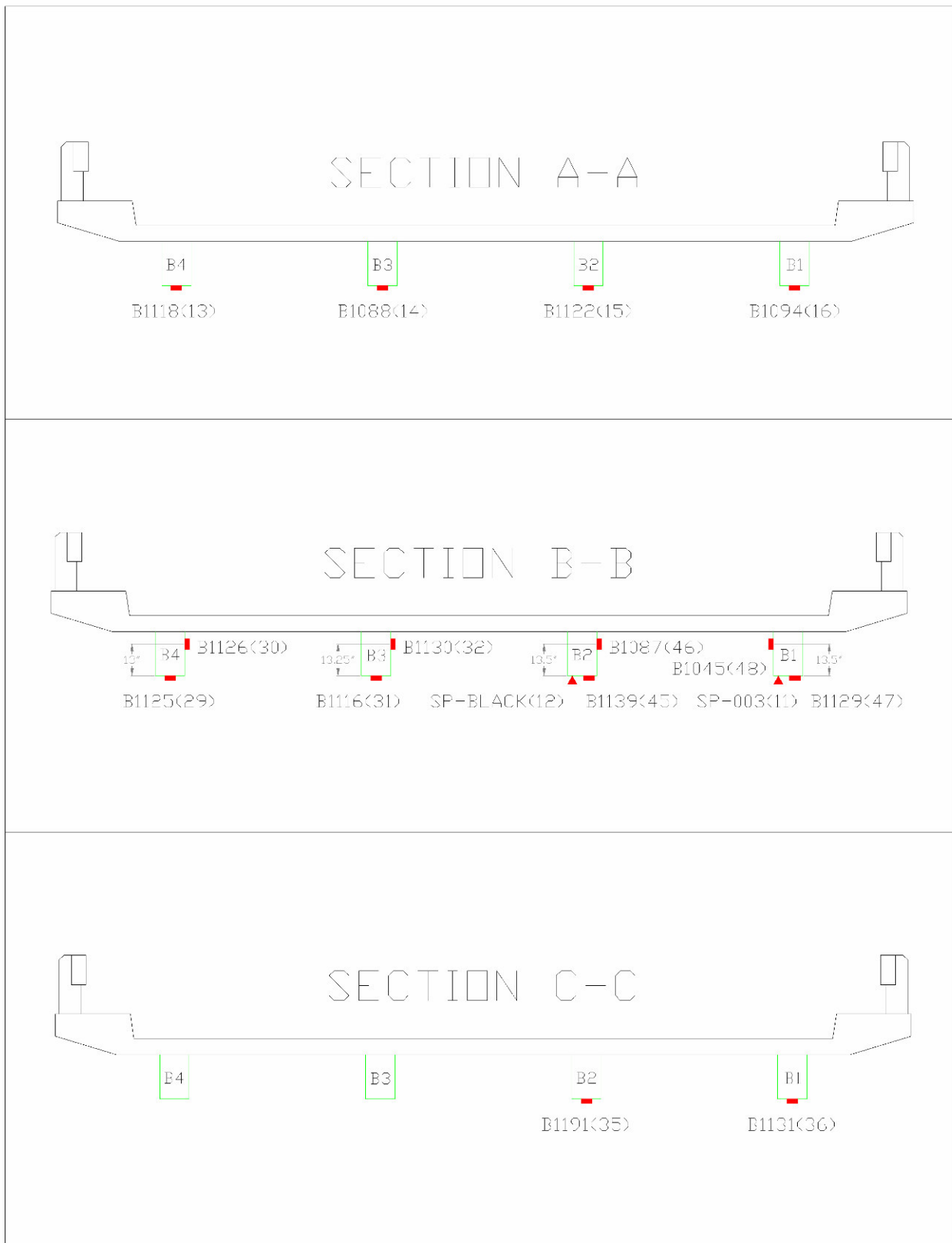


Figure 5 Instrumentation plan (cross-section view, span 2 – Test Setup 1).

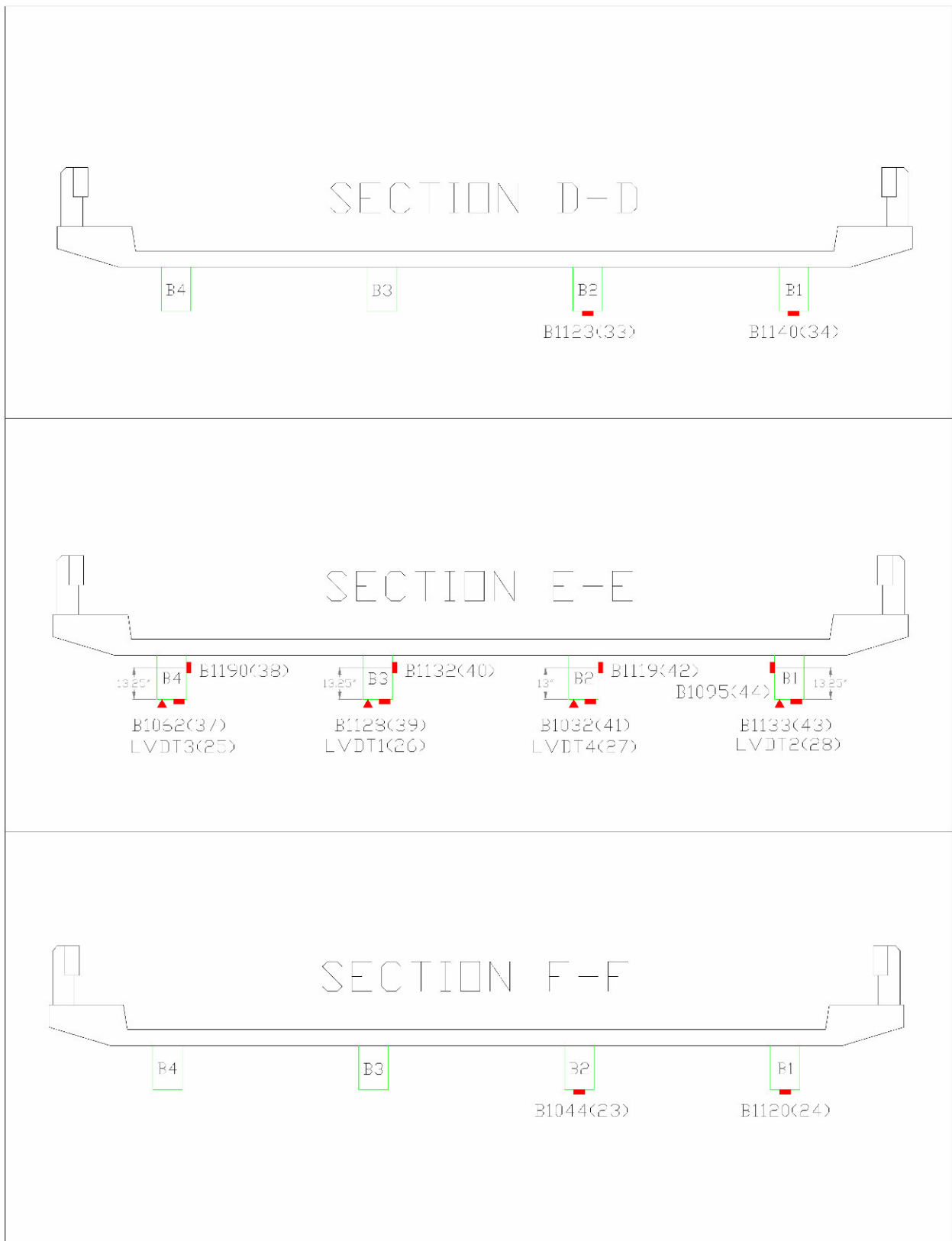


Figure 6 Instrumentation plan (cross-section view, span 3 – Test Setup 1).

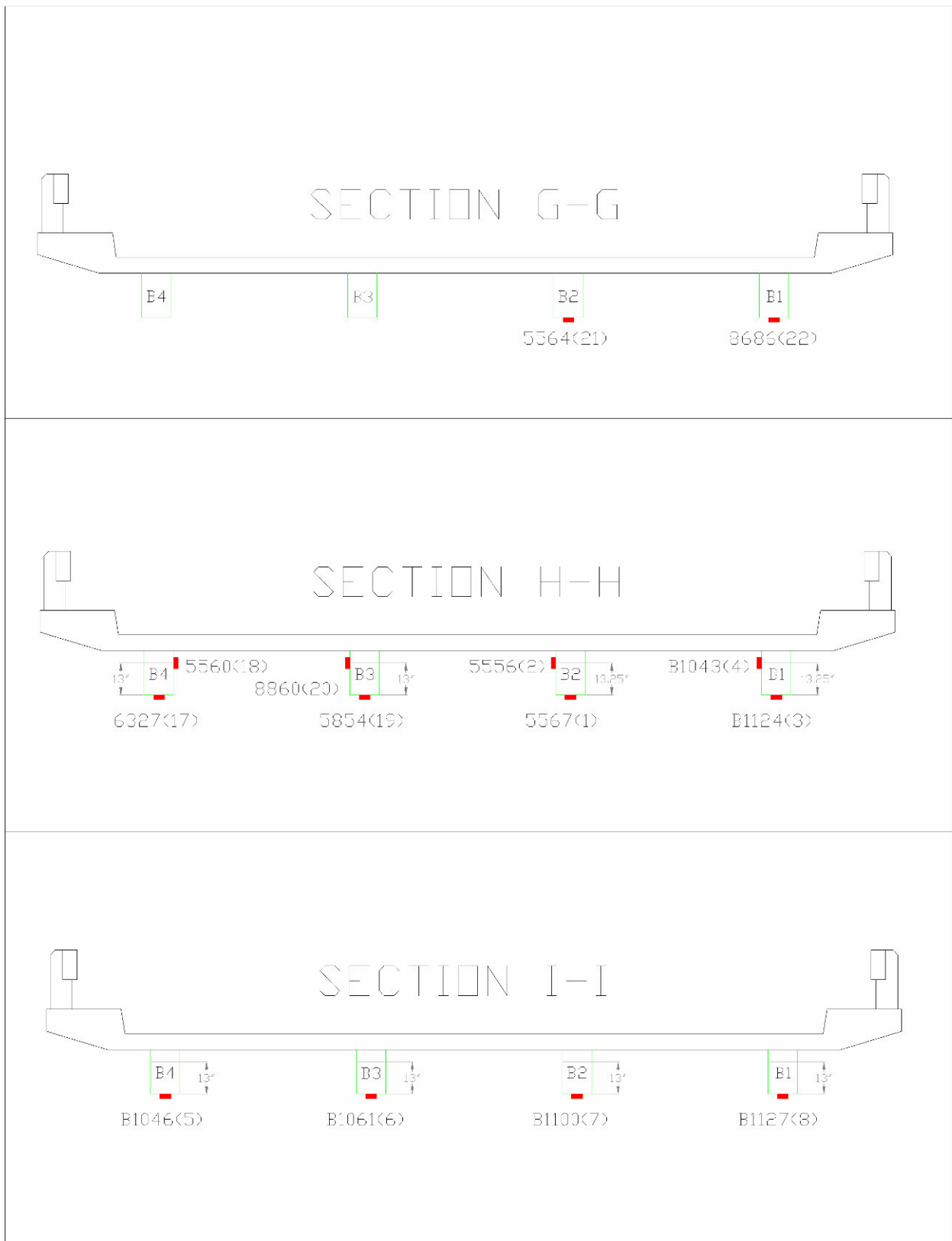


Figure 7 Instrumentation plan (cross-section view, span 4 – Test Setup 1).

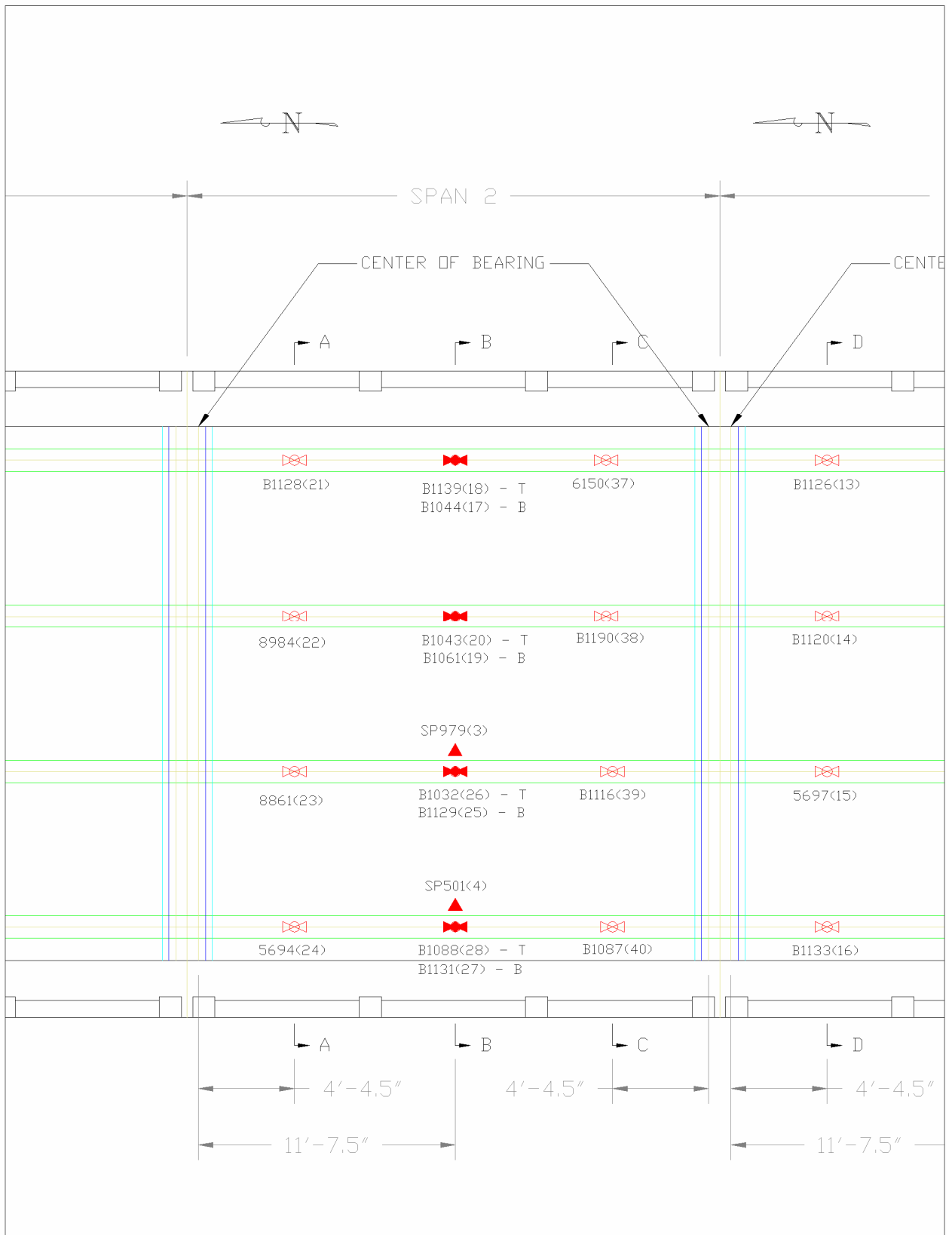


Figure 8 Instrumentation plan (span 2 gage locations – Test Setup 2).

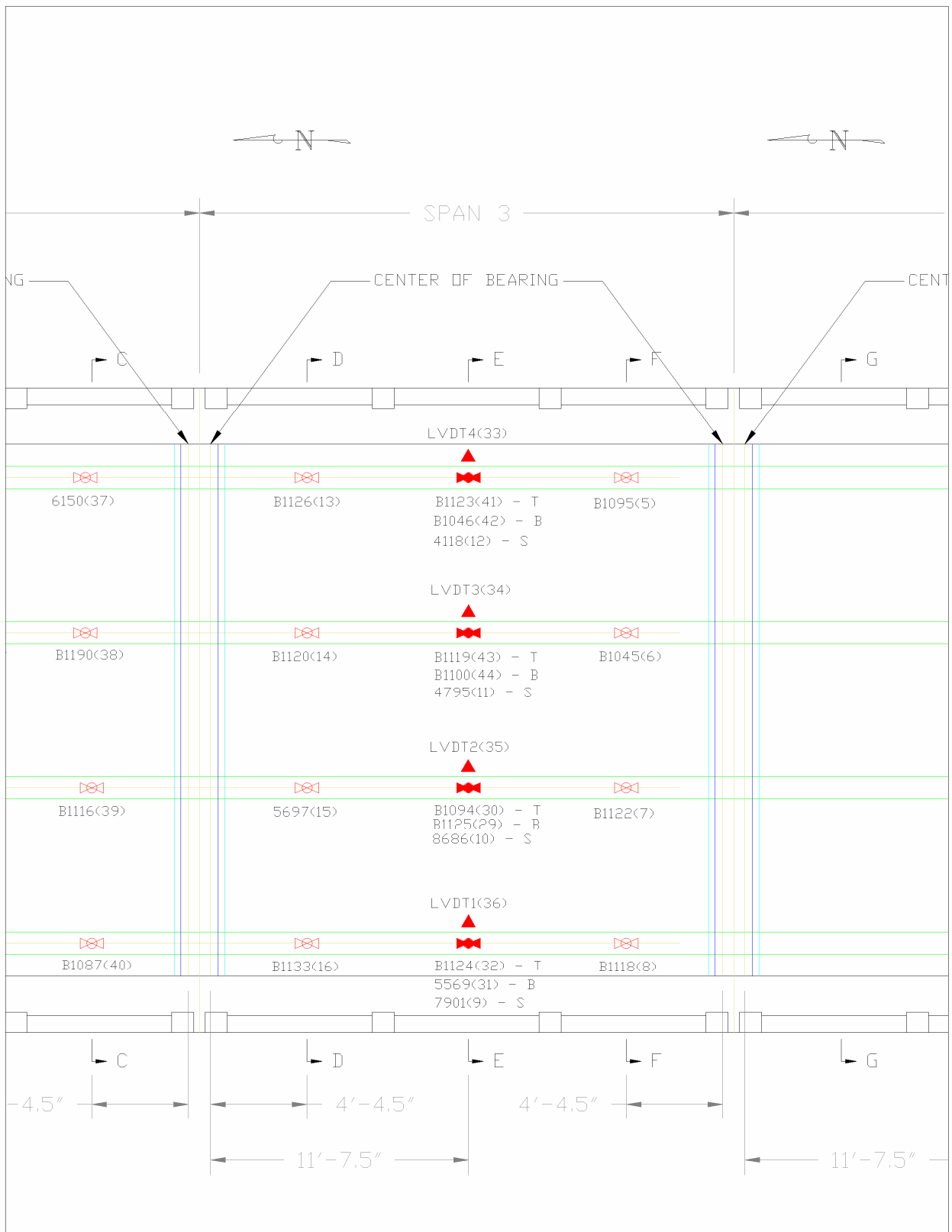


Figure 9 Instrumentation plan (span 3 gage locations – Test Setup 2).

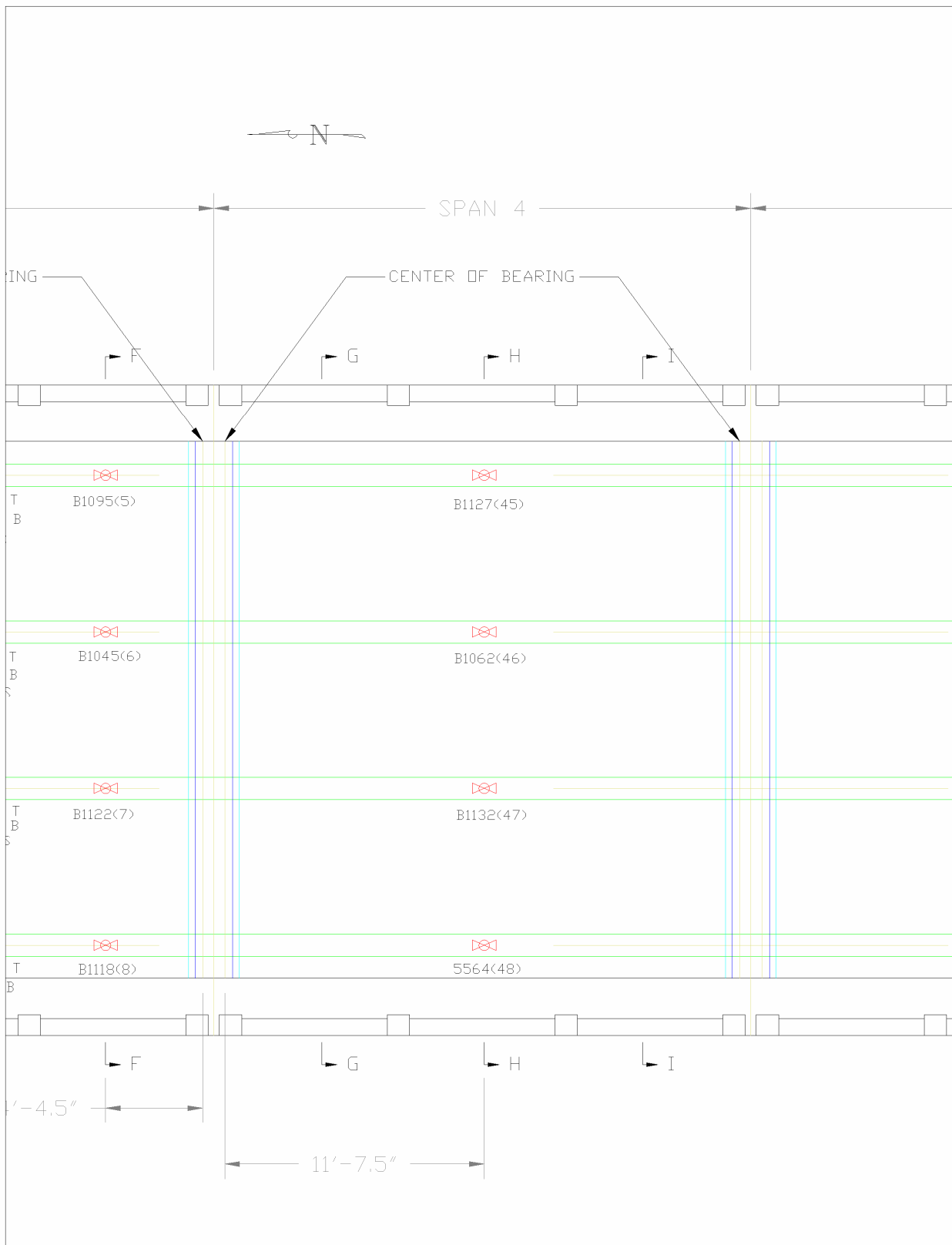


Figure 10 Instrumentation plan (span 4 gage locations – Test Setup 2).



Figure 11 Photograph showing strain and displacement instrumentation.

Table 4 Testing vehicle information.

VEHICLE TYPE - SINGLE REAR AXLE DUMP TRUCK (SEE Figure 12)	
GROSS VEHICLE WEIGHT (GVW) (same truck used during both tests)	25,900 lbs (Test 1) 25,550 lbs (Test 2)
WHEEL ROLLOUT 5 REVS	51.4' (10.28'/rev)
NO. OF SEMI-STATIC PASSES	6 passes – 3 paths
NO. OF HIGH SPEED PASSES/SPEED	2 passes – 2 paths

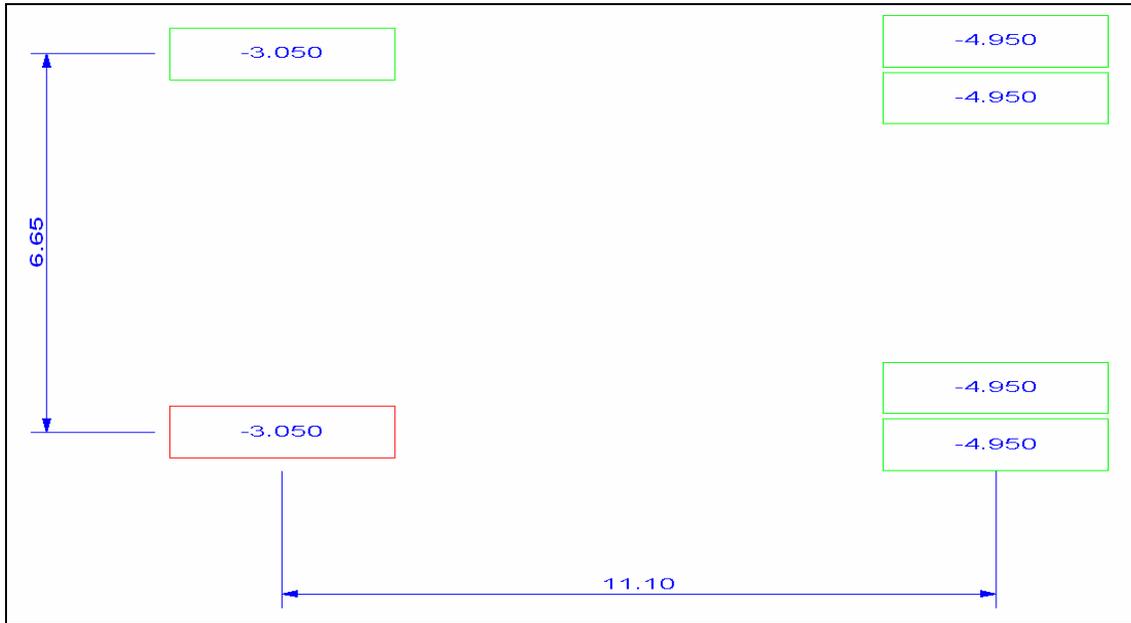


Figure 12 Test truck footprint – Single rear axle dump truck (Test 1).

Please see Appendix C for a detailed outline of the general field testing procedures, Appendix D for the specifications on the BDI Strain Transducers, and Appendix E for the specifications on the BDI Structural Testing System.

PRELIMINARY INVESTIGATION OF TEST RESULTS

All of the field data was first examined graphically to determine its quality and to provide a *qualitative* assessment of the structure's live-load response. Some of the indicators of data quality included reproducibility between identical truck crossings, elastic behavior (strains returning to zero after truck crossing), and any unusual-shaped responses that might indicate nonlinear behavior or possible gage malfunctions.

In addition to providing a data "quality check", the information obtained during the preliminary investigation was used to determine appropriate modeling procedures and helped establish the direction that the analysis should take. The majority of discussion on the bridge response behavior was obtained from the initial set of tests. A comparison of data is made between the two sets of tests to evaluate any change in performance.

PRELIMINARY DATA REVIEW OBSERVATIONS

- ***REPRODUCIBILITY & LINEARITY:*** Responses from identical truck paths were reproducible as shown in Figure 13. In addition, all strains appeared to be linear with respect to load magnitude (truck position) and all strains returned to zero, indicating that the structure was acting in a linear elastic manner. Also seen in this graph are the responses from Beam B1 at the mid-span of spans 1, 2, and 3 for the western truck path. The test was conducted by using two passes with the supplied dump truck, and all of the strain histories had a similar degree of reproducibility.
- ***DISTRIBUTION:*** The lateral load distribution of this structure was measured at several cross-sections using both strain transducers and displacement (LVDT) sensors. The results obtained from the LVDT sensors were the best representation of the lateral load distribution of the structure since the flexural cracks that were present did not affect displacement measurements as much as the strain measurements. Figure 14 displays the results from the LVDTs at maximum midspan deflection.
- ***CONTINUITY OF SPANS:*** As expected, continuity was very minimal at all tested bearing locations. End spans were not tested and therefore end-restraint due to abutments could not be analyzed. The beams that were instrumented were simply-supported at the piers and provided only minimal continuity. The small amount of continuity between spans was likely the result of slight translational movement at the top of the pier. Figure 17 shows the slight continuity observed between spans. See Figure 15 for a photo of the pier support conditions. Based on these responses and bearing type, only translational restraint springs will be used for the pier supports. A small eccentric element would also be used to connect the two spans to simulate the continuity that was observed. The condition of the bearings varied significantly. Figure 16 shows a beam bearing with substantial damage and very little bearing surface remaining. Because of this variability in condition, any end-restraint resulting from the model calibration process should be removed prior to load rating calculations.
- ***RESPONSE SYMMETRY:*** Overall, the shapes of the response histories responses indicated that the structure was responding in a symmetric manner. Displacement measurements provided the best indication of the global behavior and it was apparent from the LVDT responses in Figure 14 that responses the structures response behavior was symmetric. There was a larger

variation in strain magnitudes from beam to beam, but this is to be expected from reinforced concrete.

- *INFLUENCE OF CRACKS:* During the sensor installation, it was noticed that there were a visible flexural cracks and shear cracks. The density and size of the cracks appeared normal for a reinforced concrete bridge. While the use of transducer extensions help to minimize the effects of cracks on the measurements by averaging them over a longer gage length, the effects cannot be eliminated entirely. For example, if the gage/extension unit spans additional cracks, the output will be higher than expected. The opposite is true if there is a large crack immediately adjacent to a gage location. Figure 18 shows the response history for two locations that should have very similar magnitudes. The variation in strain magnitude indicates the measurements are likely influenced by cracks. It is important to have an idea of how much crack influence there is prior to comparing analysis results with load test data. In this case the influence of cracks was not significant enough to warrant modeling the local effects of the cracks.
- *NEUTRAL AXIS MEASUREMENTS:* Neutral axis locations were determined by examining the strain histories at multiple depths on the T-beam webs. Due to the presence of the cracks, the neutral axis locations varied slightly throughout the structure, however they were sufficiently close to the theoretical values for both the interior and exterior beams. Note that the neutral axis locations for the exterior beams were slightly higher than the interior beams indicating the curbs and railings were contributing to the exterior beam stiffness.
- *UNUSUAL RESPONSE(S):* The results recorded from all top flange gages located near supports were very low in magnitude (less than 10 micro-strain) and relatively variable since they were very close to the neutral axes locations; these gages were examined to verify basic beam cross-section properties but should not be used in the model calibration process.
- *HIGH-SPEED TESTS:* Two high-speed tests were conducted to evaluate the live-load impact on the superstructure. None of the high-speed responses showed any significant change between high speed and low speed passes along the same vehicle path. This suggests that the actual impact factor was lower than the LFD value of 30%. Figure 19 shows a direct comparison of data captured during a slow and high-speed truck crossing. Note that dynamic test was done to verify that the code specified impact factor was conservative. A much more thorough test procedure would be required to justify modifying the impact factor. There are numerous factors that influence the dynamic responses so numerous tests would need to be run with different vehicles and at many different speeds.
- *STRENGTHENING RETROFITS:* A direct comparison of the pre and post retrofit test data was made. It was expected that the small volume of FRP would have minimal effect on the structural stiffness during service loads. Since the test vehicle and test procedures were nearly identical, it was expected that the strain and displacement histories would be nearly identical. The results however, indicated that the interior beam's strain and deflection values reduced by approximately 10 percent during the second load test while the exterior beams had very similar magnitudes as shown in Figure 21 and Figure 22. While the changes were not particularly large, the observation was curious because essentially no change was expected. Furthermore, the change was relatively consistent among all three spans. There were no strengthening methods applied to Span 4 so it is not likely that the response change was related to the addition of the FRP. Figure 20 contains strain comparisons from 3 locations on an interior beam. The plot shows that the strains at the L/5 locations increased during the second test by a few micro-strain while the midspan strains decreased by

approximately the same magnitude. This response was typical of all interior beams. The basic change in magnitude with respect to the location on the beam is not consistent with what would be expected from the strengthening approach or by any changes in end-restraint at the beam bearings. The most likely cause of the change in response behavior is some type of temperature effect. The mean temperature in Zachary, LA during the second test (76°F) was 13°F degrees warmer than it was on the first test (63°F). The change in temperature may have changed how the asphalt influenced the effective depth and stiffness of the T-beams. Slight changes in neutral axis values between the two tests support this theory and it would also explain why the interior beams seem to be influenced more than the exterior beams.

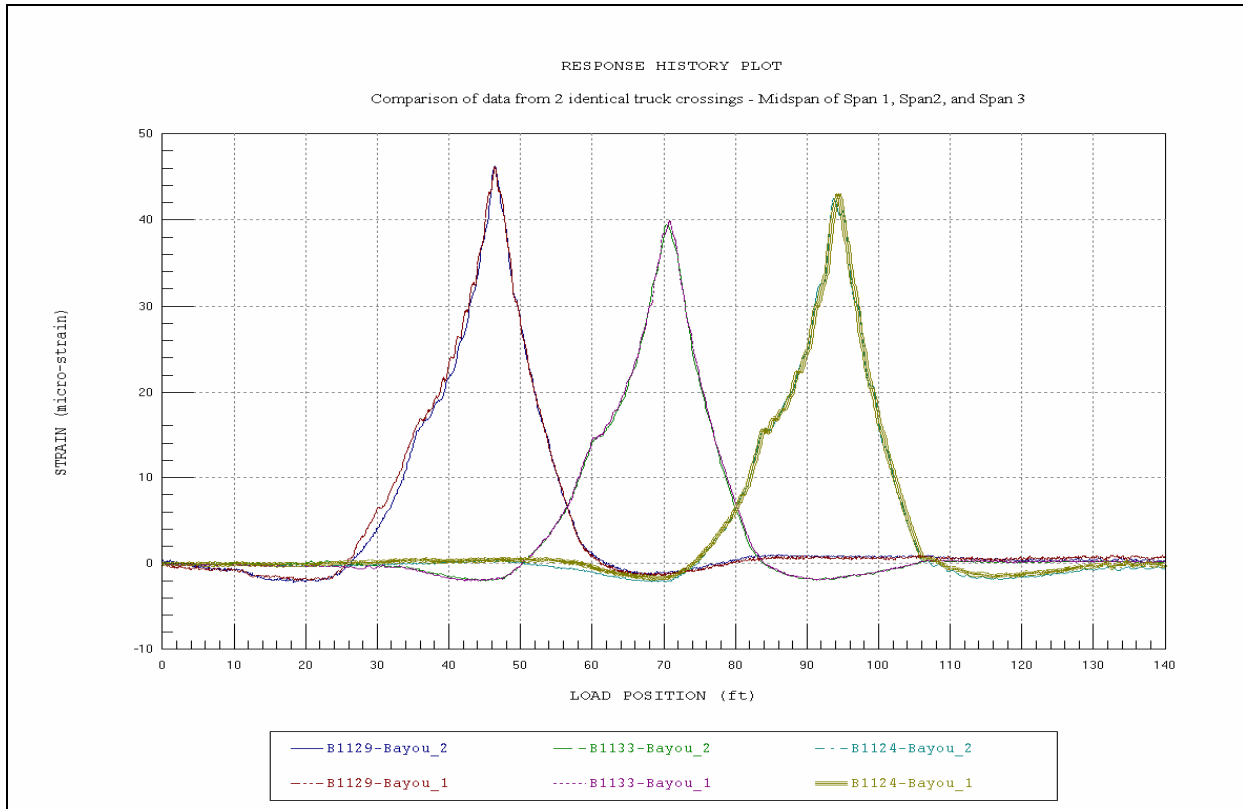


Figure 13 Reproducibility and linearity of test results.

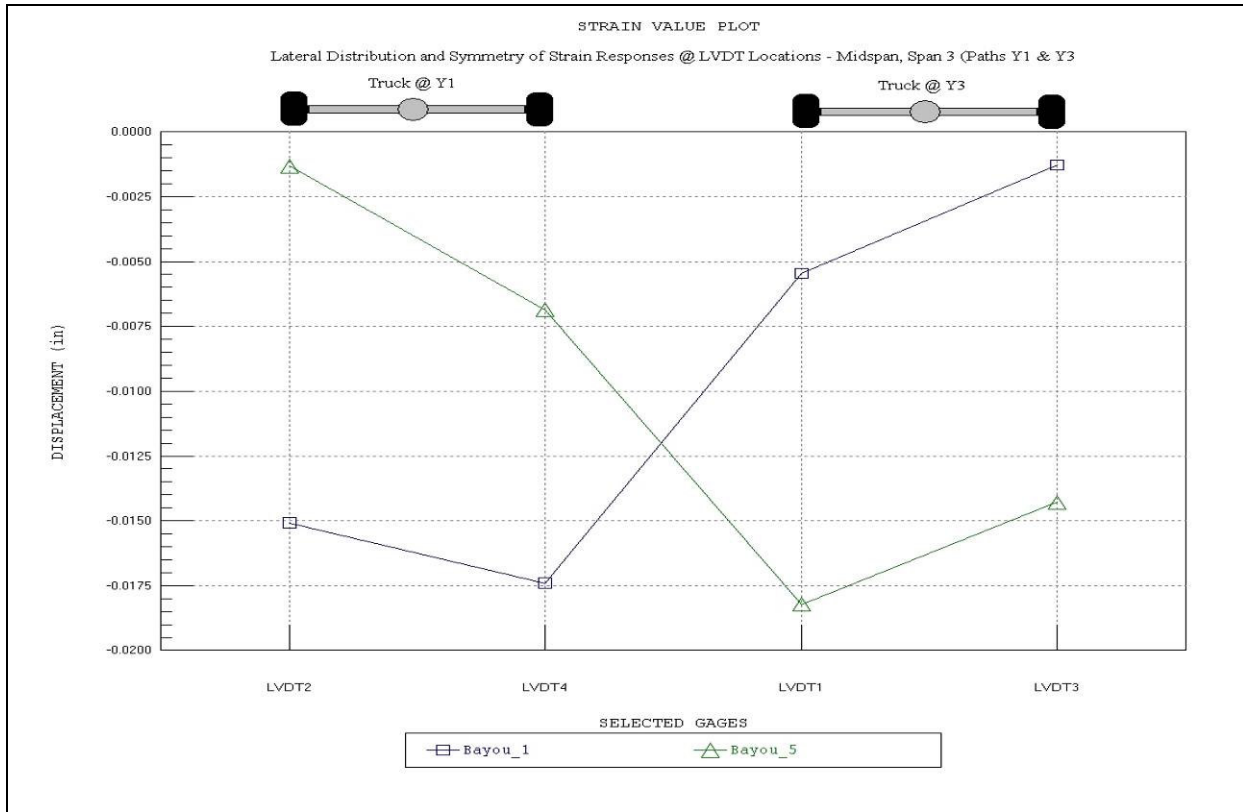


Figure 14 Lateral load distribution (LVDT results).



Figure 15 Pier support details.



Figure 16 Damaged Beam Bearing @ Pier 4.

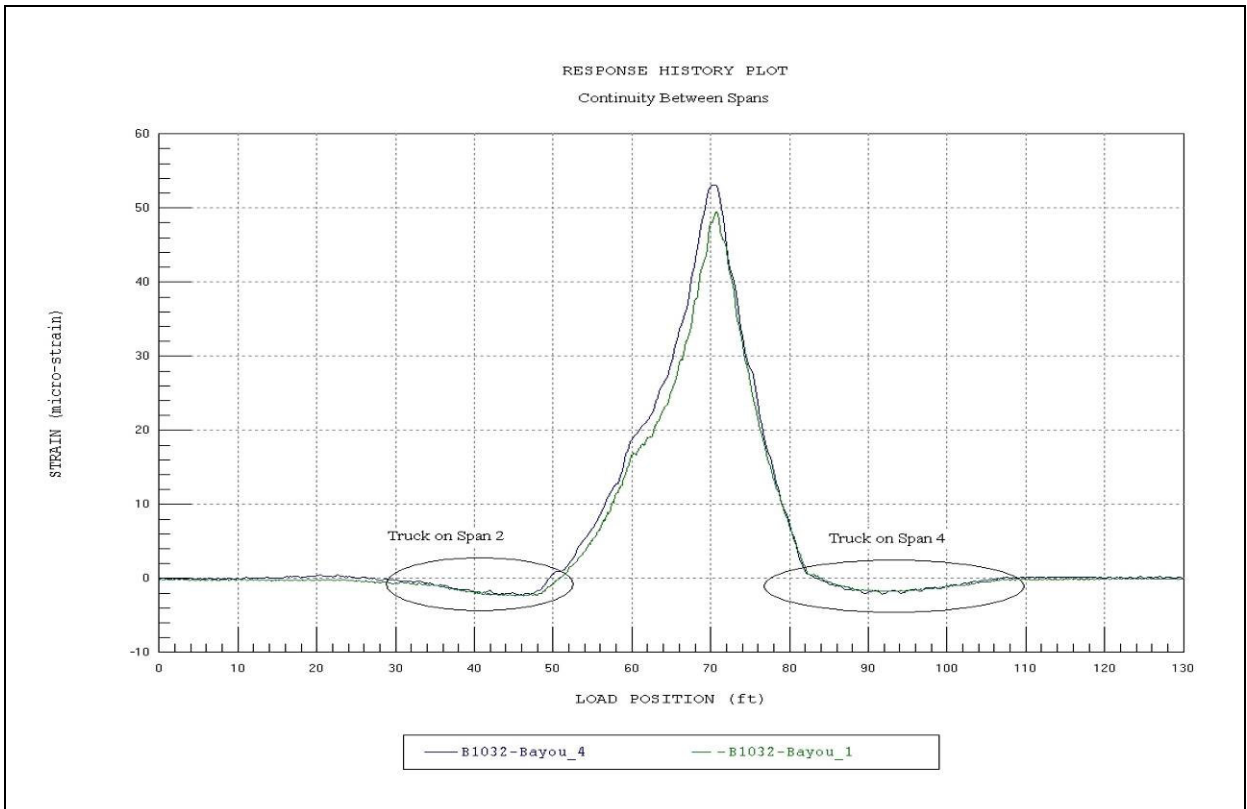


Figure 17 Slight continuity between spans.

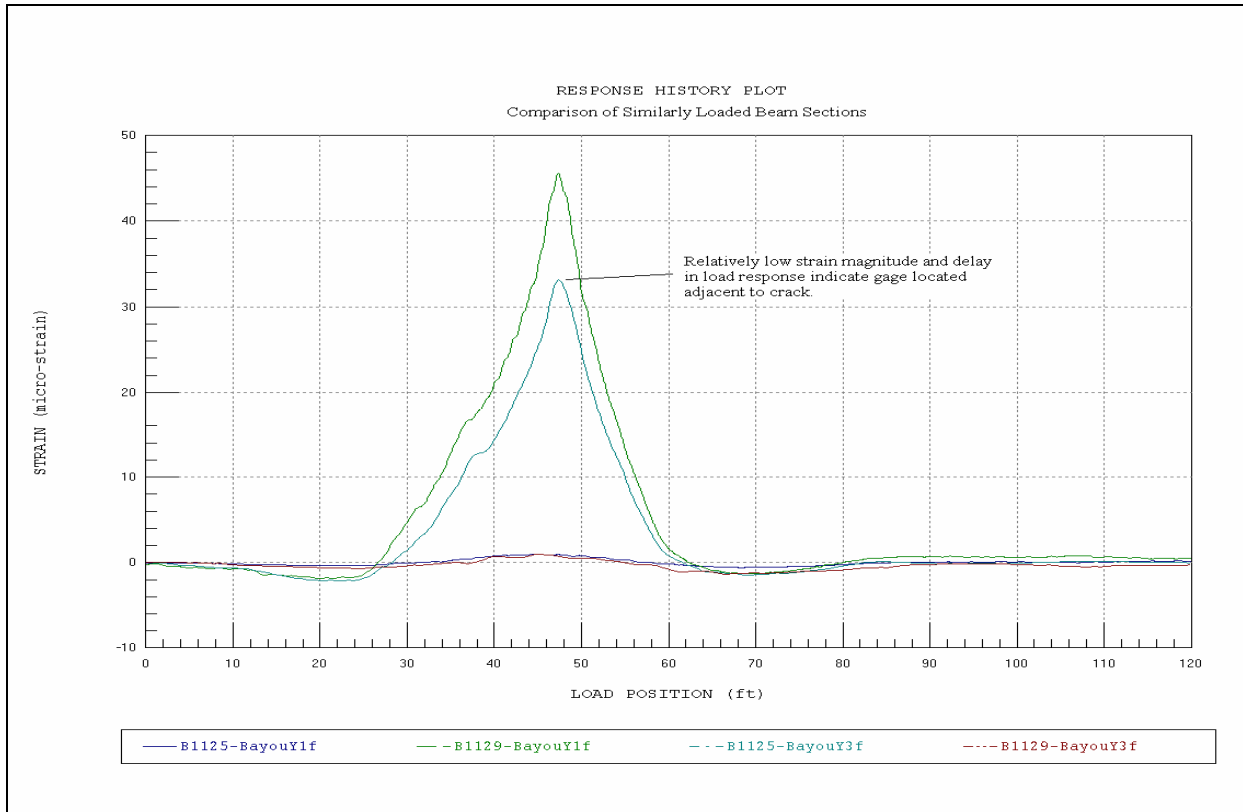


Figure 18 Influence of cracks on strain measurements.

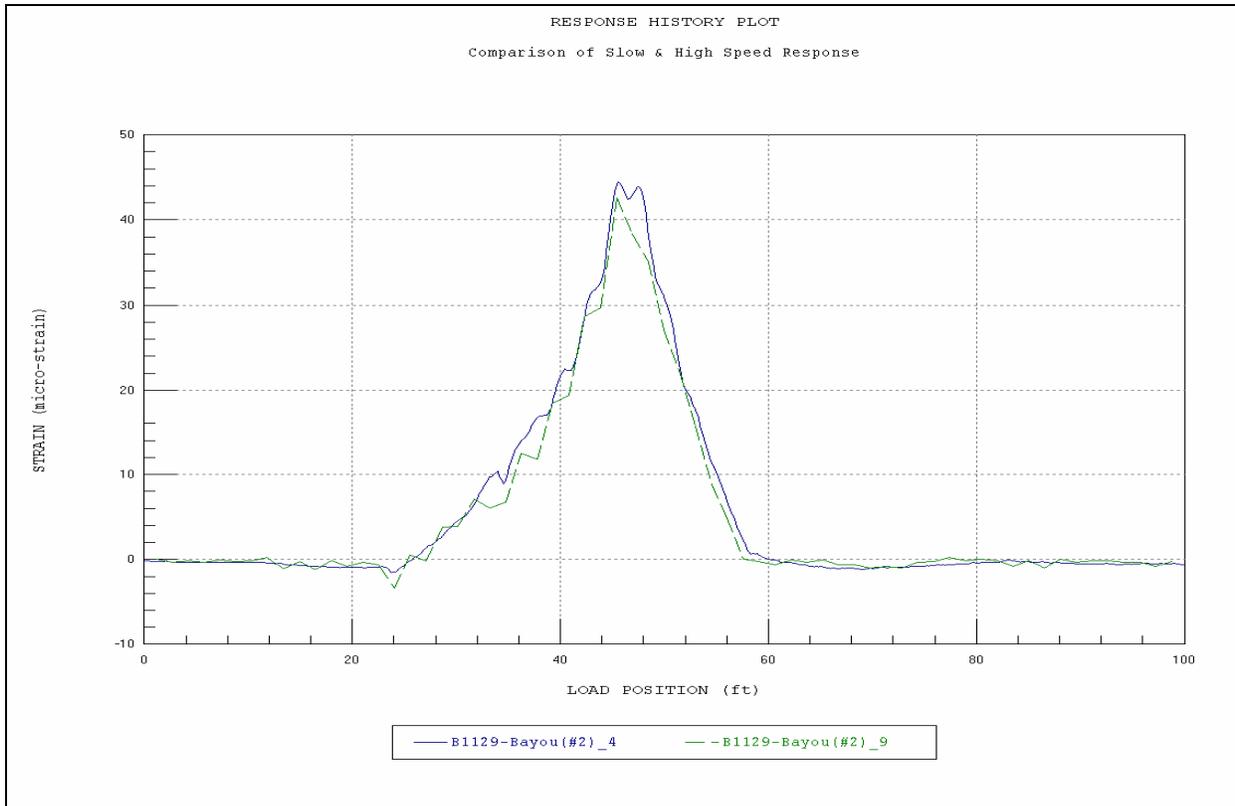


Figure 19 High-speed test results (measured impact).

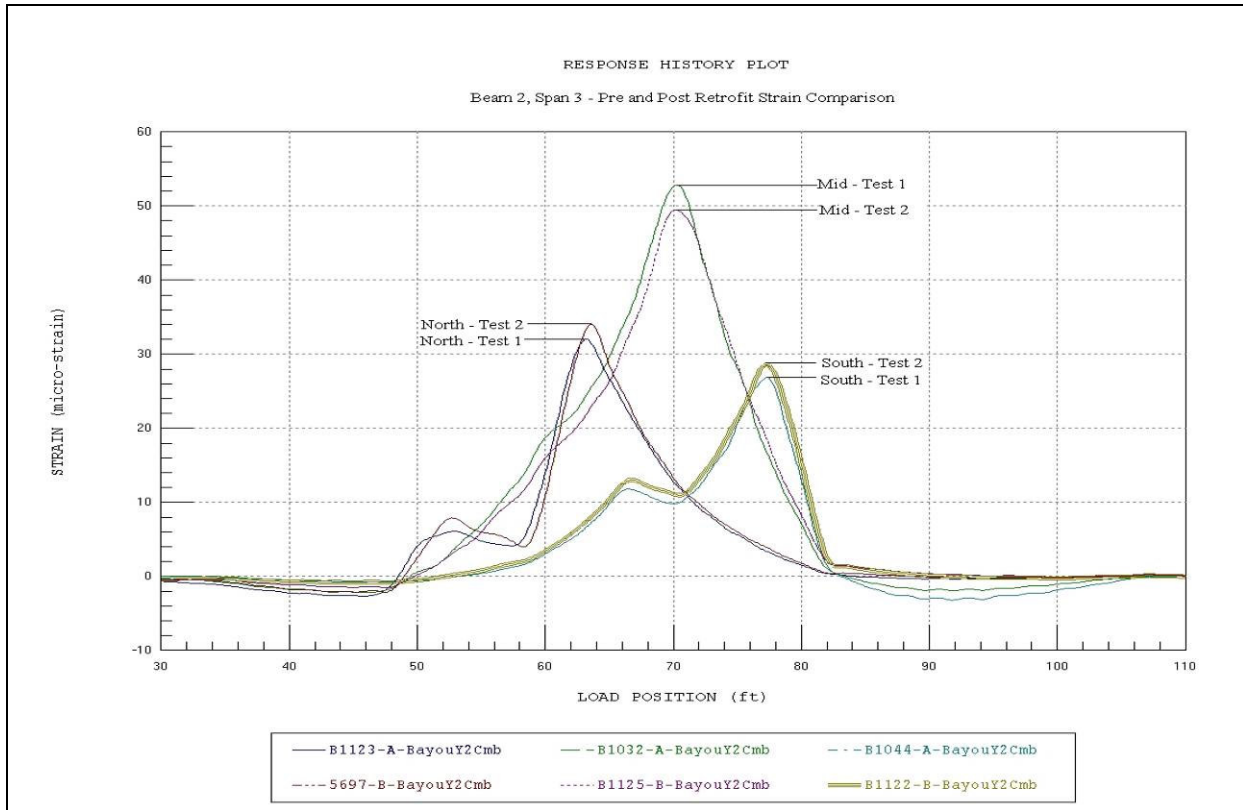


Figure 20 Pre and Post Retrofit Strain Comparison – 3 Locations on Interior Beam.

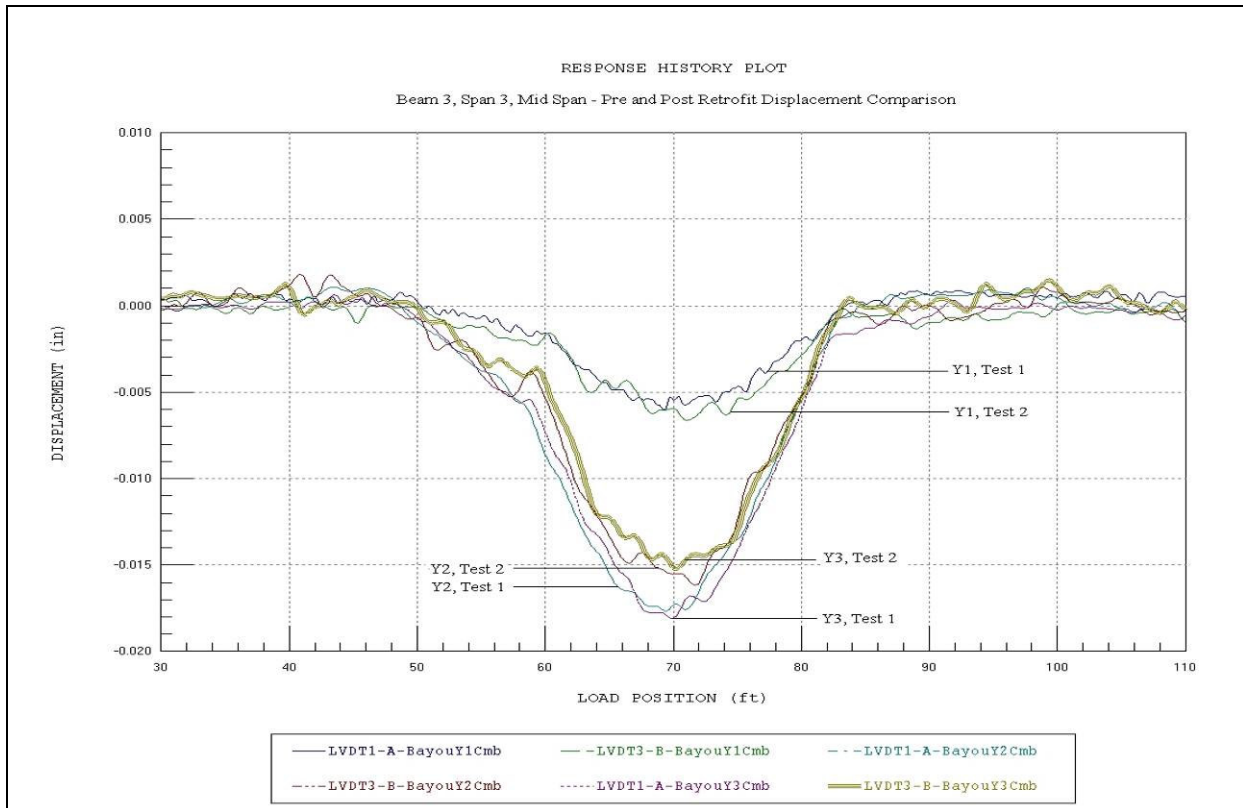


Figure 21 Pre and post retrofit displacement comparison – interior beam.

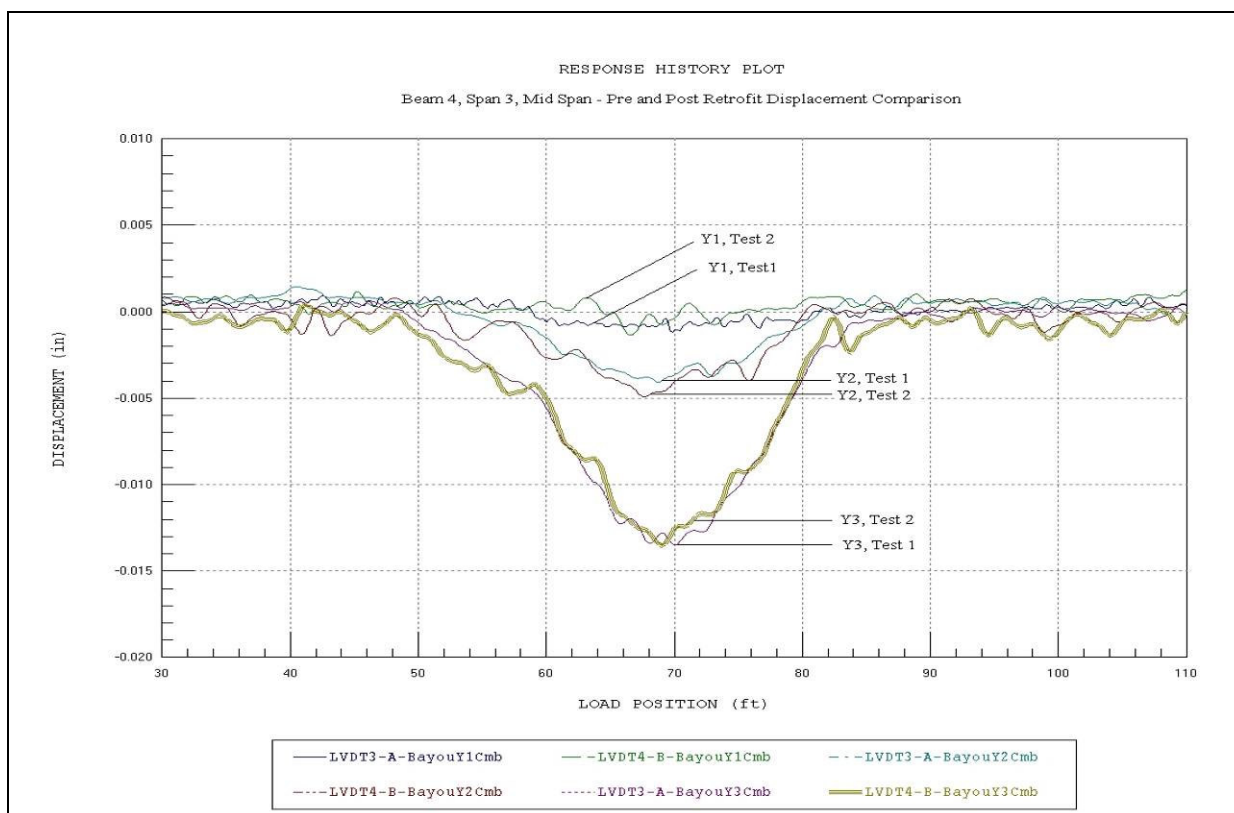


Figure 22 Pre and post retrofit displacement comparison – exterior beam.

MODELING, ANALYSIS, AND DATA CORRELATION

Note that all of the above information was determined by simply viewing the field data. Observations made during the preliminary investigation were then used by an engineer to generate a representative finite element model as seen below in Figure 23. Details regarding the structure model and analysis procedures are provided in Table 5.

Once the model was developed, the load testing procedures were essentially "reproduced" in the model. A two-dimensional "footprint" of the loading vehicle was applied to the model along the same paths that the actual test vehicle crossed the bridge. A direct comparison of strain values was then made between the analytical predictions and the experimentally-measured results. The initial model was then "calibrated" by modifying various properties and boundary conditions until the results matched those measured in the field. A complete outline of this process is provided in Appendix G.

In this case, the bridge model was calibrated using the response data from the first set of load tests (pre-retrofit). Responses from the second set of load tests were later compared with the calibrated model to evaluate any changes in response behavior.

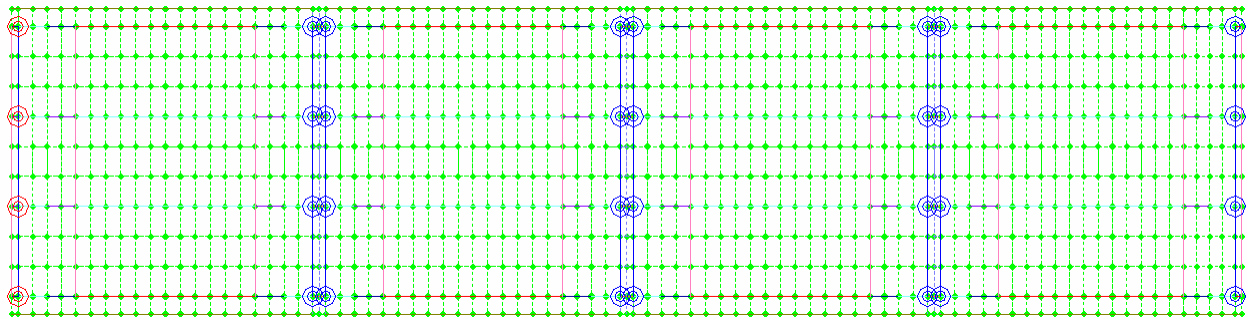


Figure 23 Finite element model of superstructure

Table 5 Analysis and model details.

Analysis Type	Linear-elastic finite element - stiffness method.
Model Geometry	Planar-grid composed of shell elements, beam elements, and springs.
Nodal Locations	Nodes placed at all bearing locations. Nodes at all four corners of each plate element.
Model Components	Plates for all slab elements. Eccentric beam elements for each beam line, diaphragm and curb. Springs elements at each support.
Live-Load	2-D footprint of test truck consisting of 6 vertical point loads for the dump truck. Truck paths simulated by series of load cases with truck moving at 2-foot increments.
Dead-Load	Self-weight of structure.
Number of Load Case Positions Compared	50 x 4 lateral load paths = 200 Load case positions compared
Total Number of Strain Comparisons	40 strain points x 200 load positions = 8000 Strain Comparisons
Model Statistics	1080 Nodes 696 Elements 12 Cross-section/Material types 50 Load Cases 40 Gage locations
Adjustable Parameters for Model Calibration	1. Rotational springs at abutment support and Piers (F_x & M_y) 3. Deck slab Young's modulus (E) 4. Exterior beams Young's modulus (E) 5. Interior beams Young's modulus (E) 6. Curb Young's modulus (E) 7. Construction Joints Young's modulus (E)

MODEL CALIBRATION RESULTS

Several stiffness parameters were modified to obtain the best correlation between the measured and computed strain responses. The parameter values used in the initial model and obtained for the final model are provided in Table 6. Note that the stiffness parameters typically selected for modification was the modulus of the beam or slab sections. The resulting element modulus represented the “effective” homogenous material stiffness and includes the effect of crack density and the volume of steel in the reinforced concrete. Resulting modulus values should therefore not be considered to be true representation of the actual concrete modulus. The relative difference in material stiffness generally provides a measure of relative crack density at the various locations on the structure. Following the optimization procedures, the model produced a .9800 correlation. The initial and final correlation and other statistical error values are provided in Table 6. See Appendix G for a description of each error value.

- ***Element stiffness:*** The effective mid-span stiffness of the interior and exterior beams increased significantly from the initial assumed values. This was also true for the end-sections of the beams. The stiffness of the end-sections was greater than that of the mid-span sections which was to be expected due to a higher crack density at midspan.
- ***Deck Stiffness:*** Overall effective stiffness of the deck increased. This could be a result of a few inches of asphalt on top of the structure and/or the significantly high strength aggregate used in the original concrete. There was talk of exceptionally hard concrete on this bridge, but the resulting modulus values were very high.
- ***Pier Support Conditions:*** Since the pier support conditions were such that there was a physical gap between the spans, axial restraint springs alone were used to simulate the friction at the beam bearings. The concrete beams were bearing directly on the pier, causing a small amount of pier movement and slight continuity between spans. At a few locations, the beam bearing location was damaged. The axial forces generated by temperature effects and end rotation are likely the cause of deterioration at the supports.
- ***Parapet/Curb Stiffness:*** The effective stiffness for the parapet/curb increased since the interaction between the parapet and exterior beams had a significant effect on the structure’s edge stiffness. This type of response significantly improved the effective lateral load distribution of the bridge deck.

Table 6 Model accuracy & parameter values.

MODELING PARAMETER (UNITS)	INITIAL MODEL VALUE	FINAL MODEL VALUE
Pier axial spring (kips/in)	0	687.3
Beam stiffness – mid-span (ksi)	3,600	9,567
Beam stiffness - end (ksi)	3,600	7,086
Beam stiffness - bearing (ksi)	3,600	2,875
Deck stiffness (ksi)	3,600	6,474
Curb stiffness (ksi)	3,600	10,700
ERROR PARAMETERS	INITIAL MODEL VALUE	FINAL MODEL VALUE
Absolute Error	41,102	8,546
Percent Error	149.3%	4.0%
Scale Error	13.2%	2.0%
Correlation Coefficient	0.9674	0.9800

LOAD RATING PROCEDURES AND RESULTS

The goal of producing an accurate model was to predict the structure's actual live-load behavior when subjected to design or rating loads. This approach is essentially identical to standard load rating procedures, except that a "field verified" model is used instead of a typical beam analysis combined with load distribution factors. Please see Appendix H for a detailed outline of the load rating procedures.

Once the finite element model was calibrated to field conditions, engineering judgment was used to address any optimized parameters that may change over time or that may be unreliable with heavy loads or future damage. In this case, the optimized stiffness values for the beams, deck and curb were used for rating since there was no evidence to support adjusting the values manually. The pier springs were reduced to zero since some of the beam bearings were damaged and because it is likely that the friction is time dependant with respect to load duration and load rates. Reducing end-restraint values is a conservative approach which results in an increase in live-load mid-span moment and a lower load rating.

Capacities were calculated using the “Standard Specifications for Highway Bridges, 17th Edition - 2002”. Load rating factors for the standard AASHTO H-20, HS-20, Type 3, Type 3-3 and Type 3S3 vehicles were computed according to the LFD rating method. Load and resistance factors used in the rating are listed in Table 7.

Table 7 Load and Resistance Factors

LOAD	TYPE	FACTOR
Dead Load	Structural	1.30
Live Load	Inventory	2.17
	Operating	1.30
Impact Factor	IM	0.30
Multiple Lane Factor, <i>m</i>	No. of Lanes	
	1	1.00
	2	1.00

Section capacities were calculated based on the set of standard Louisiana Department of Transportation Specifications which was provided for the structure. From the standards provided, it was found that the steel reinforcement allowable stress (f_s) was 20 ksi, which based on the design code at the time this bridge was built, corresponds to a yield stress (f_y) of 40 ksi. Table 8 shows a typical beam section and necessary steel information. The concrete was assumed to have a compressive strength (f'_c) of 5000 psi. This is a high compressive strength for standard reinforced concrete, but justified and still conservative based on the model optimization results. The computed shear and moment capacities for the interior and exterior girders are provided in Table 9.

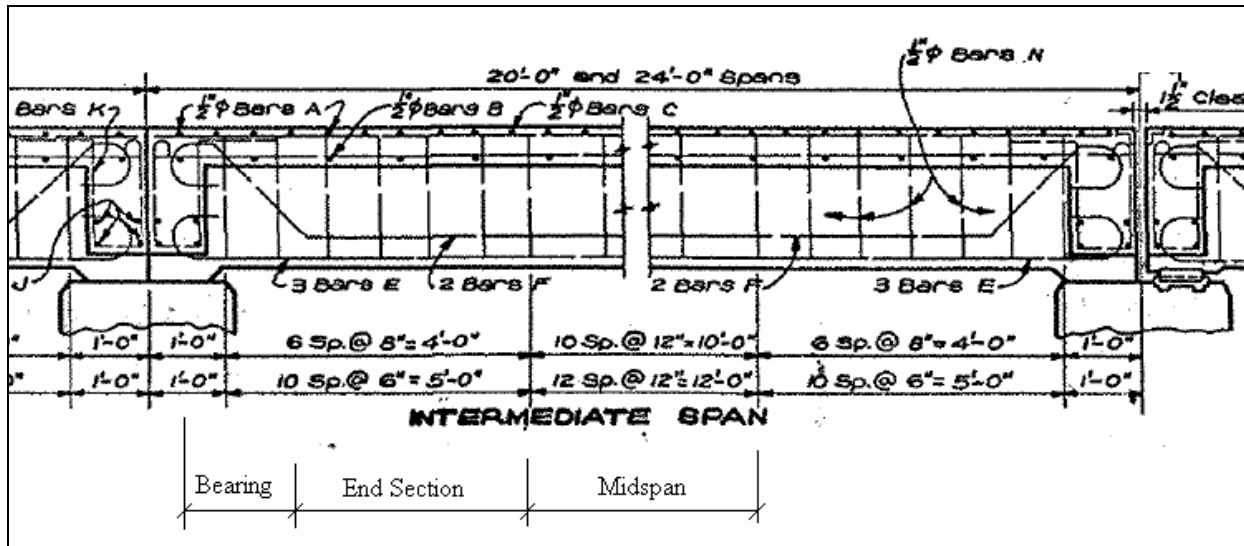


Figure 24 T-Beam Steel Details.

Table 8 Girder section and steel details.

Section	Details					
	Shear			Moment		
	V Bars	# Bars	Spacing	M Bars	# Bars	Area Steel
Midspan	#4	2	12"	1 1/8" sq.	5	6.328
End	#4	2	6"	1 1/8" sq.	5	6.328
Bearing	#4 + sloped	2 & 2	6"	1 1/8" sq.	3	3.800

Table 9 T-Beam Moment and Shear Capacities.

MEMBER	MOMENT CAPACITY $\phi_f M_n$ (kip-in)	SHEAR CAPACITY $\phi_v V_n$ (kips)
Interior Girders – Mid-span	4416.5	36.90
Interior Girders - End	4416.5	56.96
Interior Girders - Bearing	4416.5	168.15
Exterior Girders – Mid-span	4407.1	36.90
Exterior Girders - End	4407.1	56.96
Exterior Girders - Bearing	4407.1	168.15

Maximum live and dead-load shear and moment responses for each load configuration were obtained from the field verified finite-element model. The live-load shear and moment values present in Table 10 through Table 14 are the un-factored live-load and dead-load responses. Rating factors for the bridge prior to any strengthening procedures were computed for the H-20, HS-20, Type 3, Type 3-3, Type 3S3 are also provided. In all cases, the load rating factors were controlled by the shear capacity of the interior beams.

Table 10 Load rating factors for H-20.

Group	Name	Mode	RF	Element#	Node	Envelope	DL Response	LL Response
1	Ext_Girders_Midspan	+Fz	1.57	173	1	6	4.08	7.14
		-Fz	1.47	95	1	6	-3.96	-7.68
		+My	1.71	123	2	6	543.7	764.94
2	Int_Girders_Midspan	+Fz	0.89	262	1	6	5.11	11.99
		-Fz	0.87	184	1	6	-5.01	-12.38
		+My	1.03	212	2	6	647.85	1231.33
12	Int_Girders_End	+Fz	1.19	264	1	6	6.88	14.33
		-Fz	1.11	182	1	6	-6.99	-15.26
		+My	1.59	205	2	6	411.23	865.18
13	Ext_Girders_End	+Fz	2.13	175	1	6	5.63	8.24
		-Fz	1.91	93	1	6	-5.8	-9.18
		+My	2.56	160	2	6	361.6	545.46
14	Girders_Bear	+Fz	3.41	221	1	6	8.26	16.35
		-Fz	3.14	180	1	6	-8.67	-17.72

Table 11 Load rating factors for HS-20

Group	Name	Mode	RF	Element#	Node	Envelope	DL Response	LL Response
1	Ext_Girders_Midspan	+Fz	1.37	173	1	6	4.08	8.16
		-Fz	1.32	95	1	6	-3.96	-8.5
		+My	1.69	123	2	6	543.7	775.65
2	Int_Girders_Midspan	+Fz	0.81	262	1	6	5.11	13.29
		-Fz	0.81	184	1	6	-5.01	-13.33
		+My	1.03	212	2	6	647.85	1231.33
12	Int_Girders_End	+Fz	1	264	1	6	6.88	16.95
		-Fz	0.97	182	1	6	-6.99	-17.48
		+My	1.39	205	2	6	411.23	991.78
13	Ext_Girders_End	+Fz	1.74	175	1	6	5.63	10.11
		-Fz	1.63	93	1	6	-5.8	-10.73
		+My	2.2	160	2	6	361.6	633.23
14	Girders_Bear	+Fz	2.75	221	1	6	8.26	20.28
		-Fz	2.65	180	1	6	-8.67	-20.95

Table 12 Load rating factors for Type 3

Group	Name	Mode	RF	Element#	Node	Envelope	DL Response	LL Response
1	Ext_Girders_Midspan	+Fz	1.59	173	1	6	4.08	7.05
		-Fz	1.7	95	1	6	-3.96	-6.6
		+My	1.9	122	2	6	548.62	688.57
2	Int_Girders_Midspan	+Fz	0.92	262	1	6	5.11	11.71
		-Fz	0.97	184	1	6	-5.01	-11.05
		+My	1.12	211	2	6	653.87	1127.34
12	Int_Girders_End	+Fz	1.23	219	1	6	6.61	13.95
		-Fz	1.17	182	1	6	-6.99	-14.49
		+My	1.86	205	2	6	411.23	739.67
13	Ext_Girders_End	+Fz	2.23	130	1	6	5.17	7.97
		-Fz	1.99	93	1	6	-5.8	-8.82
		+My	3.08	160	2	6	361.6	453.34
14	Girders_Bear	+Fz	3.45	221	1	6	8.26	16.17
		-Fz	3.25	180	1	6	-8.67	-17.11

Table 13 Load rating factors for Type 3-3

Group	Name	Mode	RF	Element#	Node	Envelope	DL Response	LL Response
1	Ext_Girders_Midspan	+Fz	2.11	128	1	6	3.68	5.38
		-Fz	1.99	95	1	6	-3.96	-5.67
		+My	2.31	122	2	6	548.62	566.52
2	Int_Girders_Midspan	+Fz	1.22	217	1	6	4.7	8.98
		-Fz	1.15	184	1	6	-5.01	-9.34
		+My	1.37	211	2	6	653.87	923.88
12	Int_Girders_End	+Fz	1.57	219	1	6	6.61	10.9
		-Fz	1.49	182	1	6	-6.99	-11.37
		+My	2.16	205	2	6	411.23	637.57
13	Ext_Girders_End	+Fz	2.88	130	1	6	5.17	6.17
		-Fz	2.6	93	1	6	-5.8	-6.74
		+My	3.5	116	2	6	361.81	398.94
14	Girders_Bear	+Fz	4.39	221	1	6	8.26	12.72
		-Fz	4.19	180	1	6	-8.67	-13.26

Table 14 Load rating factors for Type 3S3

Group	Name	Mode	RF	Element#	Node	Envelope	DL Response	LL Response
1	Ext Girders Midspan	+Fz	1.74	173	1	6	4.08	6.43
		-Fz	1.78	95	1	6	-3.96	-6.33
		+My	2.06	122	2	6	548.62	636.54
2	Int Girders Midspan	+Fz	1.01	262	1	6	5.11	10.67
		-Fz	1.03	184	1	6	-5.01	-10.44
		+My	1.22	233	2	6	653.87	1037.54
12	Int Girders End	+Fz	1.32	264	1	6	6.88	12.87
		-Fz	1.22	182	1	6	-6.99	-13.96
		+My	1.92	227	2	6	411.23	715.39
13	Ext Girders End	+Fz	2.35	175	1	6	5.63	7.49
		-Fz	2.04	93	1	6	-5.8	-8.57
		+My	3.17	160	2	6	361.6	440.46
14	Girders Bear	+Fz	3.75	266	1	6	8.39	14.86
		-Fz	3.39	180	1	6	-8.67	-16.4

To evaluate the benefit of the various FRP strengthening procedures, load ratings were performed on each of the strengthened beam types. Modified moment capacities, based on the actual material used in the retrofits, were calculated by Paul Ziehl at the University of South Carolina. Table 15 contains the ultimate moment capacities of the original beam and each of the strengthened beam types. To provide an indication of the increased live-load capacity provided by the FRP strengthening, HS-20 load rating factors are also provided for each beam type. Because the additional strength provided by the FRP is available entirely for live-load, a substantial increase can be seen in all the load rating factors.

Table 15 Moment Capacities and Load Rating Factors of Strengthened Beams.

Beam Type	ΦM_n (kip-in)	HS-20 Load Ratings			
		RF Inv.	Tons	RF Oper.	Tons
Original T-beam	4417	1.04	37	1.74	62
Vwrap C100	5525	1.36	49	2.27	82
Carbodur S512 – Surface	5095	1.24	45	2.07	75
Carbodur S512 – NSM	5844	1.46	53	2.44	88

LONG-TERM MONITORING SYSTEM

In order to monitor the long-term performance of the strengthening methods a structural monitoring system was installed on the bridge. The long-term monitoring system includes several strain and crack measurement sensors that are monitored on a continuous basis. There are

numerous temperature sensors which obtain the ambient temperature, temperature of each displacement type sensor and the internal temperature of the concrete beams. A relative humidity sensor is also installed.

This type of monitoring system is intended to measure and record slow-speed and permanent movements such as those from temperature, settlement, creep and/or damage. The system is not intended to measure any live-load responses except under a complete static situation. Measurement cycles occur at a 60 second interval so responses due to normal traffic responses cannot be captured.

Figure 25 through Figure 27 contain the long-term instrumentation plans for Spans 2, 3, and 4. The two strengthened spans and the unmodified control span are instrumented in a manner similar to the live-load tests. In general the midspan strains are measured along with a crack opening displacement. Strain gages were installed on both the concrete and on the FRP at Span 3 where the surface mounted FRP was applied. Sensor locations designated at S# refer to strain gages, C# refer to crack displacement, and T# indicates an embedded thermistor.

The data logger setup consists of a Campbell Scientific, Inc. CR10X measurement and control device. The system is powered with a 20 watt solar panel and contains a 12 V battery to maintain operation at night. A cell modem is provided so that data can be retrieved and the logger control can be performed remotely. A custom program was written for the logger to measure the specific sensors and perform various data processing tasks. The original program was written to measure each sensor on a 60 second interval and then compute and store the averages and extreme values from each sensor once an hour. The logger operation can be controlled remotely via modem or by a PC connected directly to the logger.

An option exists to record the raw data on every measurement cycle (60 seconds). This feature is useful to run static load tests on a periodic basis. The continuous measurement cycle can be initiated and run for a couple minutes after which a specific load can then be applied to the bridge and left in place for another two minutes. Various load conditions can be applied, but each change in load condition should remain in place for at least two minutes to ensure that all sensors have been recorded with the new load condition. It will be very important to record the logger time during each load event. Following any procedures during which data is recorded continuously, it will be important to turn off the continuous recording feature. The logger memory will fill up within hours during the continuous recording; where as several months of data can be stored when only the hourly recording is performed.

All communication and control of the logger is performed with the CSI LoggerNet software. Complete instructions are available in the LoggerNet software manual. Basic information on how LoggerNet is used to communicate with the White Bayou data logger and specific details on the data-logger program are provided in Appendix D.

It is important to note that the data logger is not intended to replace visual inspection. It should be viewed as a tool to help with visual inspection and provide information as to what areas may need to be examined.

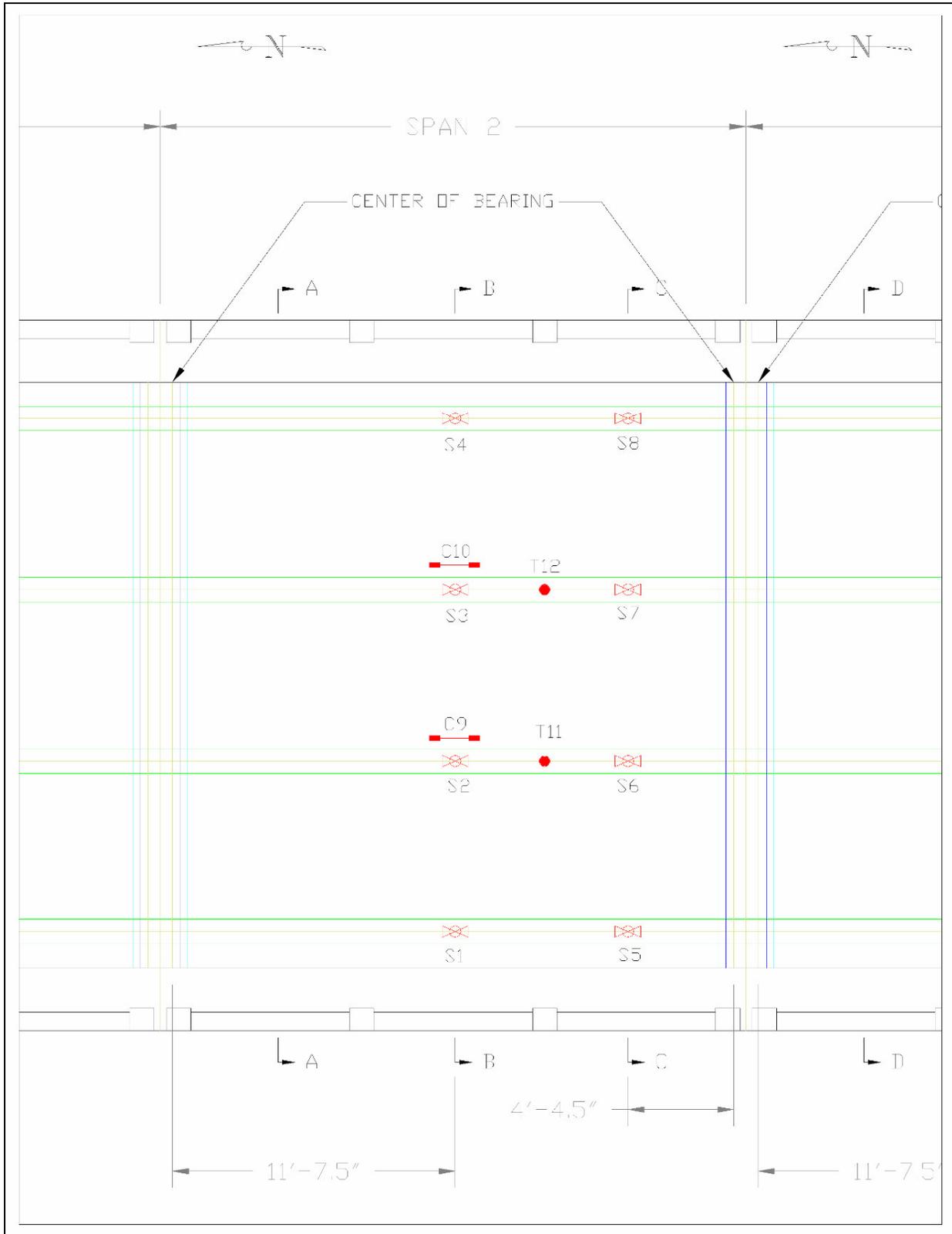


Figure 25 Long-term Instrumentation Plan – Span 2.

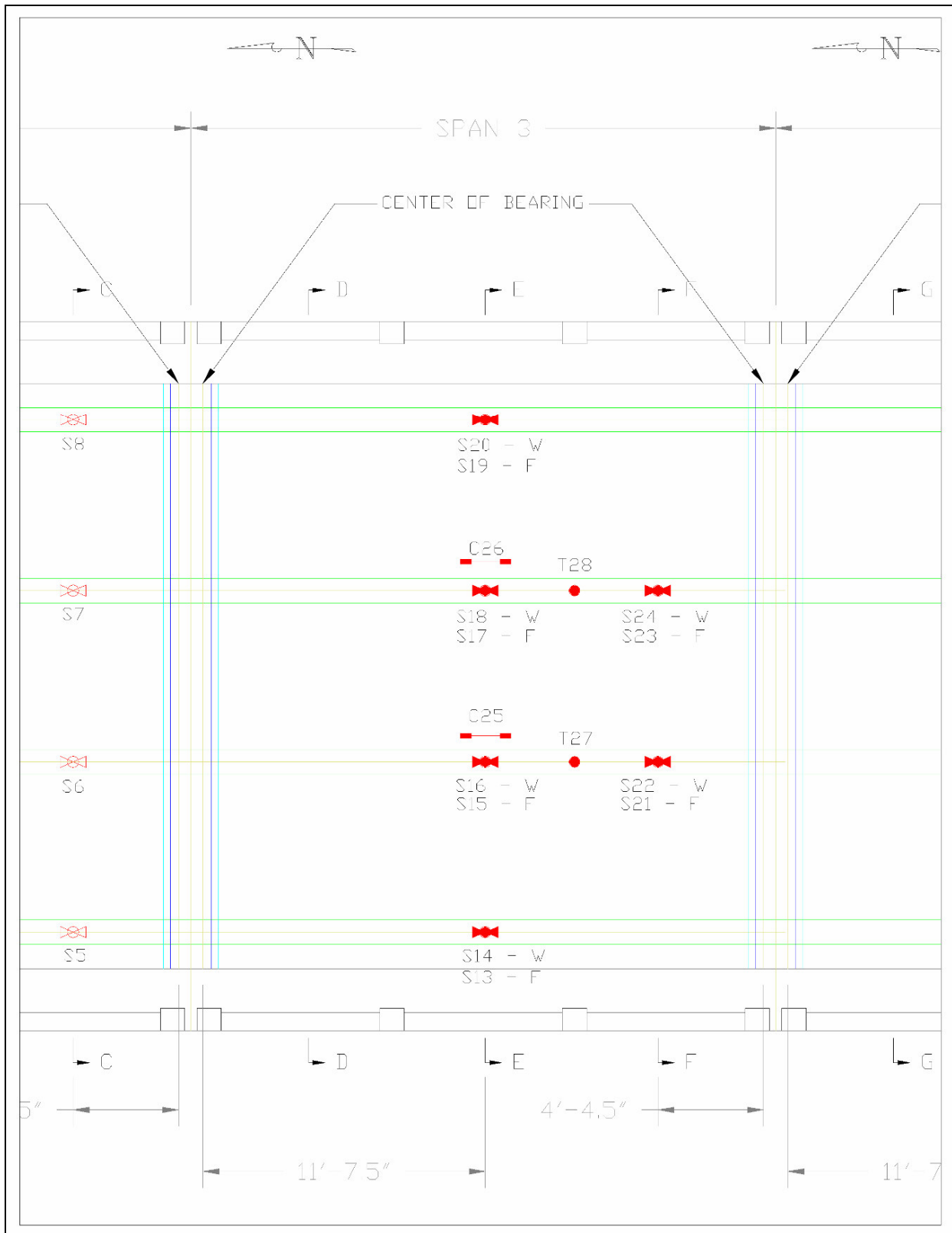


Figure 26 Long-term Instrumentation Plan – Span 3.

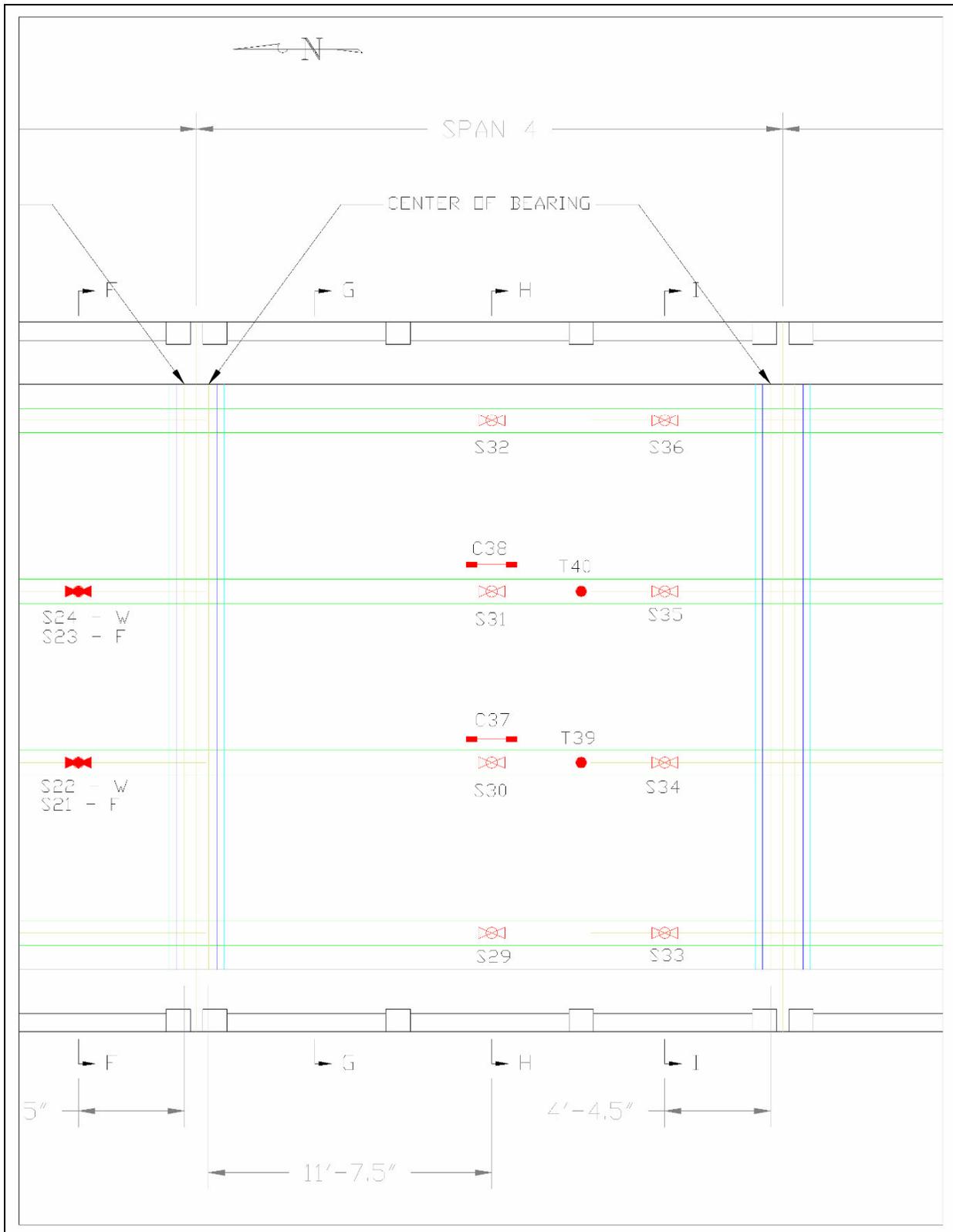


Figure 27 Long-term Instrumentation Plan – Span 4.

CONCLUSIONS AND RECOMMENDATIONS

Conclusions made directly from the load test data were qualitative in nature and indicated that the structure was behaving typical for a reinforced concrete structure. The structure appeared to be in fair condition with visible flexural and shear cracks. All strain measurements indicated that the structure was behaving linearly with respect to load magnitude (truck position) and all responses were elastic. It was also noted that some of the beam bearing locations had experienced damage. The damaged beam bearing have not yet altered the structural performance but a significant reduction in bearing area has occurred.

As is typical of RC structures, flexural cracks were observed at various locations on the beams. Load test results and subsequent model calibration indicated a higher density of cracks at mid-span (higher flexibility) than near the beam ends. This result was expected since crack formation is related to the moment magnitude. The resulting member stiffness was exceptionally high compared to what was initially assumed. Exact reasons for this are not known for sure, it is possible the actual deck thickness is greater than what was indicated by the Louisiana design standard.

Load tests were performed before and after the implementation of FRP strengthening procedures. Several beams were modified with different techniques of carbon fiber strengthening. While a change in ultimate capacity was expected, it was not expected that the responses within the serviceability limits would be noticeably different. Load test procedures and load magnitudes were nearly identical between the two load tests, yet the measurements indicated a reduction of midspan strains and displacement of approximately 10 percent on the interior girders. The same level of change was observed on the strengthened and on the unmodified spans so it did not appear that the increased stiffness was a result of the FRP application.

Load rating calculations indicated that the bridge's load capacity is limited by shear at the midspan regions of the interior girders. While the FRP strengthening did not address the shear deficiency, it had a significant effect on the load rating factors resulting from moment capacity. The primary focus of this study was to evaluate the feasibility of FRP strengthening and help evaluate the long-term performance. It was not intended to increase the actual load limit on the bridge as only 2 of the 8 spans were strengthened. Therefore it is important to note that the current posted load limit on this bridge cannot be removed due to the improved load ratings resulting from the FRP strengthening procedures.

APPENDIX A - MEASURED AND COMPUTED STRAIN COMPARISONS

While statistical terms provide a means of evaluating the relative accuracy of various modeling procedures or help determine the improvement of a model during a calibration process, the best conceptual measure of a model's accuracy is by visual examination of the response histories. The following graphs contain measured and computed stress histories from each truck path. In each graph the continuous lines represent the measured strain at the specified gage location as a function of truck position as it traveled across the bridge. Computed strains are shown as markers at discrete truck intervals.

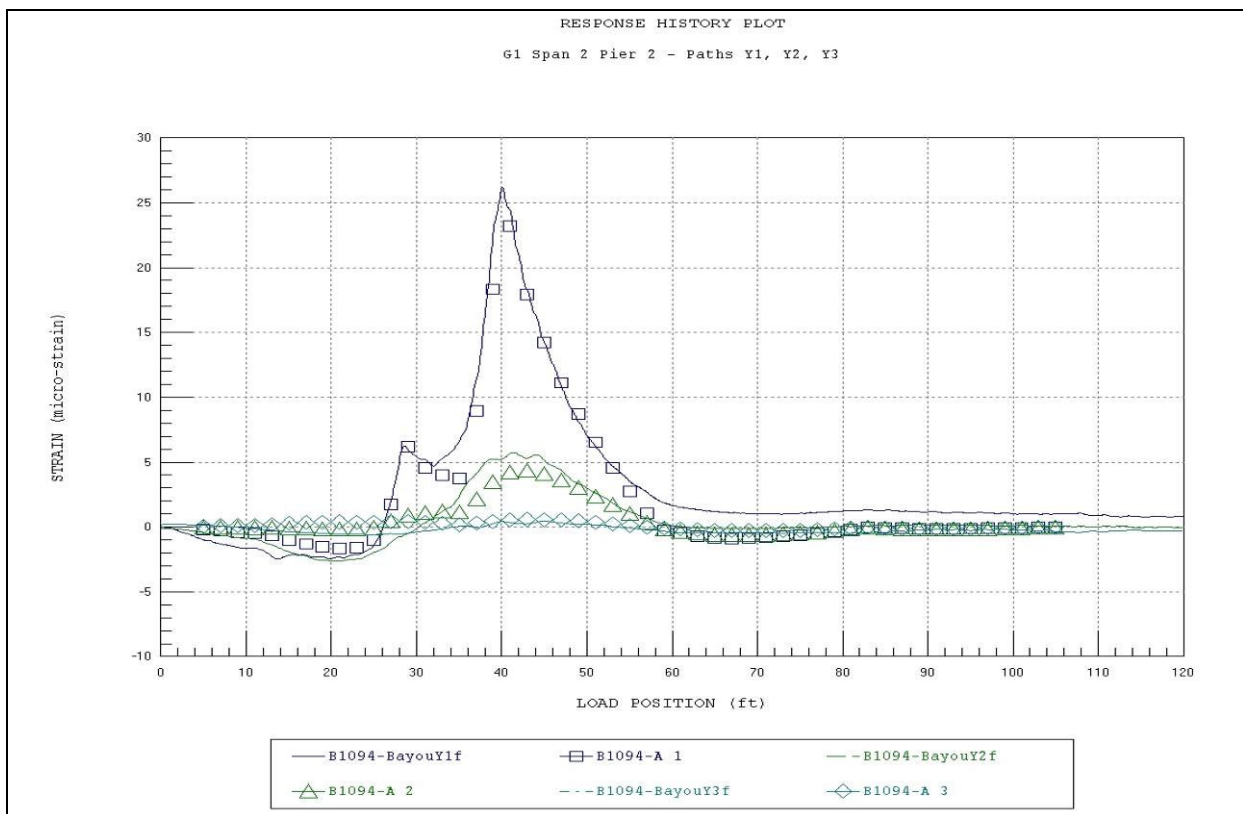


Figure 28 Beam 1, cross-section A-A – bottom.

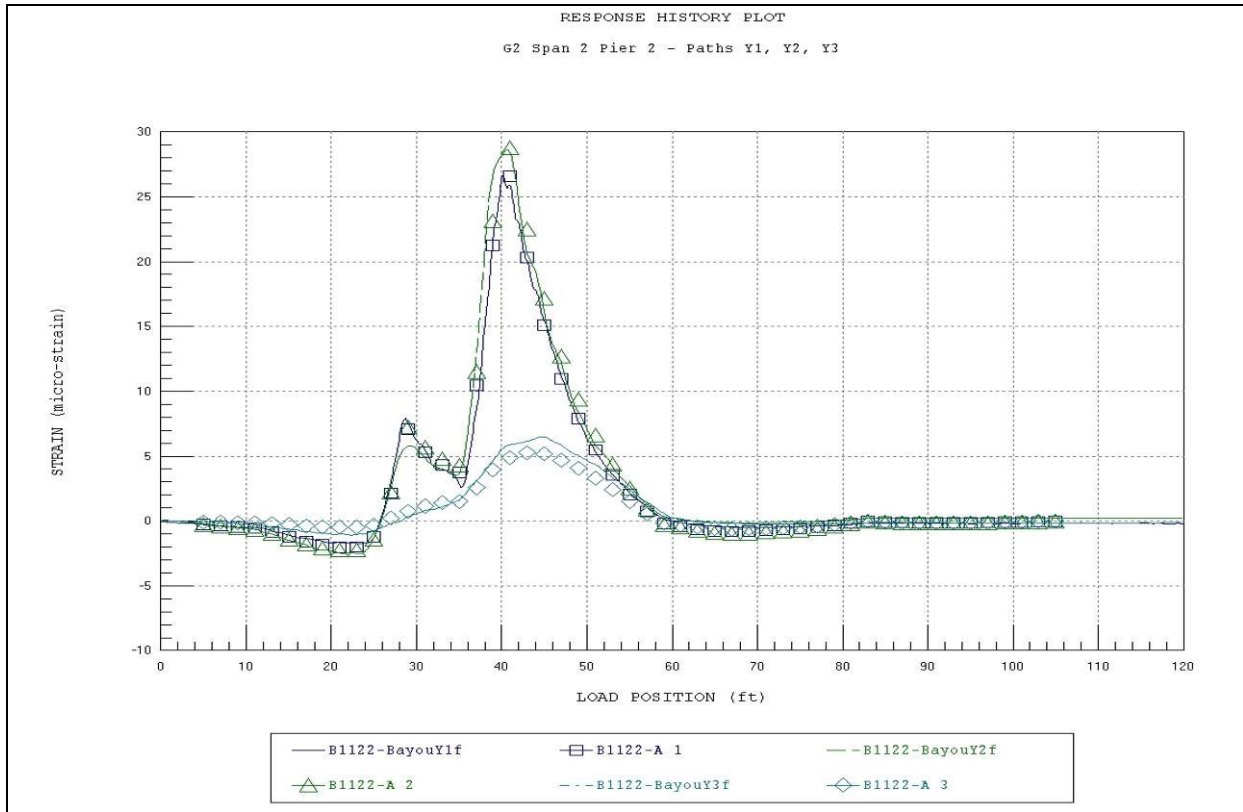


Figure 29 Beam 2, cross-section A-A – bottom.

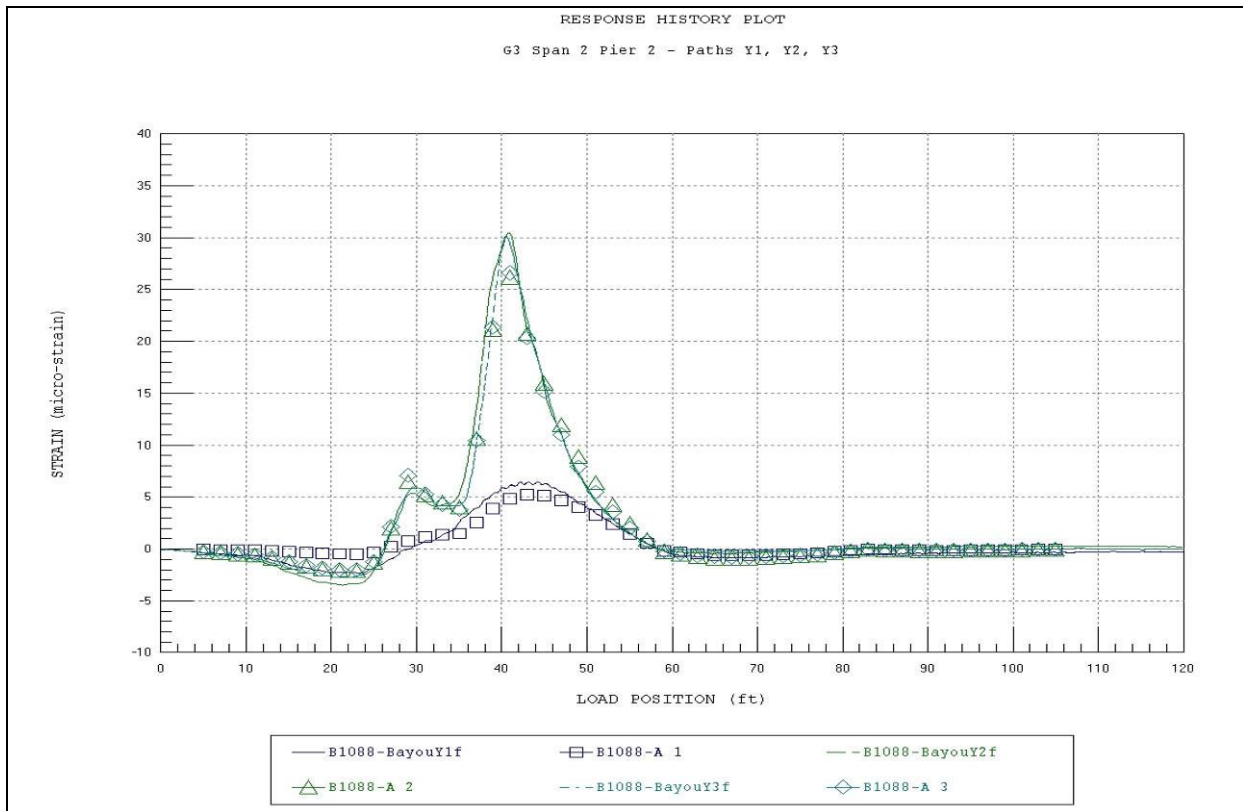


Figure 30 Beam 3, cross-section A-A – bottom.

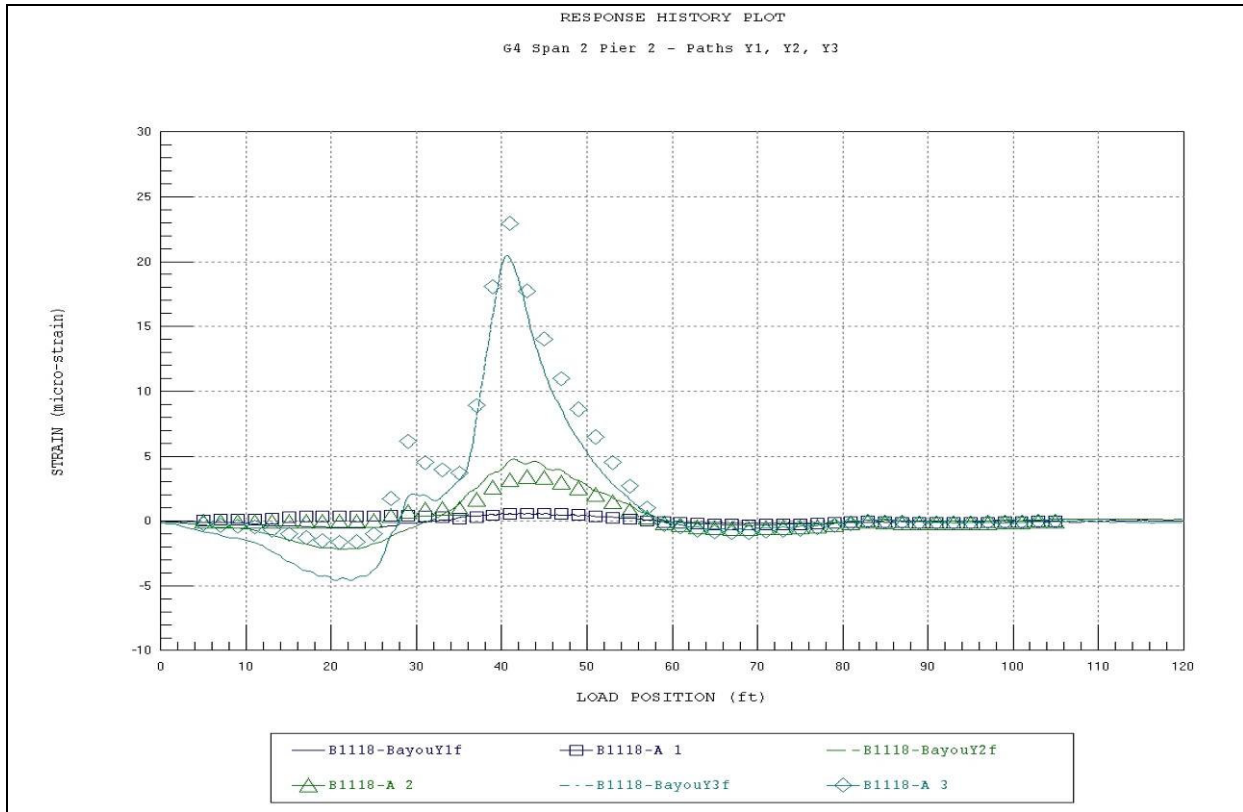


Figure 31 Beam 4, cross-section A-A – bottom.

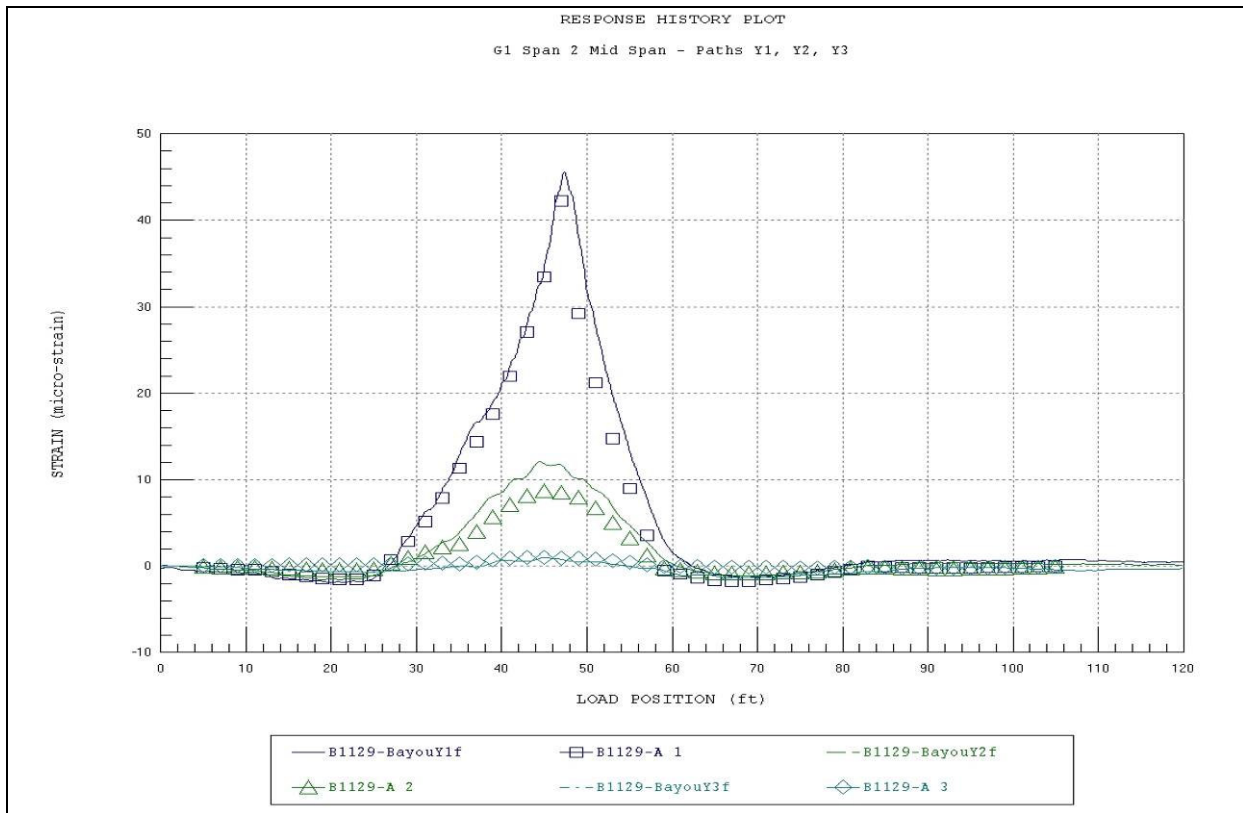


Figure 32 Beam 1, cross-section B-B – bottom.

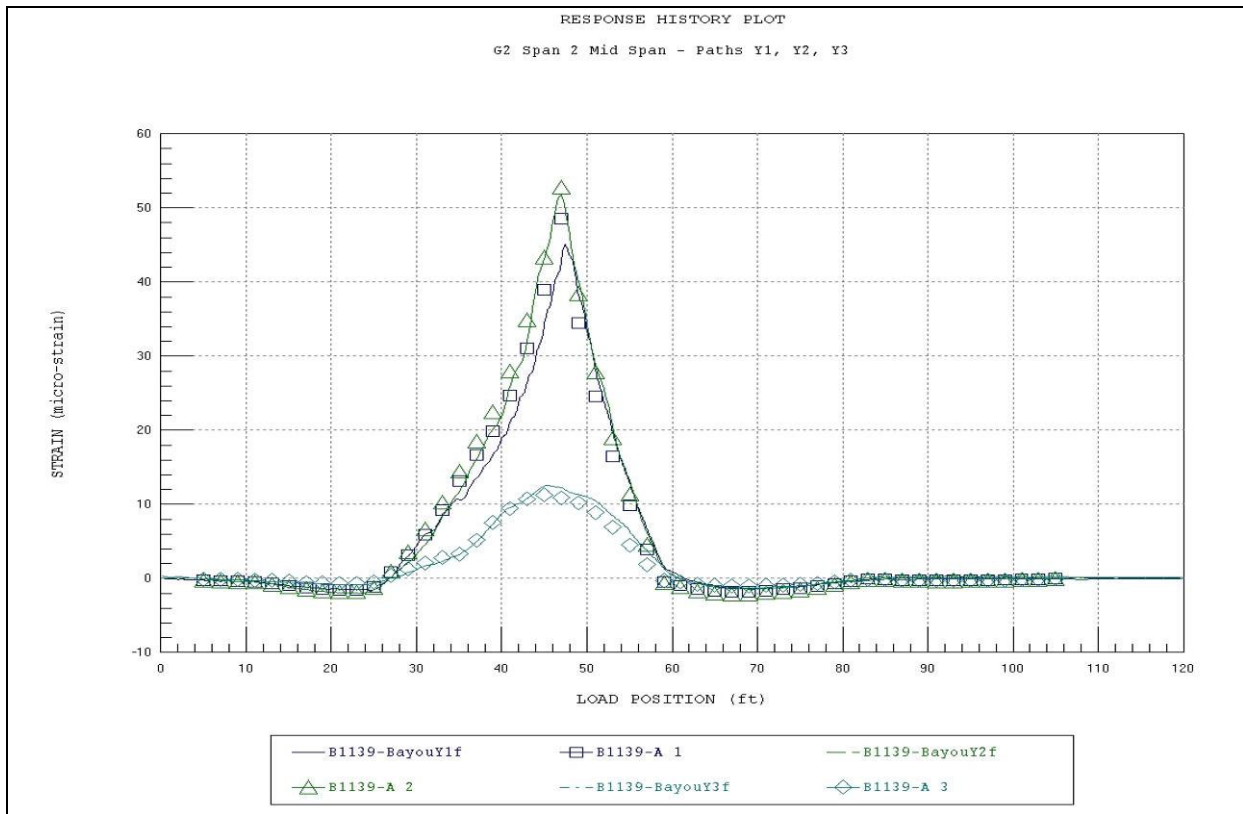


Figure 33 Beam 2, cross-section B-B – bottom.

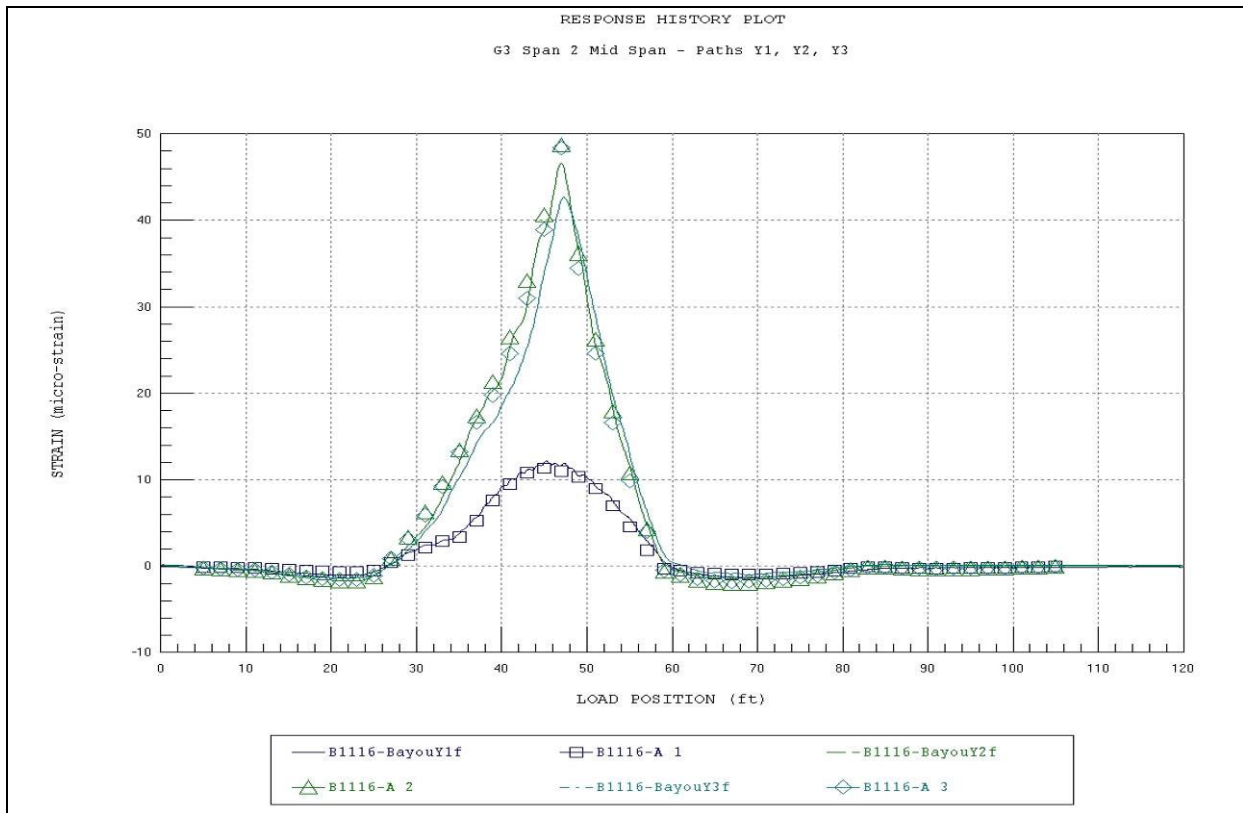


Figure 34 Beam 3, cross-section B-B – bottom.

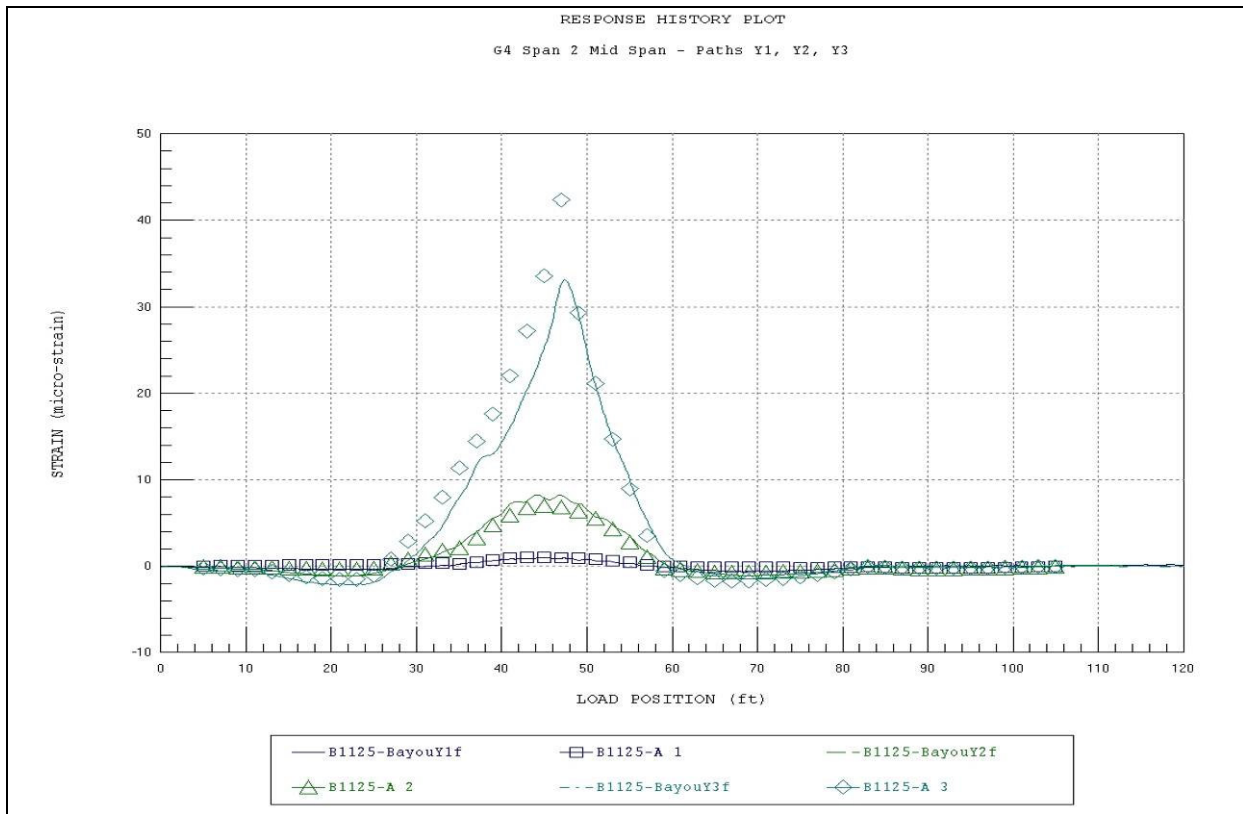


Figure 35 Beam 4, cross-section B-B – bottom.

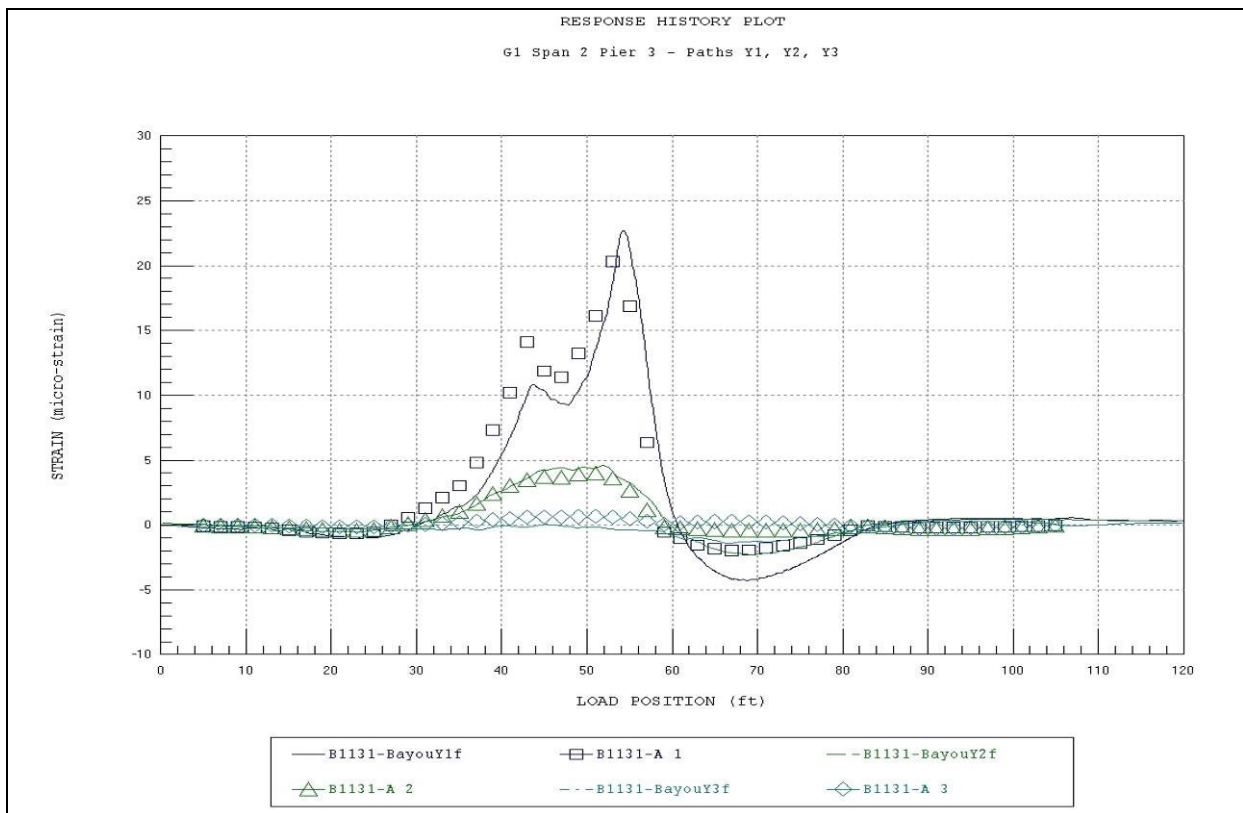


Figure 36 Beam 1, cross-section C-C – bottom.

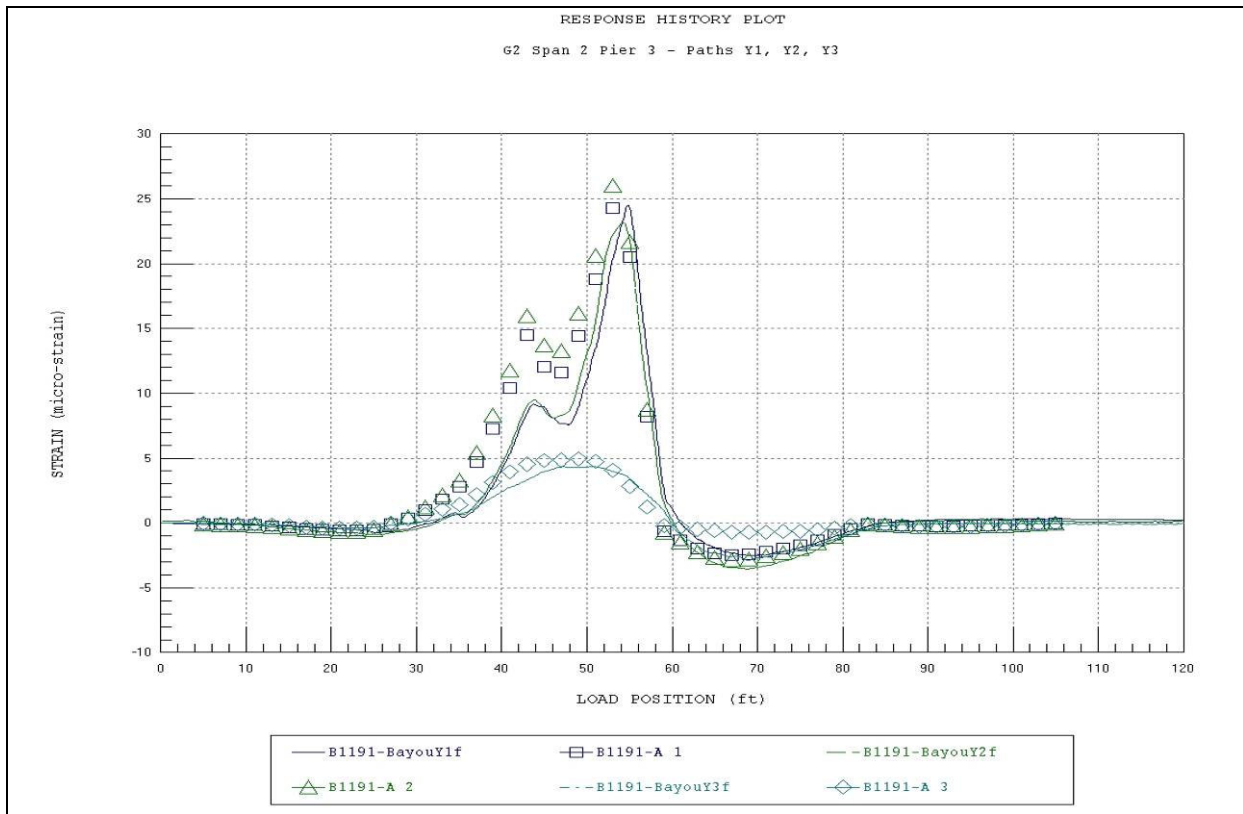


Figure 37 Beam 2, cross-section C-C – bottom.

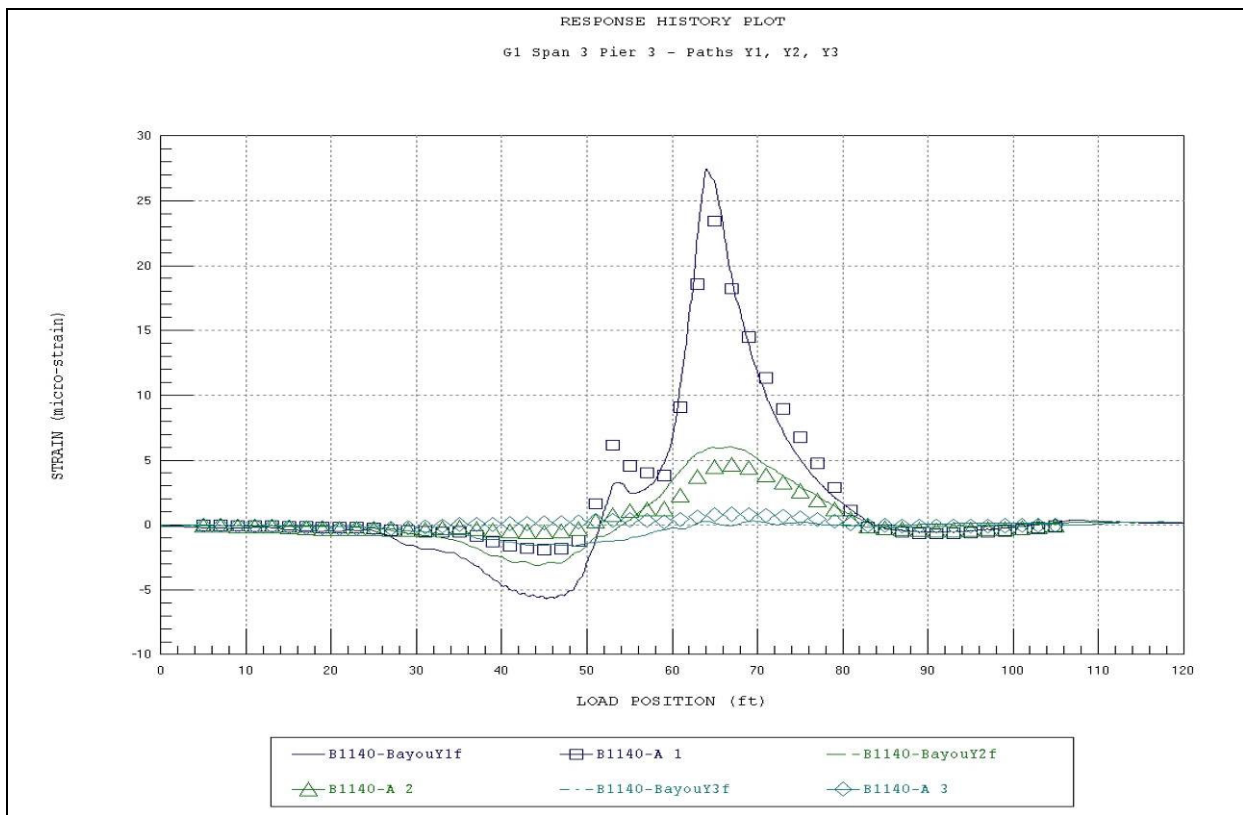


Figure 38 Beam 1, cross-section D-D – bottom.

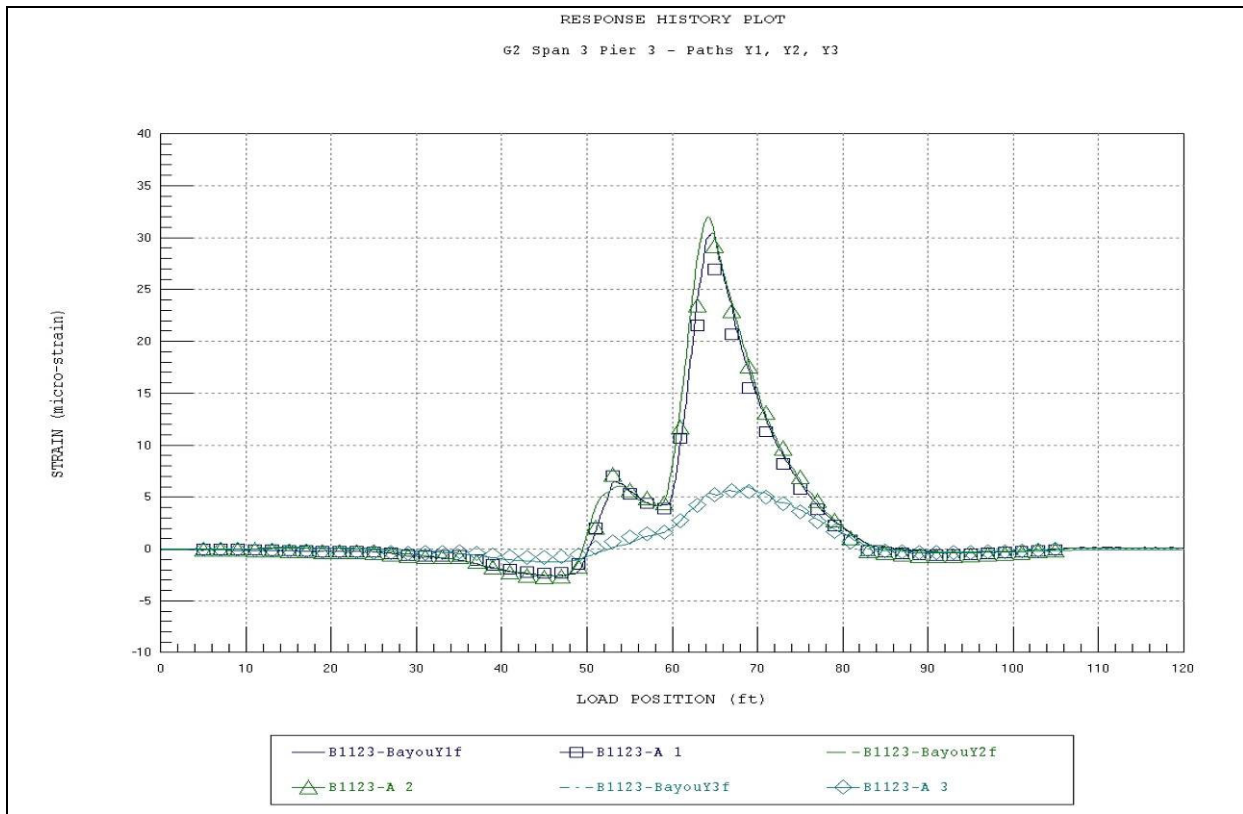


Figure 39 Beam 2, cross-section D-D – bottom.

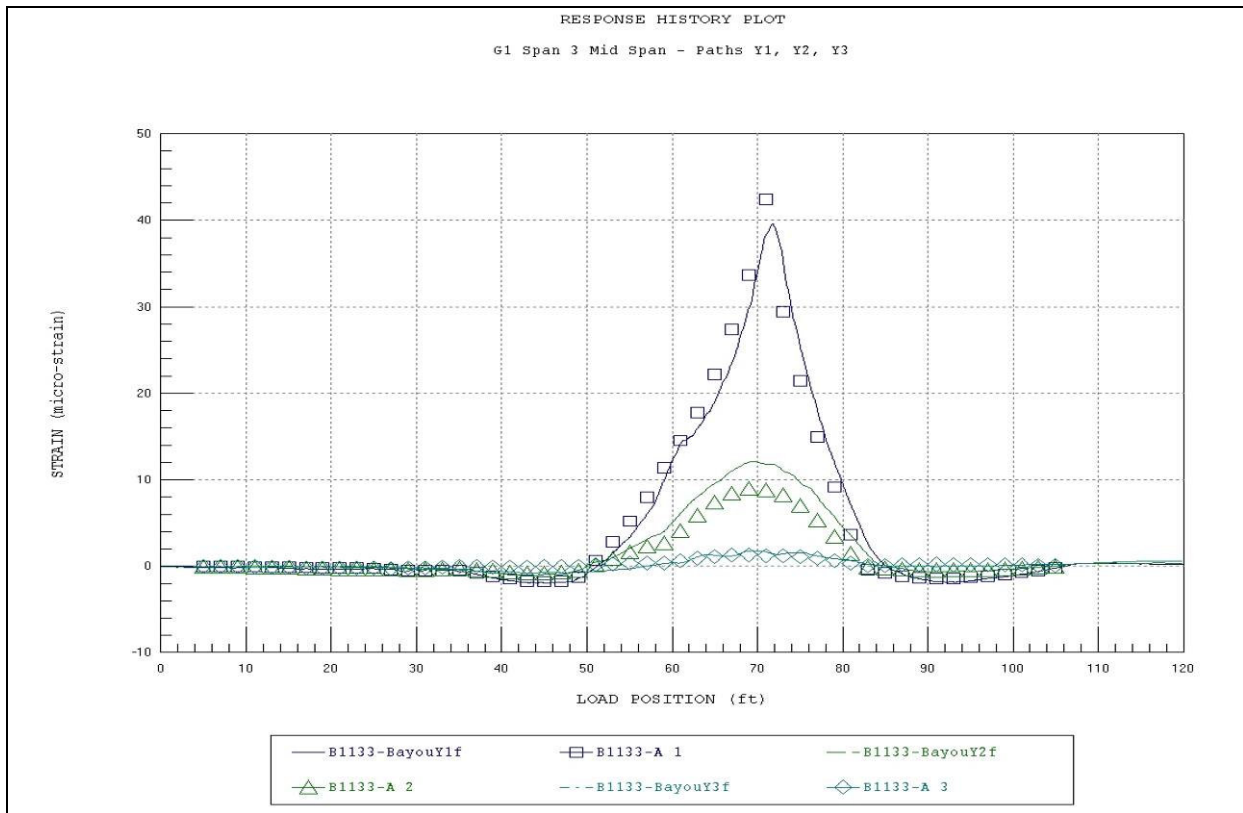


Figure 40 Beam 1, cross-section E-E – bottom.

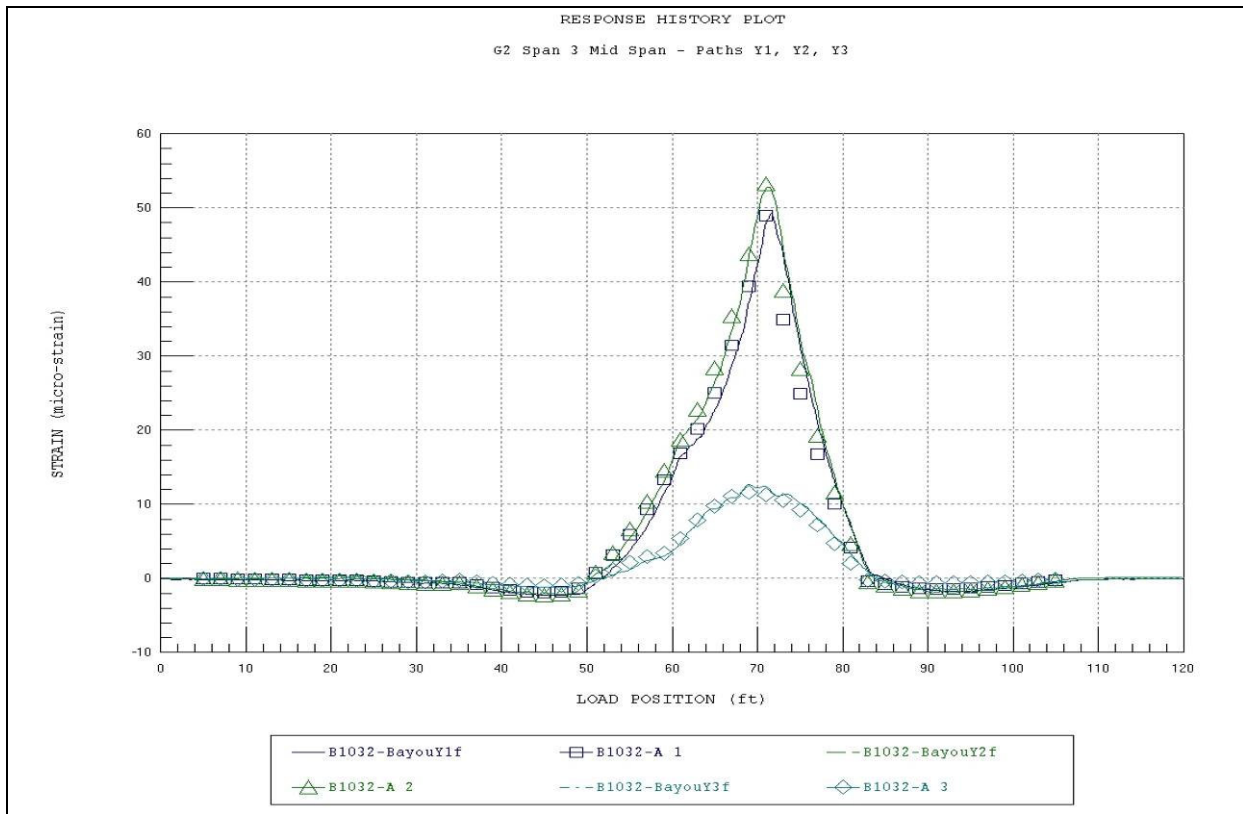


Figure 41 Beam 2, cross-section E-E – bottom.

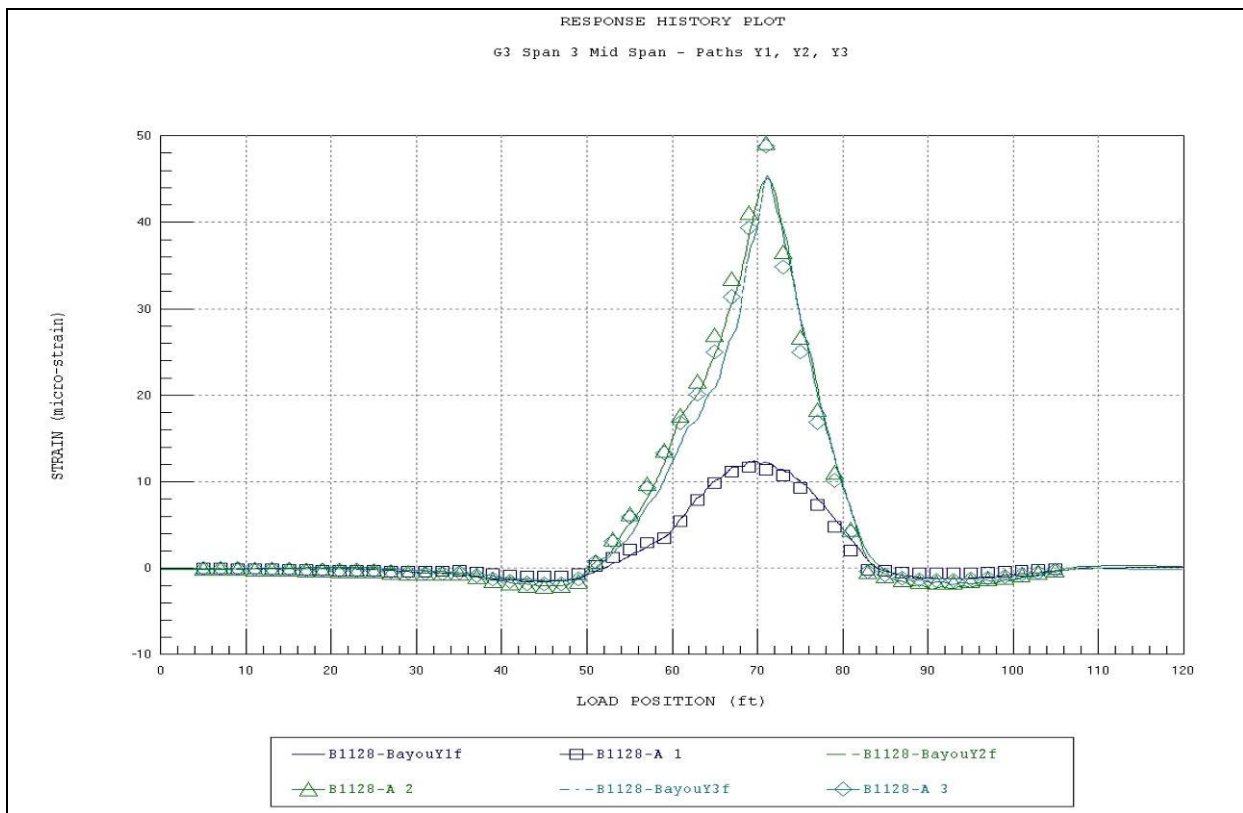


Figure 42 Beam 3, cross-section E-E – bottom.

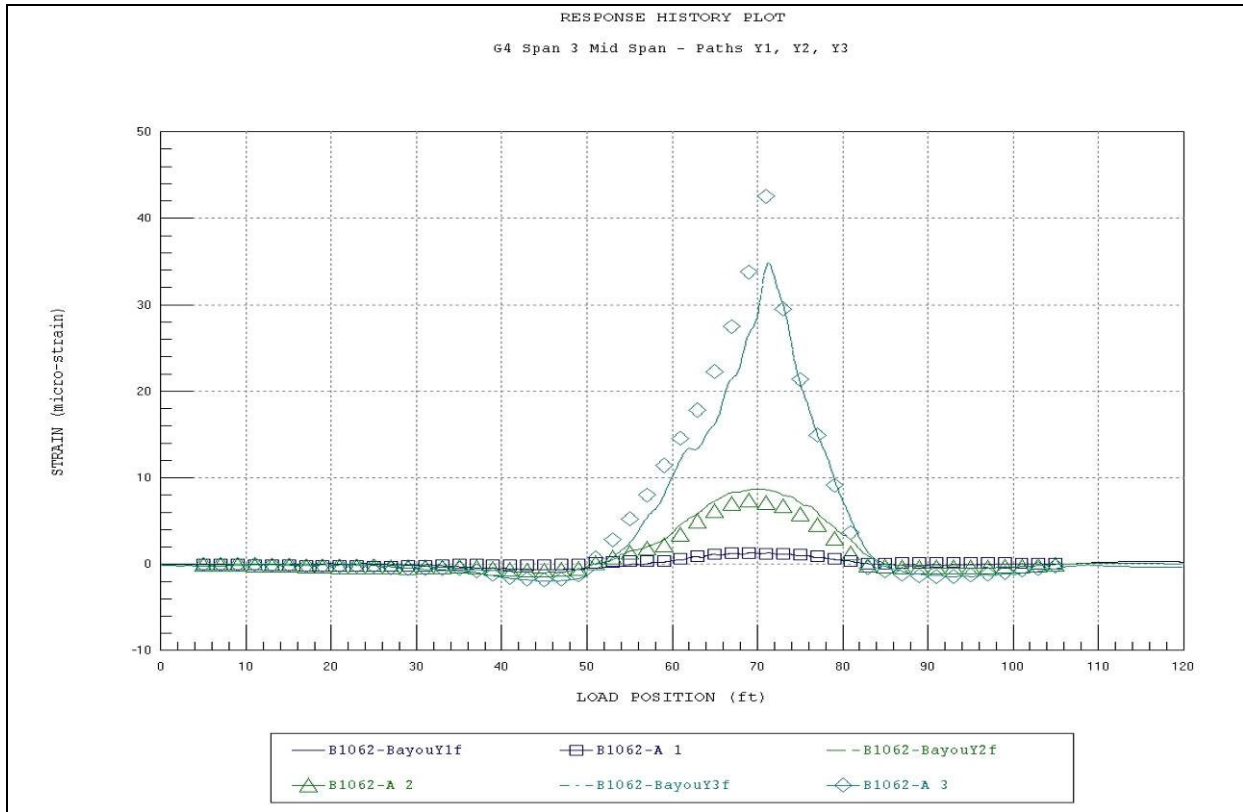


Figure 43 Beam 4, cross-section E-E – bottom.

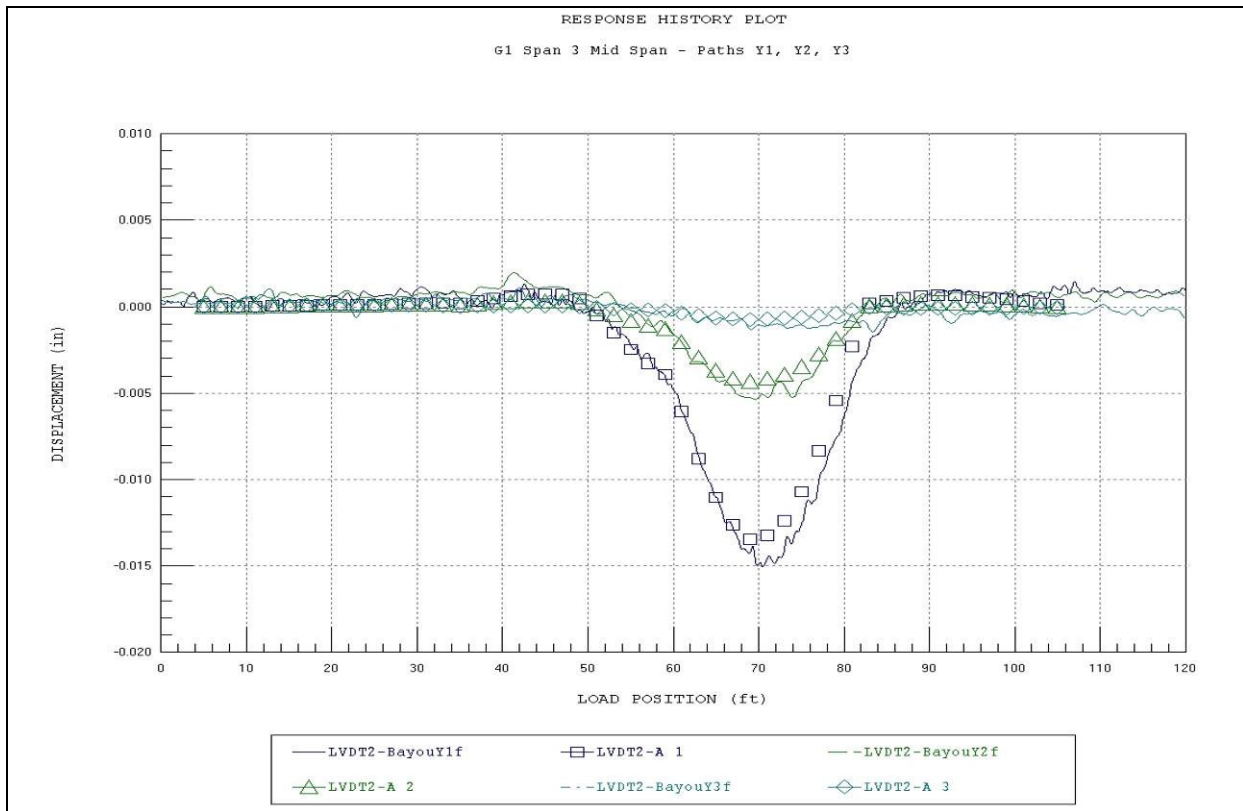


Figure 44 Beam 1, cross-section E-E – displacement.

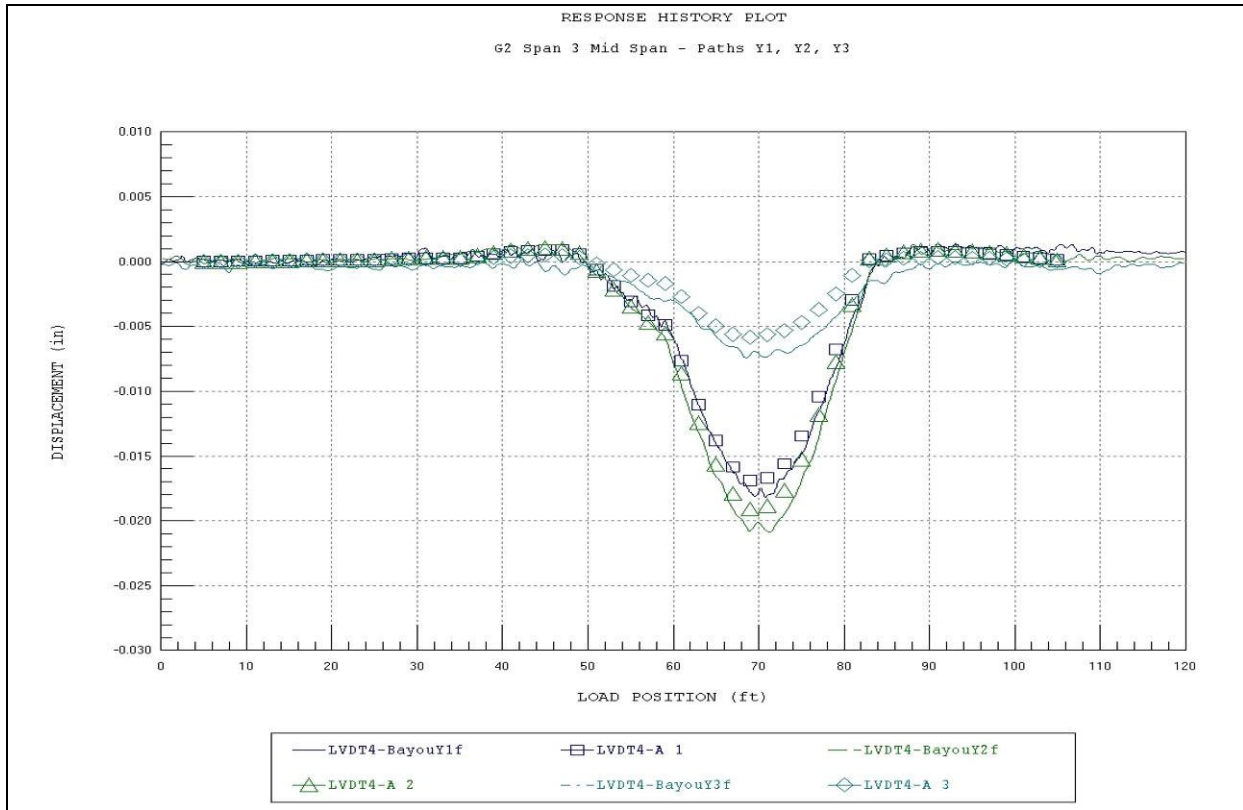


Figure 45 Beam 2, cross-section E-E – displacement.

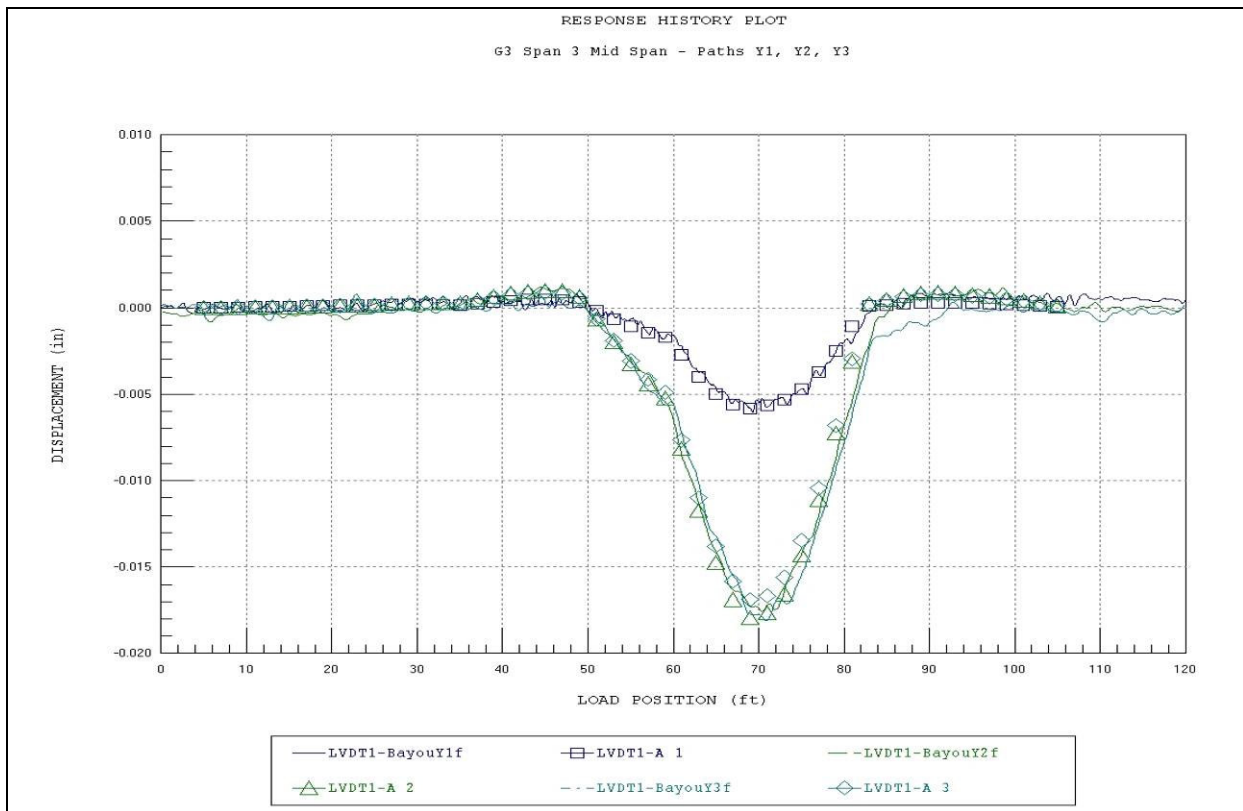


Figure 46 Beam 3, cross-section E-E – displacement.

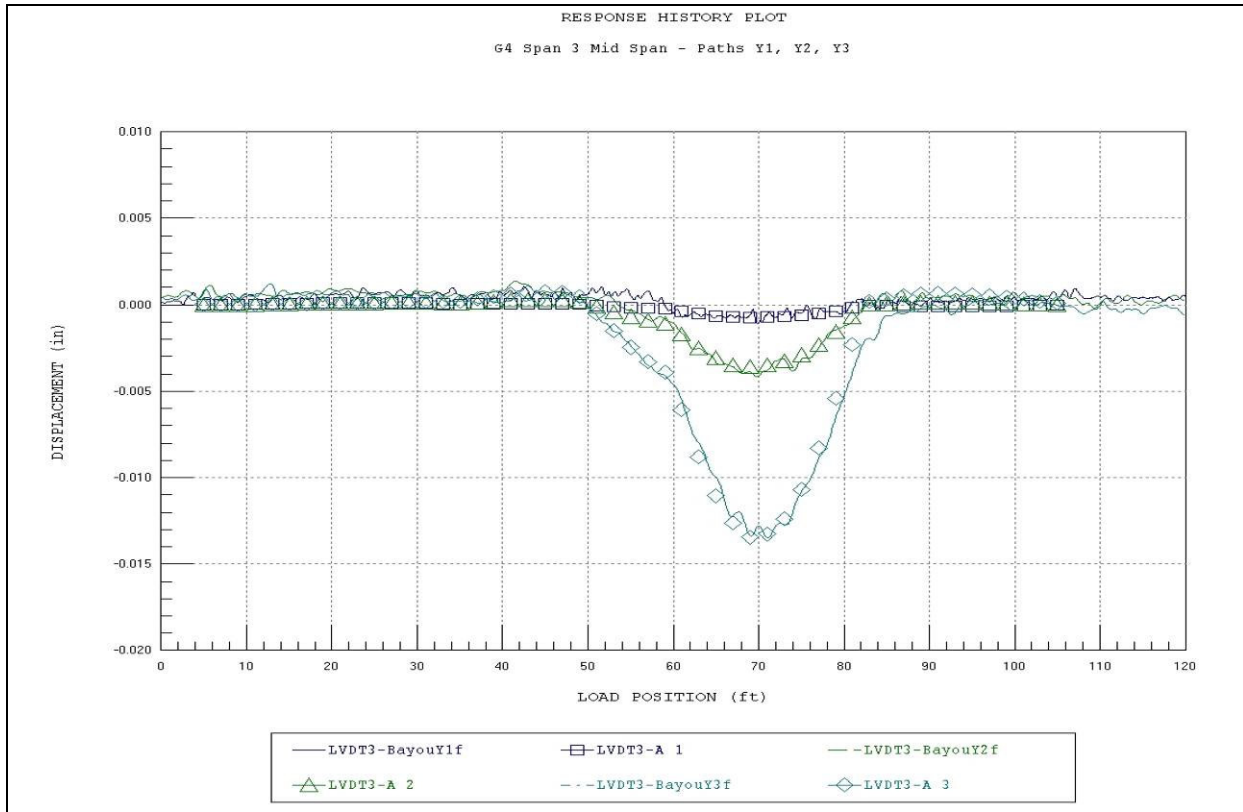


Figure 47 Beam 4, cross-section E-E – displacement.

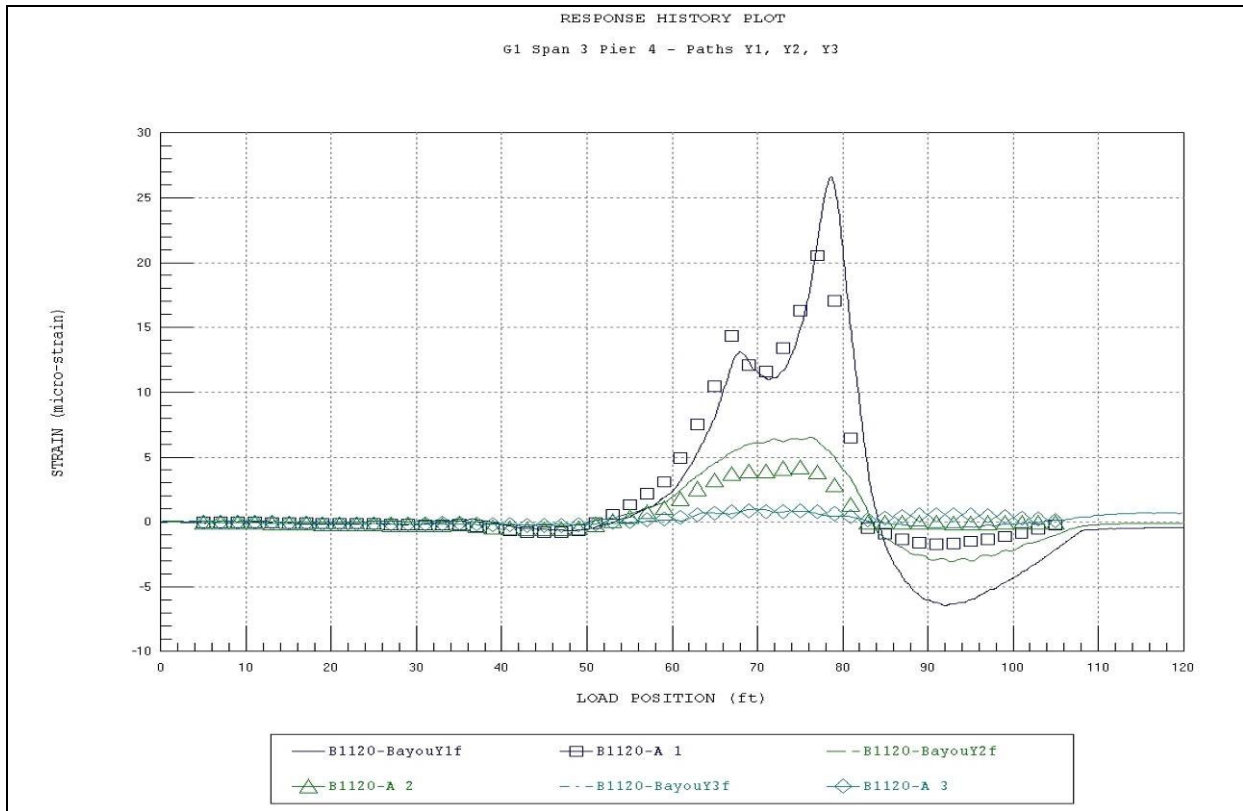


Figure 48 Beam 1, cross-section F-F – bottom.

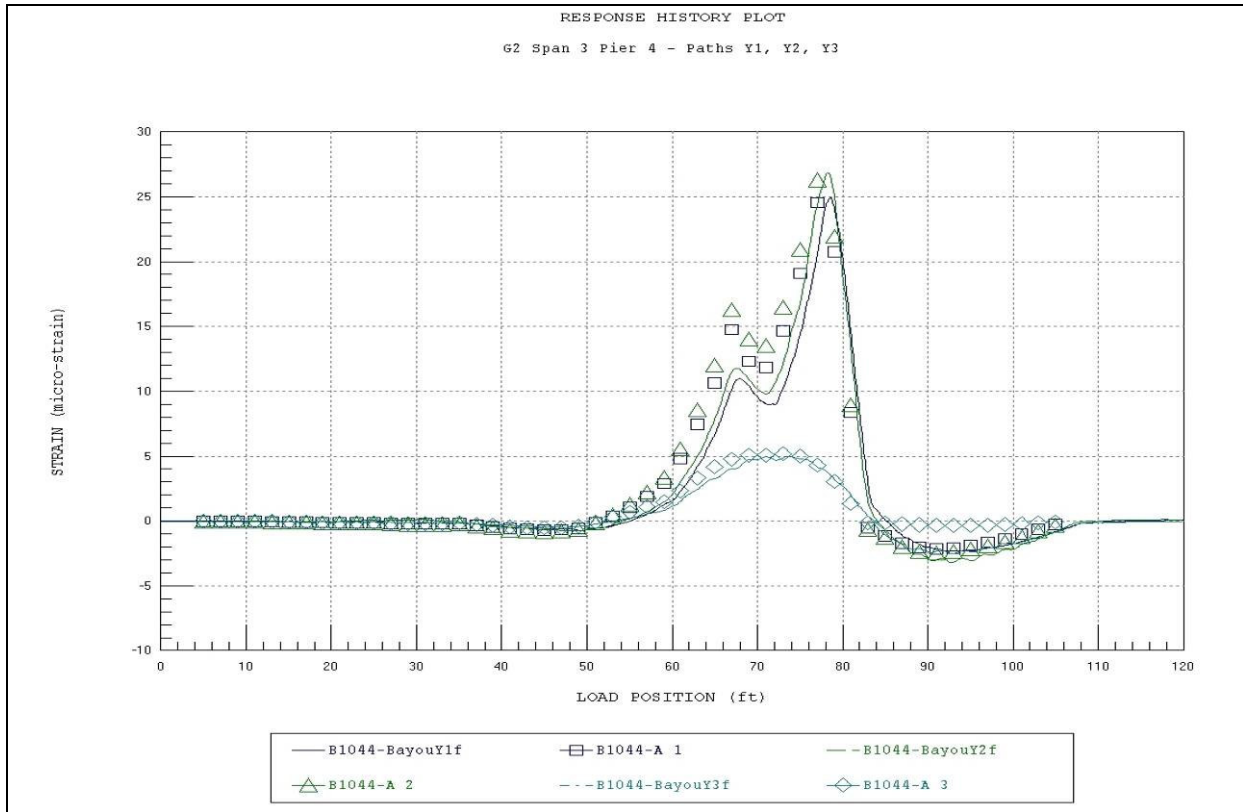


Figure 49 Beam 2, cross-section F-F – bottom.

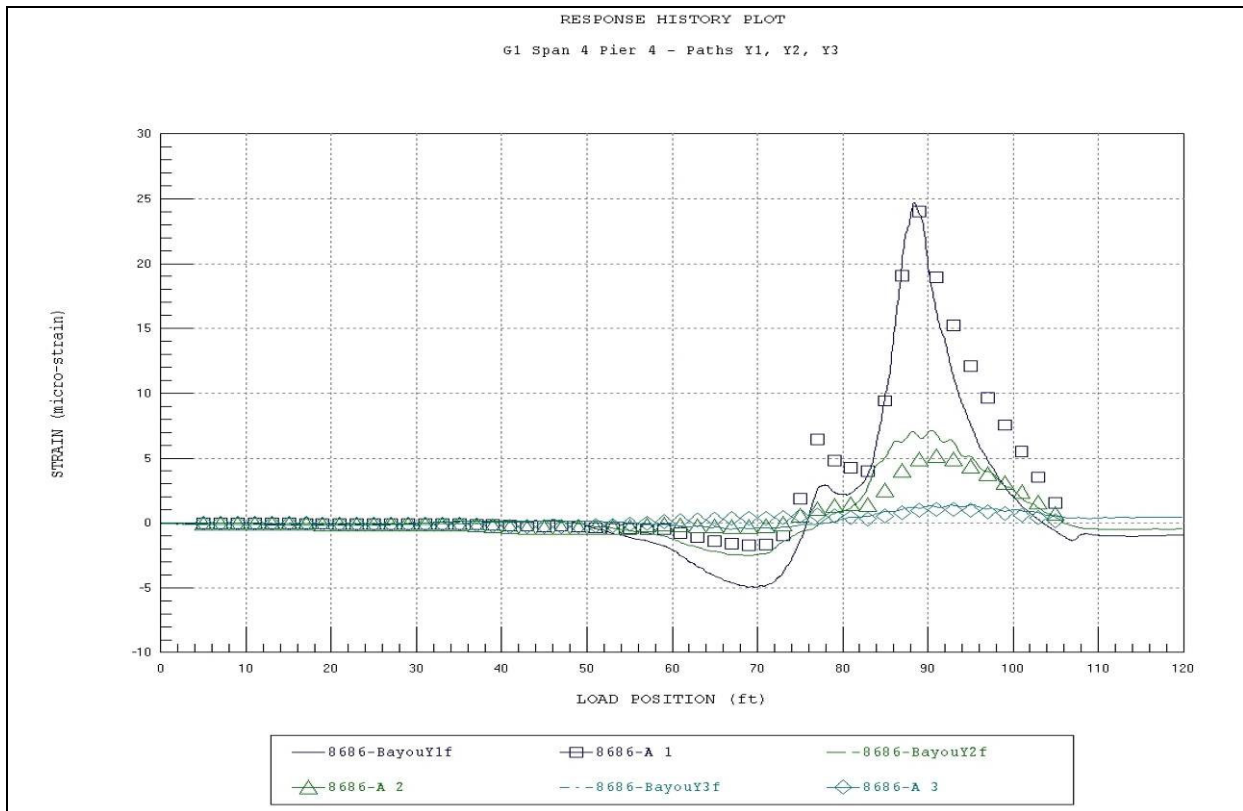


Figure 50 Beam 1, cross-section G-G – bottom.

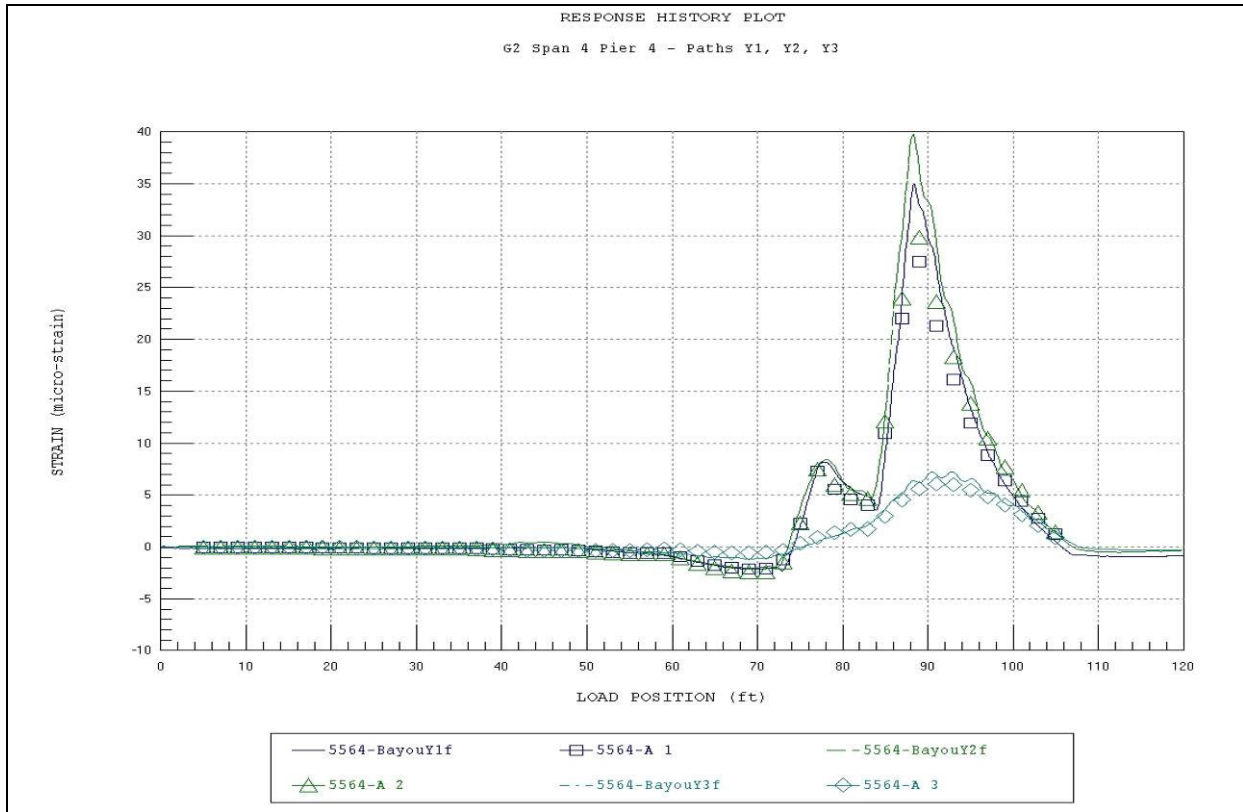


Figure 51 Beam 2, cross-section G-G – bottom.

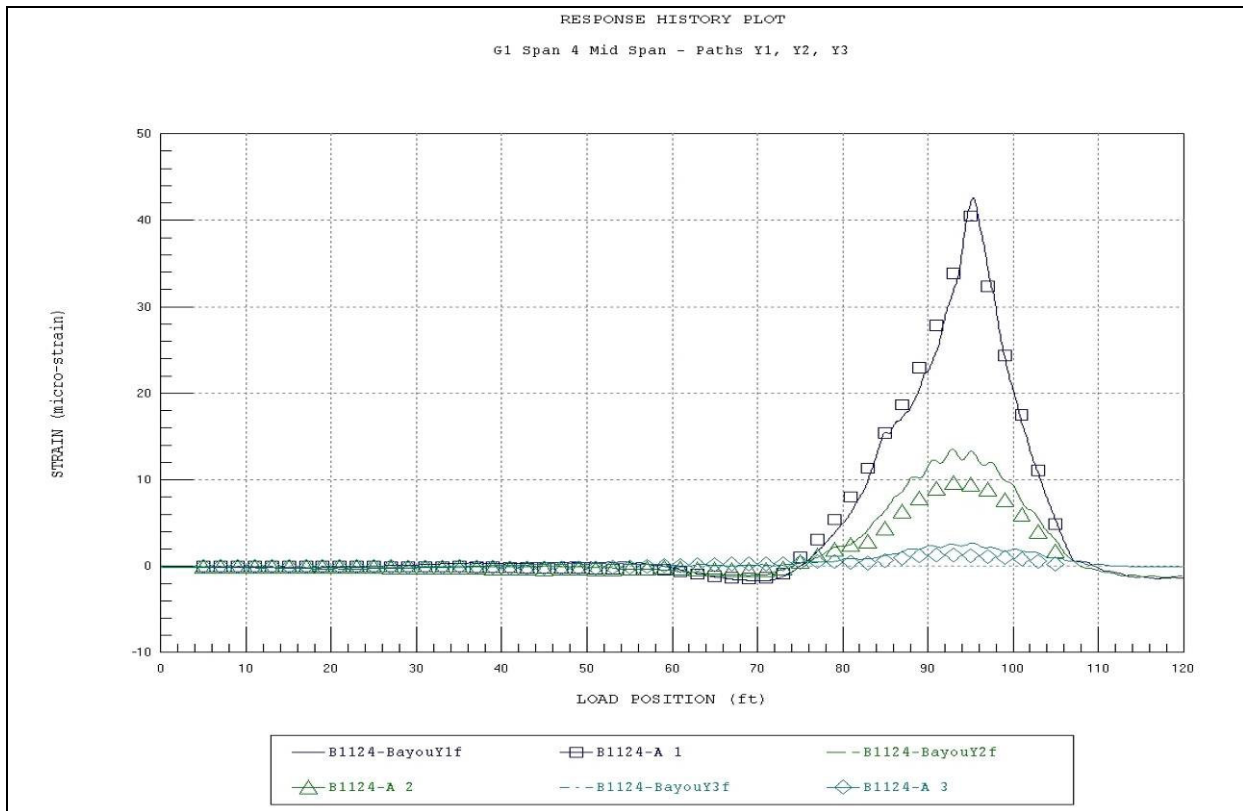


Figure 52 Beam 1, cross-section H-H – bottom.

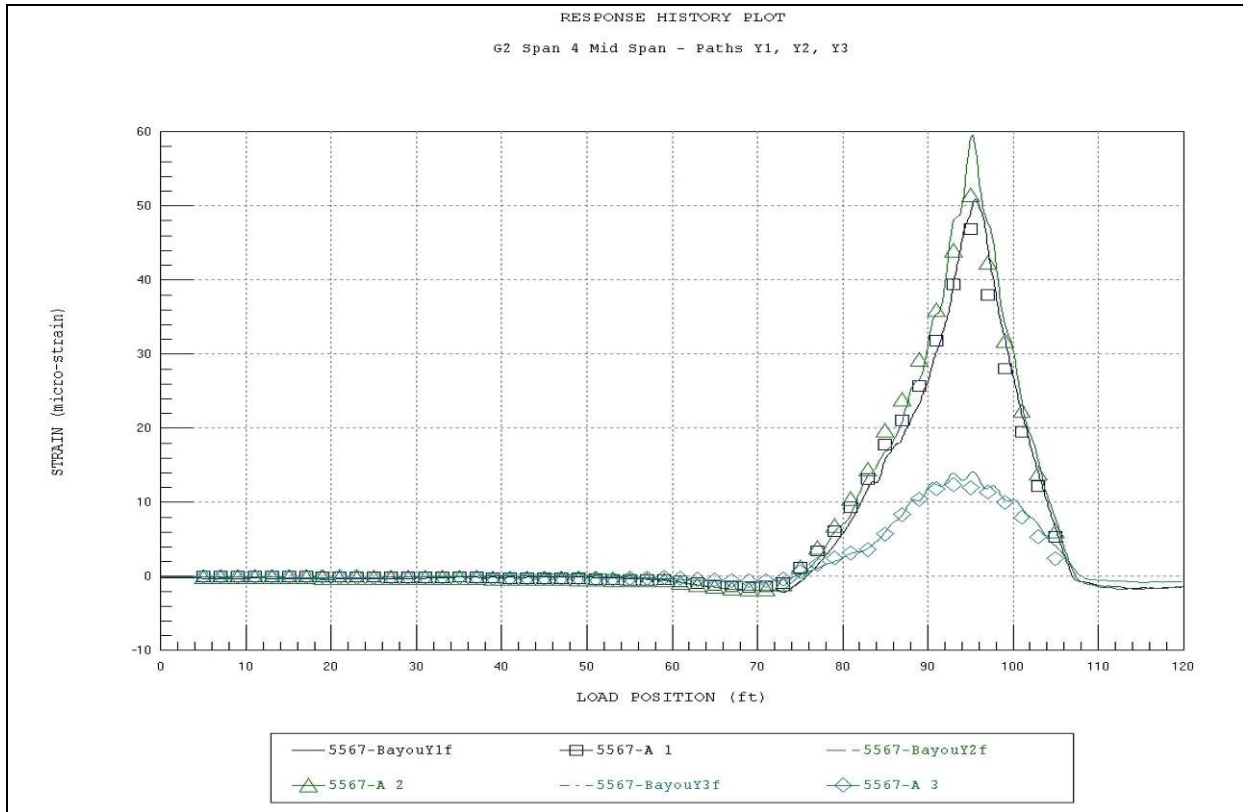


Figure 53 Beam 2, cross-section H-H – bottom.

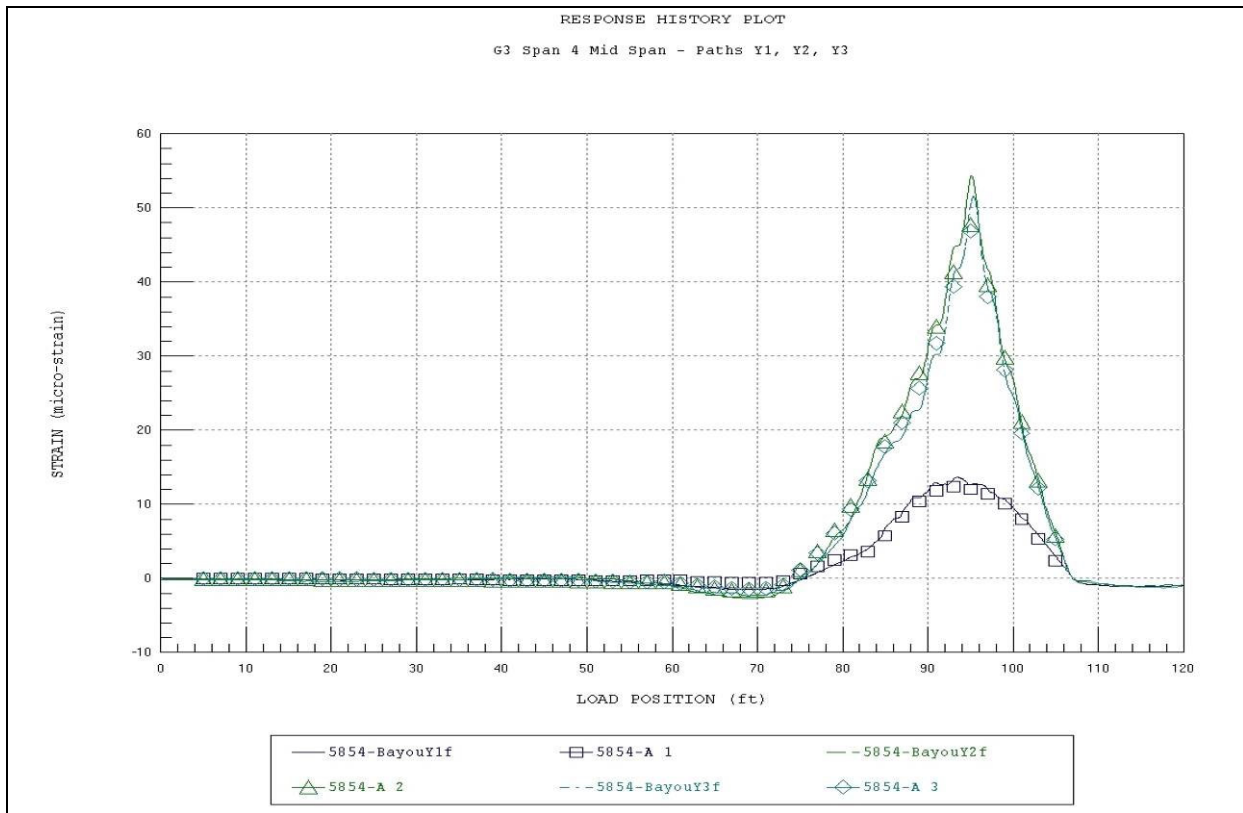


Figure 54 Beam 3, cross-section H-H – bottom.

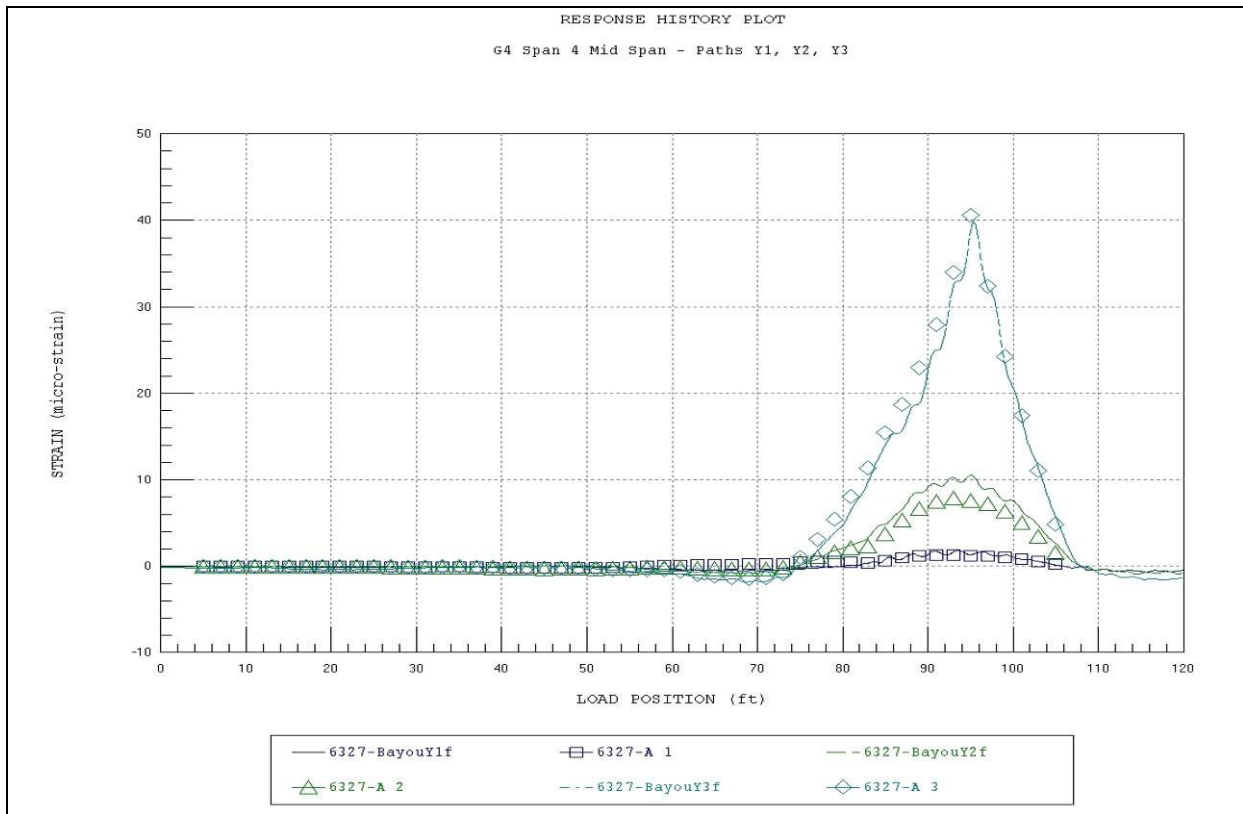


Figure 55 Beam 4, cross-section H-H – bottom.

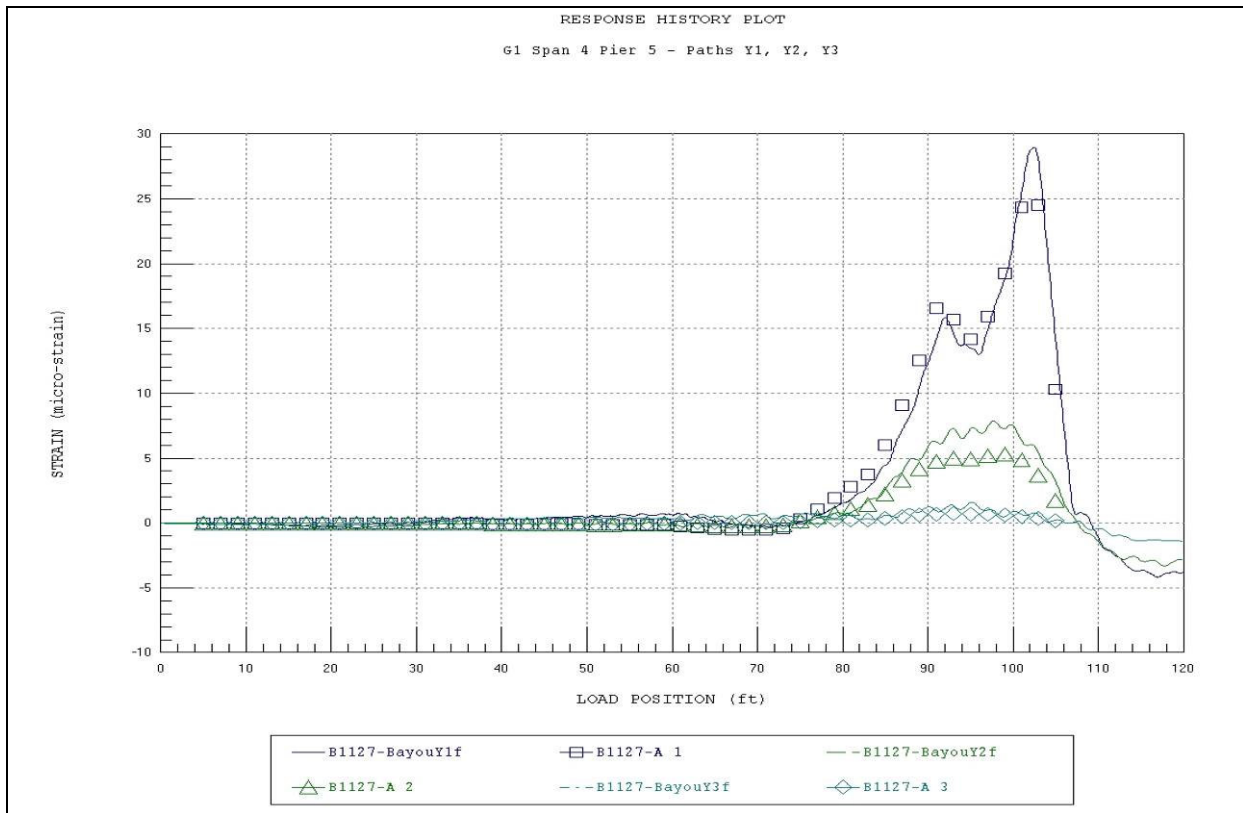


Figure 56 Beam 1, cross-section I-I – bottom.

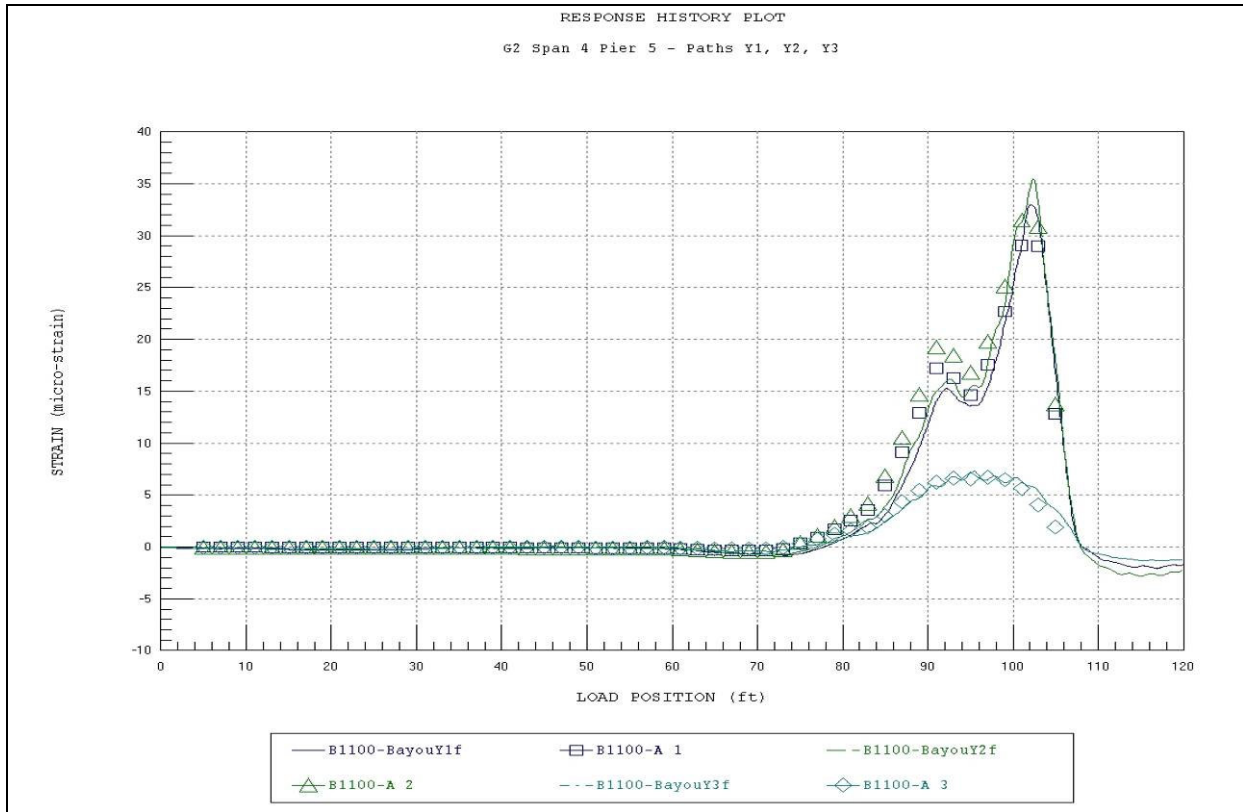


Figure 57 Beam 2, cross-section I-I – bottom.

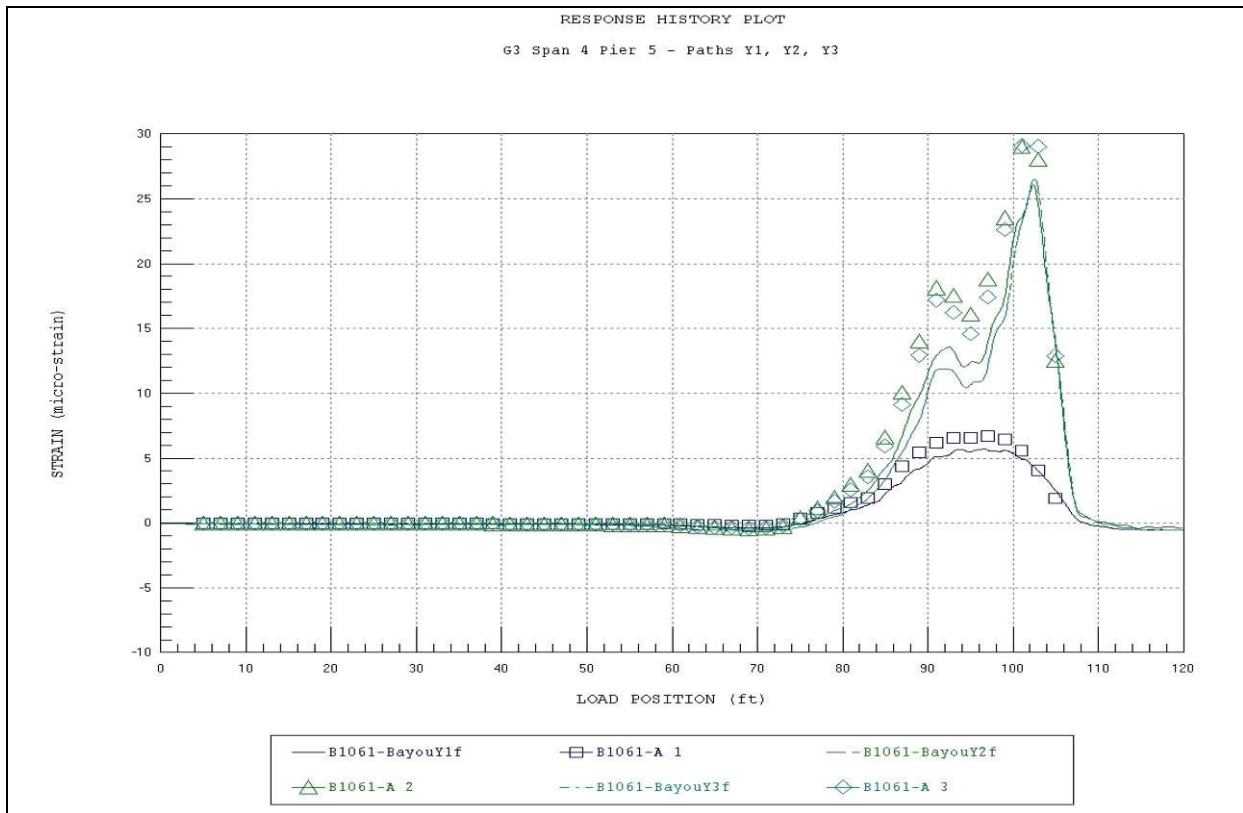


Figure 58 Beam 3, cross-section I-I – bottom.

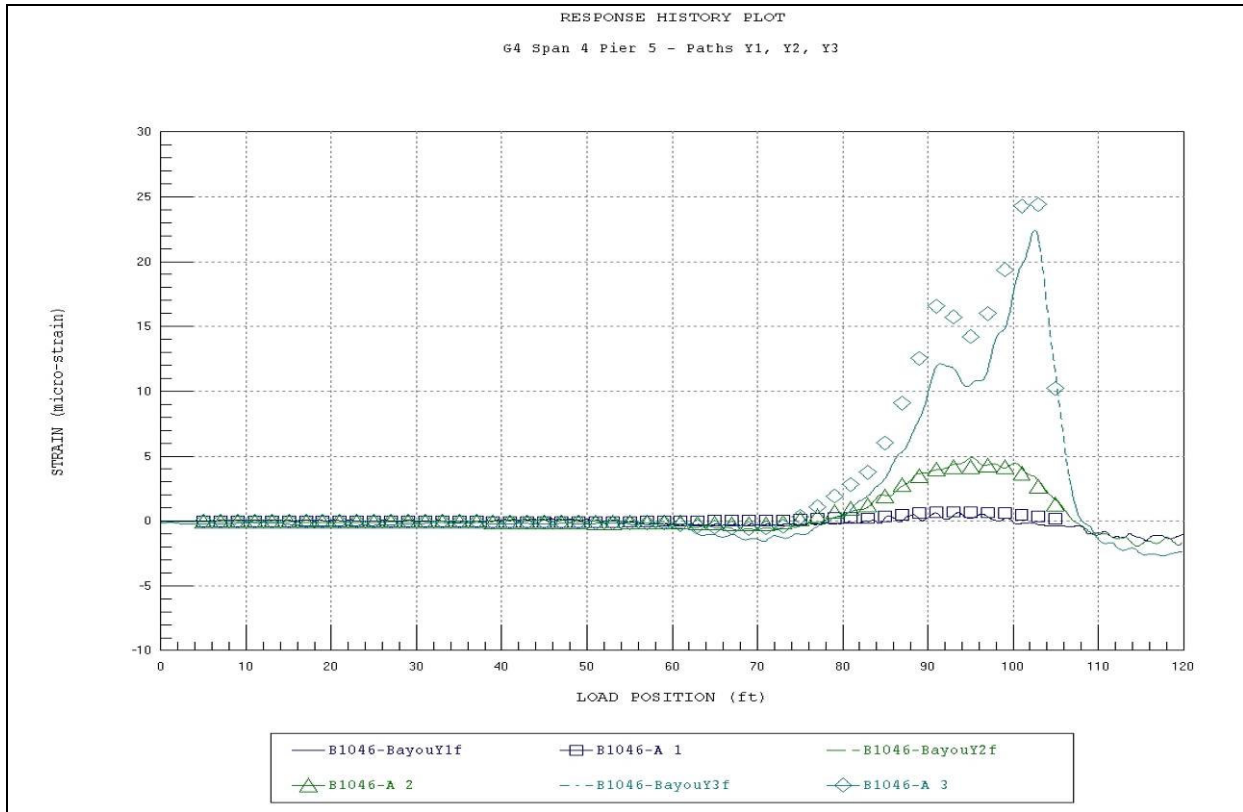


Figure 59 Beam 4, cross-section I-I – bottom.

APPENDIX B – FIELD NOTES (SCANNED)

Test #1

FIELD NOTES & TESTING CHECKLIST (TYPICAL BEAM-SLAB BRIDGES)

PROJECT NAME OR #: White Bayou Bridge.

FIELD NOTE TAKER: JLG DATE: April 17, 2007

STRUCTURE NAME OR ID: White Bayou

3 CAD DRAWINGS: 1-Gage ID, 1-Gage Dimensions, 1-General Dimensions.

MEASUREMENTS AND GAGE INSTALLATION PROCEDURES (BELOW)

SPAN LENGTH(S): In-In Diaphragm = 22' 5"

SKEW: YES NO -ANGLE: _____

BEAM SIZE: d = 16" b = 12 1/4" BEAM SPACING: 7'

DIAPHRAGM SPACING: End dim. only SIZE: b = 9" d = 14 1/2"

BENT INFO: SIZE: _____ # OF PILES: 4 PILE SPACING: Same as Beam

- GAGE INSTALLATION:
1. Measure gage location & write it on the beam.
 2. Install gage and take picture(s) w/ a reference point.
 3. Write gage ID and dimensions on CAD notes.
 4. Repeat for every gage location!!!
 5. Take multiple pics from different angles.

SUPPORT CONDITIONS: 10" bearing area from edge of beam / Diaphragm

ABUTMENT DETAILS: (Draw elevation detail)

225-231-4102 (Chad) Assistance Maintenance Engineer

DECK THICKNESS: _____ COMPOSITE: YES NO

GENERAL OBSERVATIONS: _____

Vijay > 225-802-8778
225-767-9102

Weights & Standards.

225-281-2212
(Neely)

1

MEASUREMENTS AND TESTING PROCEDURES (ABOVE)

BEGINNING OF WORLD (BOW)
(X=0, Y=0, location)

VERIFY NORTH ON PLANS: YES NO

BOW PHOTOS:

ROAD MARKINGS PHOTOS:

ROADWAY WIDTH (CURB-TO-CURB):

SYMMETRIC: YES NO

STRUCTURE WIDTH (Out-to-Out):

WEARING SURFACE: Asphalt

THICKNESS:

STARTING TEST POSITION: -10' - 1/2 rev.

DIRECTION: West

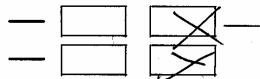
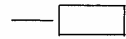
VEHICLE ROLL OUT (5 REVS!):

51.4' ^{10.28/rev}

A/C LOCATION:

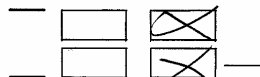
*****MAKE SURE YOU PUT THE A/C ON THE SAME WHEEL AS WAS USED TO MEASURE THE ROLL OUT*****

VEHICLE MEASUREMENTS:



6.65'

7.1



AXLE WEIGHTS:

11'

FRONT: 6,100

REAR: 19,800

GROSS: 25,900

VEHICLE PROVIDED BY: LADOTD

TRAFFIC CONTROL PROVIDED BY: LADOTD

ACCESS PROVIDED BY:

LATERAL TESTING POSITIONS: (REFERENCED FROM BOW)

Y1: <i>on Fog line</i> 1.6 ft	Y2: <i>2</i>
Y3: <i>(from edge of curb)</i> 1.6'	Y4:
Y5:	Y6:

LATERAL POSITIONS CHECKED BY:

TESTING OPERATIONS (WINSTS)

VERIFY GAGE ID & # OF CHANNELS WITH WINSTS:



RUN WINSTS TO VERIFY RESPONSES:

WEATHER CONDITIONS & AMBIENT TEMPERATURE: *75° sunny*

RUNNING THE FIELD TESTS

STS OPERATOR: *Mercino*

TRUCK OPERATOR: *JLG*

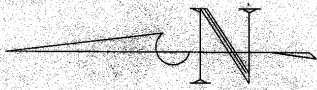
CONTROLLED SEMI-STATIC TESTS

SAMPLE RATE: *40 Hz.*

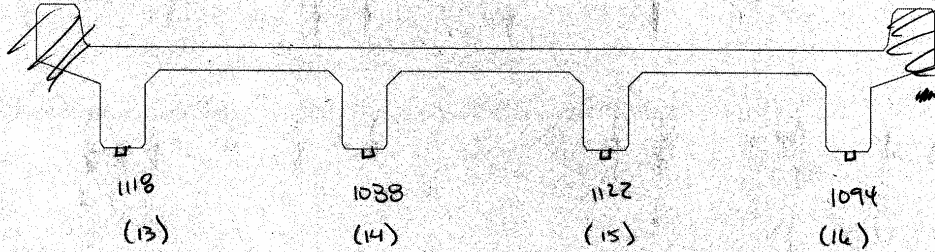
GAIN: *1000 ; 1 (LVDTs)*

cal factors for string pots are wrong.

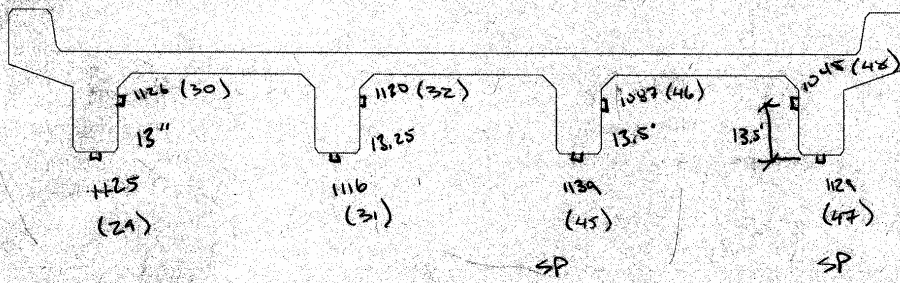
FILE NAME	LATERAL POSITION	COMMENTS
<i>Bayou - 1.cdat</i>	<i>Y1</i>	<i>Good</i>
<i>- 2.cdat</i>	<i>Y1</i>	<i>Good - truck was straighter in this run</i>
<i>- 3.dat</i>	<i>Y2</i>	<i>Good - BUT OLD LADY YELLED AT JESSE (HE GOT SAID!)</i>
<i>- 4.dat</i>	<i>Y2</i>	<i>Good</i>
<i>- 5.dat</i>	<i>Y3</i>	<i>Good</i>
<i>- 6.dat</i>	<i>Y3</i>	



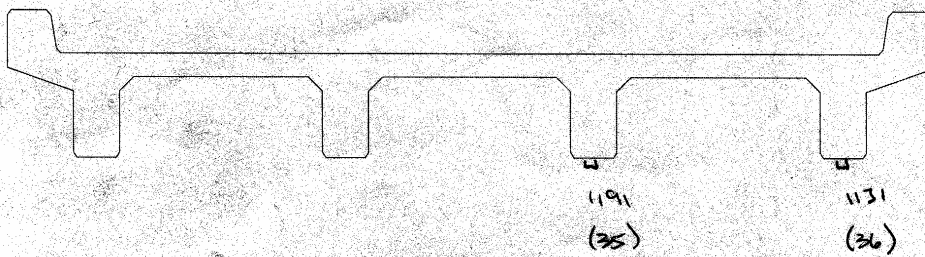
A-A

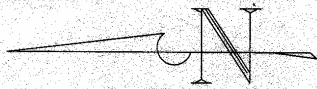


B-B

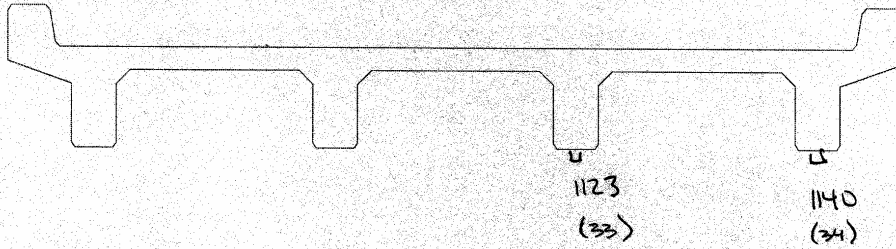


C-C

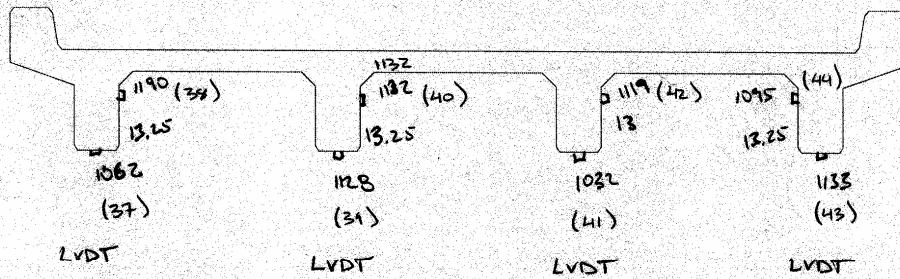




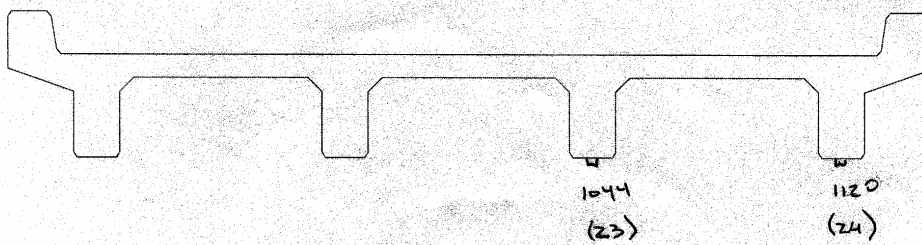
~~2-2~~ D-D

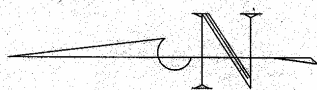


~~3-3~~ F-E

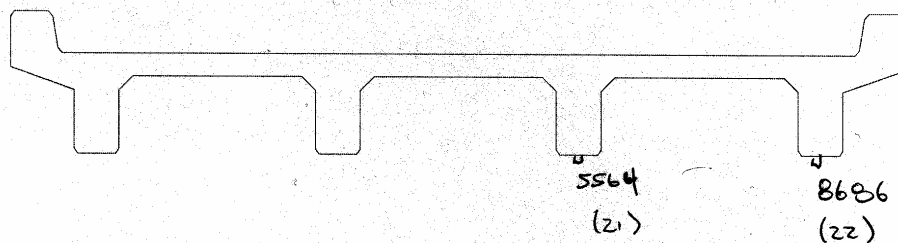


~~4-4~~ F-F

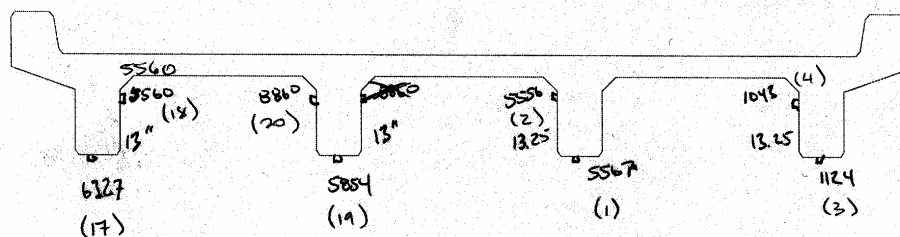




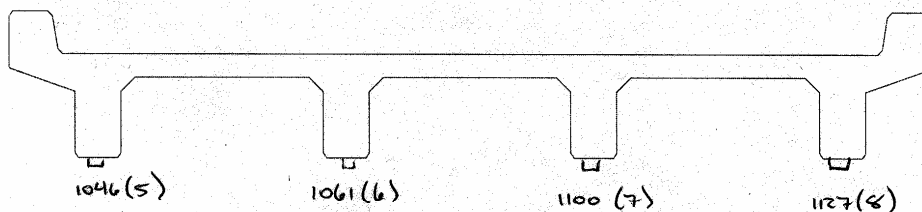
~~EF~~ G-G



~~EF~~ H-H



~~EF~~ I-I

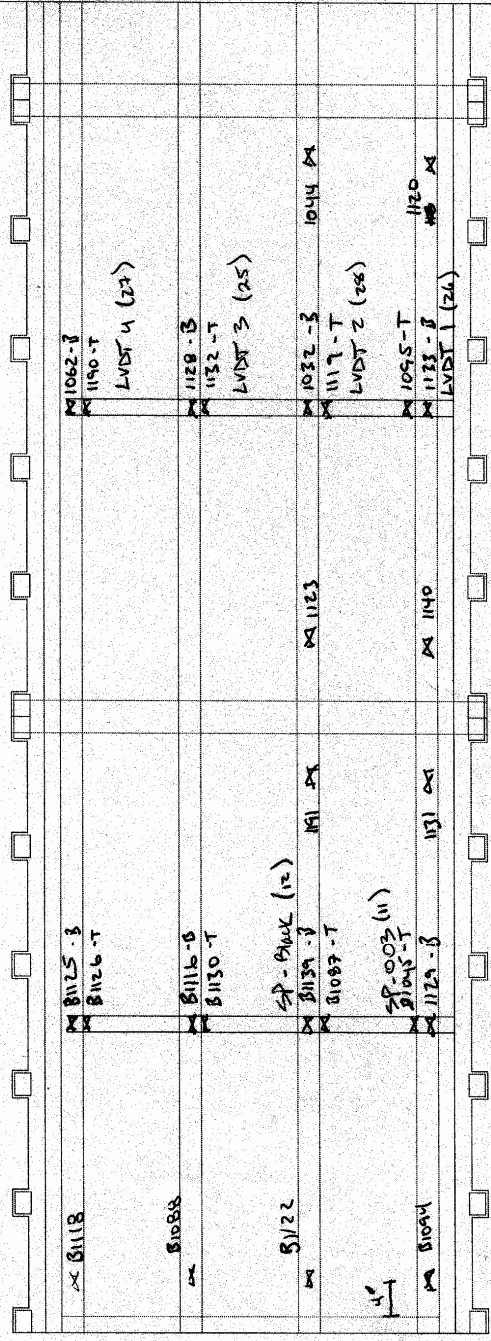


N

Span B

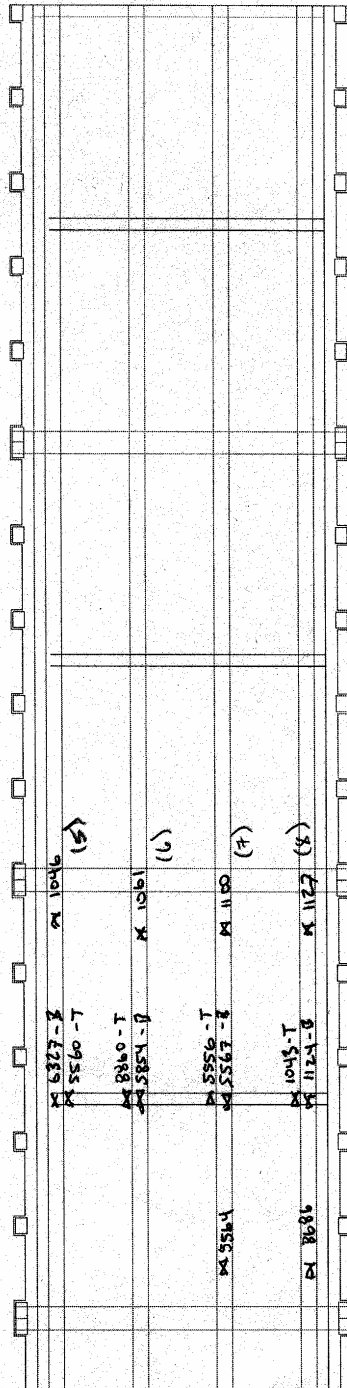
Span C

Set



Span D

MM



Test #2

FIELD NOTES & TESTING CHECKLIST
(TYPICAL BEAM-SLAB BRIDGES)

PROJECT NAME OR #: LTCD / Tulane FRP Project

FIELD NOTE TAKER: Brett Commander DATE: 5/1/07

STRUCTURE NAME OR ID: White Bayou

3 CAD DRAWINGS: 1-Gage ID, 1-Gage Dimensions, 1-General Dimensions.

MEASUREMENTS AND GAGE INSTALLATION PROCEDURES (BELOW)

SPAN LENGTH(S): 23'-3 Brg to Brg & 24'-0 c.c. Pier

SKEW: YES NO ANGLE: 0.0

BEAM SIZE: RC T-Beam 16" deep Web x 12" wide BEAM SPACING: 7'-0

DIAPHRAGM SPACING: End diaphragm only SIZE: 9" x 14" 14/9

BENT INFO: SIZE: 32' x 24' # OF PILES: 4 - under Brg PILE SPACING: 7'

- GAGE INSTALLATION:
1. Measure gage location & write it on the beam.
 2. Install gage and take picture(s) w/ a reference point.
 3. Write gage ID and dimensions on CAD notes.
 4. Repeat for every gage location!!!
 5. Take multiple pics from different angles.

SUPPORT CONDITIONS: simple bearing on bents 

ABUTMENT DETAILS: (Draw elevation detail) No end span test

DECK THICKNESS: ? COMPOSITE: YES NO

GENERAL OBSERVATIONS:

MEASUREMENTS AND TESTING PROCEDURES (ABOVE)

BEGINNING OF WORLD (BOW)
(X=0, Y=0, location)

No plans yet
VERIFY NORTH ON PLANS: YES NO

North end of deck - inside of west curb

BOW PHOTOS:

ROAD MARKINGS PHOTOS:

ROADWAY WIDTH (CURB-TO-CURB): ^S

SYMMETRIC: YES NO

STRUCTURE WIDTH (Out-to-Out):

WEARING SURFACE: *asphalt*

THICKNESS: ?

STARTING TEST POSITION: *-10' - 1/2 wheel rev*

DIRECTION: *South*

VEHICLE ROLL OUT (5 REVS!): *51.4*

A/C LOCATION: *Pass front*

*****MAKE SURE YOU PUT THE A/C ON THE SAME WHEEL AS WAS USED TO MEASURE THE ROLL OUT*****

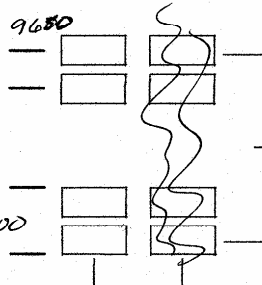
VEHICLE MEASUREMENTS:

— 3000

6.65'

— 3100

11.2'



*Weighed by
state Trooper*

AXLE WEIGHTS:

FRONT: *6100*

REAR: *19450*

GROSS: *25550*

VEHICLE PROVIDED BY: *DOTD - Dist 61*

TRAFFIC CONTROL PROVIDED BY: *DOTD " "*

ACCESS PROVIDED BY: *scaffolding under whole bridge*

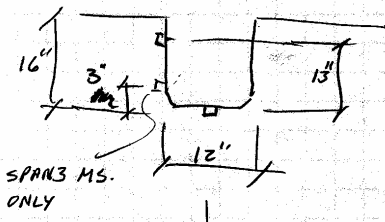
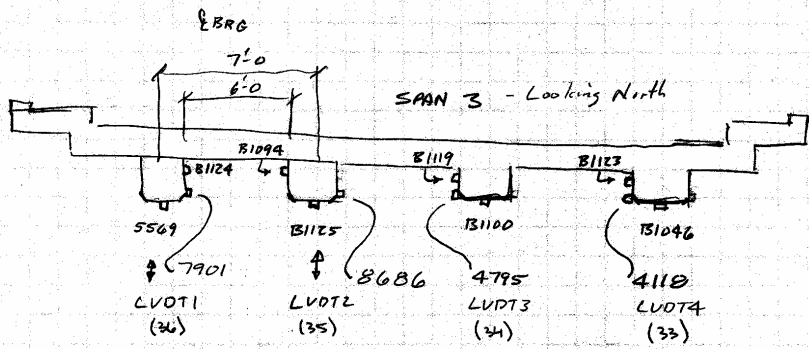
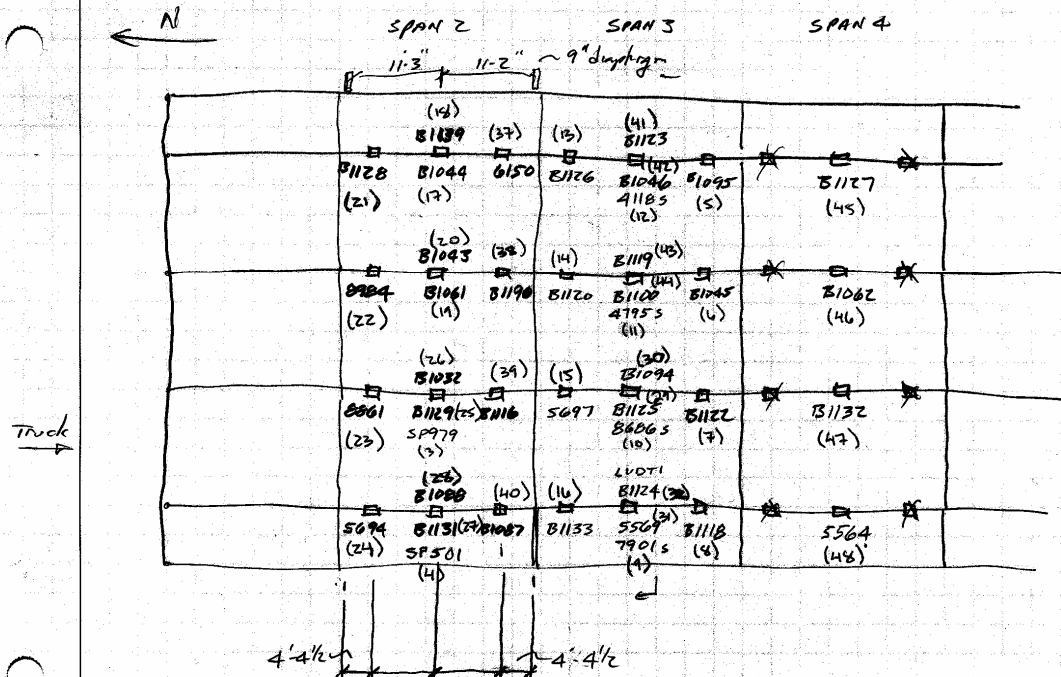
PROBLEMS

CLASS

NAME

DATE

4/30/07

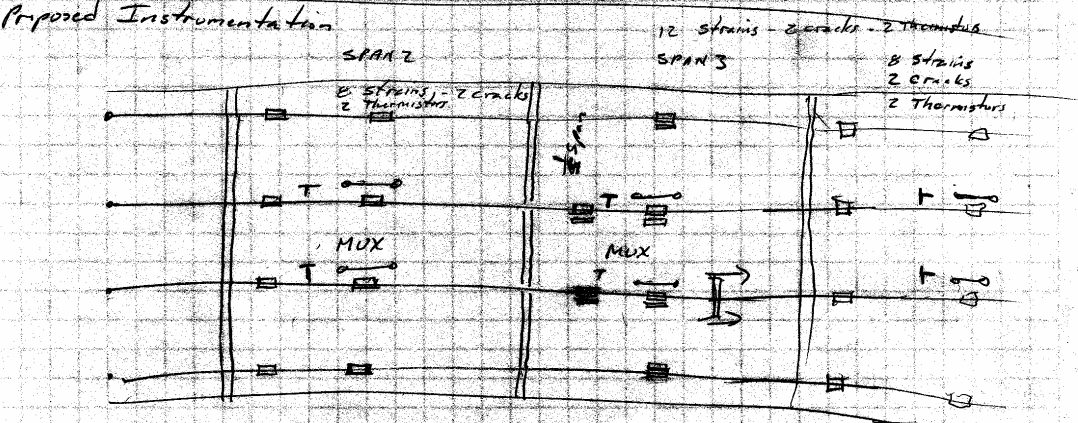


QTY	Item		
14	4420 Crack Meters 1"	- 4+2	
32	500V VW Strain gages	- 20+8	
12	PDI Strain Transducers	- LL Tests	
3	MUX CSI 16-32	- 3	
1	CRIOX cabinet w/ AWWI		
8	Thermistors 75' cable	- 4+2	Verizon Cell Service
1	reducing modem		
1	antenna		Pole / Conduit Pole / Temp
1	Solar panel		Solar panel
1	CS 500 RH/Temp prob		

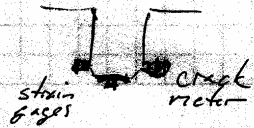
2000' blue cable
500' mux cable

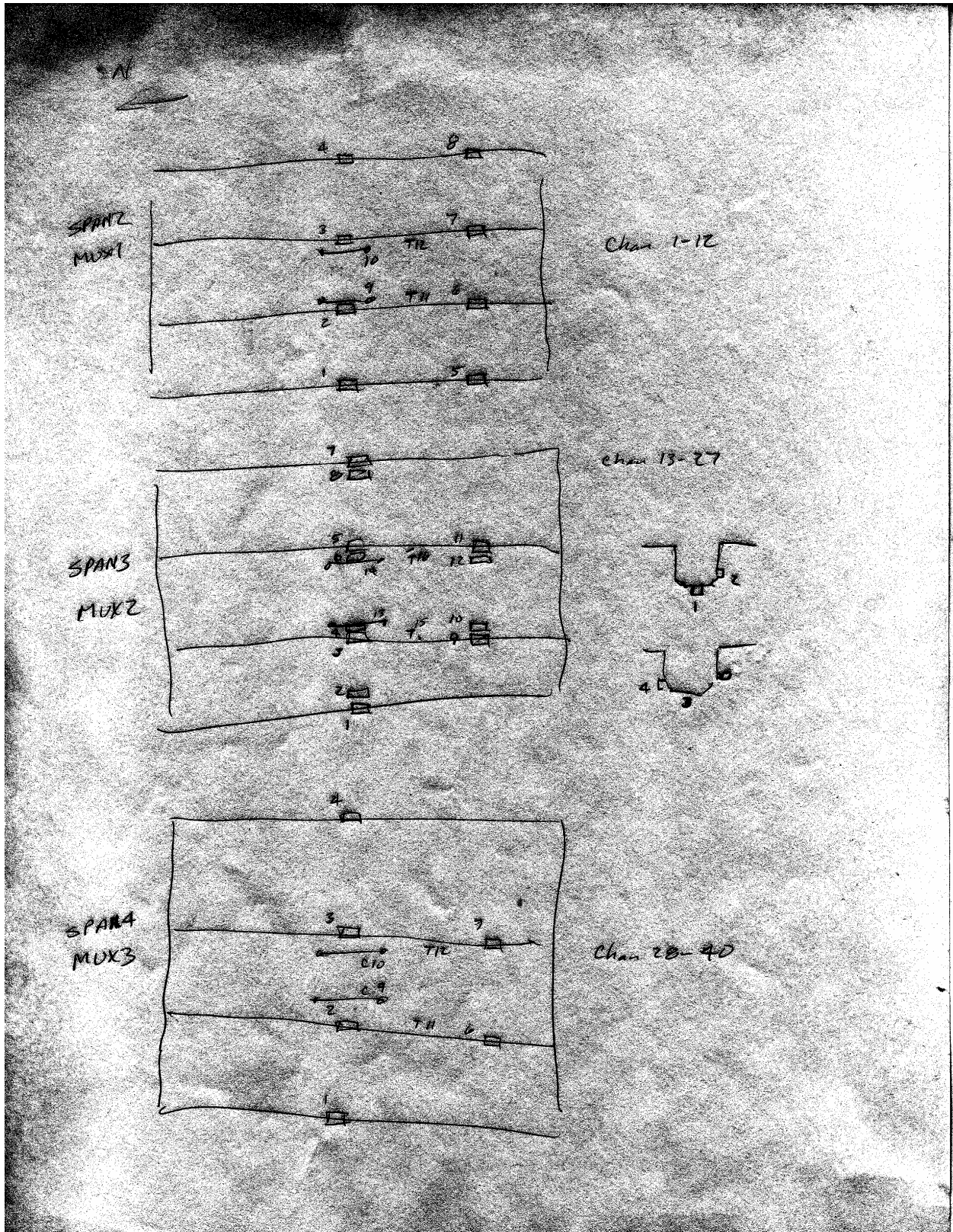
3A ULS + 6 thermistors

Proposed Instrumentation



Sample 30 sec Interval store averages hourly
Flag & store all samples





APPENDIX C - FIELD TESTING PROCEDURES

BACKGROUND

The motivation for developing a relatively easy-to-implement field-testing system was to allow short and medium span bridges to be tested on a routine basis. Original development of the hardware was started in 1988 at the University of Colorado under a contract with the Pennsylvania Department of Transportation (PennDOT). Subsequent to that project, the Integrated Technique was refined on another study funded by the Federal Highway Administration (FHWA) in which 35 bridges located on the Interstate system throughout the country were tested and evaluated. Further refinement has been implemented over the years through testing and evaluating hundreds of bridges, lock gates, and other structures.

STRUCTURAL TESTING HARDWARE

The real key to being able to complete the field-testing quickly is the use of strain transducers (rather than standard foil strain gages) that can be attached to the structural members in just a few minutes. These sensors were originally developed for monitoring dynamic strains on foundation piles during the driving process. They have been adapted for use in structural testing through special modifications, have very high accuracy, and are periodically re-calibrated to NIST standards. Please refer to Appendix D for specifications on the BDI Strain Transducers.

In addition to the strain sensors, the data acquisition hardware has been designed specifically for structural live load testing which means it is extremely easy to use in the field. Please see Appendix E for specifications on the BDI Structural Testing System. Briefly, some of the features include military-style connections for quick assembly and self-identifying sensors that dramatically reduce bookkeeping efforts. The WinSTS testing software has been written to allow easy hardware configuration and data recording operation. Other enhancements include the BDI AutoClicker which is an automatic load position indicator that is mounted directly on the vehicle. As the test truck crosses the structure along the preset path, a communication radio sends a signal to the STS that receives it and puts a mark in the data. This allows the field strains to be compared to analytical strains as a function of vehicle position, not only as a function of time. Refer to Appendix F for the AutoClicker specifications. The end result of using all of the above-described components is a system that can be used by people other than computer experts or electrical engineers. Typical testing times with the STS is usually anywhere from 20 to 60 channel tests being completed in one day, depending on access and other field conditions.

The following general directions outline how to run a typical diagnostic load test on a short-to medium-span highway bridge up to about 200 ft (60m) in length. With only minor modifications, these directions can be applied to railroad bridges (use a locomotive rather than a truck for the load vehicle), lock gates (monitor the water level in the lock chamber), amusement park rides (track the position of the ride vehicle) and other structures in which the live load can be applied easily. The basic scenario is to first instrument the structure with the required number of sensors, run a series of tests, and then removing all the sensors. These procedures can often be completed within one working day depending on field conditions such as access and traffic.

INSTRUMENTATION OF STRUCTURE

This outline is intended to describe the general procedures used for completing a successful field test on a highway bridge using the BDI-STS. For a detailed explanation of the instrumentation and testing procedures, please contact BDI and request a copy of the Structural Testing System (STS) Operation Manual.

ATTACHING STRAIN TRANSDUCERS

Once a tentative instrumentation plan has been developed for the structure in question, the strain transducers must be attached and the STS prepared for running the test. There are several methods for attaching the strain transducers to the structural members depending on whether they are steel, concrete, timber, FRP, or other. For steel structures, quite often the transducers can be clamped directly to the steel flanges of rolled sections or plate girders. If significant lateral bending is assumed to be present, then one transducer may be clamped to each edge of the flange. In general, the transducers can be clamped directly to painted surfaces. The alternative to clamping is the tab attachment method that involves cleaning the mounting area and then using a fast-setting cyanoacrylate adhesive to temporarily install the transducers. Small steel “tabs” are used with this technique and they are removed when testing is completed, and touch-up paint can be applied to the exposed steel surfaces.

Installation of transducers on pre-stressed concrete (PS/C) and FRP members is usually accomplished with the tab technique outlined above, while readily-available wood screws and a battery-operated hand drill are used for timber members. Installing transducers on reinforced concrete (R/C) is more complex in that gage extensions are used and must be mounted with concrete studs.

If the above steps are followed, it should be possible to mount each transducer in approximately five to ten minutes. The following figures illustrate transducers mounted on both steel and reinforced concrete members.



Figure 60 Strain Transducers Mounted on Steel Girder



Figure 61 Transducers w/Gage Extensions Mounted On R/C Slab

ASSEMBLY OF SYSTEM

Once the transducers have been mounted, they are connected to the four-channel STS units which are also located on the bridge. The STS units can be easily clamped to the bridge girders, or if the structure is concrete and no flanges are available to set the STS units on, transducer tabs glued to the structure and plastic zip-ties or small wire can be used to mount them. Since the transducers will identify themselves to the system, there is no special order that they must be plugged into the system. The only information that must be recorded is the transducer serial number and its location on the structure. Signal cables are then used to connect STS units together either in series or in a “tree” structure through the use of cable splitters. If several gages are in close proximity to each other, then the STS units can be plugged directly to each other without the use of a cable.

Once all of the STS units have been connected together, only one cable must be run and connected to the STS Power Supply located near the PC. Once power and communication cables are connected, the system is ready to acquire data. One last step entails installing the AutoClicker on the test vehicle as seen in Figure 62.



Figure 62 AutoClicker Mounted on Test Vehicle

ESTABLISHING LOADING VEHICLE POSITIONS

Once the structure is instrumented and the loading vehicle prepared, some reference points must be established on the deck in order to determine where the vehicle will cross. This process is important so that future analysis comparisons can be made with the loading vehicle in the same locations as it was in the field. Therefore, a “zero” or initial reference point is selected and usually corresponds to the point on the deck directly above the abutment bearing and the centerline of one of the fascia beams. All other measurements on the deck will then be related to this zero reference point. For concrete T-beams, box beams, and slabs, this can correspond to where the edge of the slab or the beam web meets the face of the abutment. If the bridge is skewed, the first point encountered from the direction of travel is used. In any case, it should be a point that is easily located on the drawings for the structure.

Once the zero reference location is known, the lateral load paths for the vehicle are determined. Often, the painted roadway lines are used for the driver to follow if they are in convenient locations. For example, for a two-lane bridge, a northbound shoulder line will correspond to Y1 (passenger-side wheel), the center dashed line to Y2 (center of truck), and the southbound shoulder line to Y3 (driver’s side wheel). Often, the structure will be symmetrical with respect to its longitudinal center line. If so, it is good practice is to take advantage of this symmetry by selecting three Y locations that are also symmetric. This will allow for a data quality check since the response should be very similar, say, on the middle beam if the truck is on the left side of the bridge or the right side of the bridge. In general, it is best to have the truck travel in each lane (at least on the lane line) and also as close to each shoulder or sidewalk as possible. When the deck layout is completed, the loading vehicle’s axle weights and dimensions are recorded.

RUNNING THE LOAD TESTS

After the structure has been instrumented and the reference system laid out on the bridge deck, the actual testing procedures are completed. The WinSTS software is initialized and configured. When all personnel are ready to commence the test, traffic control is initiated and the Run Test option is selected which places the system in an activated state. When the truck passes over the first deck mark, the AutoClicker is tripped and data is being collected at the specified sample rate. An effort is made to get the truck across with no other traffic on the bridge. When the rear axle of the vehicle completely crosses over the structure, the data collection is stopped and several strain histories evaluated for data quality. Usually, at least two passes are made at each “Y” position to ensure data reproducibility, and then if conditions permit, high speed or dynamic tests are completed.

The use of a moving load as opposed to placing the truck at discrete locations has two major benefits. First, the testing can be completed much quicker, meaning there is less impact on traffic. Second, and more importantly, much more information can be obtained (both quantitative and qualitative). Discontinuities or unusual responses in the strain histories, which are often signs of distress, can be easily detected. Since the load position is monitored as well, it is easy to determine what loading conditions cause the observed effects. If readings are recorded only at discreet truck locations, the risk of losing information between the points is great. The advantages of continuous readings have been proven over and over again.

When the testing procedures are complete, the instrumentation is removed and any touch-up work completed.

APPENDIX D - DATA LOGGER SUPPORT SOFTWARE GUIDE

CSI-LoggerNet Software

The Campbell Scientific, Inc. (CSI) software package (LoggerNet) was provided with the data logger to perform a variety of data logger functions. This software package is run from a PC and contains several programs that enable an engineer to write and compile a data logger program, communicate with the data logger to upload programs and download data, and perform automatic scheduling operations. The following table provides a brief list of the main LoggerNet options and the functions that they perform. Refer to the CSI software manual for more detailed information.

Setup	<ol style="list-style-type: none"> 1. Define data logger hardware and connection path to the PC. 2. Connection information (ports, modems, etc.) for each hardware device. 3. Name and path of data files and specify file format. 4. Setup security levels (optional). 5. Define and enable scheduled downloads from devices (data loggers).
Connect	<ol style="list-style-type: none"> 1. Enables manual connection to data loggers defined in Setup. 2. Set data logger clock with PC clock. 3. Upload data logger program to data logger. 4. Download data stored in data logger. 5. Monitor data logger input values, status of ports and flags, manually toggle settings of ports and flags.
Status	<ol style="list-style-type: none"> 1. Display list of defined hardware and tasks. 2. Shows last collection or execution attempt for each device or task. 3. Next call or execution of device or task if automatic schedule defined and enabled.
Tasks	Schedule tasks to be performed such as retrieve data from the data logger and running a program that will post process data that has been retrieved. Tasks can be done on specific schedules and subtasks can be defined to run after a primary task has been performed. For example, the primary task could be calling up the data logger and retrieving data. A secondary task could be to execute a program that post processes the data. Another subtask might rename the raw data file with the current date so that each data file contains exactly one week of data.
Edlog	Write and edit data logger programs for CR10X data loggers. The data logger program controls features such as sampling rate (program cycle), sensors to be measured, toggles ports and flags, branches control based on port and flag values, post processing of measurements to engineering units, statistical operations such as average data over period of time, comparison data values with thresholds, initiate and perform call out sequence, and data storage format.
CRBasic	Write and edit data logger programs for table based data loggers such as the CR1000, CR5000 and CR9000.

The LOGGERNET software enables a computer to communicate with the data logger via a serial connection. This can be done either through a modem or a direct connection. The first step is to define the data logger devices within the Setup Utility. If a direct connection and a modem connection are both desired from a single laptop PC, a separate device configuration must be defined for each connection type that will be used on the computer. The following steps illustrate how to connect an office computer to the CR10X via a modem and phone line:

- Start LoggerNet software and select Setup.

- Select Add Root.
- Select TAPIPort (Windows telephone modem)
- Select Add Device or right click on TAPIPort.
- Select TAPIRemote (this is the remote modem connected the datalogger).
 - Enter the phone number required to dial out to the remote modem including any extra numbers to get an outside line. Commas can be used for pauses.
- Select Add Device.
- Select data logger device (CR10x).
- Select the FSArea 1 (Final Storage Area 1) and define the filename and path where downloaded data is to be stored.

Steps required to connect a computer directly to the CR10x, via the SC32A Optically Isolated Interface, are as follows:

- Start LoggerNet software and select Setup.
- Select Add Root (If a com port is not already available on the list).
- Select Add Device or right click on Com Port.
- Select data logger device (CR10x).
- Select the FSArea 1 (Final Storage Area 1) and define the filename and path where downloaded data is to be stored.

Once the data logger device has been defined in the LoggerNet software communication parameters, data file configuration, security, scheduling and automatic clock updating parameters can be defined by selecting the various tabs on the device setup screen.

Communication with the data logger is initiated from the LoggerNet-Connect option. From this program, the connection to a specific data logger can be made, the data logger clock can be set, programs (LTRC_WB.DLD) can be sent to or retrieved from the data logger, data can be downloaded manually, and the data can be monitored numerically or graphically. The following outline lists the procedures used to communicate and control the data logger:

- Start LoggerNet software and select Connect.
- Select device from the list on the left hand side of the window.
- Click on Connect button. If the connection fails, check the device configuration in the Setup program.
 - Common connection problems include the use of the wrong com port or modem settings. If the connection works but is unstable, try using a smaller packet size (512) and adding extra response time for the logger and the ComPort.
- After connecting to the logger, set the logger clock with the PC clock (if required).
- If a new program is to be uploaded, enter the program filename (LTRC_WB.DLD) and click on **Send**. The program is checked for errors after loading and an error message will be appear if any errors are encountered. When a program is sent to the logger, that program is automatically used to associate variable names to data input locations. Otherwise, if connecting to a data logger that is already running a program, it may be necessary to use the "Associate DLD Program" option to assign variable names to data cells. It is important to download any existing data from the data logger before uploading a new program because all data logger memory, port settings, and flag settings will be reset.
- Click on the **Numeric** display button to monitor logger data values.
 - A grid of data cells will be displayed. Use **Add** button to display the desired data values. Three separate numeric grids can be displayed.
- Click on the **Graphs** display button to monitor value time histories.

- A time history graph will be displayed on which 12 series can be plotted. Three separate graphs windows can be displayed.
- Depending on the data logger program, it may be necessary to manually set Ports or Flags to control the program operation. Click the **Ports/Flags** button to display the status and control the values of Ports and Flags.
- Data can be downloaded manually from the Connect window. Select the **Collect Now** button to download data to the default file using the default file attributes (format, append, etc.). To download data to a different data file or to download data from a different memory range other than the default, select the **Custom** collect button.

The status of Device or Task schedules can be viewed from the LoggerNet Status page. A window shows the current data logger devices and tasks along with information about the last attempted access, the range of data downloaded, and the next scheduled access. Manual downloads or access can be controlled from Status page as well as the Connect page.

LTRC_WB.DLD Data Logger Program Operation

A data logger program was written specifically to operate the instruments provided with the Tulane/LTRC 48 channel long-term structural monitoring system. This section provides an outline of the LTRC_WB.DLD data logger program features. Keep in mind that the data logger program can, and most likely will be, modified. Any changes in the operation should be noted and updated in this manual.

When first uploaded, the LTRC_WB.DLD data logger program initializes all port and flag settings to off. The ports and flags will be set to off anytime the power is cycled on the data-logger. Control Flags 1 & 2 can be toggled manually (via the LoggerNet software) to control the program operation. No program functions are performed until Control Flag 1 is manually turned on (Set High). This is done by clicking on the Flag 1 button in the LoggerNet-Connect-Ports/Flags window. After the Flag 1 is turned on, the program will instruct the data logger to sample all of the sensors at a specified program interval (60 seconds). Control Flag 2 is used to specify whether data is to be stored after each interval. Average values and extreme values will be updated with each program loop and stored each hour regardless of the status of Flag 2. The following table contains a list of each Control Flag and its effect on the LTRC_WB.DLD program.

Flag	Status	Program Control
1	On	Executes instructions of the LTRC_WB.DLD data logger program.
	Off	Halts execution of program.
2	On	Causes data from each sensor cycle to be stored after each program interval (60 second intervals). Hourly average and extreme values are also stored at the top of the hour.
	Off	(Default) Only hourly average and extreme values are stored.
3	On	Reset baseline readings used for the computation of delta values (changes in strain or displacement). Flag 3 will be turned so that baseline readings can be initialized on the first program loop when the program is loaded.
	Off	(Default)The LTRC_WB.DLD program will automatically turn Flag 3 off after the baseline readings are obtained.
4	On	Not used.
	Off	Not used.
5	Off	Not used.
6	Off	Not used.
7	On/Off	Program controlled flag that turns on every hour to signal that average and

		extreme values are to be written to long-term storage.
8	On	(Default) Disable logger call back.
	Off	Logger will attempt a call back – no phone number implemented in program.

Several hundred input values are defined and stored during program operation. These input fields are addressed by an integer number and have a name associated with the memory location. The value of each data field is controlled by the program operation and can be representative of a sensor value, a threshold limit, calibration constant, a calculated value, etc. The current values of the each data field can be monitored from the **LoggerNet-Connect-Numeric Display** window. A total of 156 data values can be viewed at one time. The data fields to be viewed in each cell are defined by the user by selecting a cell or range of cells and then clicking on the **Add** button. In order for the data field names to be displaced with each input location, the correct data logger program must be identified in the **LoggerNet-Connect-Tools-Associate DLD Program** option.

The amount of time between required data downloads varies depending on the setting of Flag 2. With initial memory configuration (2 MB extended memory), the data logger can store approximately 600000 data points. Approximately 100 data points are stored once a minute if Flag 2 is turned on and 200 data points are stored once an hour regardless of the Flag 2 setting. The following table contains approximate maximum download intervals based on Flag 2 settings. These values are based on the assumption that the Flag 2 setting remains constant. Keep in mind that data storage may change if the data logger program is modified. To avoid data loss it is highly recommended that data be downloaded on a more frequent interval than that allowed by the available memory. Useful information can be obtained with frequent monitoring such as the condition of the power supply or if any sensors have malfunctioned.

Flag 2	Values / Record	Records / Hour	Maximum Download Interval
Off	200	1	3000 hours (125 days)
On	100	60	100 hours (4 days)

*Assuming a 60-second program interval.

Scheduling

Automatic scheduling of data downloads is accomplished from the **LoggerNet-Setup** page or from the **Tasks** page. Select the data logger for which to perform automatic downloads. Select the Data Collection tab and check the "Schedule on" check box. The appropriate file properties can be selected as follows (Data logged since last call, append to end of file, ASCII comma separated) and the file name can be defined. It is highly recommended that the data file be located on the computers local hard drive rather than a mapped network drive. This is because the stability of the network can cause the LoggerNet software to not find an existing data file when appending data to it. In which case the file is overwritten instead of appended to. The download timing can be defined by selecting the Schedule tab and filling in the appropriate date and time values for "calling interval" and "next call". In the original configuration, the LTRC-WB data logger can store approximately 4 months worth of data before overwriting. It is recommended however, that automatic downloads be performed weekly to reduce the amount of data that could be potentially lost due to a loss of system. This will also result in shorter phone calls to the data logger.

Post-processing programs can also be initiated through the **Tasks** feature. A software application residing on the PC can be defined as a Task. A task can be associated with a specific logger and performed after any scheduled download or it can be a standalone task that

has its own schedule. All tasks can have sub-tasks that are performed upon successful completion of the previous task. If several downloads are to be performed between post processing operations, then a separate Task Schedule is the best option. For example it maybe desirable to have the data logger downloaded data on a daily basis. Then you may want to rename the raw data file once a week and post-process the week's worth of data. The program that renames the data file and post-processes the data should have its own task schedule.

Data Logger Data Format

Data downloaded from the data logger can be stored in a variety of formats. Comma-delimited, ASCII-text provides the most portability for importing into spreadsheet programs. Regardless of the format, data generated by the LTRC_WB.DLD program contains the same information. Each record (line) contains measurements from all active data channels. Each field (column) contains data for a specific variable or sensor. The Array ID at the beginning of each record is used to determine the type of data present in the record. Table 16 through Table 21 contain information about the data from each Array type

Table 16 Array 1 Data Format – Average Sensor Values – Recorded Hourly.

Item	Columns	Description/Units
Array ID	1	1
Year	2	Year
Day	3	Julian day of year
Hr/Min	4	Hour and minute code. Last two digits are minutes; first one or two digits are hours in 24 hour format.
Sensor Values	5-44	Average sensor data value that occurred in hour time interval

Table 17 Array 2 Data Format – Average Temperatures – Recorded Hourly.

Item	Columns	Description/Units
Array ID	1	2
Year	2	Year
Day	3	Julian day of year
Hr/Min	4	Hour and minute code. Last two digits are minutes; first one or two digits are hours in 24-hour format.
Sensor Temperatures	5-44	Temperature at time of data sample (°F).
Ambient Temperatures	45	Temperature at time of data sample (°F).
Relative Humidity	46	Percent humidity
CR10x Temperature	47	Internal CR10 Temperature at time of data sample (°F).
CR10x Voltage	48	Battery voltage supplied to CR10x

Table 18 Array 3 Data Format – Minimum Sensor Values – Recorded Hourly.

Item	Columns	Description/Units
Array ID	1	1
Year	2	Year
Day	3	Julian day of year
Hr/Min	4	Hour and minute code. Last two digits are minutes; first one or two digits are hours in 24 hour format.
Sensor Values	5-44	Minimum sensor data value occurring within hour time interval.

Table 19 Array 4 Data Format – Maximum Sensor Values – Recorded Hourly.

Item	Columns	Description/Units
Data Code = 4	1	1
Year	2	Year
Day	3	Julian day of year
Hr/Min	4	Hour and minute code. Last two digits are minutes; first one or two digits are hours in 24 hour format.
Sensor Values	5-44	Maximum sensor data value occurring within hour time interval.

Table 20 Array 5 Data Format – sensor values – recorded @ 60 sec interval (Flag 2 On).

Item	Columns	Description/Units
Data Code = 4	1	11
Year	2	Year
Day	3	Julian day of year
Hr/Min	4	Hour and minute code. Last two digits are minutes; first one or two digits are hours in 24 hour format.
Sensor Values	5-44	Maximum sensor data value occurring within hour time interval.

Table 21 Array 6 Data Format – temperatures – recorded @ 60 sec interval (Flag 2 On).

Item	Columns	Description/Units
Array ID	1	12
Year	2	Year
Day	3	Julian day of year
Hr/Min	4	Hour and minute code. Last two digits are minutes; first one or two digits are hours in 24-hour format.
Sensor Temperatures	5-44	Temperature at time of data sample (°F).
Ambient Temperatures	45	Temperature at time of data sample (°F).
Relative Humidity	46	Percent humidity
CR10x Temperature	47	Internal CR10 Temperature at time of data sample (°F).
CR10x Voltage	48	Battery voltage supplied to CR10x

Instrumentation Notes

The LTRC-WB long-term data logger was configured and programmed to take measurements from 36 vibrating wire sensors (30 strain gages and 6 crack meters). All of the sensors utilize vibrating wire technology and are activated by a single vibrating wire interface (CSI-AVW1). Sensors are connected to the AVW1 and read sequentially with the use of three 16-channel multiplexers (CSI-AM416). Sensor values generated by the data logger program are all stored in engineering units; for example inches for displacement and micro-strain (in⁻⁶/in) for strain.

Figure 63 shows the location of each long-term sensor on the structure along with the associated data-logger channel number. The associated multiplexer channel number, calibration factor, and memory location name are provided in Table 22.

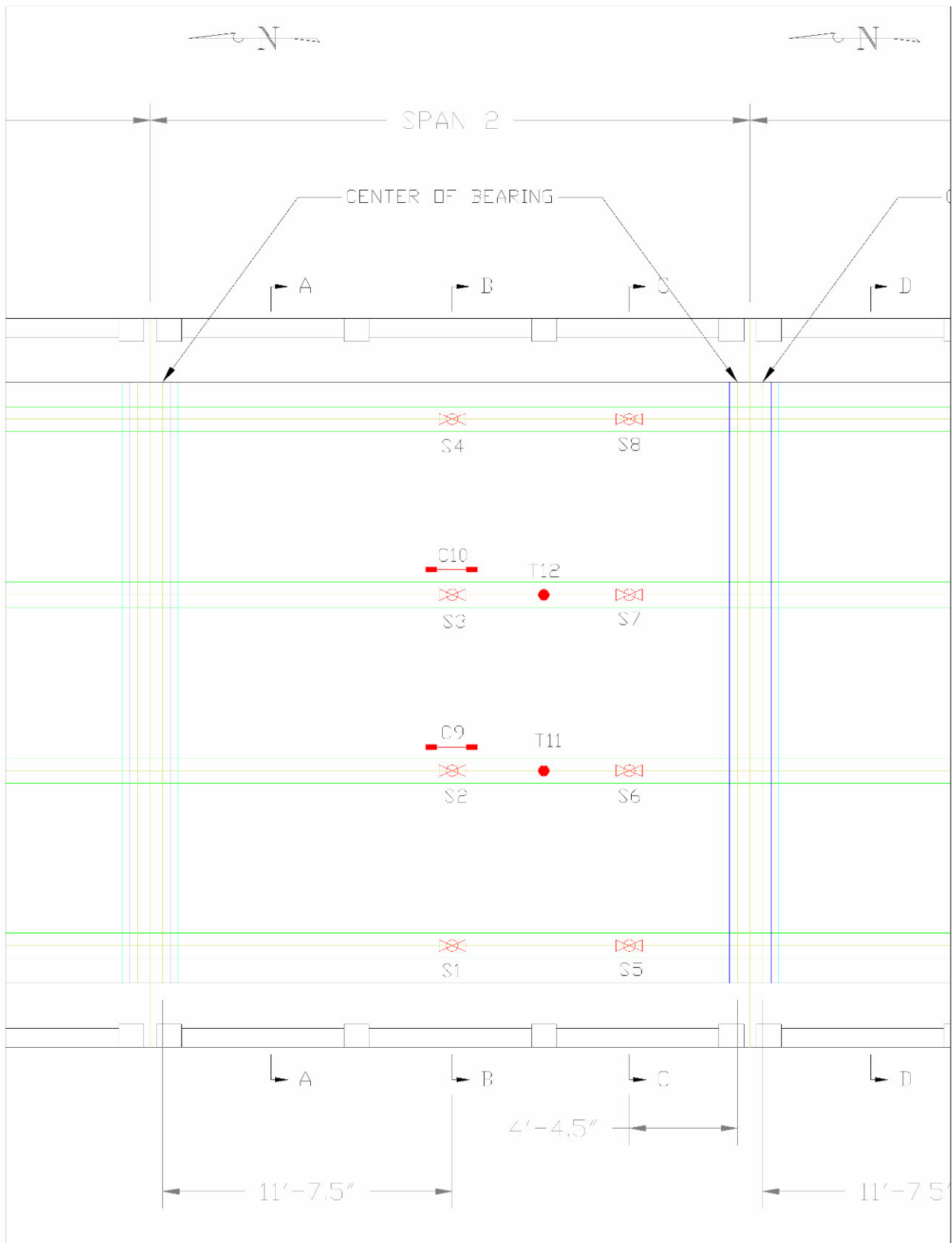


Figure 63 Long-term Instrumentation Plan – Span 2.

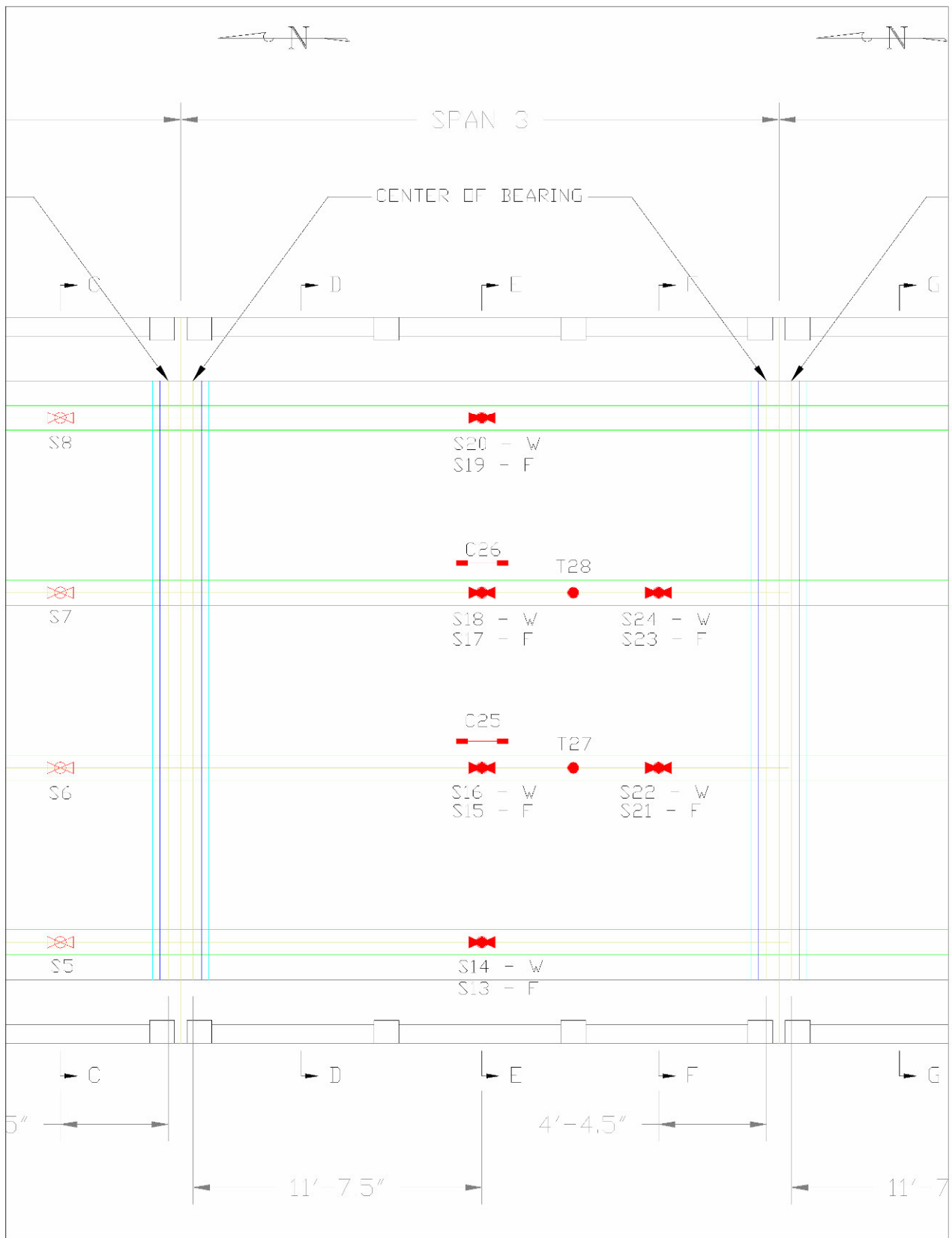


Figure 64 Long-term Instrumentation Plan – Span 3.

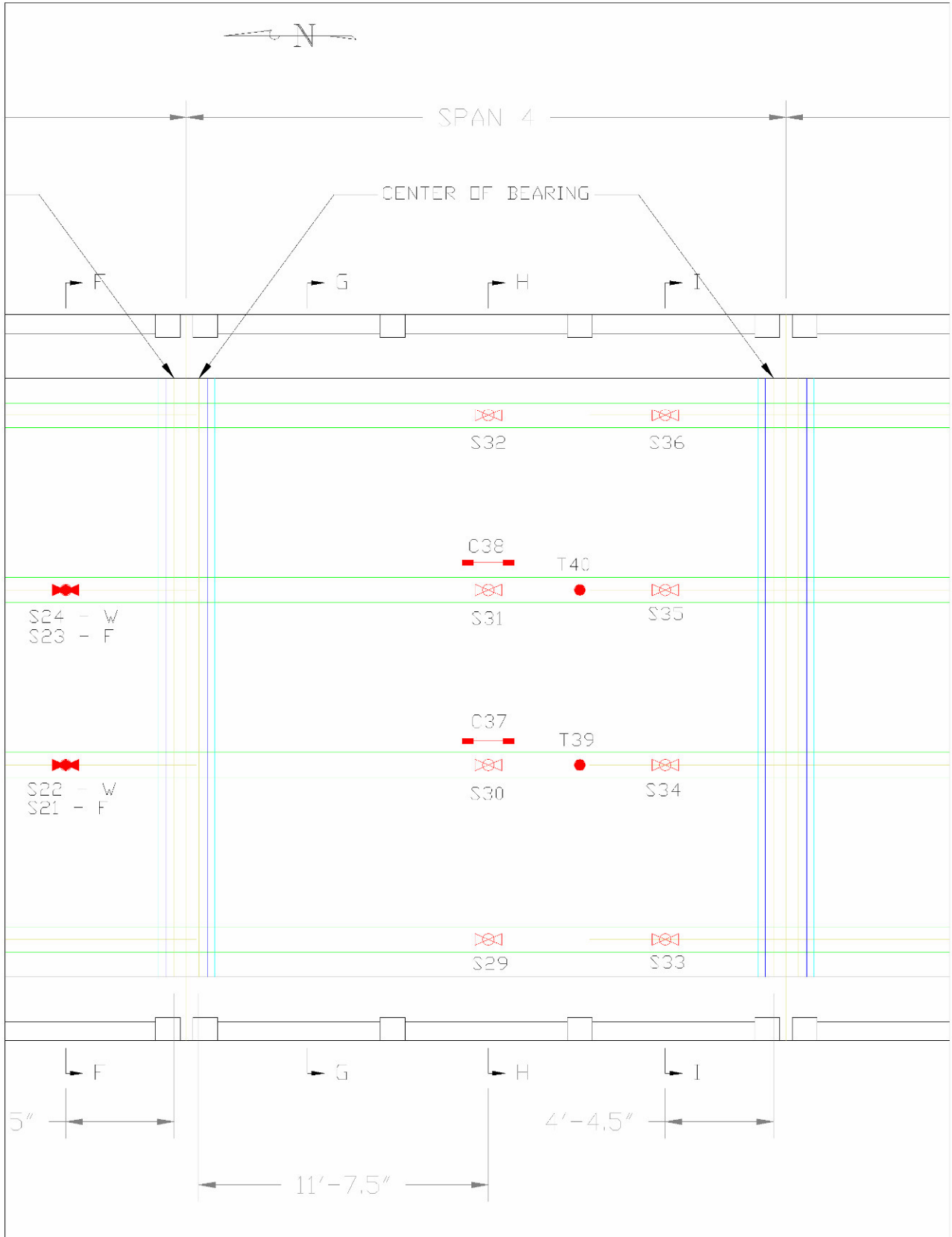


Figure 65 Long-term Instrumentation Plan – Span 4.

Table 22 Instrumentation connectivity and channel numbers.

Gage ID	Structure Location	Sensor Type	Calibration Factor	Mux	Mux Channel
Span 2 Sensors					
1	Midspan Bm 1	Strain Gage 4000	3837	1	1
2	Midspan Bm 2	“ “ “	“	1	2
3	Midspan Bm 3	“ “ “	“	1	3
4	Midspan Bm 4	“ “ “	“	1	4
5	4/5 th Pnt Bm 1	“ “ “	“	1	5
6	4/5 th Pnt Bm 2	“ “ “	“	1	6
7	4/5 th Pnt Bm 3	“ “ “	“	1	7
8	4/5 th Pnt Bm 4	“ “ “	“	1	8
9	Midspan Bm 2	Crack meter	0.1800	1	9
10	Midspan Bm 3	“ “	0.1800	1	10
11	Midspan Bm 2	Thermistor only	N/A	1	11
12	Midspan Bm 3	“ “	N/A	1	12
Span 3 Sensors					
13	Midspan Bm 1 FRP	Strain Gage 4000	3837	2	1
14	Midspan Bm 1 Web	“ “ “	“	2	2
15	Midspan Bm 2 FRP	“ “ “	“	2	3
16	Midspan Bm 2 Web	“ “ “	“	2	4
17	Midspan Bm 3 FRP	“ “ “	“	2	5
18	Midspan Bm 3 Web	“ “ “	“	2	6
19	Midspan Bm 4 FRP	“ “ “	“	2	7
20	Midspan Bm 4 Web	“ “ “	“	2	8
21	4/5 th Pnt Bm 3 FRP	“ “ “	“	2	9
22	4/5 th Pnt Bm 3 Web	“ “ “	“	2	10
23	4/5 th Pnt Bm 4 FRP	“ “ “	“	2	11
24	4/5 th Pnt Bm 4 Web	“ “ “	“	2	12
25	Midspan Bm 2	Crack meter	0.1800	2	13
26	Midspan Bm 3	“ “	0.1800	2	14
27	Midspan Bm 2	Thermistor only	N/A	2	15
28	Midspan Bm 3	“ “	N/A	2	16
Span 4 Sensors					
29	Midspan Bm 1	Strain Gage 4000	3837	3	1
30	Midspan Bm 2	“ “ “	“	3	2
31	Midspan Bm 3	“ “ “	“	3	3
32	Midspan Bm 4	“ “ “	“	3	4
33	4/5 th Pnt Bm 1	“ “ “	“	3	5
34	4/5 th Pnt Bm 2	“ “ “	“	3	6
35	4/5 th Pnt Bm 3	“ “ “	“	3	7
36	4/5 th Pnt Bm 4	“ “ “	“	3	8
37	Midspan Bm 2	Crack meter	0.1800	3	9
38	Midspan Bm 3	“ “	0.1800	3	10
39	Midspan Bm 2	Thermistor only	N/A	3	11
40	Midspan Bm 3	“ “	N/A	3	12

All vibrating wire sensors have the same number of cable wires and color code and should be connected in the arrangement listed in Table 23.

Table 23. Gage Wiring Sequence

Gage Wire Color	AM416 Wire Nut
Red	H1
Black	L1
Green	H2
White	L2
Bare	Shield

APPENDIX E – SPECIFICATIONS: BDI STRAIN TRANSDUCERS



Effective gage length:	3.0 in (76.2 mm). Extensions available for use on R/C structures.
Overall Size:	4.4 in x 1.2 in x 0.5 in (110 mm x 33 mm x 12 mm).
Cable Length:	10 ft (3 m) standard, any length available.
Material:	Aluminum
Circuit:	Full wheatstone bridge with four active 350Ω foil gages, 4-wire hookup.
Accuracy:	± 2%, individually calibrated to NIST standards.
Strain Range:	Approximately ±4000 $\mu\epsilon$.
Force req'd for 1000 $\mu\epsilon$:	Approximately 9 lbs. (40 N).
Sensitivity:	Approximately 500 $\mu\epsilon$ /mV/V,
Weight:	Approximately 3 oz. (88 g),
Environmental:	Built-in protective cover, also water resistant.
Temperature Range:	-60°F to 250°F (-50°C to 120°C) operation range.
Cable:	BDI RC-187: 22 gage, two individually-shielded pairs w/drain.
Options:	Fully waterproofed, Heavy-duty cable, Special quick-lock connector.
Attachment Methods:	C-clamps or threaded mounting tabs & quick-setting adhesive.

APPENDIX F – SPECIFICATIONS: BDI STRUCTURAL TESTING SYSTEM



Channels	4 to 128, Expandable in multiples of 4
Hardware Accuracy	± 0.2% (2% for Strain Transducers)
Sample Rates	0.01 to 1,000 Hz sample rate. Internal over-sampling rate is 15 KHz.
Max Test Lengths	20 minutes at 100 Hz. 128K samples per channel maximum test length.
Gain Levels	1, 250, 500, 1000
Digital Filter	Fixed by selected sample rate
Analog Filter	200 Hz, -3db, 3rd order Bessel
Max. Input Voltage	±10V
Power	85 - 264 VAC, 47-440 Hz -25 to 55 degrees C
12VDC Power	External inverter included
Excitation Voltages: Standard: LVDT:	5VDC @ 200mA ±15VDC @ 200mA
A/D Resolution	2.44 uV/bit (14-Bit ADC)
PC Requirements	Windows 2000, XP
PC Interface	USB 1.1 Port (Compatible with USB 2.0)
Self-Balancing Range	± 20 mV @ input with 350Ω Wheatstone bridge
Enclosures	Aluminum splash resistant
Cable Connections	All aluminum military grade, circular bayonet "snap" lock.
Vehicle Tracking:	See "AutoClicker" Specifications
Sensors	See "BDI Strain Transducer" Specifications Also supports LVDT's, foil strain gages, accelerometers, various DC output sensors. Single RS232 serially-interfaced sensor.
Weights: Power Unit: STS Unit	6.2 lbs (2.8 kg) 1.6 lbs (0.7 kg)
Dimensions: Power Unit: STS Unit:	13.5" x 9.5" x 2.4" (343mm x 242mm x 61 mm) 11.8" x 3.4" x 1.7" (300mm x 87mm x 44mm)

APPENDIX G – SPECIFICATIONS: BDI AUTOCLICKER



3 Handheld Radios	Motorola P1225 2-Channel (or equal) modified for both “Rx” and “Tx”.
Power	9V battery
Mounting	Universal front fender mounting system
Target	Retroreflective tape mounted on universal wheel clamp
Bands/Power	VHF/1 Watt or UHF/2 Watt
Frequencies	User-specified
Data Acquisition System Requirements	TTL/CMOS input (pull-up resistor to 5V)
Output	Isolated contact closure (200V 0.5A max switch current)

APPENDIX H - MODELING AND ANALYSIS: THE INTEGRATED APPROACH

INTRODUCTION

In order for load testing to be a practical means of evaluating short- to medium-span bridges, it is apparent that testing procedures must be economic to implement in the field and the test results translatable into a load rating. A well-defined set of procedures must exist for the field applications as well as for the interpretation of results. An evaluation approach based on these requirements was first developed at the University of Colorado during a research project sponsored by the Pennsylvania Department of Transportation (PennDOT). Over several years, the techniques originating from this project have been refined and expanded into a complete bridge rating system.

The ultimate goal of the Integrated Approach is to obtain realistic rating values for highway bridges in a cost effective manner. This is accomplished by measuring the response behavior of the bridge due to a known load and determining the structural parameters that produce the measured responses. With the availability of field measurements, many structural parameters in the analytical model can be evaluated that are otherwise conservatively estimated or ignored entirely. Items that can be quantified through this procedure include the effects of structural geometry, effective beam stiffness, realistic support conditions, effects of parapets and other non-structural components, lateral load transfer capabilities of the deck and transverse members, and the effects of damage or deterioration. Often, bridges are rated poorly because of inaccurate representations of the structural geometry or because the material and/or cross-sectional properties of main structural elements are not well defined. A realistic rating can be obtained, however, when all of the relevant structural parameters are defined and implemented in the analysis process.

One of the most important phases of this approach is a qualitative evaluation of the raw field data. Much is learned during this step to aid in the rapid development of a representative model.

INITIAL DATA EVALUATION

The first step in structural evaluation consists of a visual inspection of the data in the form of graphic response histories. Graphic software was developed to display the raw strain data in various forms. Strain histories can be viewed in terms of time or truck position. Since strain transducers are typically placed in pairs, neutral axis measurements, curvature responses, and strain averages can also be viewed. Linearity between the responses and load magnitude can be observed by the continuity in the strain histories. Consistency in the neutral axis measurements from beam to beam and as a function of load position provides great insight into the nature of the bridge condition. The direction and relative magnitudes of flexural responses along a beam line are useful in determining if end restraints play a significant role in the response behavior. In general, the initial data inspection provides the engineer with information concerning modeling requirements and can help locate damaged areas.

Having strain measurements at two depths on each beam cross-section, flexural curvature and the location of the neutral axis can be computed directly from the field data. Figure 66 illustrates how curvature and neutral axis values are computed from the strain measurements.

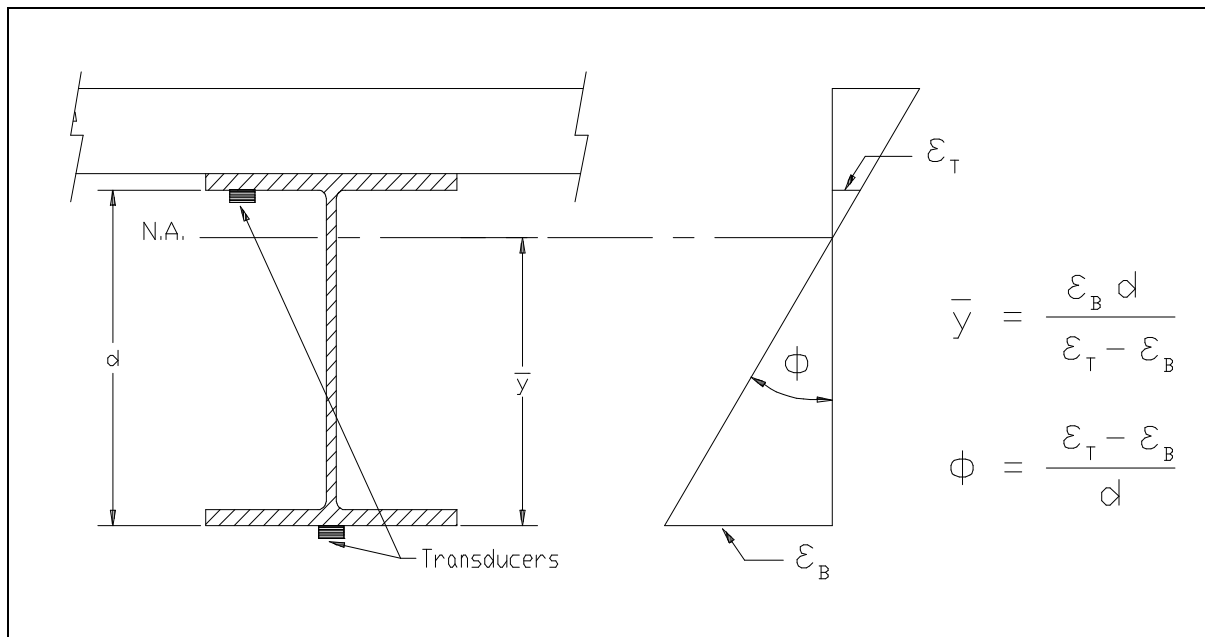


Figure 66 Illustration of Neutral Axis and Curvature Calculations

The consistency in the N.A. values between beams indicates the degree of consistency in beam stiffness. Also, the consistency of the N.A. measurement on a single beam as a function of truck position provides a good quality check for that beam. If for some reason a beam's stiffness changes with respect to the applied moment (i.e. loss of composite action or loss of effective flange width due to a deteriorated deck), it will be observed by a shift in the N.A. history.

Since strain values are translated from a function of time into a function of vehicle position on the structure and the data acquisition channel and the truck position tracked, a considerable amount of book keeping is required to perform the strain comparisons. In the past, this required manipulation of result files and spreadsheets which was tedious and a major source of error. This process is now performed automatically by the software and all of the information can be verified visually.

FINITE ELEMENT MODELING AND ANALYSIS

The primary function of the load test data is to aid in the development of an accurate finite element model of the bridge. Finite element analysis is used because it provides the most general tool for evaluating various types of structures. Since a comparison of measured and computed responses is performed, it is necessary that the analysis be able to represent the actual response behavior. This requires that actual geometry and boundary conditions be realistically represented. In maintaining reasonable modeling efforts and computer run times, a certain amount of simplicity is also required, so a planar grid model is generated for most structures and linear-elastic responses are assumed. A grid of frame elements is assembled in the same geometry as the actual structure. Frame elements represent the longitudinal and transverse members of the bridge. The load transfer characteristics of the deck are provided by attaching plate elements to the grid. When end restraints are determined to be present, elastic spring elements having both translational and rotational stiffness terms are inserted at the support locations.

Loads are applied in a manner similar to the actual load test. A model of the test truck, defined by a two-dimensional group of point loads, is placed on the structure model at discrete locations along the same path that the test truck followed during the load test. Gage locations identical to those in the field are also defined on the structure model so that strains can be computed at the same locations under the same loading conditions.

EVALUATION OF ROTATIONAL END RESTRAINT

A common requirement in structural identification is the need to determine effective spring stiffnesses that best represent in-situ support conditions. Where as it is generally simple to evaluate a spring constant in terms of moment per rotation, the value generally has little meaning to the engineer. A more conceptual approach is to evaluate the spring stiffness as a percentage of a fully restrained condition. For example: 0% being a pinned condition and 100% being fixed. This is best accomplished by examining the ratio of the beam or slab stiffness to the rotational stiffness of the support.

As an illustration, a point load is applied to a simple beam with elastic supports, see Figure 67. By examining the moment diagram, it is apparent that the ratio of the end moment to the midspan moment (M_e/M_m) equals 0.0 if the rotational stiffness (K_r) of the springs is equal to 0.0. Conversely, if the value of K_r is set to infinity (rigid) the moment ratio will equal 1.0. If a fixity term is defined as the ratio (M_e/M_m), which ranges from 0 to 100 percent, a more conceptual measure of end restraint can be obtained.

The next step is to relate the fixity term to the actual spring stiffness (K_r). The degree to which the K_r effects the fixity term depends on the beam or slab stiffness to which the spring is attached. Therefore the fixity term must be related to the ratio of the beam/spring stiffness. Figure 68 contains a graphical representation of the end restraint effect on a simple beam. Using the graph, a conceptual measure of end-restraint can be defined after the beam and spring constants are evaluated through structural identification techniques.

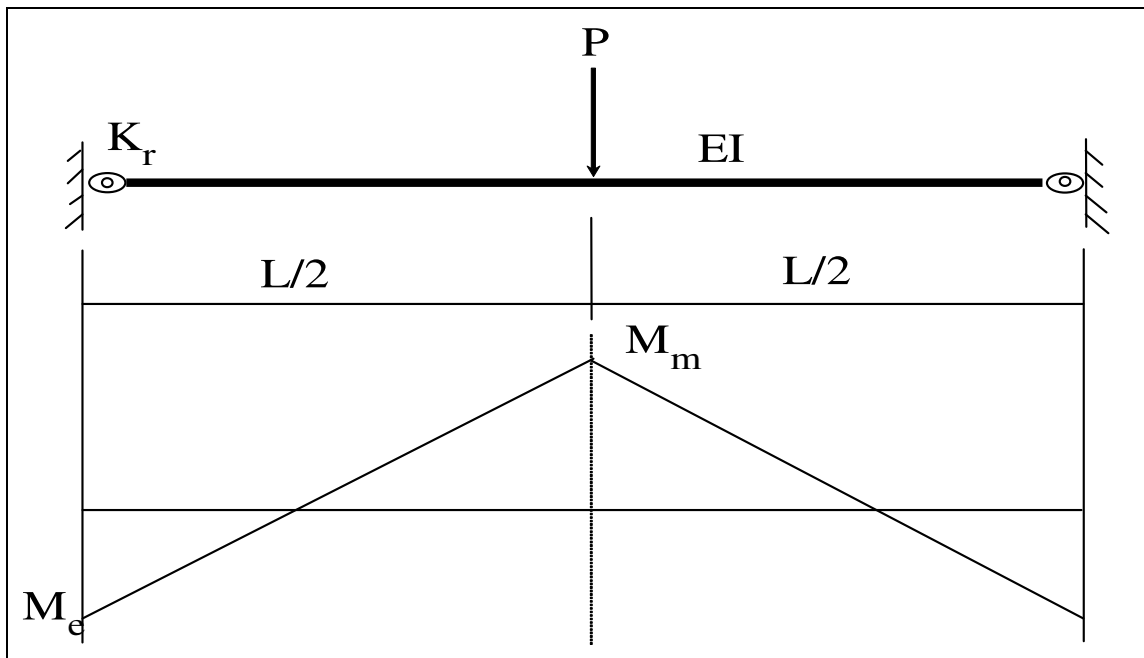


Figure 67 Moment Diagram of Beam with Rotational End Restraint.

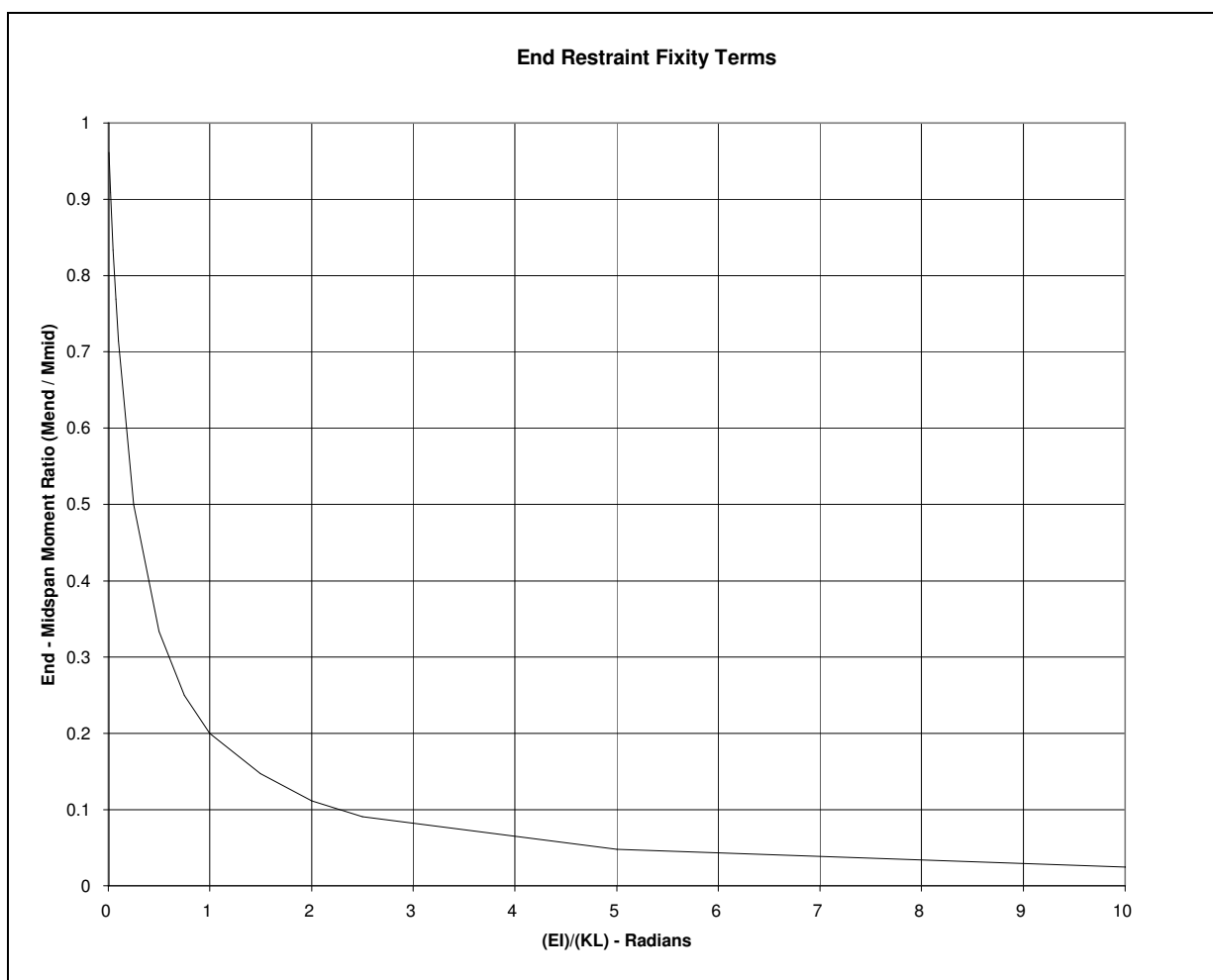


Figure 68 Relationship Between Spring Stiffness and Fixity Ratio.

MODEL CORRELATION AND PARAMETER MODIFICATION

The accuracy of the model is determined numerically by the analysis using several statistical relationships and through visual comparison of the strain histories. The numeric accuracy values are useful in evaluating the effect of any changes to the model, where as the graphical representations provide the engineer with the best perception for why the model is responding differently than the measurements indicate. Member properties that cannot be accurately defined by conventional methods or directly from the field data are evaluated by comparing the computed strains with the measured strains. These properties are defined as variable and are evaluated such that the best correlation between the two sets of data is obtained. It is the engineer’s responsibility to determine which parameters need to be refined and to assign realistic upper and lower limits to each parameter. The evaluation of the member property is accomplished with the aid of a parameter identification process (optimizer) built into the analysis. In short, the process consists of an iterative procedure of analysis, data comparison, and parameter modification. It is important to note that the optimization process is merely a tool to help evaluate various modeling parameters. The process works best when the number of parameters is minimized and reasonable initial values are used.

During the optimization process, various error values are computed by the analysis program that provides a quantitative measure of the model accuracy and improvement. The error is quantified in four different ways, each providing a different perspective of the model's ability to represent the actual structure; an absolute error, a percent error, a scale error and a correlation coefficient.

The **absolute error** is computed from the absolute sum of the strain differences. Algebraic differences between the measured and theoretical strains are computed at each gage location for each truck position used in the analysis; therefore, several hundred strain comparisons are generally used in this calculation. This quantity is typically used to determine the relative accuracy from one model to the next and to evaluate the effect of various structural parameters. It is used by the optimization algorithm as the objective function to minimize. Because the absolute error is in terms of micro-strain ($m\epsilon$) the value can vary significantly depending on the magnitude of the strains, the number of gages and number of different loading scenarios. For this reason, it has little conceptual value except for determining the relative improvement of a particular model.

A **percent error** is calculated to provide a better qualitative measure of accuracy. It is computed as the sum of the strain differences squared divided by the sum of the measured strains squared. The terms are squared so that error values of different sign will not cancel each other out, and to put more emphasis on the areas with higher strain magnitudes. A model with acceptable accuracy will usually have a percent error of less than 10%.

The **scale error** is similar to the percent error except that it is based on the maximum error from each gage divided by the maximum strain value from each gage. This number is useful because it is based only on strain measurements recorded when the loading vehicle is in the vicinity of each gage. Depending on the geometry of the structure, the number of truck positions, and various other factors, many of the strain readings are essentially negligible. This error function uses only the most relevant measurement from each gage.

Another useful quantity is the **correlation coefficient**, which is a measure of the linearity between the measured and computed data. This value determines how well the shape of the computed response histories match the measured responses. The correlation coefficient can have a value between 1.0 (indicating a perfect linear relationship) and -1.0 (exact opposite linear relationship). A good model will generally have a correlation coefficient greater than 0.90. A poor correlation coefficient is usually an indication that a major error in the modeling process has occurred. This is generally caused by poor representations of the boundary conditions or the loads were applied incorrectly (i.e. truck traveling in wrong direction).

The following table contains the equations used to compute each of the statistical error values:

Table 24 Error Functions

ERROR FUNCTION	EQUATION
Absolute Error	$\sum \epsilon_m - \epsilon_c $
Percent Error	$\sum (\epsilon_m - \epsilon_c)^2 / \sum (\epsilon_m)^2$
Scale Error	$\frac{\sum \max \epsilon_m - \epsilon_c _{gage}}{\sum \max \epsilon_m _{gage}}$
Correlation Coefficient	$\frac{\sum (\epsilon_m - \bar{\epsilon}_m)(\epsilon_c - \bar{\epsilon}_c)}{\sum \sqrt{(\epsilon_m - \bar{\epsilon}_m)^2 (\epsilon_c - \bar{\epsilon}_c)^2}}$

In addition to the numerical comparisons made by the program, periodic visual comparisons of the response histories are made to obtain a conceptual measure of accuracy. Again, engineering judgment is essential in determining which parameters should be adjusted so as to obtain the most accurate model. The selection of adjustable parameters is performed by determining what properties have a significant effect on the strain comparison and determining which values cannot be accurately estimated through conventional engineering procedures. Experience in examining the data comparisons is helpful; however, two general rules apply concerning model refinement. When the shapes of the computed response histories are similar to the measured strain records but the magnitudes are incorrect this implies that member stiffness must be adjusted. When the shapes of the computed and measured response histories are not very similar then the boundary conditions or the structural geometry are not well represented and must be refined.

In some cases, an accurate model cannot be obtained, particularly when the responses are observed to be non-linear with load position. Even then, a great deal can be learned about the structure and intelligent evaluation decisions can be made.

APPENDIX I - LOAD RATING PROCEDURES

A load-rating factor is a numeric value indicating a structure's ability to carry a specific load. Load rating factors were computed by applying standard design loads along with the structure's self-weight and asphalt overlay. Rating factors are computed for various structural components and are equal to the ratio of the component's live load capacity and the live load applied to that component; including all appropriate load factors. A load-rating factor greater than 1.0 indicates a member's capacity exceeds the applied loads with the desired factors of safety. A rating factor less than 1.0 indicates a member is deficient such that a specific vehicle cannot cross the bridge with the desired factor of safety. A number near 0.0 indicates the structure cannot carry its own dead weight and maintain the desired safety factor. The lowest component rating-factor generally controls the load rating of the entire structure. Additional factors are applied to account for variability in material, load application, and dynamic effects. Two levels of load rating are performed for the bridge. An Inventory Level rating corresponds to the design stress levels and/or factors of safety and represents the loads that can be applied on a daily basis. The Operating Rating levels correspond to the maximum load limits above which the structure may experience damage or failure.

For borderline bridges (those that calculations indicate a posting is required), the primary drawback to conventional bridge rating is an oversimplified procedure for estimating the load applied to a given beam (i.e. wheel load distribution factors) and a poor representation of the beam itself. Due to lack of information and the need for conservatism, material and cross-section properties are generally over-estimated and beam end supports are assumed to be simple when in fact even relatively simple beam bearings have a substantial effect on the midspan moments. Inaccuracies associated with conservative assumptions are compounded with complex framing geometries. From an analysis standpoint, the goal here is to generate a model of the structure that is capable of reproducing the measured strains. Decisions concerning load rating are then based on the performance of the model once it is proven to be accurate.

The main purpose for obtaining an accurate model is to evaluate how the bridge will respond when standard design loads, rating vehicles or permit loads are applied to the structure. Since load testing is generally not performed with all of the vehicles of interest, an analysis must be performed to determine load-rating factors for each truck type. Load rating is accomplished by applying the desired rating loads to the model and computing the stresses on the primary members. Rating factors are computed using the equation specified in the AASHTO Manual for Condition Evaluation of Bridges - see Equation (1).

It is important to understand that diagnostic load testing and the integrated approach are most applicable to obtaining Inventory (service load) rating values. This is because it is assumed that all of the measured and computed responses are linear with respect to load. The integrated approach is an excellent method for estimating service load stress values but it generally provides little additional information regarding the ultimate strength of particular structural members. Therefore, operating rating values must be computed using conventional assumptions regarding member capacity. This limitation of the integrated approach is not viewed as a serious concern, however, because load responses should never be permitted to reach the inelastic range.

Operating and/or Load Factor rating values must also be computed to ensure a factor of safety between the ultimate strength and the maximum allowed service loads. The safety to the public is of vital importance but as long as load limits are imposed such that the structure is not damaged then safety is no longer an issue.

Following is an outline describing how field data is used to help in developing a load rating for the superstructure. These procedures will only complement the rating process, and must be used with due consideration to the substructure and inspection reports.

1. **Preliminary Investigation:** Verification of linear and elastic behavior through continuity of strain histories, locate neutral axis of flexural members, detect moment resistance at beam supports, and qualitatively evaluate behavior.
2. **Develop representative model:** Use graphic pre-processors to represent the actual geometry of the structure, including span lengths, girder spacing, skew, transverse members, and deck. Identify gage locations on model identical to those applied in the field.
3. **Simulate load test on computer model:** Generate 2-dimensional model of test vehicle and apply to structure model at discrete positions along same paths defined during field tests. Perform analysis and compute strains at gage location for each truck position.
4. **Compare measured and initial computed strain values:** Various global and local error values at each gage location are computed and visual comparisons made with post-processor.
5. **Evaluate modeling parameters:** Improve model based on data comparisons. Engineering judgment and experience is required to determine which variables are to be modified. A combination of direct evaluation techniques and parameter optimization are used to obtain a realistic model. General rules have been defined to simplify this operation.
6. **Model evaluation:** In some cases it is not desirable to rely on secondary stiffening effects if it is likely they will not be effective at higher load levels. It is beneficial, though, to quantify their effects on the structural response so that a representative computer model can be obtained. The stiffening effects that are deemed unreliable can be eliminated from the model prior to the computation of rating factors. For instance, if a non-composite bridge is exhibiting composite behavior, then it can conservatively be ignored for rating purposes. However, if it has been in service for 50 years and it is still behaving compositely, chances are that very heavy loads have crossed over it and any bond-breaking would have already occurred. Therefore, probably some level of composite behavior can be relied upon. When unintended composite action is allowed in the rating, additional load limits should be computed based on an allowable shear stress between the steel and concrete and an ultimate load of the non-composite structure.
7. **Perform load rating:** Apply HS-20 and/or other standard design, rating and permit loads to the calibrated model. Rating and posting load configuration recommended by AASHTO are shown in Figure 69.
8. The same rating equation specified by the **AASHTO - Manual for the Condition Evaluation of Bridges** is applied:

$$RF = \frac{C - \gamma_{DC}(DC) - \gamma_{DW}(DW) \pm \gamma_P(P)}{\gamma_L(LL + IM)} \quad (1)$$

where:

RF = Rating Factor for individual member.

C = Member Capacity.

γ_{DC} = LRFD load factor for structural components and attachments.

DC = Dead-load effect due to structural components.

γ_{DW} = LRFD load factor for wearing surfaces and utilities.

DW = Dead-load effect due to wearing surface and utilities.

γ_p = LRFD load factor for permanent loads other than dead loads = 1.0

P = Permanent loads other than dead loads.

LL = Live-load effect.

IM = Impact effect, either AASHTO or measured.

The only difference between this rating technique and standard beam rating programs is that a more realistic model is used to determine the dead-load and live-load effects. Two-dimensional loading techniques are applied because wheel load distribution factors are not applicable to a planar model. Stress envelopes are generated for several truck paths, envelopes for paths separated by normal lane widths are combined to determine multiple lane loading effects.

9. **Consider other factors:** Other factors such as the condition of the deck and/or substructure, traffic volume, and other information in the inspection report should be taken into consideration and the rating factors adjusted accordingly.

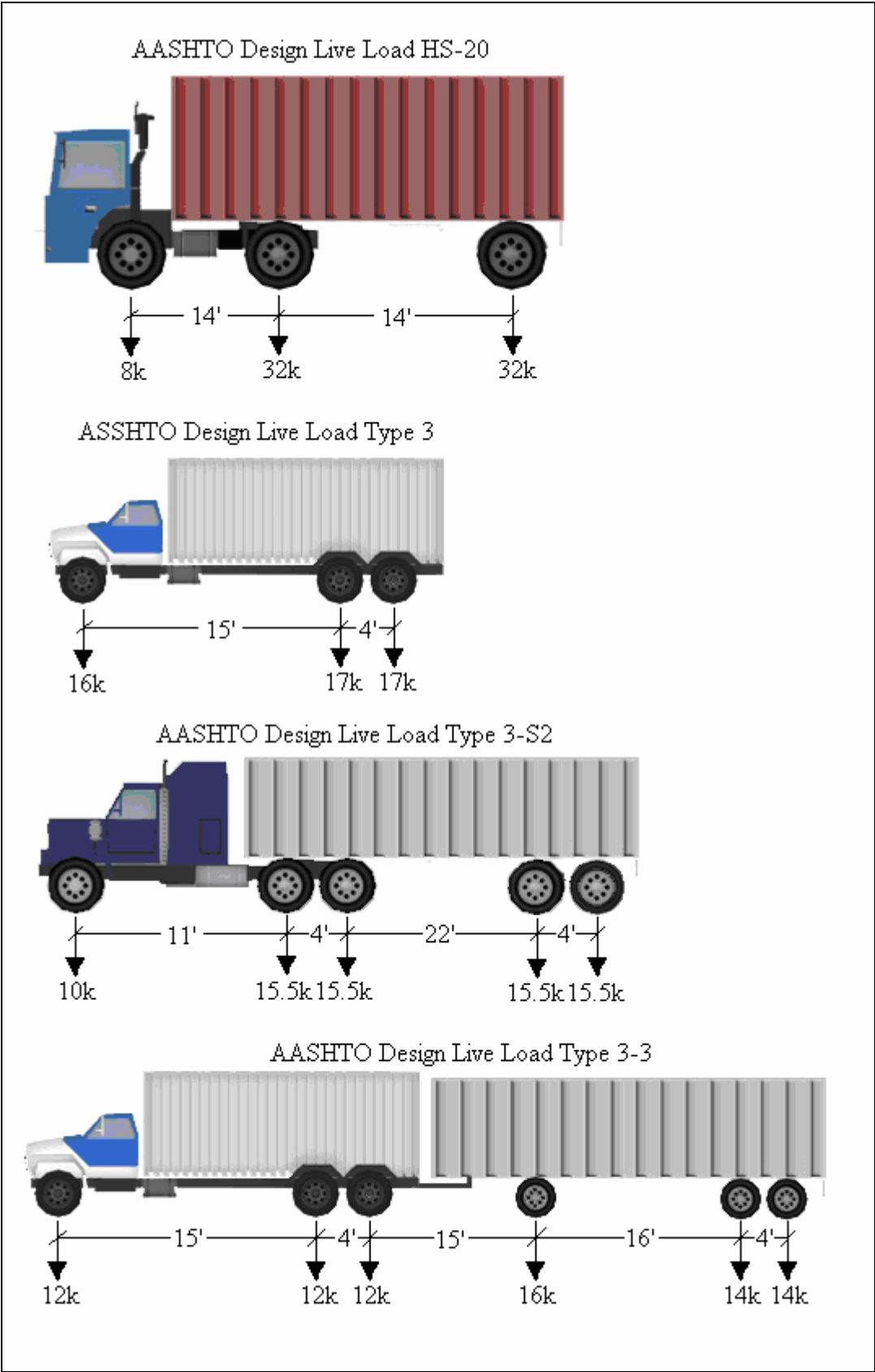


Figure 69 AASHTO Rating and Posting Load Configurations.

APPENDIX J - REFERENCED MATERIAL

AASHTO (2003). "AASHTO LRFD Bridge Design Specifications." Washington, D.C.

AASHTO, (2003). "Manual for the Condition Evaluation and Load and Resistance Factor Rating (LRFR) of Highway Bridges", Washington, D.C.

Commander, B., (1989). "An Improved Method of Bridge Evaluation: Comparison of Field Test Results with Computer Analysis." Master Thesis, University of Colorado, Boulder, CO.

Gerstle, K.H., and Ackroyd, M.H. (1990). "*Behavior and Design of Flexibly-Connected Building Frames.*" Engineering Journal, AISC, 27(1),22-29.

Goble, G., Schulz, J., and Commander, B. (1992). "Load Prediction and Structural Response." Final Report, FHWA DTFH61-88-C-00053, University of Colorado, Boulder, CO.

Lichtenstein, A.G.(1995). "Bridge Rating Through Nondestructive Load Testing." Technical Report, NCHRP Project 12-28(13)A.

Schulz, J.L. (1989). "Development of a Digital Strain Measurement System for Highway Bridge Testing." Masters Thesis, University of Colorado, Boulder, CO.

Schulz, J.L. (1993). "In Search of Better Load Ratings." *Civil Engineering*, ASCE 63(9),62-65.

APPENDIX B

Shear Rating Calculations

Inventory Rating Level

It results in a live load which can safely utilize an existing structure for an indefinite period of time.

Operating Rating Level

It results in a maximum permissible live load to which the structure may be subjected. Allow unlimited numbers of vehicles to use the bridge at Operating Level may shorten the life of the bridge.

General Note: Compressive strength of concrete will be taken as 5,000 psi instead of the original strength of 3,000 psi. Yield stress of steel is taken as 40,000 psi.

$$A_s := 6.3285 \text{ in}^2 \quad SpL := 23 \text{ ft} \quad \text{GirdSpa} := 7 \cdot \text{ft} \quad \text{ft} \equiv 12 \text{ in}$$

$$f_y := 40000 \frac{\text{lb}}{\text{in}^2} \quad b := 69 \text{ in} \quad \text{Bearing} := 10 \text{ in}$$

$$h := 22.5 \text{ in} \quad \text{GirdSpa} = 84 \cdot \text{in}$$

$$f_c := 5000 \frac{\text{lb}}{\text{in}^2} \quad b_w := 12 \cdot \text{in} \quad \text{ton} \equiv 2000 \cdot \text{lb}$$

$$E_s := 30000000 \frac{\text{lb}}{\text{in}^2} \quad h_f := 6.5 \text{ in} \quad k \equiv 1000 \text{ lb}$$

$$\beta_1 := 0.85 - 0.05 \cdot \left(\frac{f_c - 4000 \frac{\text{lb}}{\text{in}^2}}{1000 \frac{\text{lb}}{\text{in}^2}} \right) \quad \beta_1 = 0.8 \quad a := \frac{A_s \cdot f_y}{\beta_1 \cdot f_c \cdot b} \quad a = 0.917 \cdot \text{in}$$

Statement := $\begin{cases} \text{"Treat as a Rectangular Section"} & \text{if } a < h_f \\ \text{"T-beam section"} & \text{otherwise} \end{cases}$

Statement = "Treat as a Rectangular Section"

$$b_{eff} := \min \left[\frac{SpL}{4}, (16 \cdot h_f + b_w), \text{GirdSpa} \right] \quad b_{eff} = 69 \cdot \text{in}$$

$$c_g := \frac{(2 \cdot 1.125 \cdot 1.125) \cdot (3 + 1.5) + (3 \cdot 1.125 \cdot 1.125) \cdot (1.5)}{(2 + 3) \cdot (1.125 \cdot 1.125)} \cdot 1 \text{ in}$$

$$c_g = 2.7 \cdot \text{in}$$

Beam is now 72 in x 22.5 in

$$d := h - cg \quad d = 19.8 \cdot \text{in} \quad \epsilon_c := 0.003 \quad \phi := 0.90 \quad \epsilon_y := \frac{f_y}{E_s} \quad \epsilon_y = 1.333 \times 10^{-3}$$

$$c1 := \frac{a}{\beta_1} \quad c1 = 1.1 \cdot \text{in} \quad \text{Ratio} := \frac{c1}{d} \quad \text{Ratio} = 0.058$$

Check Strain in steel $\epsilon_s := \frac{(d - c1)}{c1} \cdot \epsilon_c \quad \epsilon_s = 0.049$

$$\text{Statement1} := \begin{cases} \text{"Steel has yielded!!!!"} & \text{if } \epsilon_y < \epsilon_s \\ \text{"Steel has not yielded!!!!"} & \text{otherwise} \end{cases}$$

$$\text{Statement1} = \text{"Steel has yielded!!!!"}$$

$$M_n := A_s \cdot f_y \cdot \left(d - \frac{a}{2} \right) \quad M_n = 408 \cdot \text{ft} \cdot \text{k}$$

$$M_u := \phi \cdot M_n \quad M_u = 4406.5 \cdot \text{k} \cdot \text{in} \quad M_{u1} := M_u \quad M_{u1} = 367.2 \cdot \text{k} \cdot \text{ft}$$

From Paul's computations

$$M_{\text{paul}} := 4416.5 \cdot \text{ft} \cdot \text{k} \quad M_{\text{paul1}} := \frac{M_{\text{paul}}}{12} \quad M_{\text{paul1}} = 368 \cdot \text{ft} \cdot \text{k}$$

$$\text{There is a difference of } := M_{u1} - M_{\text{paul1}} \quad \text{There is a difference of } = -0.8 \cdot \text{ft} \cdot \text{k}$$

$$d = 19.8 \cdot \text{in}$$

Critical Section at $d = 19.8$ in from face of support

Critical Section at $d = 0.5 \cdot \text{bearing depth} + d$

$$CS := \frac{\text{Bearing}}{2} + d \quad CS = 24.8 \cdot \text{in} \quad CS = 2.1 \cdot \text{ft}$$

DL on Girder

$$\text{Structural} := \frac{[b \cdot hf + bw \cdot (h - hf)]}{144 \frac{\text{in}^2}{\text{ft}^2}} \cdot 150 \frac{\text{lb}}{\text{ft}^3} \quad \text{Structural} = 0.667 \cdot \frac{\text{k}}{\text{ft}} \quad d = 1.65 \cdot \text{ft}$$

$$\text{Structural} = 0.667 \cdot \frac{\text{k}}{\text{ft}}$$

$$\text{AC overlay is 5 inches} \quad \text{Act} := 5 \text{in} \quad \text{AC} := \frac{b \cdot \text{Act}}{144 \frac{\text{in}^2}{\text{ft}^2}} \cdot 144 \frac{\text{lb}}{\text{ft}^3} \quad \text{AC} = 0.345 \cdot \frac{\text{k}}{\text{ft}}$$

$$Wdl := \text{Structural} + AC \quad Wdl = 1.012 \cdot \frac{k}{ft}$$

$$\text{Max Shear is at end} \quad V_{max} := Wdl \cdot \frac{SpL}{2} \quad V_{maxdl} := V_{max} \quad V_{maxdl} = 11.6 \cdot k$$

$$\text{Max Shear at d from face of support} \quad V_{maxd} := \frac{V_{max} \cdot (SpL - CS)}{SpL} \quad V_{maxd} = 10.6 \cdot k$$

$$DF := \frac{GirdSpa}{6ft} \quad DF = 1.167 \quad IF := \frac{50}{\left(SpL \cdot \frac{1}{ft} - CS \cdot \frac{1}{ft} + 125 \right)} \quad IF = 0.343$$

$$UseIF := \begin{cases} 0.3 & \text{if } IF > 0.3 \\ IF & \text{otherwise} \end{cases} \quad UseIF = 0.3$$

For a 23 ft span girder, the influence line method gives: $V_{maxL} := 19.48k$ $V_{maxLCS} := 16.4 \cdot k$

$$V_{maxLI} := V_{maxLCS} \cdot DF \cdot (1 + UseIF) \quad V_{maxLI} = 24.9 \cdot k$$

$$\text{Shear Capacity of Section} \quad A_v := 2 \cdot 0.22 \text{in}^2 \quad A_v = 0.44 \cdot \text{in}^2 \quad \text{Spacing} := 6\text{in}$$

$$V_c := 2 \frac{\text{lb}^{0.5}}{\text{in}} \cdot f_c^{0.5} \cdot b_w \cdot d \quad V_c = 33.6 \cdot k \quad \phi_1 := 0.85$$

$$V_s := A_v \cdot f_y \cdot \frac{d}{\text{Spacing}} \quad V_s = 58.1 \cdot k \quad V_n := V_c + V_s \quad V_n = 91.7 \cdot k$$

$$\phi V_n := \phi_1 \cdot V_n \quad \phi V_n = 77.9 \cdot k \quad V_u := \phi V_n \quad V_u = 77.9 \cdot k$$

$$\text{Moment Capacity Rating} \quad M_d := \frac{Wdl \cdot SpL^2}{8} \quad M_d = 66.9 \cdot k \cdot \text{ft}$$

From AAHTO and for L=23 ft $MHS := 92.0 \text{ft} \cdot k$ No Impact $UseIF = 0.3$ $DF = 1.2$

$$ML := MHS \cdot DF \quad ML = 107.3 \cdot k \cdot \text{ft}$$

$$MLI := ML \cdot (1 + UseIF) \quad MLI = 139.5 \cdot \text{ft} \cdot k$$

$$RF_{opr} := \frac{Mu - 1.3M_d}{1.3 \cdot MLI} \quad RF_{opr} = 1.54 \quad R_{opr} := RF_{opr} \cdot 36 \cdot \text{ton} \quad R_{opr} = 56 \cdot \text{ton}$$

$$RF_{inv} := \frac{Mu - 1.3M_d}{1.3 \cdot \left(\frac{5}{3} \right) \cdot MLI} \quad RF_{inv} = 0.93$$

$$R_{inv} := RF_{inv} \cdot 36 \cdot \text{ton} \quad R_{inv} = 33 \cdot \text{ton}$$

HS31
HS18

Shear Capacity Rating

$$V_{\max d} = 10.6 \cdot k \quad V_{\max LI} = 24.9 \cdot k$$

$$RF_{\text{oprs}} := \frac{V_u - 1.3 V_{\max d}}{1.3 \cdot V_{\max LI}}$$

$$RF_{\text{oprs}} = 1.98$$

$$R_{\text{oprs}} := RF_{\text{oprs}} \cdot 36 \cdot \text{ton} \quad R_{\text{oprs}} = 71 \cdot \text{ton}$$

HS40

$$RF_{\text{invs}} := \frac{V_u - 1.3 V_{\max d}}{1.3 \cdot \left(\frac{5}{3}\right) \cdot V_{\max LI}}$$

$$RF_{\text{invs}} = 1.19$$

$$R_{\text{invs}} := RF_{\text{invs}} \cdot 36 \cdot \text{ton} \quad R_{\text{invs}} = 43 \cdot \text{ton}$$

HS19

Strength of the section:

1. Moment:

$$\text{Section Capacity: } \phi M_n := \phi \cdot M_n \quad \phi M_n = 367.2 \cdot \text{ft} \cdot \text{k}$$

$$\text{Applied Loads: } M_d = 66.9 \cdot \text{ft} \cdot \text{k} \quad M_{LI} = 139.5 \cdot \text{ft} \cdot \text{k}$$

$$M_{u2} := 1.3 \cdot \left(M_d + \frac{5}{3} \cdot M_{LI} \right) \quad M_{u2} = 389.33 \cdot \text{ft} \cdot \text{k}$$

$$\text{Statement2} := \begin{cases} \text{"Section is inadequate in flexure"} & \text{if } \phi M_n < M_{u2} \\ \text{"Section is adequate in flexure"} & \text{otherwise} \end{cases}$$

$$\text{Statement2} = \text{"Section is inadequate in flexure"}$$

2. Shear:

$$\text{Section Capacity: } \phi V_n := \phi \cdot V_n \quad \phi V_n = 77.93 \cdot k$$

$$\text{Applied Loads: } V_{\max d} = 11.6 \cdot k \quad V_{\max LI} = 24.9 \cdot k$$

$$V_{u2} := 1.3 \cdot \left(V_{\max d} + \frac{5}{3} \cdot V_{\max LI} \right) \quad V_{u2} = 69 \cdot k$$

$$\text{Statement3} := \begin{cases} \text{"Section is inadequate in shear"} & \text{if } \phi V_n < V_{u2} \\ \text{"Section is adequate in shear"} & \text{otherwise} \end{cases}$$

$$\text{Statement3} = \text{"Section is adequate in shear"}$$

VWrap C100

Flexure Only!

Mu3 := 5525·in·k

$$RF_{opr3} := \frac{Mu3 - 1.3Md}{1.3 \cdot MLI}$$

$$RF_{opr3} = 2.06$$

$$R_{opr3} := RF_{opr3} \cdot 36 \cdot \text{ton} \quad R_{opr3} = 74 \cdot \text{ton}$$

HS40

$$RF_{inv3} := \frac{Mu3 - 1.3Md}{1.3 \cdot \left(\frac{5}{3}\right) \cdot MLI}$$

$$RF_{inv3} = 1.24$$

$$R_{inv3} := RF_{inv3} \cdot 36 \cdot \text{ton} \quad R_{inv3} = 44 \cdot \text{ton}$$

HS24

Carbodur S512-96 Surface Flexure Only!!

Mu4 := 5095·in·k

$$RF_{opr4} := \frac{Mu4 - 1.3Md}{1.3 \cdot MLI}$$

$$RF_{opr4} = 1.86$$

$$R_{opr4} := RF_{opr4} \cdot 36 \cdot \text{ton} \quad R_{opr4} = 67 \cdot \text{ton}$$

HS37

$$RF_{inv4} := \frac{Mu4 - 1.3Md}{1.3 \cdot \left(\frac{5}{3}\right) \cdot MLI}$$

$$RF_{inv4} = 1.12$$

$$R_{inv4} := RF_{inv4} \cdot 36 \cdot \text{ton} \quad R_{inv4} = 40 \cdot \text{ton}$$

HS22

Carbodur S512-96 NSM

Flexure Only!!

Mu5 := 5844·in·k

$$RF_{opr5} := \frac{Mu5 - 1.3Md}{1.3 \cdot MLI}$$

$$RF_{opr5} = 2.21$$

$$R_{opr5} := RF_{opr5} \cdot 36 \cdot \text{ton} \quad R_{opr5} = 79 \cdot \text{ton}$$

HS44

$$RF_{inv5} := \frac{Mu5 - 1.3Md}{1.3 \cdot \left(\frac{5}{3}\right) \cdot MLI}$$

$$RF_{inv5} = 1.32$$

$$R_{inv5} := RF_{inv5} \cdot 36 \cdot \text{ton} \quad R_{inv5} = 48 \cdot \text{ton}$$

HS26

This public document is published at a total cost of \$250. 42 copies of this public document were published in this first printing at a cost of \$250. The total cost of all printings of this document including reprints is \$250. This document was published by Louisiana Transportation Research Center to report and publish research findings as required in R.S. 48:105. This material was duplicated in accordance with standards for printing by state agencies established pursuant to R.S. 43:31. Printing of this material was purchased in accordance with the provisions of Title 43 of the Louisiana Revised Statutes.